

Université Pierre et Marie Curie

École Doctorale 158 : Cerveau-Cognition-Comportement

L'Institut du Cerveau et de la Moelle/ UMR_S 1127

**Mechanisms of Central Nervous System Nodes of
Ranvier Assembly**

Par : Sean Anthony FREEMAN

Thèse de doctorat de Neurosciences

Dirigée par Mme. Catherine LUBETZKI et Mme. Nathalie SOL-FOULON

Présentée et soutenue publiquement le 2 juillet 2015

Devant un jury composé de :

M. Peter J. BROPHY	- <i>Examineur</i>
M. François COURAUD	- <i>Président du jury</i>
Mme. Bénédicte DARGENT	- <i>Rapporteur</i>
Mme. Catherine LUBETZKI	- <i>Directrice de la thèse</i>
Mme. Nathalie SOL-FOULON	- <i>Co-directrice de la thèse</i>
M. Nicolas TRICAUD	- <i>Rapporteur</i>

Table of Contents

Abbreviations	4
Part I: Introduction	13
Chapter I: The myelinated nerve.....	14
1.1 Historical perspective of the nerve fiber	14
1.2 Structure and molecular composition of myelinated nerve fibers	17
1.2.1 The myelin sheath	17
1.2.1.1 Myelinated regions and structure	18
1.2.1.2 Myelin composition	20
1.2.1.2.1 Lipid composition.....	20
1.2.1.2.2 Protein composition	21
1.2.1.3 Oligodendrocyte differentiation and myelination	23
1.2.2 The nodes of Ranvier (Nodes)	26
1.2.2.1 Nodal ultrastructure	28
1.3 Molecular composition of excitable and axo-glial domains	33
1.3.1 Voltage-gated ion channels	35
1.3.1.1 Voltage-gated sodium channels (Na _v)	35
1.3.1.2 Voltage-gated potassium channels (K _v)	45
1.3.2 Cellular adhesion molecules of the immunoglobulin superfamily	48
1.3.2.1 L1-CAMs.....	48
1.3.2.2 GPI-anchored CAMs	57
1.3.2.3 Neurexin-related CAMs.....	60
1.3.3 Cytoskeletal scaffolding proteins.....	64
1.3.3.1 Spectrins	66
1.3.3.2 Ankyrins	70
1.3.4 Other scaffolding molecules	72
1.3.5 Schwann cell microvilli and extracellular matrix (ECM) proteins	73
1.3.5.1 Schwann cell microvilli	73

1.3.5.2 ECM	76
1.3.6 Signaling molecules	78
Chapter II: Action potential conduction along myelinated fibers in healthy and diseased states	82
2.1 Signal conduction along unmyelinated axons	82
2.2 Signal conduction along myelinated axons	86
2.3 Factors affecting conduction velocity in myelinated axons	90
2.3.1 Paranodal junctions	90
2.3.2 Nodes of Ranvier	90
2.4 The transition to saltatory conduction along myelinated axons	93
2.5 Action potential conduction in the diseased state	94
2.5.1 Multiple sclerosis (MS)	94
2.5.2 Disruption to the nodal architecture alters axonal conduction.....	95
Chapter III: Mechanisms of nodes of Ranvier assembly and transport of nodal components in the PNS and CNS	100
3.1 Mechanisms of PNS nodes of Ranvier assembly.....	100
3.1.1 Heminodal clustering mechanism	101
3.1.2 Paranodal-junction dependent mechanism	104
3.2 Mechanisms of CNS nodes of Ranvier assembly	107
3.2.1 Extrinsic mechanisms of CNS nodes of Ranvier formation	107
3.2.1.1 Paranodal junctions	107
3.2.1.2 ECM	110
3.2.1.3 Oligodendroglial secreted proteins.....	111
3.2.1.4 Nodal CAMs and Nav β -Subunits	114
3.2.2 Intrinsic mechanisms of CNS nodes of Ranvier formation	115
3.2.2.1 Cytoskeletal Scaffolds	115
3.2 Trafficking and targeting of neuronal nodal components	120
3.2.1 Mechanisms for the transition of voltage-gated channels at the nodes of Ranvier	125

3.3 Aim of the dissertation	129
Part II: Results	132
Acceleration of conduction velocity linked to clustering of nodal components precedes myelination	133
Study of the trafficking of nodal components by live imaging in dissociated hippocampal cultures	153
Part III: Discussion	178
1.1 Prenodes form along GABAergic interneurons in the absence of myelination: Developmental function and beyond	179
1.2 Do prenodes determine where myelination takes place?	180
2.1 Prenodal assembly requires extrinsic and intrinsic factors	181
2.1.1 What is the nature of the oligodendrocyte secreted factor(s)?	182
2.1.2 The action of the oligodendrocyte secreted factor(s)	183
2.2 The role of ankyrinG	185
2.3 The transition of ion channels at prenodes	186
3.1 The roles of prenodes in action potential conduction	189
3.1.2 Would conduction speed increase when myelination occurs and do prenodes permit saltatory conduction?	191
3.1.3 Prenodes in the pathological state	193
Conclusion.....	197
References.....	199
Summary	237

Table of Figures

Figure 1: Ultrastructure and overview of myelinated domains.....	19
Figure 2: Oligodendrocyte lineage and myelination.....	25
Figure 3: Louis-Antoine and his drawings of the “ <i>étranglements annulaires</i> ”	27
Figure 4: Ultrastructure of the nodes of Ranvier	31
Figure 5: Overview of the molecular architecture of the CNS and PNS excitable domains and perinodal domains	34
Figure 6: Structure and distribution of mammalian voltage-gated sodium channel α -subunits	36
Figure 7: Immunolocalization of Nav subunits at the AIS and nodes of Ranvier	39
Figure 8: Structure, expression, and localization of voltage-gated potassium channels.....	44
Figure 9: General Structure of L1-CAMs.....	49
Figure 10: Neurofascin isoforms.....	49
Figure 11: Neurofascin186 at the AIS and nodes of Ranvier	52
Figure 12: Paranodal localization of Nfasc155 in the PNS and CNS.....	54
Figure 13: Expression of contactin in the CNS and PNS.....	58
Figure 14: Expression of TAG-1, and loss of TAG-1 results in aberrant K _v 1 localization	58
Figure 15: Caspr is a molecular marker for paranodal junction formation.....	61
Figure 16: Expression of Caspr2 and the juxtaparanodes	63
Figure 17: General structure of the spectrin family of scaffolding proteins	65
Figure 18: General structure of the ankyrin family of scaffolding proteins	65
Figure 19: Immunolocalization of spectrin scaffolding proteins at excitable and perinodal domains.....	67
Figure 20: AnkyrinG maintains AIS components	69
Figure 21: AnkyrinG is a nodal and paranodal component.	69
Figure 22: Gliomedin structure, cleavage sites, and immunolocalization in the PNS	74

Figure 23: Summary of the molecular architecture of CNS and PNS excitable domains and perinodal domains	79
Figure 24: Action potential conduction along unmyelinated axons	83
Figure 25: Action potential conduction along myelinated axons	87
Figure 26: Conduction is altered when the paranodes and nodes of Ranvier are disturbed.....	91
Figure 26: Changes in nodal architecture during demyelination.....	96
Figure 27: Heminodal clustering mechanism in the PNS	102
Figure 28: Role of paranodal junctions in forming PNS nodes of Ranvier.....	105
Figure 29: Role of paranodal junctions in forming CNS nodes of Ranvier	108
Figure 30: Oligodendrocyte secreted factors induces node-like clustering in the CNS.....	112
Figure 31: Cre-lox systems utilized to study the roles of ankyrinG in CNS nodes of Ranvier assembly.....	118
Figure 32: Overview of the trafficking pathways axonal proteins to be delivered to specific axonal domains	121
Figure 33: Neurofascin186 is selectively retained at PNS nodes of Ranvier.....	124
Figure 34: Transition from Na _v 1.2 to Na _v 1.6 in the developing optic nerve	126
Figure 35: Summary of the assembly mechanisms governing prenode formation and the functional role of nodal clusters prior to myelination	195

Abbreviations

2',3'-cyclic-nucleotide 3'phosphodiesterase:	CNPase
A disintegrin and metalloproteinase:	ADAM
Action potential:	AP
Adenomatous polyposis coli:	APC
Adenosine triphosphate:	ATP
Ankyrin-binding domain:	ABD
Axon initial segment:	AIS
Brain-specific hyaluronan-binding link protein:	Bral1
Calmodulin kinase II:	CaMKII
Casein kinase 2	CK2
Cell adhesion molecule:	CAM
Central nervous system:	CNS
Cerebroside sulfotransferase:	CST
Chondroitin sulfate proteoglycans:	CSPG
Close homolog of L1:	CHL-1
Contactin associated protein:	Caspr
Days <i>in vitro</i> :	DIV
Dorsal root ganglion:	DRG
Extracellular matrix:	ECM
Ezrin/Radixin/Moesin:	ERM
Fibronectin type III:	FNIII
Galactocerebroside:	GalC
Galactosyltransferase:	CGT
Gamma-aminobutyric acid:	GABA

Glutamate decarboxylase:	GAD
Glycophorin, Neurexin IV, Paranodin:	GNP
Glycosylphosphatidylinositol:	GPI
Green fluorescent protein:	GFP
Heparin sulfate proteoglycan:	HSPG
Human influenza hemagglutinin:	HA
Immunoglobulin:	Ig
IQ Motif Containing J-Schwannomin Interacting Protein 1:	IQCJ-SCHIP-1
Kinesin-like protein	KIF
Membrane associated guanylate kinase:	MAGUK
micro RNA:	miRNA
Microtubule-associated protein 2:	MAP2
Multiple sclerosis:	MS
Myelin basic protein:	MBP
Myelin-associated glycoprotein:	MAG
Neural/glial antigen 2:	NG2
Neurofascin:	Nfasc
Neuron conditioned medium:	NCM
Neuron-glia CAM related:	NrCAM
Oligodendrocyte	OL
Oligodendrocyte conditioned medium:	OCM
Oligodendrocyte precursor cell:	OPC
Peripheral nervous system:	PNS
Platelet derived growth factor receptor alpha:	PDGF-alpha
Proline, alanine, threonine:	PAT
Proteolipid protein:	PLP
PSD-95/disc large/zonula occludens-1:	PDZ

Retinal ganglion cell:	RGC
Short Hairpin RNA:	shRNA
Transient axonal glycoprotein-1:	TAG-1
Vesicular glutamate transporter:	VGAT
Voltage-gated potassium channel:	K _v
Voltage-gated sodium channel:	Na _v

Part I: Introduction

Chapter I: The Myelinated Nerve

1.1 Historical Perspective of the Nerve Fiber

In the early 19th century, the first drawings of the nervous cell came to light through the observations of the German anatomist Gabriel Gustav Valentin (1810-1863). Before this time, microscope instrumentation and histological tools were too crude to detail the fine structure of nervous system cells; however, it was through the very development of the achromatic lens in compound microscopes coupled with improvements in histological tools that the drawings of Valentin and those of his contemporaries saw the light of day. Great improvement of Valentin's work was followed by beautifully detailed studies in the cerebellum from the Czech anatomist Jan Evangelista Purkinje (1787-1869). In his observations, he described tear-like shapes in rows with short processes emanating towards the outside grey matter surface, which we now call the Purkinje cell.

Another pioneering anatomist during this time, Robert Remak (1815-1865), first described, unintentionally, the axon. He observed, nearly at the same time by the German physiologist Theodor Schwann (1810-1882), that there were fibers that were myelinated and those that were unmyelinated, which he called "Remak bands" and "Remak fibers", respectively. However, it was not until 27 years later that drawings by the young German neuroanatomist Otto Friedrich Karl Deiters (1834-1863) would produce the clearest observations yet of the nervous cell. With the help of better microscopes and better histological techniques, he was able to describe branches radiating from the cellular soma and a long cylindrical process emanating from the cell body. What Deiters referred to as "protoplasmic processes" and "axis cylinder" were renamed in 1889 by Wilhelm His (1831-1904) to be "dendrites", and by Rudolph Albert von Kölliker (1817-1905) as the "axon". Furthermore, he was able to characterize a portion of the axon proximal to the cell body, which we now

describe as the axon initial segment (AIS). In between the time of renaming the neurite processes, the German anatomist Heinrich Wilhelm von Waldeyer (1836-1921) also put a name to the nerve cell itself, which he labeled as the “neuron”.

On the myelinating glia front, studies in the mid 1800’s by the German pathologist Rudolf Virchow (1821-1902) advanced the original work of his predecessors Remak and Schwann. At this time, he described a sheath around axons and labeled it, although misnamed, “myelin” since it resembled bone marrow, and “myelos” is Greek for “marrow”. It was not until 1871 with the work of Louis-Antoine Ranvier (1835-1922) that we would redefine the Remak bands as a specific myelinating cells in the peripheral nervous system as Schwann cells, and later on in 1878 the gaps in between the myelinating segments as nodes of Ranvier.

The next significant progress for neurons occurred with the development of a new stain by the Italian physician Camillo Golgi (1843-1926). This stain, which bears his name as the Golgi stain, was able to specifically impregnate neurons, and further improved the ability of anatomists to follow the trajectories of the neurite processes. Following this useful new technique, a convergence of ideas from some of the greatest European scientists took place to conceptualize the cellular basis of the nervous system. One school of thought called the reticular theory, led by Golgi, suggested that nerve cells were so densely packed together there could not be a possible way of transmission between nervous cells. Thusly, he argued, nervous tissue must be continuous.

The other school, advanced by the prodigious Spanish histologist Santiago Ramón y Cajal (1852-1934), stated that the neuron is the basic cellular and functional unit of the nervous system. This concept, which we currently hold today, would later take shape to be called the “Neuron Doctrine”. Ramón y Cajal came to this conclusion based on an improved Golgi staining technique, which allowed him to visualize more closely the fine structures of axonal projections and dendritic arborizations. He observed that axon terminals were located in the regions of dendritic arbors, and therefore this suggested to him that there was directionality in the flow of information from the cell body, down the axon, and into the dendrite.

These key anatomical observations led to the law of dynamic polarization, and in 1906, together with Golgi, a Nobel Prize in Medicine and Physiology.

It was not until the work of Cajal's Spanish colleague Pio del Rio Hortega (1882-1945), along with the help of the Canadian neurosurgeon Wilder Penfield (1891-1976), that the myelinating cells of the central nervous system would be visualized. Utilizing a new staining method, Hortega was able to describe in 1921 cells called "oligodendrocytes", which are derived from the Greek words "oligo" meaning "few", "dendro" meaning tree, and "cyte" meaning cell. Yet, Hortega was unable to come up with a functional role for these cells.

Further developments, such as electron microscopy and electrophysiological techniques, in the mid 20th century allowed us to understand the intimate relationship between myelinating glia and the axon, and the functional proprieties of the neuron. Electron microscopy work by Richard and Mary Bunge allowed for visualization of the interaction between myelinating glia and the axon. Important electrophysiological work detailed the presence of voltage-gated ion channels along the neuronal membrane, and provided further information regarding the location of axon potential initiation and direction of electrical conduction (further discussed in chapter II).

Today, we now know that the myelinated fiber is indeed a highly specialized structure comprised of several subspecialized domains with important functions. The AIS is responsible for initiation of the electrical nervous signal called the action potential (AP) (Palmer and Stuart, 2006; Khaliq and Raman, 2006; Meeks and Mennerick, 2007; Shu *et al.*, 2007; Hu *et al.*, 2009; Popovic *et al.*, 2011) and maintenance of neuronal polarity (Hedstrom *et al.*, 2008; Sobotzki *et al.*, 2009; Galiano *et al.*, 2012), while nodes of Ranvier, together with the myelin sheath, are important for rapidly and efficiently propagating that signal down the nervous fiber (Poliak and Peles, 2003; Salzer, 2003; Sherman and Brophy, 2005).

1.2 Structure and molecular composition of myelinated nerve fibers

1.2.1 The myelin sheath

One of the last evolutionary steps of the vertebrate nervous system was myelination of axons by glial cells nearly 420 million years before present in jawed fish (Zalc *et al.*, 2008). The myelin sheath is a lipid rich multilamellar structure that wraps around axonal membranes. Originally described by Rudolf Virchow (1821-1902) in 1854 as a substance produced by neurons, we now know that myelin is produced in the central nervous system (CNS) and peripheral nervous system (PNS) by oligodendrocytes and Schwann cells, respectively. Oligodendrocytes are able to envelop several axons simultaneously, while Schwann cells wrap individually around one axon (for review see Sherman and Brophy, 2005).

The myelin sheath provides numerous functional benefits to the neuron. Firstly, one important specialized function of myelin is to provide vertebrates with a means to greatly increase neural conduction along axons through electrical insulation. The compacted myelin sheath allows vertebrate axons to conduct action potentials in the order of 50 to 100 times in magnitude faster than that of the non-myelinated invertebrate axon (Zalc and Colman, 2008). Indeed, this insulating function of myelinating glia has major implications, and will be revisited in chapter II.

Another important function of myelinating glia is that they provide trophic support to neurons. Since glial cells cover large portions of the axonal surface with myelin, the axonal surface has a very limited area only in the breaks between myelinating segments where it is able to interact with extracellular metabolites (Nave *et al.*, 2010). Recent reports have made strides in uncovering the trophic support roles of myelinating glia (Funfschilling *et al.*, 2012; Lee *et al.*, 2012). Funfschilling *et al.* (2012) reported that oligodendrocytes are able to provide nutritional support to neurons via lactate transport, suggesting that myelinating glia impart an important role in meeting the metabolic demands of the neuron.

Finally, myelin also provides a protective covering around axons. In conditions where myelin destruction occurs, called demyelination, neurons are vulnerable to axonal damage. This further damage to the axon could be the result of lymphocytes or related cytokine-induced cytotoxicity or dysfunction of axonal ion channel homeostasis, which in turn leads to neurodegeneration (Friesse *et al.*, 2014).

1.2.1.1 Myelinated Regions and Structure

Several experimental advances, particularly those in electron microscopy, have advanced our knowledge of myelin structure. PNS Schwann cells and CNS oligodendrocytes wrap extensive spirally myelinating sheaths around axons that eventually become thinner through compaction (Fig. 1A). Compacted alternating double membrane leaflets of membrane with a periodicity of 12 nm that are electron-dense and electron-light are resolved through electron microscopy (Aggarwal *et al.*, 2011). The thicker electron-dense region resulting from the apposition of two internal faces of the lipid bilayer is called the major dense line, while the thinner electron-dense layer resulting from the apposition of two external myelin wraps is the intraperiod line.

Specific regions along the internal myelinating segment, called the internode, remain uncompacted. In the PNS, Schmidt-Lanterman incisures are small regions of cytoplasm that remain during the Schwann cell myelination process. These regions are important because they allow for communication and exchange of metabolites between the superficial and deep layers of myelin with the Schwann cell cytoplasm. Additionally, an uncompacted portion at the extremity of each myelin lamellae, called a paranodal loop (Fig. 1B), in both CNS and PNS myelinating segments organize to form the paranode (Fig. 1C; Aggarwal *et al.*, 2011).

Important to note is that the compacted myelin sheath and the internodal region of the axon are separated by a periaxonal space—but by looking at a longitudinal cross section near the edges of a myelinated segment, we observe that

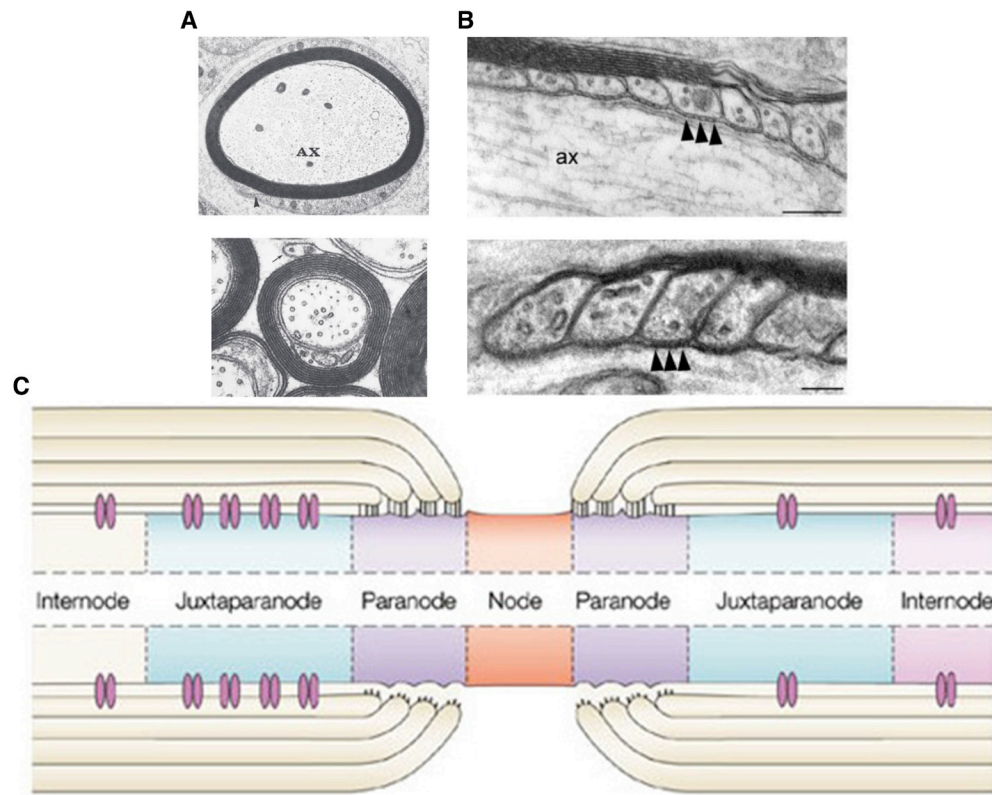


Figure 1: Ultrastructure and overview of myelinated domains. **(A)** Cross section of a myelinated PNS axon (ax) in the top panel and a cross section of a myelinated CNS axon in the lower panel. Adapted from Quarles *et al.*, 2006. **(B)** Ultrastructure of the paranodal junctions formed between the paranodal loops and the axon in both panels with a higher magnification observed in the lower panel. Of note are the septate-like junctions denoted by the black arrowheads. Adapted from Schaeren-Wiemers *et al.* 2004. **(C)** Overview of the myelinated domains along a CNS axon. The domains are similar in the PNS. Adapted from Poliak and Peles, 2003.

septate-like junctions form at paranodes between the cytoplasmic filled paranodal loops of the myelinating glial cell membrane and axolemma (Fig. 1B). While the paranodal junctions provide an efficient restriction barrier between the voltage-gated sodium channels at nodes of Ranvier and the voltage-gated potassium channels at the juxtaparanodes, these junctions are permeable to small metabolites and ions (Mierzwa *et al.*, 2010). As we will discuss later, there are a number of cell adhesion molecules (CAMs) located at the paranodal junctions that are implicated in both the formation and maintenance of the macromolecular complex at the nodes of Ranvier.

The section separating the paranode and the internode is the juxtaparanode (Fig. 1C). This region is well defined as a passively excitable region enriched in voltage-gated potassium channels and various CAMs. Further description of these protein classes will be reserved for the section on molecular composition of excitable and axo-glial domains.

1.2.1.2 Myelin Composition

The composition of myelin is unique in that it is a poorly hydrated structure (40% water) that is more enriched in lipids than proteins. Indeed, the dry weight of myelin is between 70-85% lipid compared to 15-35% protein, while in most other cellular membranes it is the reverse. This is not surprising though considering the insulating functions of myelin that permit rapid action potential propagation, which would favor a membrane low in water content and rich in lipids.

1.2.1.2.1 Lipid Composition

The major lipids of the myelin membrane are separated into three groups: glycolipids, cholesterol, and phospholipids. The molar ratios between the three groups of lipids range from 2:4:3 to 2:4:4 (Baumann and Pham-Dinh, 2001). Our discussion, however, will only be limited to the most typical myelin lipids: glycolipids.

Glycolipids

One group in particular, the galactolipids, dominates the glycolipid family of myelin lipids. The galactolipids galactocerebroside (GalC) and its sulfated derivative sulfatide make up nearly one-third of the total mature myelin lipid mass (Dupree *et al.*, 1998). Galactocerebroside is a lipid composed of galactose and ceramide, enzymatically linked to the first position hydroxyl group by ceramide galactosyltransferase (CGT), while sulfatide is formed from the sulfation of galactocerebroside via the enzyme cerebroside sulfotransferase (CST; Morell and Radin, 1969).

The galactolipids have been intensely studied due to their abundance and early expression in oligodendroglia. Utilizing *CGT*-null mice (therefore lacking galactocerebroside and sulfatide), several studies have shown that these mice have abnormal myelin ultrastructure, breakdown of the paranodal junctions, and reduction in axonal conduction velocity (Basio *et al.*, 1996; Coetzee *et al.*, 1996; Dupree *et al.*, 1998). Looking more closely at the roles of sulfatide, Pfeiffer and colleagues reported through immunological perturbations that sulfatide has been found to be a key molecule for oligodendrocyte development (Bansal *et al.*, 1988, 1989; Bansal and Pfeiffer, 1989) and it is seen to play a role in the enhanced rate of differentiation in cultured oligodendrocytes (Bansal *et al.* 1999). Since the studies utilizing *CGT* mutants could not differentiate the functions between galactocerebroside and sulfatide, a *CST*-deficient mouse was developed. Using this mouse, Honke *et al.* (2002) and Marcus *et al.* (2006) reported that sulfatide was necessary for proper paranodal junctions structure and maintenance. Together, these results suggest that sulfatide is an important regulatory molecule in OL development and in maintaining myelin structure.

1.2.1.2.2 Protein Composition

As stated earlier, proteins comprise a lower fraction of mature myelin dry weight; however, they are important because they are specific for myelin and glial

cells. In this context, the protein composition of oligodendrocyte myelin is mainly comprised of myelin basic protein (MBP) and proteolipid protein (PLP), while Schwann cell myelin is primarily composed of P₀ and peripheral myelin protein 22.

While there are large variety of myelin proteins, the following section will be dedicated to four specific proteins: proteolipid protein (PLP), myelin basic protein (MBP), 2',3'-cyclic-nucleotide 3'phosphodiesterase (CNPase), and myelin-associated glycoprotein (MAG). Other myelin protein components that are involved in axo-glial junction formation will be described in the section on molecular composition of excitable and axo-glial domains.

Proteolipid proteins (PLP and DM-20)

The largest proteinaceous component of CNS myelin is PLP. PLP is a low molecular weight glycoprotein with four hydrophobic alpha helical transmembrane segments, and both C- and N- termini localize at the intraperiodic lines of myelin (Baumann and Pham-Dinh, 2001). The mRNA can go through alternative splicing and gives rise to another isoform called DM-20. PLP is normally expressed in mature oligodendrocytes, but the DM-20 isoform has been observed to be expressed in a subpopulation of OPCs (Spassky *et al.*, 2001). Through genetic ablation studies of the *PLP* gene, PLP and DM-20 do not appear to be necessary for either myelination or myelin compaction (Klugmann *et al.*, 1997). However, these mutant lines show reduction in the physical stability of myelin, suggesting that PLP/DM-20 play a role in stabilizing the myelin membrane (Boison *et al.*, 1995). Further studies also suggest that PLP/DM-20 play a role in neuronal integrity since in both mice and patients that lack PLP, axonal swellings and ultimately axonal degeneration occur (Griffiths *et al.*, 1998; Garbern *et al.*, 2002).

Myelin Basic Protein (MBP)

MBP, which constitutes 30% of protein, rounds out the second largest component of CNS myelin proteins. MBP has several isoforms through alternative transcription and can also go through alternative splicing, thus creating a large

MBP protein family (Baumann and Pham-Dinh, 2001). MBP is located in the cytoplasmic region of the major dense line of compact myelin, and its localization to these regions is important since the MBP-deficient *shiverer* mouse display hypomyelination and absence of the major dense line in CNS myelin (Privat *et al.*, 1979).

2',3'-cyclic-nucleotide 3'phosphodiesterase (CNPase)

CNPase constitutes 4% of the myelin proteins in the CNS. *In vitro*, CNPase has been observed to hydrolyze 2', 3'-cyclic nucleotides, an artificial substrate that does not exist in nature since in living species nucleotides are cyclized in 3'-5'. The expression of CNPase is notably absent from compact myelin, but it is expressed in the cytoplasmic cell membrane of oligodendrocytes and in the paranodal regions of the myelinated sheath. Functions of CNPase remain elusive; however, oligodendrocytes overexpressing CNPase have aberrant myelin sheaths (Gravel *et al.*, 1996), and loss of CNPase has been shown to affect paranodal junctions (Rasband *et al.*, 2005) and axonal integrity without any obvious effect on myelination (Lappe-Siefke *et al.*, 2003).

Myelin-Associated Glycoprotein (MAG)

At around 1%, MAG represents a relatively small fraction of the protein content found in CNS myelin. MAG is a transmembrane protein that contains a large extracellular domain with five segments of internal homology that resemble immunoglobulin domains (Salzer *et al.*, 1987). In the CNS, MAG is enriched in the periaxonal domains of myelinating oligodendrocytes. Myelin appears to be normal in MAG-deficient mice; yet, MAG mutant mice have a slight delay in myelin compaction (Montag *et al.*, 1994).

1.2.1.3 Oligodendrocyte differentiation and myelination

The differentiation of migrating and proliferating oligodendrocyte precursor cells (OPC) to myelinating oligodendrocytes (OL) can be defined

morphologically and through expression of specific antigenic markers that are either kept or lost throughout its lineage. Through the sequential expression of these biochemical markers, the oligodendroglial differentiation process is categorically subdivided into six defining stages: Oligodendrocyte progenitor, oligodendrocyte precursor cell (OPC), pre-oligodendrocyte, immature oligodendrocyte, non-myelinating mature oligodendrocyte, and myelinating oligodendrocyte (Fig. 2A).

Both *in vitro* and *in vivo*, early OPCs are morphologically defined by their bipolar shape and are further defined by their surface expression of PDGFR α (platelet derived growth factor receptor alpha; Pringle and Richardson, 1993), the chondroitin sulfate proteoglycan NG2 (neural/glial antigen 2; Nishiyama *et al.*, 1999), and the ganglioside A2B5 (Raff *et al.*, 1983). At this stage OPCs are highly proliferative and migratory. OPCs then progress into the pre-OL stage where they are morphologically defined by their multiple processes and surface expression of O4 (sulfatide; Bansal and Pfeiffer, 1989). The pre-OLs are less migratory, but remain proliferative at this stage since they are receptive to the mitogenic properties of PDGF (Barres *et al.*, 1992, 1993). Once losing their proliferative capacities, the pre-OLs transition into the highly branched immature OLs. The immature OLs begin to express new markers such as O1 (GalC), CNP (Zalc *et al.*, 1981), and the tumor suppressor protein APC (adenomatous polyposis coli; Bhat *et al.*, 1996). The maturation process of the immature OL then continues over the next days (3-5) where they become further arborized and begin to express specific myelin proteins such as PLP, MAG, and MBP (Martini and Schachner, 1986). The stage of the non-myelinating OL then begins, defined by their flat sheets of myelin membrane and establishment of axonal contacts. The final step is transitioning into myelinating OLs that wrap axonal processes and express the molecular marker MOG (Solly *et al.*, 1996).

Once oligodendrocytes reach a mature state, they begin to myelinate several axons. Surprisingly, this process occurs very rapidly over a short period of

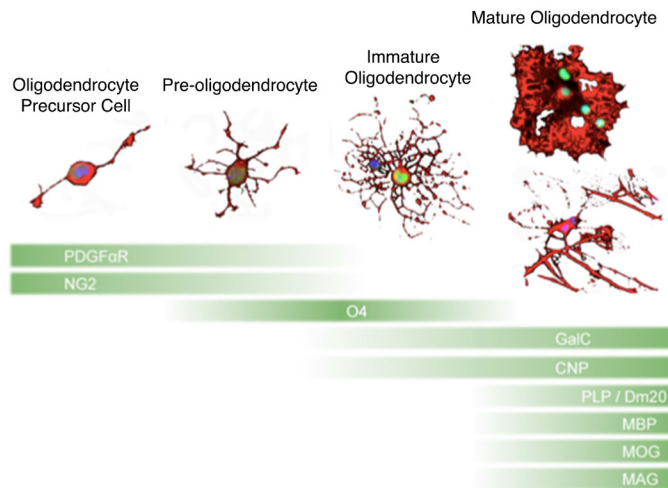
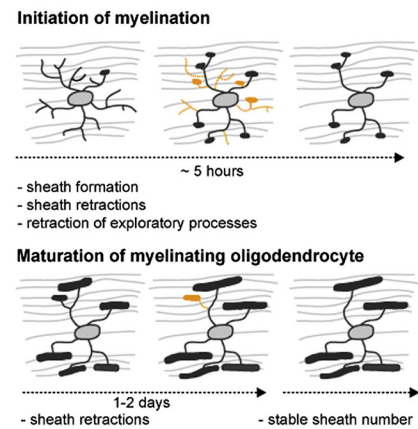
A**B**

Figure 2: Oligodendrocyte lineage and myelination. **(A)** Oligodendrocytes express several markers that define their lineage from an oligodendrocyte precursor to a myelinating oligodendrocyte. Adapted from Dr. Sarah Moyon. **(B)** Oligodendrocytes have a finite window in which that must initiate the myelination process. This is followed by retraction of some myelin sheaths and stabilization of the number of myelinated segments. Adapted from Czopka *et al.*, 2013.

time (Fig. 2B, Watkins *et al.*, 2008; Czopka *et al.*, 2013). In fact, it is in the order of several hours (Czopka *et al.*, 2013). Utilizing the zebrafish (*Danio rerio*) model system, Czopka *et al.* (2013) demonstrated that oligodendrocytes produce new myelin sheaths in a time window of around five hours, and afterwards oligodendrocytes change their behavior by stopping the production of new sheaths (Fig. 2B). Changes following this window are retractions of very few myelinated sheaths for about 1 to 2 days (Czopka *et al.*, 2013). These results suggest that the time window for myelin production is an intrinsic feature to the oligodendrocyte.

1.2.2 The Nodes of Ranvier (Nodes)

The first studies laying the foundation for nodes of Ranvier began with Louis-Antoine Ranvier's histological work in 1871. While working alongside Claude Bernard at Collège de France, Ranvier embraced Bernard's approach in cellular nutrition. In Ranvier's view, the impermeability of the myelin sheath prevented the exchange of nutrient materials between the nerve fiber and oxygenated blood, and therefore begged the question: How does nutritional exchange between the myelinated nerve and the blood occur? To Ranvier, it was through the short non-myelinated regions between myelinating sheaths called "*étranglements annulaires*".

Meticulously detailed in one of his first pioneering histological manuals entitled, "*Leçons sur l'histologie du système nerveux*" (Ranvier, 1878), Ranvier showed that an aqueous solution of ammonium picrocarminate was able to first enter through discrete regions along rabbit sciatic nerves, which he called "*étranglements annulaires*" (or "annular constrictions"), and then diffused along the nerve fiber. Additionally, by using rat thoracic nerves stained with reduced sodium nitrate solution, Ranvier then further observed what he described as "small black crosses" located at the same regions as the "annular constrictions" (Fig. 3B and C; Ranvier, 1878). He postulated that these regions, which now bear his name as the nodes of Ranvier, could therefore be important for nutrition of the nerve cell (Ranvier, 1878).

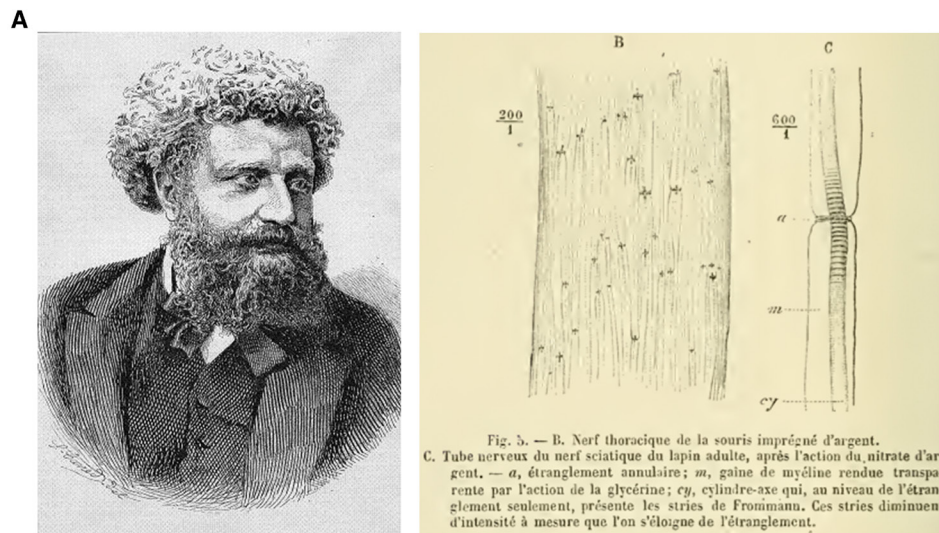


Figure 3: Louis-Antoine and his drawings of the “*étranglements annulaires*”. **(A)** Portrait of Louis-Antoine Ranvier. **(B)** and **(C)** Original drawings of sciatic nerves stained with silver nitrate by Ranvier’s talented artist, M. Karmanski. Adapted from Ranvier, 1878.

However, it was not until Ranvier's later work on nerve degeneration where he interpreted their true main role in nerve conduction. Utilizing a living rabbit with both sciatic nerves denuded, he exposed one nerve to pure water at 56°C and the other with 1 to 200 concentration of salt water at the same temperature (Ranvier, 1878). He observed that in the nerve exposed to pure water, the myelin sheath swelled and the nodes of Ranvier disappeared, resulting in a loss of nerve function by either mechanical or electrical stimulation after 20 minutes. While he still observed similar histological changes to the nerve exposed salt water, the nerve was still excitable through mechanical or electrical stimulation after five hours, thus suggesting to Ranvier that the nodes of Ranvier may be implicated in nerve conduction (Ranvier, 1878; Barbara, 2007).

1.2.2.1 Nodal Ultrastructure

As mentioned previously in the introductory portion of this section, Ranvier's description of the nodes of Ranvier was made through various chemical staining procedures, but the continual development of electron microscopy and the freeze-fracture technique have further allowed us to look more closely at both the ultrastructure of the nodal axolemma and its external axoplasm. Because the PNS and CNS nodes of Ranvier vary slightly in their overall ultrastructural architectures, the first section will highlight the similarities shared between the two nervous systems, and the second will discuss their dissimilarities, in particular at the extranodal space, in order to provide further clarity on their ultrastructural differences.

The Similarities in Nodal Ultrastructure

Typically, the size of the node of Ranvier itself ranges between 1.0-2.0 μm (Salzer, 2003). The axonal diameter at the nodes of Ranvier is reduced in size by around one half compared to the internode, but the nodal axonal caliber is slightly larger than that of the paranodal region (Landon and Williams, 1963). As the quantity of neurofilament and axonal caliber are proportionally related (Friede and

Samorajski, 1970), this size difference mainly demonstrates the reduction in the mean number of neurofilaments found at the node of Ranvier, and also the reduced post-translational phosphorylation of lysine-serine-proline repeats that occurs extensively along the neurofilament chain (Pannese, 2015; Salzer, 2003). However, even though there are fewer neurofilaments, their number per unit area of axoplasm at both the nodes of Ranvier and internode are similar (Pannese, 2015), suggesting a higher order packing arrangement of neurofilaments at the nodes (Salzer, 2003). Interestingly, the number of microtubules increases at the node of Ranvier, and it has been furthermore observed that there are a number of fasciculated microtubules, which are notably observed at the AIS, at the proximal ends of nodes of Ranvier in sensory and motor axons in the spinal root (Nakazawa and Ishikawa, 1995). This latter result suggests that cross-linking proteins that are necessary for microtubule fasciculation are also transported to proximal nodes.

Along with the microtubule densities, there are a number of membranous organelles that are associated to the microtubule tracks, and elements of smooth endoplasmic reticulum (Pannese, 2015). Lysosomal vesicles have been observed near the nodal axolemma, where they are suggested to play a role in nodal protein turnover (Zagoren, 1984). Inversely to lysosomal vesicles, exocytotic vesicles are also observed at the node of Ranvier, and most likely play an important role for docking nodal proteins to the developing node of Ranvier (Wiley-Livingston and Ellisman, 1980). Furthermore, studies on the rhesus monkey oculomotor nucleus have also shown that there are synaptic vesicles present where nodes of Ranvier make synaptic contact with dendrites (Waxman, 1974).

Beneath and slightly separated from the nodal axolemma is an electron-dense granular cytoplasmic undercoating of around 25-35 nm that ends at the paranodal junction (Salzer, 2003). This osmiophilic layer, which is also present at the AIS, is thought to be specific to regions with excitable domains and speculated to play a role in neuronal excitability (Waxman and Quick, 1977). Additionally, as these regions are enriched in scaffolding proteins that anchor voltage-gated

channels to the actin cytoskeleton, this layer most likely corresponds to a dense cytoskeletal network of ankyrins and spectrins (Rosenbluth, 1983).

The development of the freeze fracture technique has furthered our understanding of the node of Ranvier axolemmal ultrastructure. Notably, Rosenbluth (1976) showed that a high density (in the order of $1200/\mu\text{m}^2$) of 20 nm sized intramembraneous particles were accumulated on the E-face of the nodal axolemma in frog brain (Fig. 4A). As voltage-gated ion channels and ATPases are highly enriched at the nodal axolemma in both the PNS and the CNS, it was speculated that these particles corresponded to either voltage-gated sodium channels or Na^+/K^+ -ATPases (Rosenbluth, 1976). However, in support of the former conclusion, the concentration of these large particles is significantly higher at the nodes compared to the paranodal and internodal regions (which have a relatively low concentration in Na_v channels; Rosenbluth, 1976), and that ATPases are mainly found at the P-face of the nodal axolemma. This was partially confirmed through raising antibodies against the voltage-gated sodium channel and using either binding assays or immunocytochemistry to show that Na_v is indeed enriched at the nodes (Richie and Rogart, 1977; Ellisman and Levinson, 1982; Haimovich *et al.*, 1984), and the diffuse pattern of immunolabeling of all Na^+/K^+ -ATPase subunits along myelinated axons in the PNS and CNS (McGrail *et al.*, 1991; Gerbi *et al.*, 1999).

Differences in PNS and CNS Nodal Ultrastructure

Several defining ultrastructure features of the extranodal space differentiate the PNS and the CNS. In the PNS, the Schwann cell wraps around an axon in a one to one relationship and then forms a tight collar where they eventually meet at the nodes of Ranvier. As these two domains converge, it is easy to see through longitudinal sections that invaginated finger-like projections abutting from the ends of each Schwann cell protrude into the nodal axoplasm (Fig. 4B). These cytoplasm filled projections, called Schwann cell microvilli, vary in size between 50 and 80 nm

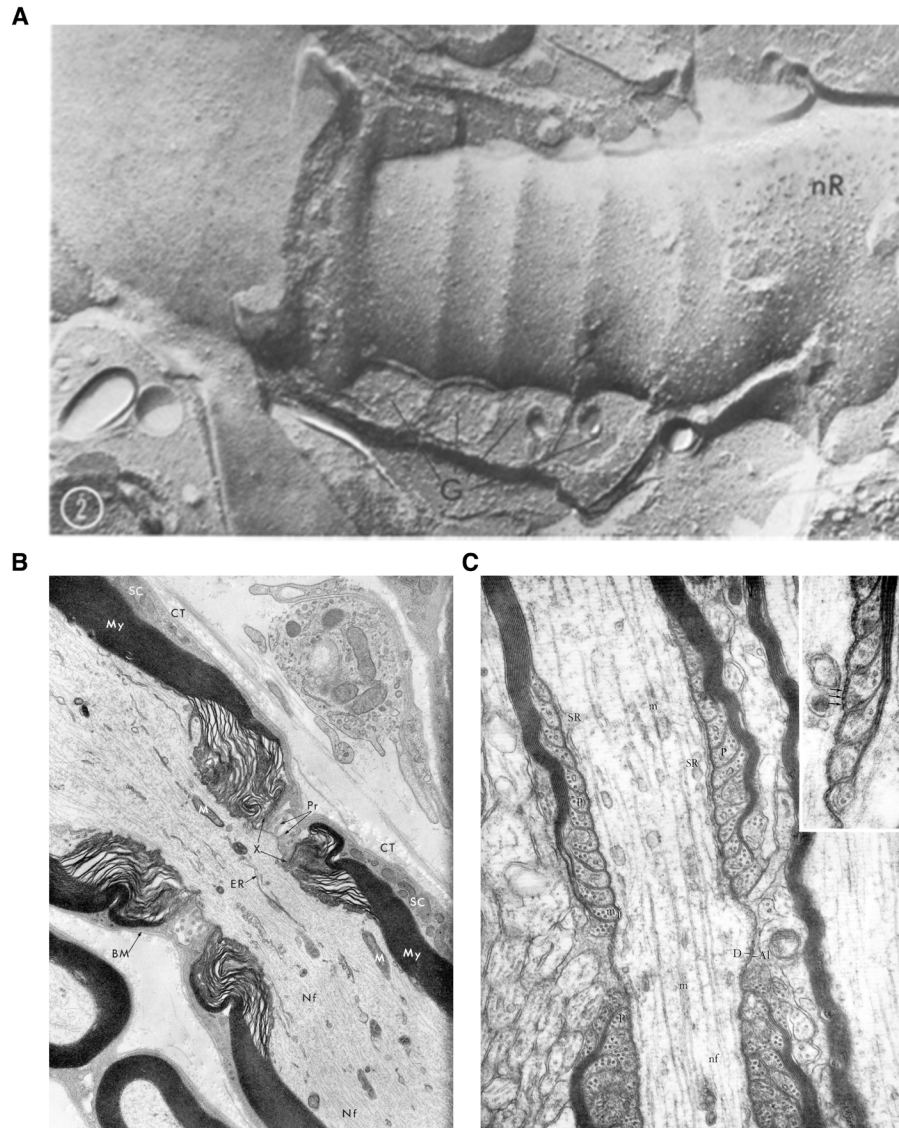


Figure 4: Ultrastructure of the nodes of Ranvier. **(A)** Freeze-fracture of frog brain axon. Nodes of Ranvier contain large densities of intramembraneous particles (nR). Glial loops are denoted by (G). Adapted from Rosenbluth, 1976. **(B)** PNS nodal ultrastructure of a mouse sciatic nerve. Connective tissue and basement membrane (BM) covers the surface of a Schwann cell (SC). Microvilli (Pr) invade the nodal region. Myelin (My) covers the axon and SC form junctions (X) with the axon. The axoplasm contains neurofilaments (Nf), mitochondria (M), and endoplasmic reticulum (ER). Adapted from Porter and Bonneville, 1973. **(C)** CNS nodal ultrastructure of rat basal ganglion. Dense coating (D) is observed at the nodes of Ranvier, which are flanked by paranodal loops (P) of the myelinating oligodendrocyte. The axoplasm contains neurofilaments (nf), mitochondria (m) and smooth endoplasmic reticulum (SR). Adapted from Peters *et al.*, 1976.

in diameter (depending on species) and contain longitudinal filaments of around 10 nm (Landon and Williams, 1963). Typically, these Schwann cell microvilli are densely packed at the extranodal space, and are separated 3-5 nm away from the nodal axolemma (Zagoren, 1984). The functional significance of Schwann cell microvilli has only until recently been elucidated, and will be further discussed in chapter III. Another ultrastructural feature of the PNS node is a basal lamina consisting of proteoglycans that extends continuously along the axonal fiber (Landon and Hall, 1976). Importantly, this basal lamina does not impede the movement of ions across the nodal axolemma (Landon and Hall, 1976). Furthermore, between the basal lamina and the nodal axolemma is a filamentous matrix. Both this material and the basal lamina have been thought to play a role in buffering ions and acting as a cation reservoir (Landon and Langley, 1971). Indeed, there is an abundance of aggregated heparin sulfate proteoglycans (HSPGs) at the PNS nodes of Ranvier, and their identification and respective roles will be discussed later in the molecular composition of the AIS, nodes of Ranvier and outerlying domains.

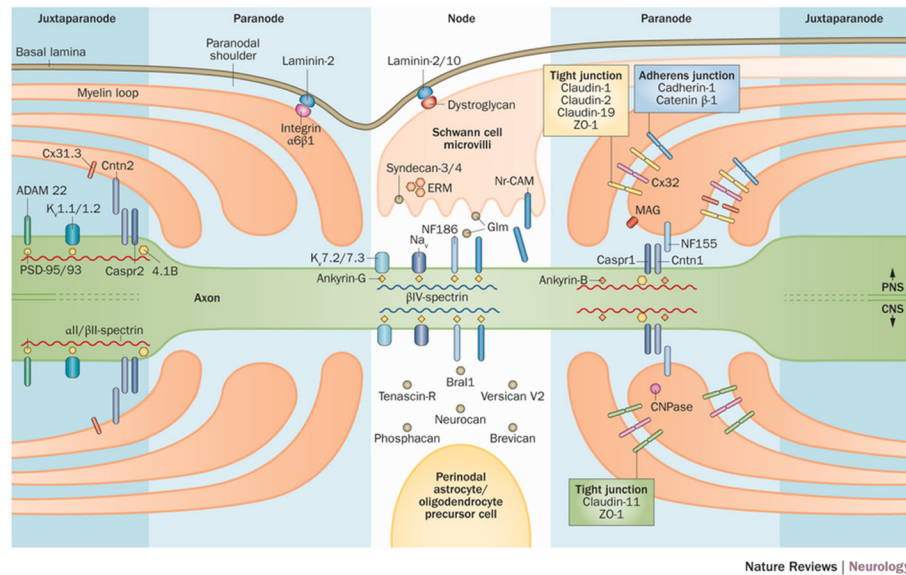
Clearly differentiating CNS nodes from PNS nodes are the evident lack of Schwann cell microvilli and a basal lamina (Fig. 4C). The perinodal junctions between the axon oligodendroglial myelin wraps do not give rise to microvilli. Instead, occasionally replacing the microvillar processes are perinodal astrocytes (or otherwise called synantocytes; Butt *et al.*, 2002), which have been shown through immunogold labeling to contact the nodes of Ranvier in rat optic nerve (Ffrench-Constant *et al.*, 1986) and by confocal microscopy in the anterior medullary velum (Butt *et al.*, 2002). Furthermore, the lack of basal lamina exposes CNS nodes to the extracellular space that is also occupied by a filamentous extracellular-matrix (ECM).

In further discussing the ultrastructural differences between the PNS and CNS nodes, it is worth revisiting the subject of organelles. A more debated subject regarding organelles is the presence and enrichment of mitochondria between the two nervous system nodes of Ranvier. Early studies have demonstrated that there

are mitochondria located at PNS nodes (Berthold, 1978; Fabricius *et al.*, 1993), and more recently it has been shown that the density of mitochondria at PNS nodes and paranodes is greater than the internodal region (Perkins and Ellisman, 2011). On the other hand, in the CNS, it has been described that there are either similar densities of mitochondria in the nodal, paranodal and internodal area (Edgar *et al.*, 2008), or there is a notable absence of mitochondria at the nodes altogether (Edgar *et al.*, 2008; Kidd *et al.*, 2011; Ohno *et al.*, 2011). These differences may point to two different possibilities: 1.) The motility of these organelles—large mitochondria remain stationary at points of high-energy consumption such as paranodal regions enriched in K_v channels and Na^+/K^+ ATPases, while small motile mitochondria freely move through the axon to regions where they may be needed. 2.) An interesting hypothesis outlined in Zhang *et al.* (2010), and in relation to the aforementioned possibility, suggests that the differences in mitochondrial localization in the PNS and CNS is related to differential Ca^{2+} signaling along axons. CNS axons display spatially uniform Ca^{2+} signaling, while in the PNS it is localized to the nodes of Ranvier, and in turn, recruits mitochondria to the nodal region (Zhang *et al.*, 2010). Nevertheless, as most of these studies were done through immunofluorescence/electron microscopy or short time-lapse imaging, the conclusions inferred from these studies may therefore only represent a “snap-shot” of the true distribution of these mobile organelles. This question may be partially resolved by looking at the distribution of mitochondria during developmental formation of PNS and CNS nodes through long time-lapse imaging.

1.3 Molecular Composition of Excitable and Axo-Glial Domains

Through the use of various biochemical tools, our understanding of the molecular composition of the excitable domains has expanded from just that of the voltage-gated ion channel. There exists a large repertoire of cell-adhesion molecules, cytoskeletal scaffolding proteins, and extracellular matrix proteins at the AIS, the nodes, and their surrounding regions (see Fig. 5 for a general overview). As these varying protein classes are located at multiple regions along the axon, this section

A

Nature Reviews | Neurology

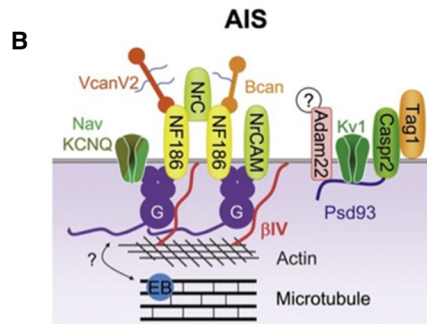


Figure 5: Overview of the molecular architecture of the CNS and PNS excitable domains and perinodal domains. **(A)** Detailed schematic of PNS and CNS nodes of Ranvier. From Stathopoulos *et al.*, 2015. **(B)** Detailed schematic of the axon initial segment (AIS). Adapted from Chang and Rasband, 2013.

will take an in depth look at each of these protein classes and detail their distribution at the AIS, and PNS and CNS nodes of Ranvier, paranodes and juxtaparanodes. Furthermore, where permitted, the roles of certain molecules with respect to the AIS, juxtaparanodal, and paranodal assembly or maintenance will be described. The main roles of paranodal, ECM, and nodal components in the assembly of PNS and CNS nodes of Ranvier will be reserved for chapter III.

1.3.1 Voltage-Gated Ion Channels

The first experimental studies detailing the presence of voltage-gated ion channels came in the 1930s by John Z. Young (1907-1997) on the squid axon. Later seminal work by Hodgkin (1914-1998), Huxley (1917-2012) and Katz (1911-2003) in the 1950s and Hille in the 1960s detailed a movement of sodium and potassium ions through axonal pores, affirming the presence of voltage-gated ion channels in nervous cells. Since then, a tremendous amount of effort has gone into elucidating the different voltage-gated ion channels, their subtypes, and their temporal and spatial distributions in the nervous system. At both the AIS and at nodes of Ranvier, the expression of both voltage-gated sodium (Na_v) and potassium (K_v) channels has been observed. At these regions, Na_v channels play an essential role in action potential initiation and propagation, while K_v channels function to modulate action potential initiation and alter axonal conduction. Interestingly, a subset of K_v channels is restricted to the juxtaparanodal region where they regulate the internodal resting membrane potential. This section will outline the different ion channel subtypes, their subunits, and their temporal and spatial distribution at the AIS, CNS and PNS nodes of Ranvier, and juxtaparanodes.

1.3.1.1 Voltage-Gated Sodium Channels (Na_v)

Alpha subunits

The *SCNA* family encodes for ten different sodium channel α -subunit isoforms (Fig. 6B). Structurally, the α -subunit forms a pore containing four homologous domains (I-IV), each consisting of six transmembrane α -helical segments (S1-S6), that are connected through inner pore loops from S6 to S1 (Fig.

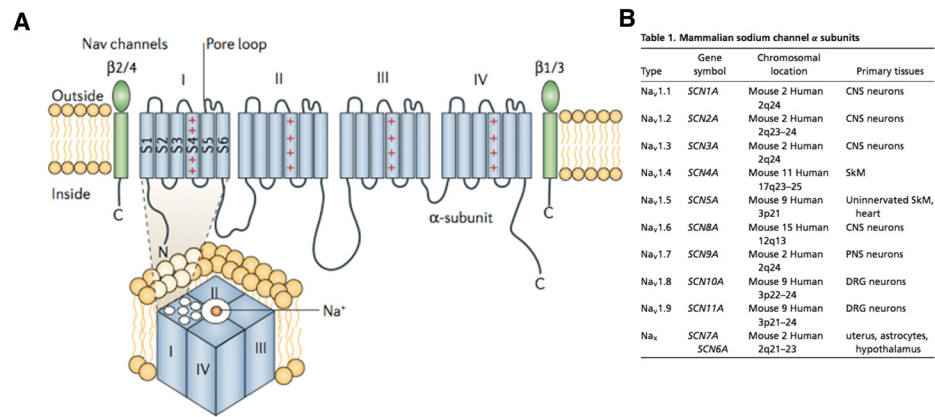


Figure 6: Structure and distribution of mammalian voltage-gated sodium channel α -subunits. **(A)** General structure of the voltage-gated sodium channel. Adapted from Lai and Jan, 2006. **(B)** Table of the mammalian voltage-gated sodium channel α -subunits and their distribution in various tissues. Adapted from Catterall, 2012.

6A; Catterall, 2012). The S4 segment of each homologous domain permits the activation of the α -subunit, while the intracellular loop connecting the III and IV homologous domain is responsible for inactivation of the α -subunit during sustained depolarization (Catterall, Goldin, and Waxman, 2005).

Six neurotoxin receptor sites have been found on the sodium channel α -subunit, and thereby make them sensitive to pharmacological inactivation or activation with drugs such as tetrodotoxin, α - and β -scorpiotoxin, and saxotoxin. These agents act upon various regions of the α -subunit, and some in particular act in a stoichiometric 1:1 ratio (*i.e.* saxotoxin). Using these drugs has not only given us better understanding of sodium channel function, but has also been cleverly exploited in order to isolate and uncover the expression patterns of α -subunits. By using ^{125}I -labelled scorpion toxin, Beneski and Catterall (1980) isolated 260-kDa and 30-40 kDa fragments from neuroblastoma cells. The larger fragment was later found to correspond to the α -subunit of the sodium channel, while the smaller fragment would be the β -subunit (Hartshorne and Catterall, 1984; Messner and Catterall, 1985). Together, the voltage-gated sodium channels forms a heterotrimeric complex of α - and β -subunits, wherein one α -subunit is linked to two different β -subunits (Messner and Catterall, 1985; O'Malley and Isom, 2015). A summary of the expression of the 10 different sodium channels can be found in the table in Figure 6B. Discussion will be limited to the three main sodium channel α -subunits shared between the CNS and PNS nodes of Ranvier: $\text{Na}_v1.1$, $\text{Na}_v1.2$ and $\text{Na}_v1.6$

$\text{Na}_v1.1$

$\text{Na}_v1.1$ has seen to be highly enriched at the AIS in the mammalian CNS, and at nodes of Ranvier in the rodent CNS and PNS (Fig. 7A and C; Ogiwara *et al.*, 2007; Van Wart *et al.*, 2007; Duflocq *et al.*, 2008; Lorincz and Nusser, 2008; O'Malley *et al.*, 2009; Luo *et al.*, 2014; Tian *et al.*, 2014). Primarily, enrichment of $\text{Na}_v1.1$ in the mouse spinal cord appears at P7 at the AIS and at P14 in CNS nodes of Ranvier, and gradually increases to a plateau of enrichment at both

compartments in adulthood (Duflocq *et al.*, 2008). In mouse PNS nodes of Ranvier, $\text{Na}_v1.1$ is observed to be present at P2, peaks at P5, decreases rapidly at P7, and then is absent at P21 (Luo *et al.*, 2014). In rodent adult spinal cord and retinal ganglion cells, $\text{Na}_v1.1$ is primarily enriched at the proximal region of the AIS (Fig. 7B; Van Wart *et al.*, 2007; Duflocq *et al.*, 2008; Lorincz and Nusser *et al.*, 2008); however, $\text{Na}_v1.1$ distribution is homogenous at the AISs of short axon cells of the olfactory bulb (Lorincz and Nusser *et al.*, 2008). Interestingly, $\text{Na}_v1.1$ is enriched exclusively in GABAergic interneurons at the AIS in both rodent and human cortex and at nodes in the rodent hippocampus (Ogiwara *et al.*, 2007; Lorincz and Nusser *et al.*, 2008; Tian *et al.*, 2014). Nevertheless, $\text{Na}_v1.1$ AIS and nodal enrichment has also been observed in adult mouse retinal ganglion cells and optic nerve, respectively (Van Wart *et al.*, 2007; O'Malley *et al.*, 2009).

Additionally, $\text{Na}_v1.1$ is functionally involved in action potential initiation, conduction and repetitive neuronal firing (Catterall *et al.*, 2005). Mutations or deletions of the *SCN1A* gene have furthermore been observed to play a pathophysiological role in causing generalized epilepsy with febrile seizures plus and severe myoclonic epilepsy in infants (Catterall *et al.*, 2005), in which the latter may be related to a reduction in sodium current or spike firing in GABAergic interneurons (Kalume *et al.*, 2007; Ogiwara *et al.*, 2007).

$\text{Na}_v1.2$

$\text{Na}_v1.2$ is expressed early at the immature AIS (Fig. 7A) and is preferentially accumulated in a proximal-distal gradient in mammalian AISs (Hu *et al.*, 2009, Tian *et al.*, 2014). Due to its high-threshold and preferential enrichment at the proximal AIS, $\text{Na}_v1.2$ is believed to play a functional role in action potential backpropagation towards the soma (Hu *et al.*, 2009).

Beyond the AIS, axonal expression of $\text{Na}_v1.2$ has been shown to be diffuse along rat unmyelinated hippocampal mossy fiber and Schaffer collateral tracks, and along unmyelinated zones of rat retinal ganglion cell axons (Westenbroek *et al.*,

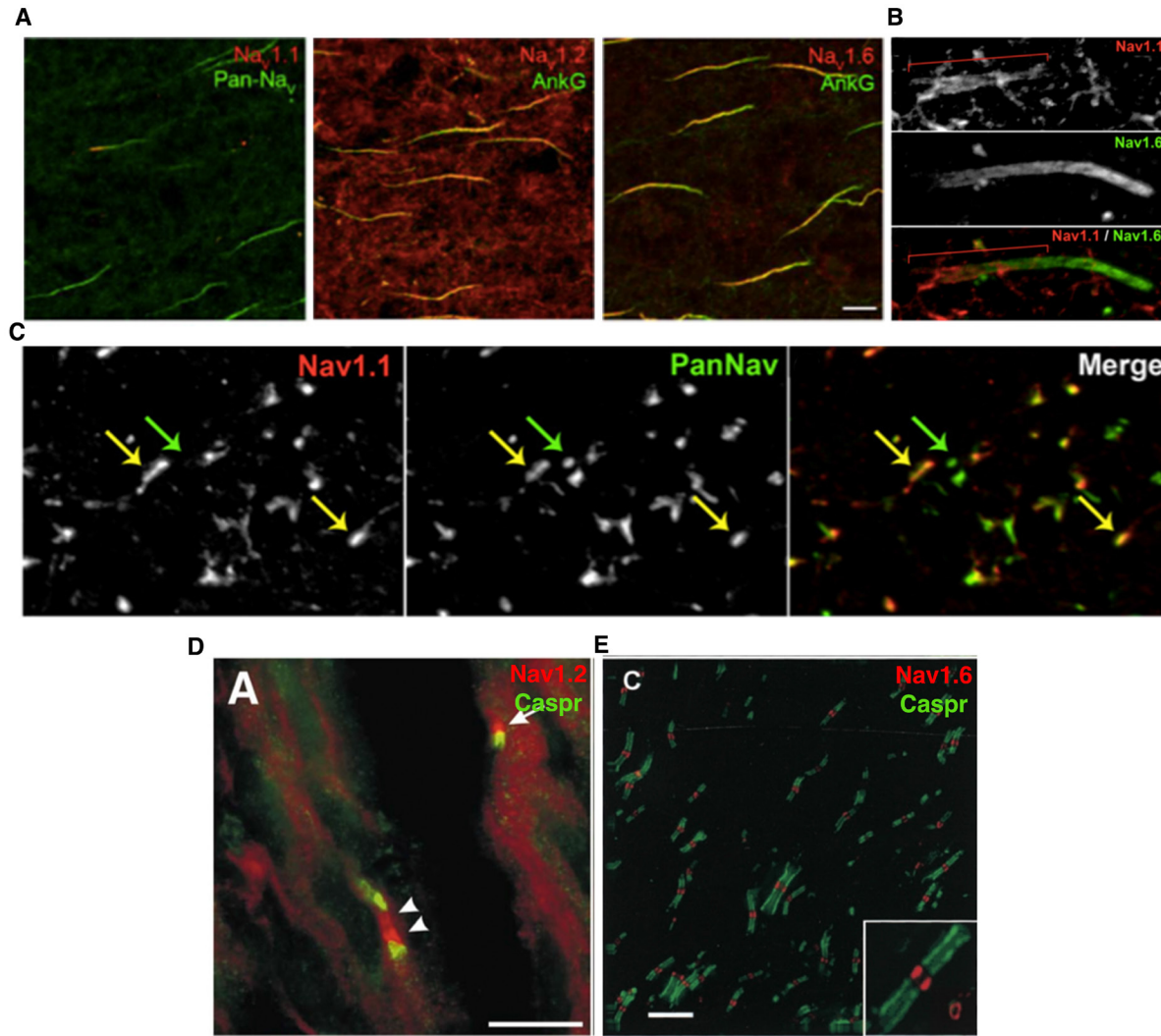


Figure 7: Immunolocalization of Nav subunits at the AIS and nodes of Ranvier. **(A)** Expression of $\text{Nav}1.1$, $\text{Nav}1.2$, and $\text{Nav}1.6$ at the AIS of cortical neurons in human tissue. Adapted from Tian *et al.*, 2014. **(B)** $\text{Nav}1.1$ (red) is restricted to the proximal portion of the AIS, while $\text{Nav}1.6$ is present at the distal AIS. Adapted from Duflocq *et al.*, 2008. **(C)** Colocalization of $\text{Nav}1.1$ (red) and Pan Nav (green) at nodes of Ranvier in adult spinal cord (yellow arrows). Of note, some nodes of Ranvier are $\text{Nav}1.1$ -negative (green arrows). Adapted from Duflocq *et al.*, 2008. **(D)** $\text{Nav}1.2$ immunolabeling (red) at the developing sciatic nerve. Arrowheads represent two heminodal clusters converging to form a node and the full arrow denotes a heminodal cluster flanked by Caspr (green). Adapted from Rasband and Trimmer 2001. **(E)** Immunolabeling of nodal $\text{Nav}1.6$ (red) flanked by Caspr (green) in the optic nerve. Adapted from Caldwell *et al.*, 2001.

1992, Gong *et al.*, 1999, Boiko *et al.*, 2001). However, enrichment of $\text{Na}_v1.2$ has been observed in node-like clusters along rat retinal ganglion cell axons *in vitro* (Kaplan *et al.*, 2001). In the rodent PNS, $\text{Na}_v1.2$ is first detected at nodes at P1 (Fig. 7D), progressively disappears between P2.5-5, and then is rarely detected between P7-28 (Boiko *et al.*, 2001; Luo *et al.*, 2014). During rat optic nerve development, it has been observed that $\text{Na}_v1.2$ is localized to immature nodes and then declines rapidly after the second postnatal week (Boiko *et al.*, 2001). This nodal $\text{Na}_v1.2$ regulation corresponds to the myelination time course in the rat optic nerve, suggesting that $\text{Na}_v1.2$ is replaced at the nodes as CNS myelination proceeds (see chapter III; Boiko *et al.*, 2001). Conversely, in adult human tissue, $\text{Na}_v1.2$ has been observed to be enriched in a subpopulation of nodes of Ranvier in the cortex (Tian *et al.*, 2014).

Similar to $\text{Na}_v1.1$, $\text{Na}_v1.2$ is functionally involved in action potential initiation, conduction and repetitive firing (Catterall *et al.*, 2005). Knocking out the *SCN2A* gene in mice results in hypoxic perinatal death and a sharp attenuation of sodium channel currents in mouse hippocampal cultures (Catterall, Goldin, and Waxman, 2005; Planells-Cases *et al.*, 2000). Point mutations of *SCN2A* have also been observed in a Japanese patient, which resulted in febrile and afebrile seizures (Sugawara *et al.*, 2001).

$\text{Na}_v1.6$

Axonal expression of $\text{Na}_v1.6$ at the AIS appears to be late compared to its $\text{Na}_v1.2$ counterpart in the rodent (Boiko *et al.*, 2003). Juxtaposing $\text{Na}_v1.2$, $\text{Na}_v1.6$ is preferentially enriched at the distal end of the AIS in rodent and human AISs (Fig. 7B; Van Wart *et al.*, 2007; Hu *et al.*, 2009, Tian *et al.*, 2014); however, $\text{Na}_v1.6$ AIS expression is uniform in rat layer 5 pyramidal neurons (Lorincz and Nusser, 2008). Electrophysiological experiments have reported that distal enrichment of low-threshold $\text{Na}_v1.6$ is important for electrogenesis since its spatially enriched location at the AIS determines action potential initiation (Hu *et al.*, 2009).

Further along the axon, $\text{Na}_v1.6$ is expressed along non-myelinated PNS fibers (Black *et al.*, 2002), but also clusters at developing and adult PNS and CNS nodes

(Fig. 7E; Caldwell *et al.*, 2000; Krzemien *et al.*, 2000; Tzoumaka *et al.*, 2000; Black *et al.*, 2002; Luo *et al.*, 2014). The time course of rodent CNS nodal $\text{Na}_v1.6$ clustering appears to coincide with myelination (Kaplan *et al.*, 2001; Boiko *et al.*, 2001). Indeed, $\text{Na}_v1.2$ is localized to immature nodes of Ranvier in rat optic nerve, which progressively gets replaced by $\text{Na}_v1.6$ as myelination proceeds (see chapter III, Boiko *et al.*, 2001).

Functionally, $\text{Na}_v1.6$ plays a central role in axon potential generation and conduction, resurgent and persistent current in Purkinje cells, and tunes the spike timing of cerebellar granule cells (Catterall *et al.*, 2005; Raman *et al.*, 1997; Osorio *et al.*, 2010). Mutations to the gene encoding for $\text{Na}_v1.6$ in mice result in disrupted firing patterns of Purkinje cells, development of motor endplate disease, and causes cerebellar ataxia (Catterall *et al.*, 2005).

Beta Subunits

Mammalian sodium channel β -subunits form a family of five proteins ($\beta1\text{Na}_v$, $\beta1\text{BNa}_v$, $\beta2\text{Na}_v$, $\beta3\text{Na}_v$, and $\beta4\text{Na}_v$) that are encoded by four *SCNB* genes. Each isoform contains an N-terminal extracellular Ig-like fold similar to proteins of the Ig superfamily of CAMs, a single transmembrane-spanning segment, and a short intracellular C-terminus (O'Malley and Isom, 2015). Of note, Na_v β -subunits interact with α -subunits through two different types of interactions: $\beta1\text{Na}_v$ and $\beta3\text{Na}_v$ noncovalently interact with α -subunits through their N- and C-terminal domains, while $\beta2\text{Na}_v$ and $\beta4\text{Na}_v$ interact with α -subunits through disulfide linkage of Cys-26 ($\beta2$) and Cys-28 or 58 ($\beta4$) in the N-terminal Ig-like fold (Chen *et al.*, 2012; Gilchrist *et al.*, 2013; Buffington and Rasband, 2013; O'Malley and Isom, 2015).

Na_v β -subunits are described as “auxillary” subunits, but they play critical roles in regulating the rate of α -subunit activation and inactivation (Patton *et al.*, 1994; Kazen-Gillespie *et al.*, 2000), regulating the amount of resurgent sodium current and sodium current density (Isom *et al.*, 1995; McEwen *et al.*, 2004; Aman *et al.*, 2009), and trafficking α -subunits and regulating their plasma membrane insertion (Chen *et al.*, 2002; Schmidt and Catterall, 2002). Furthermore, Na_v β -

subunits have been shown to interact with voltage-gated potassium channels and modulate their activation (Nguyen *et al.*, 2012; Marionneau *et al.*, 2012). Therefore, $\text{Na}_v \beta$ -subunits are key players in ion channel functioning and sodium channel recruitment to regions of excitability. So far, three $\text{Na}_v \beta$ -subunit isoforms have been reported to cluster at the nodes of Ranvier (O'Malley and Isom, 2015): $\beta 1\text{Na}_v$, $\beta 2\text{Na}_v$, and $\beta 4\text{Na}_v$. This section will discuss these isoforms in detail below.

$\beta 1\text{Na}_v$

$\beta 1\text{Na}_v$ has been reported to be enriched in the mouse at the AIS and nodes of Ranvier. At the AIS, $\beta 1\text{Na}_v$ is highly enriched in both glutamatergic neurons and GABAergic interneurons (primarily somatostatin and parvalbumin⁺ interneurons), and associates with $\text{Na}_v 1.1$, $\text{Na}_v 1.2$, $\text{Na}_v 1.6$ in the mouse somatosensory cortex (Brackenbury *et al.*, 2010; Wimmer *et al.*, 2015). At CNS nodes of Ranvier, $\beta 1\text{Na}_v$ has so far been observed in the mouse adult corpus callosum and ventral funiculi of the cervical spinal cord (Wimmer *et al.*, 2015; Desmazières *et al.*, 2014), while in the PNS it has been reported in mouse sciatic nerve nodes starting at P3 and continues into the adult (Ratcliff *et al.*, 2000; Chen *et al.*, 2004; Desmazières *et al.*, 2014).

Like all $\text{Na}_v \beta$ -subunits, $\beta 1\text{Na}_v$ contains an extracellular Ig-like fold domain that allows it to act as a CAM, thereby permitting $\beta 1\text{Na}_v$ to interact in *trans* homophilic and *cis/trans* heterophilic interactions. *Trans* homophilic interactions of $\beta 1\text{Na}_v$ permit neurite outgrowth through fyn kinase (Davis *et al.*, 2004; Brackenbury *et al.*, 2008). Heterophilically, $\beta 1\text{Na}_v$ can interact with the extracellular domains of various other nodal and paranodal CAMs such as neurofascin186 and 155 (Ratcliff *et al.*, 2001; McEwen and Isom, 2004), contactin (Kazarinova-Noyes *et al.*, 2001) and NrCAM (McEwen and Isom, 2004). As well, $\beta 1\text{Na}_v$ can interact with extracellular matrix proteins such as Tenascin-R (Xiao *et al.*, 1999), and with other $\text{Na}_v \beta$ -subunits such as $\beta 2\text{Na}_v$ (McEwen and Isom, 2004).

$\beta 1\text{Na}_v$ can increase the cell surface expression and gating of Na_v and $\text{K}_v \alpha$ -subunits (thereby modifying electrical properties), but these data vary substantially

depending on the genetic background, cell type, and ion channel α -subunit being studied (reviewed in Calhoun and Isom, 2014).

$\beta 2\text{Na}_v$

In cultured rat retinal ganglion cells (RGCs) and hippocampal neurons, $\beta 2\text{Na}_v$ has been observed to be enriched at the level of the AIS (Kaplan *et al.*, 2001; Chen *et al.*, 2012). Their localization has also been observed at node-clusters in rat hippocampal neurons associated to $\text{Na}_v 1.2$ (Kaplan *et al.*, 2001), at nodes of Ranvier in mouse sciatic nerve, and mouse white matter tracts of the cerebellum (Chen *et al.*, 2002).

$\beta 2\text{Na}_v$ can be further processed through posttranslational modifications by γ -secretase cleavage, thereby permitting the intracellular domain to enter the nucleus and increase transcription of *Scn1a* (Kim *et al.*, 2007). Additionally, $\beta 2\text{Na}_v$ increases functional expression of sodium channels, modifies their gating, and increases plasma membrane surface area in *Xenopus* oocytes (Isom *et al.*, 1995). Along with these reports, $\beta 2\text{Na}_v^{-/-}$ mice display increased seizure susceptibility, a reduction in the amount of plasma membrane associated sodium channels and reduced optic nerve conduction. Extracellularly, $\beta 2\text{Na}_v$ can interact with Tenascin-C (Srinivasan *et al.*, 1998).

$\beta 4\text{Na}_v$

$\beta 4\text{Na}_v$, the most recently discovered and least described Na_v β -subunit, is expressed in multiple regions in the adult rat brain and spinal cord (Yu *et al.*, 2003). Subcellular enrichment of $\beta 4\text{Na}_v$ has also been reported at the AISs of fast-spiking GABAergic interneurons, and in a subset of rat PNS and CNS nodes of Ranvier (Buffington and Rasband, 2013). These immunohistological observations correlate with functional electrophysiological studies since $\beta 4\text{Na}_v$ has been shown to be associated with resurgent sodium current, which aids in high-frequency repetitive firing (Khaliq *et al.*, 2003; Grieco *et al.*, 2005).

Similar to $\beta 2\text{Na}_v$, $\beta 4\text{Na}_v$ requires a disulfide bond at Cys-28 in order to localize to the AIS and nodes of Ranvier (Buffington and Rasband, 2013). AnkyrinG

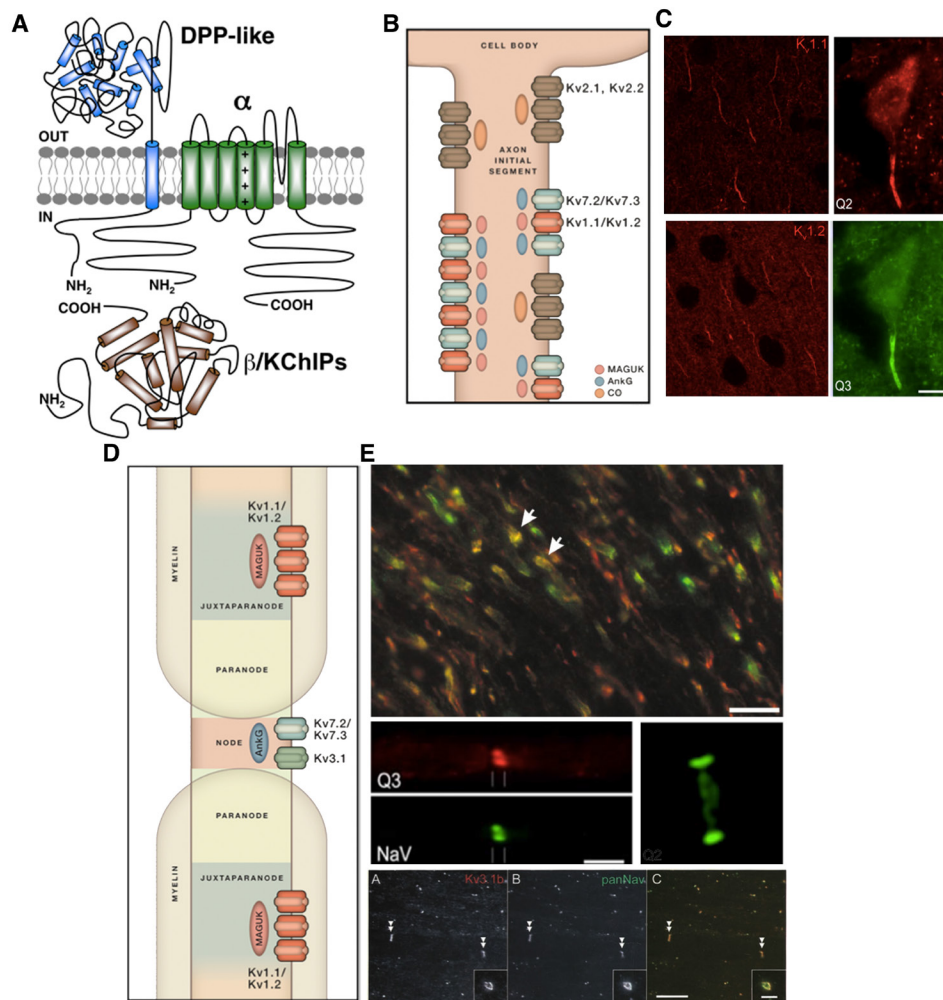


Figure 8: Structure, expression, and localization of voltage-gated potassium channels. **(A)** Structure of the voltage gated potassium channels. Adapted from Vacher *et al.*, 2008. **(B)** Overview of the voltage-gated potassium channels at the axon initial segment alongwith their interacting partners. Adapted from Trimmer, 2015. **(C)** K_v1 and K_v7 localize to the AIS of various regions in the brain. Adapted from Lorincz and Nusser 2008 and Pan *et al.*, 2006. **(D)** Overview of the voltage-gated potassium channels at the nodes and juxtaparanodes. Adapted from Trimmer, 2015. **(E)** $K_v1.1$ (green) and $K_v1.2$ (red) are localized to paranodes in the optic nerve (top panel). $K_v7.2$ (red, top middle panel) and $K_v7.3$ (green, middle right panel) localize to the nodes of Ranvier. $K_v3.1b$ (red, bottom panel) is also a component of the nodes of Ranvier and colocalize (arrowheads) with Na_v (green). Adapted from Rasband, 2004 (E top panel), Pan *et al.*, 2006 (middle panels), and Devaux *et al.*, 2003 (bottom panels).

and sodium channel α -subunits are also necessary for $\beta 4\text{Na}_v$ to localize to the AIS (Buffington and Rasband, 2013).

1.3.1.2 Voltage-Gated Potassium Channel Alpha Subunits (K_v)

K^+ channels comprise the largest and most diverse group of ion channels in mammals (Trimmer, 2015). Indeed, ~ 90 genes code for K^+ α - and β -subunits, and the heteromeric channel pore is often comprised of a combination of different α -subunits and various splice isoforms, thus leading to a wide diversity and complexity in the K^+ channel family. Almost half of these 90 genes encode for voltage dependent potassium channels, which allow for passage of K^+ ions via changes in membrane potential. In vertebrates, 41 genes encode for K_v1 through K_v12 , and each subfamily can be broken down further into a number of different K_v isoforms (Trimmer, 2015).

The quaternary structure of the K_v channel ion pore is a tetrameric complex of α -subunits, wherein each α -subunit is comprised of six transmembrane segments (S1-S6) (Fig. 8A; Vacher *et al.*, 2008). K_v channels are also composed of auxiliary β -subunits such as $K_v\beta$, KChIP, and DPP-like (Vacher *et al.*, 2008). Of the large family of K_v channels, only two subfamilies have been observed to be compartmentalized at the nodes: K_v7 (KCNQ) and K_v3 (Fig. 8D and E). Interestingly, other K_v channels have been observed (notably K_v1 , and more recently BK/Slo1 channels) at the AIS, paranode, and juxtaparanode (Fig. 8B-E). Our discussion will therefore focus on three families (K_v1 , K_v3 , and K_v7) in detailing their subcellular distribution and roles at excitable axonal domains.

K_v1

K_v1 is the *Shaker*-type family (name originated from *Drosophila*) of voltage-gated potassium channels that is comprised of eight isoforms ($K_v1.1$ - $K_v1.8$). Only $K_v1.1$, $K_v1.2$, $K_v1.4$, and $K_v1.5$ have been reported to be enriched near or at subcellular excitable domains. Notwithstanding, expression and functional roles of

K_v1.1 and K_v1.2 have been extensively studied, and therefore this section will only detail these two K_v1 subtypes.

K_v1.1 and K_v1.2 are highly enriched in the distal compartment of the AIS in human neocortical pyramidal cells, and in both excitatory and inhibitory neurons of multiple rat brain regions (Fig. 8C; Inda *et al.*, 2006; Van Wart *et al.*, 2007; Lorincz and Nusser, 2008). Together, K_v1.1 and K_v1.2 are observed to be extensively co-labeled at the AIS, suggesting that these channels most likely form heteromeric channels (Lorincz and Nusser, 2008). Localization of K_v1.1 and K_v1.2 to the AIS depends on the interaction with the PDZ (PSD-95/disc large/zonula occludens-1) domain of the MAGUK (membrane associated guanylate kinase) PSD-93/Chapsyn-110 (Horresch *et al.*, 2008; Ogawa *et al.*, 2008).

K_v1.1 and K_v1.2 are both also clustered together as heteromultimers at the juxtaparanodal regions of the mammalian CNS and PNS myelinated axon (Fig. 8E; Wang *et al.*, 1994; Rasband *et al.*, 1999; Howell *et al.*, 2006). Clustered underneath the myelin sheath and spatially separated from the node by paranodal junctions, these channels most likely regulate the internodal resting potential and diminish repetitive firing (see chapter II; Arancibia-Carcamo and Attwell, 2014). K_v1.1 and K_v1.2 appear first at the nodes and paranodes during the first postnatal week in rat, but then subsequently become restricted to the juxtaparanodes between P14 and P28 (Vabnick *et al.*, 1998).

K_v3

K_v3 are a family of four K⁺ channels isoforms: K_v3.1-K_v3.4. In the rat CNS, K_v3.1b, one of the two splice variant isoforms of K_v3.1, clusters at nodes of Ranvier (Fig. 8D and E) but is not enriched at the AIS (Devaux *et al.*, 2003). K_v3.1b first appears at a few nodes starting at P8 in the ventral column of the spinal cord, and then increases rapidly in expression to a point where it then reaches its adult levels by P12 (Devaux *et al.*, 2003). Furthermore, K_v3.1b clusters at nodes of Ranvier prior to K_v1.2 clustering at juxtaparanodes, and K_v3.1b appears to be mostly associated with mature nodes (Devaux *et al.*, 2003). As for the PNS, K_v3.1b is observed in only

a few sciatic nerve nodes of Ranvier, of both large and small diameter, starting at P12 and increasing in number between P15 and P21 (Devaux *et al.*, 2003).

The functional role of K_v3.1b at nodes has yet to be fully uncovered. Experiments using 4-AP, a pharmacological blocker of K⁺ channels, and performing CAP recordings on optic nerve did not yield any changes to AP repolarization (Devaux *et al.*, 2003). Yet, genetic ablation of K_v3.1 resulted in a reduction in AP frequency (Espinosa *et al.*, 2001). Interestingly, K_v3.1b has been observed to be enriched in hippocampal parvalbumin⁺ interneurons (Weiser *et al.*, 1995), and is corroborated by the fact that K_v3 conductance has been observed to play an important role in permitting high-frequency firing in fast-spiking interneurons (Lien and Jonas, 2003).

K_v7 (KCNQ)

The K_v7 family, or otherwise called KCNQ, are a form of delayed rectifier K⁺ channels comprised of five isoforms: K_v7.1 to K_v7.5. So far, only K_v7.2 and K_v7.3 have been described to be enriched in mammalian AISs and nodes of Ranvier (Fig. 8B-E; Trimmer, 2015). AIS expression of K_v7.2 and K_v7.3 appear in multiple nervous system regions including the brainstem, striatum, hippocampus, cerebellar cortex, and neocortex (Devaux *et al.*, 2004; Pan *et al.*, 2006; Klinger *et al.*, 2011).

K_v7.2 and K_v7.3 are restricted to rodent adult PNS and CNS nodes, but K_v7.3 exhibits heterogenous nodal expression in both systems (Fig. 8E; Devaux *et al.*, 2004; Pan *et al.*, 2006; Schwarz *et al.*, 2006; Battefeld *et al.*, 2014). Indeed, enrichment of K_v7.2, together with K_v7.3, is observed in rat sciatic nerve fibers and rat neocortical axons whose diameters are >6 μm and between 1 and 3 μm, respectively (Schwarz *et al.*, 2006; Battefeld *et al.*, 2014). K_v7.3 is absent from nodes in sciatic nerve fibers above >10 μm, while K_v7.2 is always present (Schwarz *et al.*, 2006; Pan *et al.*, 2006).

1.3.2 Cellular Adhesion Molecules of the Immunoglobulin Superfamily (IgCAMs)

Cellular adhesion molecules (CAMs) are important proteins that mediate cell-cell interactions during the development of nervous and non-nervous tissues. CAMs comprise a wide variety of glycoprotein families such as integrins, selectins, netrins, cadherins, and immunoglobulins (Igs). Importantly, members of the Ig-domain superfamily have been highly implicated in nervous tissue development. Looking at the subcellular level of myelinated axons, three different subgroups of the Ig-domain superfamily of CAMs have been described to be enriched at excitable axonal domains: L1-CAMs, glycosylphosphatidylinositol (GPI)-anchored CAMs, and neurexin related proteins. This section on CAMs will outline the different protein classes with respect to their distribution to excitable domains, and will explore their molecular intracellular and extracellular interactions.

1.3.2.1 L1-CAMs

L1-CAM family members are expressed in nervous tissue of invertebrate and vertebrate species. Their role in the nervous system ranges from myelination, maintenance and organization of excitable domains, to axon growth and guidance (Barbin *et al.*, 2004; Panicker *et al.*, 2003; Zonta *et al.*, 2011; Desmazieres *et al.*, 2014; Thaxton *et al.*, 2011; Zonta *et al.*, 2008; Zhang *et al.*, 2015; Pillai *et al.*, 2009; Sherman *et al.*, 2005; Buttermore *et al.*, 2012; Sakurai, 2012). The structure of mostly all L1-CAM family members include six Ig domains on the aminoterminal side, three to five fibronectin type III (FNIII) domains, and a single transmembrane segment (Fig. 9; Hortsch *et al.*, 2000). The Ig domains allow for these molecules to engage in homophilic and heterophilic interactions with other CAMs, sodium channel subunits, and the extracellular matrix. Intracellularly, L1-CAMs contain a conserved ankyrin-binding domain (ABD) motif that permits interaction with scaffolding protein ankyrinG (Fig. 9; Davis and Bennett, 1994; Hortsch *et al.*, 2009). Vertebrate members of the L1-CAM family include L1, CHL1 (Close Homolog of L1), NgCAM (Neuron-glia CAM), NrCAM/Bravo (Neuron-glia CAM related), and

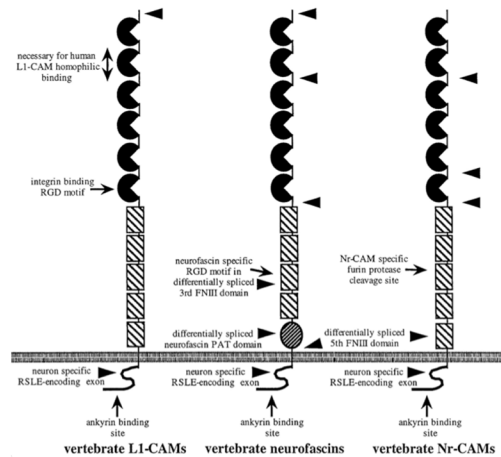


Figure 9: General Structure of L1-CAMs. The black circles represent the Ig domains on the extracellular regions of the protein. The lined boxes represent the fibronectin III (FNIII) domains, and the lined circle represents the mucin or PAT domain of neurofascins. Arrowheads indicate the different splice isoforms present through alternative splicing, while full arrows represent either the ankyrinG binding site in the intracellular region of the L1-CAMs or the cleavage site for NrCAM. Adapted from Horsch, 2000.

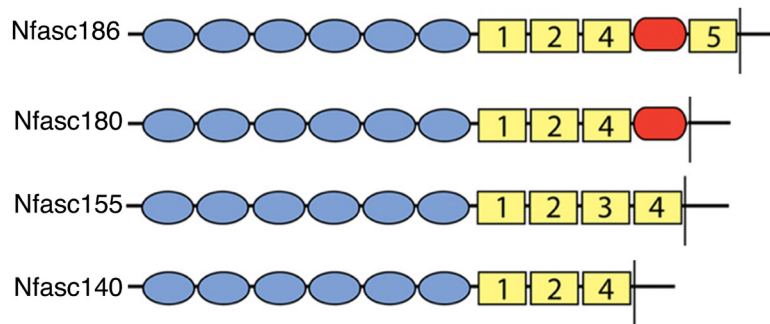


Figure 10: The four different neurofascin isoforms expressed in the nervous system. Blue circles represent the Ig domains, the green squares represent the FNIII domains, and the red ovals represent the mucin domain. Adapted from Zhang *et al.*, 2015.

neurofascin (Fig. 9; Hortsch *et al.*, 2000). So far, only NrCAM and neurofascin have been reported to be enriched at excitable domains. Therefore, discussion of nodal L1-CAM family members will only detail these two molecules.

Neurofascin

Neurofascin (Nfasc), first described in the chick brain, is an important member of the Ig superfamily that has been observed to be involved in axonal fasciculation, neurite extension or inhibition, action potential initiation, myelination, maintenance and organization of excitable domains (for review see Kriebel *et al.*, 2012).

Processing of the Nfasc precursor mRNA results in a large variety of splice isoforms that are expressed in neurons and glial cells. The main neuronal Nfasc polypeptides are Nfasc186, Nfasc180 and Nfasc140, while Nfasc155 is the main glial Nfasc isoform (Fig. 10). The variability of Nfasc splice variants is mainly determined by the incorporation of the mucin-like [otherwise called PAT (proline, alanine, threonine)] domain, or the inclusion of the third or fifth FNIII-type domain (for a detailed review on Nfasc splice variants see Kriebel *et al.*, 2012).

Neurofascins are also further processed beyond their splice isoforms as they can go through multiple posttranslational modifications. The extracellular region of neurofascins can be modified through *N*-linked or *O*-linked glycosylation, which permits further interactions with extracellular partners (Volkmer *et al.*, 1996; Pomicter *et al.*, 2010; Kriebel *et al.*, 2012). The transmembrane domain can be palmitoylated and thereby allows neurofascins to be localized to specialized membrane domains (Ren and Bennett, 1998). Lastly, the FIGQY motif in the cytoplasmic region of neurofascins can be tyrosine phosphorylated (this motif is also conserved in other L1-CAM family members). In the phosphorylated state, neurofascins are able to bind to doublecortin, while the dephosphorylated state permits binding to ankyrinG (Garver *et al.*, 1997; Tuvia *et al.*, 1997; Kizhatil *et al.*, 2002).

The various Nfasc isoforms are spatially and temporally separated. For example, Nfasc180 and Nfasc140 are typically associated with the early brain development and play important functional roles in the immature neuron (Kriebel *et al.*, 2012). Nfasc186, however, is temporally expressed later than these other isoforms and is generally associated with the mature neuron (Kriebel *et al.*, 2012).

Neurofascins at the levels of the AIS and Nodes of Ranvier

The two Nfasc isoforms that have been described to be enriched at excitable domains are Nfasc140 and Nfasc186. Nfasc140 lacks the mucin-like domain and the third and fifth of the five FNIII domain, whereas Nfasc186 contains the mucin-like domain and contains all five FNIII except the third (Fig. 10). Western blot analyses of mouse hindbrain have shown that the expression of Nfasc140 appears to be at its strongest during mid-embryonic stages (E13) and steadily declines thereafter at the onset of myelination (Zhang *et al.*, 2015).

Unlike Nfasc140, Nfasc186 is expressed early in rodent PNS and CNS embryonic stages and is continually expressed into the adult (Davis *et al.*, 1993, Tait *et al.*, 2000; Basak *et al.*, 2007; Zhang *et al.*, 2015). Nfasc186 has been observed to be enriched at the AIS of neurons in multiple brain regions (Davis *et al.*, 1996; Tait *et al.*, 2000; Xu and Shrager, 2005; Hedstrom *et al.*, 2007), while more recent studies through transgenic mice have found that Nfasc140 is also enriched at the AIS of P8 mouse Purkinje neurons (Zhang *et al.*, 2015).

Importantly, Nfasc186 has been observed to play various critically functional roles in context to the AIS. In the cerebellum, innervation of Purkinje cell AISs by pinceau synapses from basket interneurons depends on a gradient of Nfasc186 at the AIS. Loss of Nfasc186 results in mislocalization of basket cell axon innervation and reduction in pinceau synapses (Ango *et al.*, 2004; Zonta *et al.*, 2011; Buttermore *et al.*, 2012). Lentiviral shRNA knockdown of Nfasc186 in adult rat brain results in reduction in GABAergic synaptic terminals at the AIS, suggesting that Nfasc186 is important in maintaining axo-axonic synapses (Kriebel *et al.*, 2011). Moreover, conditional loss of Nfasc186 at the mature AIS in mouse Purkinje cells results in

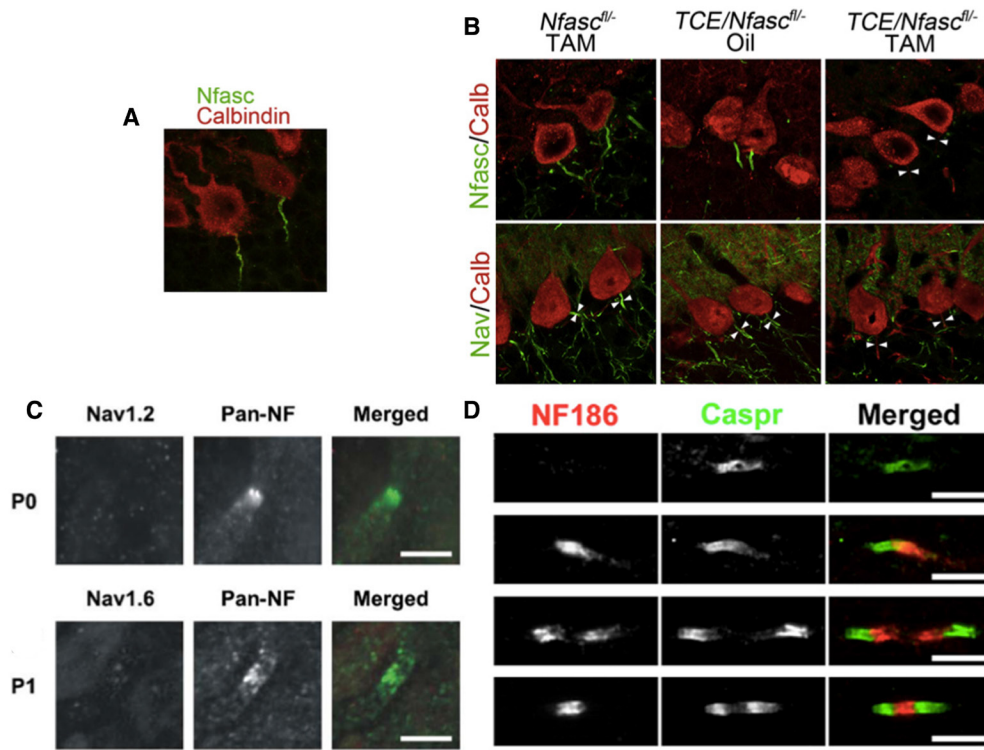


Figure 11: Neurofascin186 at the AIS and nodes of Ranvier. **(A)** Immunolocalization of Nfasc186 (green) to the AIS of Purkinje neurons (red). **(B)** Neurofascin is essential for maintaining the components of the AIS. Loss of Nav (green bottom panels) is observed at the AISs (arrowheads) of Purkinje neurons (red) when conditionally ablating Nfasc186 (far right panels). A and B adapted from Zonta *et al.*, 2011. **(C)** Nfasc186 (green) appears before Nav isoforms (red) in the PNS. Adapted from Schafer *et al.*, 2006. **(D)** Coimmunolabeling of Nfasc186 (red) and Caspr (green) in optic nerve from P10 (top panels) to adult (bottom panels). Adapted from Susuki *et al.*, 2013.

disintegration of the AIS components such as Nav, ankyrinG and NrCAM, and abolishment of spontaneous action potential firing (Fig. 11A and B; Zonta *et al.*, 2011). These results suggest that Nfasc186 at the mature AIS acts as an anchor point for recruitment of newly synthesized AIS components (Zonta *et al.*, 2011).

An additional role of Nfasc186 at the AIS is its ability to interact with extracellular matrix molecules. ShRNA knockdown of Nfasc186 at the AIS of rat cortical neurons results in loss of ECM protein brevican at the AIS, while overexpression of Nfasc186 in rat hippocampal neurons results in the enrichment of brevican in the somatodendritic regions of the neuron (Hedstrom *et al.*, 2007). Altogether, these results confirm an indispensable role for Nfasc186 in axo-axonic synapse formation, Purkinje cell AIS maintenance and function, and for maintaining the ion buffering extracellular matrix around the AIS of cortical and hippocampal neurons.

In the PNS, Nfasc186 has been reported to be one of the first axonal components to arrive at the developing node of Ranvier (Fig. 11C; Lambert *et al.*, 1997; Schafer *et al.*, 2006). At P0, more than half of the developing nodes of the rat sciatic nerve are void of Nav1.2 or Nav1.6 (Schafer *et al.*, 2006); additionally, at P2, Nfasc186 is observed to cluster at developing nodes, while ankyrinG is diffusely labeled (Lambert *et al.*, 1996). CNS expression of Nfasc186 at nodes appears to follow a different time course than its PNS counterpart. Clustering of Nfasc186 in the mouse optic nerve is first observed at P10, where it is observed with nodal scaffolding components and flanked by clusters of Caspr (Fig. 11D; Susuki *et al.*, 2013). Rarely is Nfasc186 observed at nodes without a nodal scaffolding protein or paranodal Caspr (Susuki *et al.*, 2013). Expression of Nfasc186 becomes expressed in more optic nerve nodes by P13 and reaches peak adult levels by P17 (Susuki *et al.*, 2013). In contrast to Nfasc186, enrichment of Nfasc140 at the nodes of Ranvier have only until now been observed since there is no specific antibody for this neurofascin isoform. Recently, Zhang *et al.* (2015) showed that transgenically expressed Nfasc140 is enriched in both mouse PNS and CNS nodes of Ranvier.

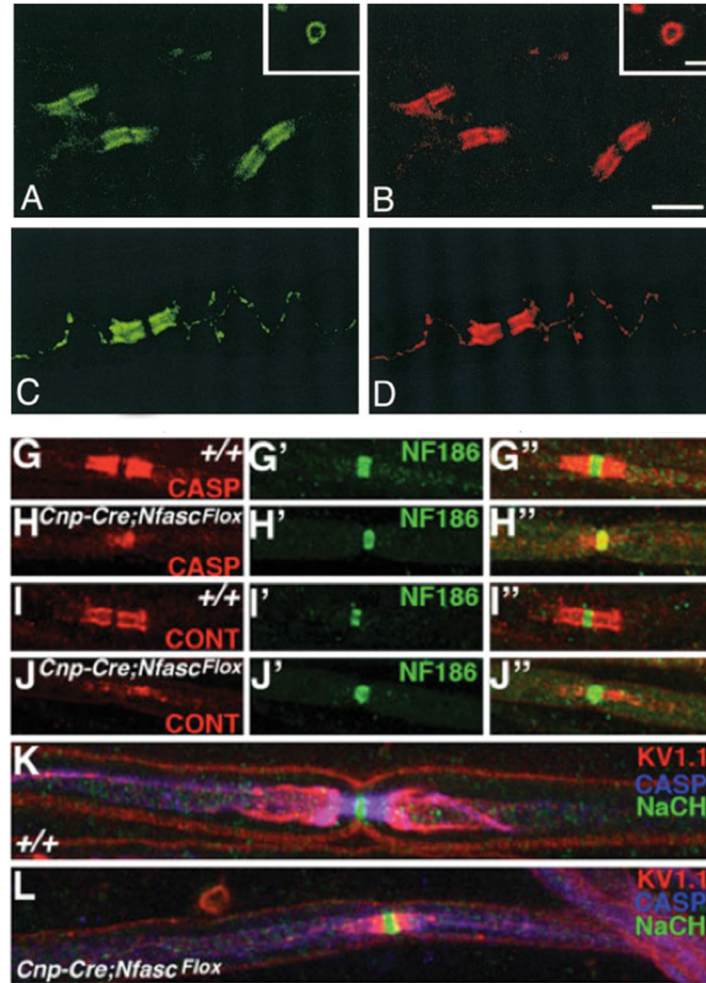


Figure 12: Paranodal localization of Nfasc155 in the PNS and CNS. (A) and (B): Colocalization of Nfasc155 (green) and Caspr (red) in optic nerve. (C) and (D): Colocalization of Nfasc155 (green) and Caspr (red) in teased sciatic nerve. Adapted from Tait *et al.*, 2000. Glial specific loss of Nfasc155 disrupts the paranodal components Caspr (red in H and blue in L) contactin (red in I), and juxtaparanodal localization of K_v1.1 (red in L). Adapted from Pillai *et al.*, 2009.

Nfasc186 and Nfasc140 play a crucial role in recruiting other nodal components to the developing node, and its role will be discussed further in mechanisms of nodal and paranodal development and maintenance.

Neurofascin at the Paranodal Junction

The glial specific neurofascin splice isoform, Nfasc155, is highly clustered at developing and adult PNS and CNS paranodal junctions (Fig. 12A and B; Davis *et al.*, 1996; Tait *et al.*, 2000). Different from both Nfasc186 and Nfasc140, this isoform contains the third FNIII domain and lacks the mucin-like domain (Fig. 10; Davis *et al.*, 1996).

Nfasc155 interacts extracellularly with the Caspr/Contactin complex to form the paranodal junction complex (Tait *et al.*, 2000; Charles *et al.*, 2002). Recently the cytoplasmic domain of Nfasc155 has been shown to interact with glial ankyrinG and ankyrinB (Chang *et al.*, 2014). Partitioning Nfasc155 to the paranodal junctions requires the Ig 5-6 on the extracellular surface (Thaxton *et al.*, 2010). Furthermore, a subpopulation of Nfasc155 has been described to have developmentally regulated association to lipid rafts (Schafer *et al.*, 2004). These lipid rafts are thought to stabilize the interaction between the Caspr and Nfasc155 at the paranode (Schafer *et al.*, 2004), while ankyrins are believed to either target Nfasc155 to the paranodal junctions or stabilize the developing paranodal junction (Chang *et al.*, 2014).

Nfasc155 is implicated in maintaining the paranodal junction (Fig. 12H and J; Sherman *et al.*, 2005; Zonta *et al.*, 2008; Pillai *et al.*, 2009; Thaxton *et al.*, 2010). Loss of Nfasc155 results in disrupted PNS and CNS paranodal junctions, which in turn results in diffusion of juxtaparanodal K_v1 channels to the paranodes (Fig. 12L; Zonta *et al.*, 2008; Pillai *et al.*, 2009). This K_v1 diffusion to the paranodes is a recurring phenotype in most mutants that have disruptions to the paranodal junctions.

NrCAM

NrCAM, also known as Bravo, is an additional L1-CAM that has been observed to play a role in axon growth, axon guidance, and formation of excitable domains (Grumet *et al.*, 1997; Custer *et al.*, 2003; Eshed *et al.*, 2005, 2007; Feinberg *et al.*, 2010). First cloned in the chick, NrCAM is expressed in multiple mammalian nervous system tissues and in various cell types, particularly neurons and glial cells (Davis *et al.*, 1996; Feinberg *et al.*, 2010). The structure of NrCAM contains six Ig-like aminoterminal domains, five FNIII-like repeats, and a transmembrane domain. While NrCAMs full-length peptide is 200-kDa, most studies have only been able to isolate either a 140-kDa or 170-kDa protein. These two products are a result of two sites of cleavage located on the extracellular region of NrCAM (Grumet *et al.*, 1997). The first site lies within the third FNIII-like domain and is the furin cleavage site, resulting in the 140-kDa product (Kayyem *et al.*, 1992; Hosaka *et al.*, 2001), while the second is an ADAM cleavage site that is located within the transmembrane domain and produces the 170-kDa product (Susuki *et al.*, 2013). Cleaving NrCAM sheds the extracellular portion of the protein and allows it to become secreted and to interact with the extracellular matrix and the nodes of Ranvier (Eshed *et al.*, 2007; Feinberg *et al.*, 2010; Susuki *et al.*, 2013).

NrCAM is enriched at the AIS of many rodent neuronal cell types such as motoneurons, Purkinje cells, and hippocampal neurons (Davis *et al.*, 1996; Custer *et al.*, 2003; Hedstrom *et al.*, 2007; Zonta *et al.*, 2011). NrCAMs role at the AIS appears to be ancillary since knockdown of NrCAM in rat hippocampal cultures does not disturb clustering of other AIS components (Hedstrom *et al.*, 2007), and *NrCAM-null* mutants do not display a phenotype related to neuronal excitability (Custer *et al.*, 2003).

In PNS nodes of Ranvier, NrCAM is expressed in axons and is also secreted from Schwann cell microvilli; however, some NrCAM remains in the Schwann cell microvilli in its transmembrane form (Feinberg *et al.*, 2010). PNS nodal expression of NrCAM in rodent sciatic nerve fibers has been observed as early as E21, and in 60% of cases absent of Na_v coclusters (Custer *et al.*, 2003). In addition, while

ankyrinG/NrCAM coclusters are found in rodent P2 sciatic nerve, there are a number of NrCAM absent of ankyrinG (Lambert *et al.*, 1997). Yet, its timing of PNS nodal clustering seems to be concomitant with Nfasc186.

NrCAM is also observed in adult CNS nodes of Ranvier, where it is, unlike PNS nodes of Ranvier, solely expressed in its 140-kDa-secreted form (Susuki *et al.*, 2013). Whether NrCAM expressed at CNS nodes is secreted from oligodendroglia or neurons awaits identification. Additionally, timing of NrCAM clustering relative to other CNS nodal components remains an open question.

1.3.2.2 GPI-anchored CAMs

GPI-anchored CAMs have also been described to have important functions during neuronal development such as axonal growth, synaptic function, and organization of excitable domains (Labasque and Faivre-Sarrailh, 2010). Members of the GPI-anchor family found at excitable domains include Contactin/F3/F11 and TAG-1/Contactin-2/Axonin-1. The structural properties of contactin and TAG-1 are slightly similar to the L1-CAM family members: the N-terminal extracellular regions are comprised of six C2 type Ig domains, four FNIII domains, and a GPI tail rounding out the C-terminus. For TAG-1, however, the fifth and sixth Ig domains fold over toward the third and fourth Ig domains in a U-shape in order to enhance *trans* homophilic interactions (Mortl *et al.*, 2007). Extracellular interactions of contactin and TAG-1 include other CAMs, sodium channels, and extracellular matrix proteins (Labasque and Faivre-Sarrailh, 2010).

Contactin

Contactin is a neuronal and oligodendroglial GPI-anchored CAM that is involved in several neuronal developmental processes (Volkmer *et al.*, 1998; Rathjen *et al.*, 1987; Çolakoğlu *et al.*, 2014), and interacts with a variety of nodal and paranodal constituents (Volkmer *et al.*, 1998; Rios *et al.* 2000; Kazarinova-Noyes *et al.*, 2001; Çolakoğlu *et al.*, 2014).

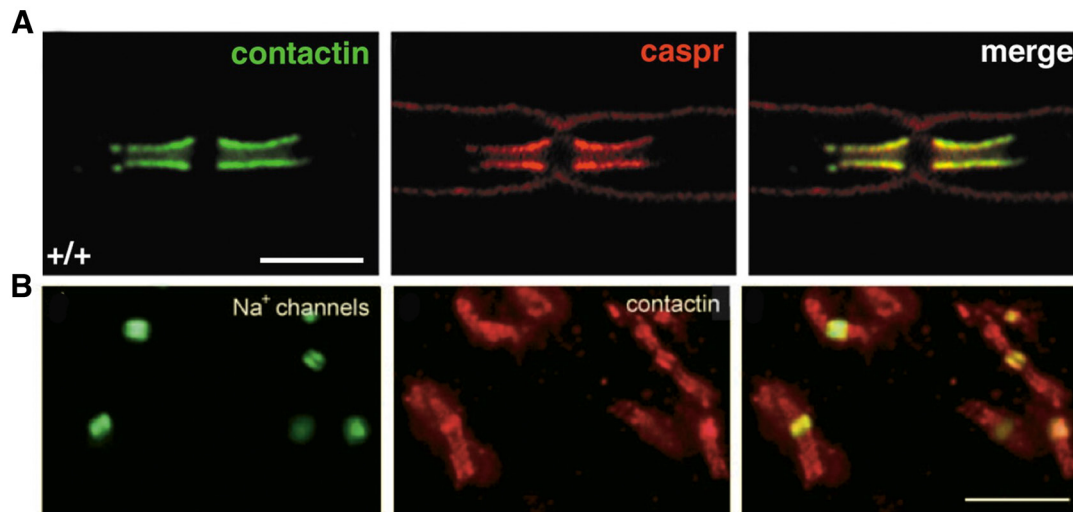


Figure 13: Expression of contactin in the CNS and PNS. **(A)** Contactin is expressed at the paranodes in the PNS and colocalizes with the paranodal junction protein Caspr. Adapted from Boyle *et al.*, 2001. **(B)** Paranodal and nodal expression of contactin. At nodes, contactin colocalizes with Nav. Adapted from Kazarinova-Noyes *et al.*, 2001.

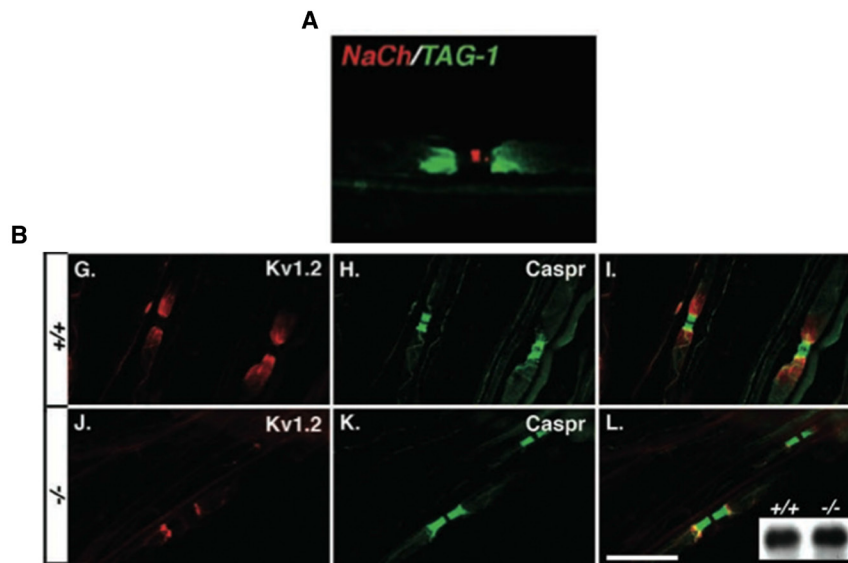


Figure 14: Expression of TAG-1, and loss of TAG-1 results in aberrant Kv1 localization. **(A)** Immunolocalization of TAG-1 to the juxtaparanodes in the sciatic nerve. The space between Pan-Na_v and TAG-1 is the paranode. **(B)** Loss of TAG-1 (lower three panels) results in diffusion of juxtaparanodal Kv1.2 (red) even though its overall expression (inset in lower righthand panel) remains the same in the PNS. Paranodal junctions (green Caspr immunostaining) are unaffected in the TAG-1 mutant mouse. **(A)** and **(B)** are both adapted from Poliak *et al.*, 2003.

Paranodal enrichment of contactin has been observed in both the PNS and CNS (Fig. 13A and B; Boyle *et al.*, 2001; Rios *et al.* 2000; Kazarinova-Noyes *et al.*, 2001; Çolakoğlu *et al.*, 2014). Rodent PNS expression of contactin is diffuse along the axonal surface around P0; but as the myelination process proceeds during the first postnatal week, contactin becomes clustered at the developing paranodal junction (Boyle *et al.*, 2001). Similarly, in the CNS, contactin clustering at the paranode follows the time course of the myelination process in the rat optic nerve (Çolakoğlu *et al.*, 2014). Although paranodal contactin is most likely to be axonal, oligodendrocytes precursor cells (OPCs) also express contactin (Einheber *et al.*, 1997; Çolakoğlu *et al.*, 2014), which then becomes downregulated as the OPCs progress into the stage of a myelinating oligodendrocyte (Çolakoğlu *et al.*, 2014).

Interestingly, contactin is observed to be clustered only at CNS nodes of Ranvier (Rios *et al.* 2000; Kazarinova-Noyes *et al.*, 2001; Çolakoğlu *et al.*, 2014). Here, through its interaction with the Na_vβ1 subunit, contactin most likely is involved in increasing Na_v channel expression and current density (Kazarinova-Noyes *et al.*, 2001).

Loss of contactin results in disrupted paranodal junctions and diffusion of K_v1 to the paranodal junction (Boyle *et al.*, 2001). Contactin is dependent on Caspr in order to cluster at the paranodes (Bhat *et al.*, 2001; Gollan *et al.*, 2002, 2003), but not at the CNS nodes of Ranvier (Rios *et al.*, 2000).

TAG-1

One GPI-anchored family protein localized to the juxtaparanodal region is TAG-1/Contactin2/Axonin-1 (Traka *et al.*, 2002). TAG-1 is also expressed at the AIS (Ogawa *et al.*, 2008), but its expression and role at this domain will not be discussed. At the cellular level, TAG-1 is expressed by both PNS and CNS myelinating glia and neurons (Traka *et al.*, 2002, 2003; Poliak *et al.*, 2003). Interestingly, TAG-1 can interact extracellularly between the myelinating glial cell and the neuronal membrane in *trans*, and further extracellular heterophilic

interactions of TAG-1 include Caspr2 (contactin-associated protein 2; Traka *et al.*, 2003) and NrCAM (Lustig *et al.*, 1999).

Expression of TAG-1 appears in ensheathing rodent Schwann cells at P6, followed by TAG-1 distribution to juxtaparanodal region in maturely myelinated sciatic nerve fibers where it is coclustered with K_v1 channels (Fig. 14A and B; Traka *et al.*, 2002, 2003). In the CNS, TAG-1 is expressed by P12 in the rodent spinal cord, and eventually becomes clustered at the juxtaparanodal regions by adult stages (Traka *et al.*, 2002).

The important role of TAG-1 is to cluster K_v1 at the CNS and PNS juxtaparanode. *TAG-1*-null mice fail to cluster K_v1 to the juxtaparanodes (Fig. 14B), while there is little reduction in the concentration of axonal K_v1, suggesting that TAG-1 is involved in localizing K_v1 to the juxtaparanodes (Traka *et al.*, 2003; Poliak *et al.*, 2003).

1.3.2.3 Neurexin-related CAMs

One important neurexin-related (neurexin is originally described in *Drosophila*) protein family found at the paranodes and juxtaparanodes is Contactin associated protein (Caspr)/Paranodin/NeurexinIV. This protein is a transmembrane glycoprotein that consists of an aminoterminal discoidin domain, two EGF-like domains flanked by laminin G-like domains, and a cytoplasmic GNP (glycophorin, neurexin IV, paranodin) domain that allows it to bind to 4.1B (Faivre-Sarrailh *et al.*, 2000; Horresh *et al.*, 2010). Not only do Caspr interact with cytoskeletal linker proteins, Caspr is also able to interact with other CAMs.

Caspr

Caspr, also described independently as Paranodin (Menegoz *et al.*, 1997), is a glycoprotein of the neurexin superfamily that was first identified to interact with contactin (Peles *et al.*, 1997). Expression of Caspr in the nervous system is strictly neuronal (Einheber *et al.*, 1997; Menegoz *et al.*, 1997). Its subcellular expression can be observed at the “para”-AIS (Duflocq *et al.*, 2011), and also at the septate-like

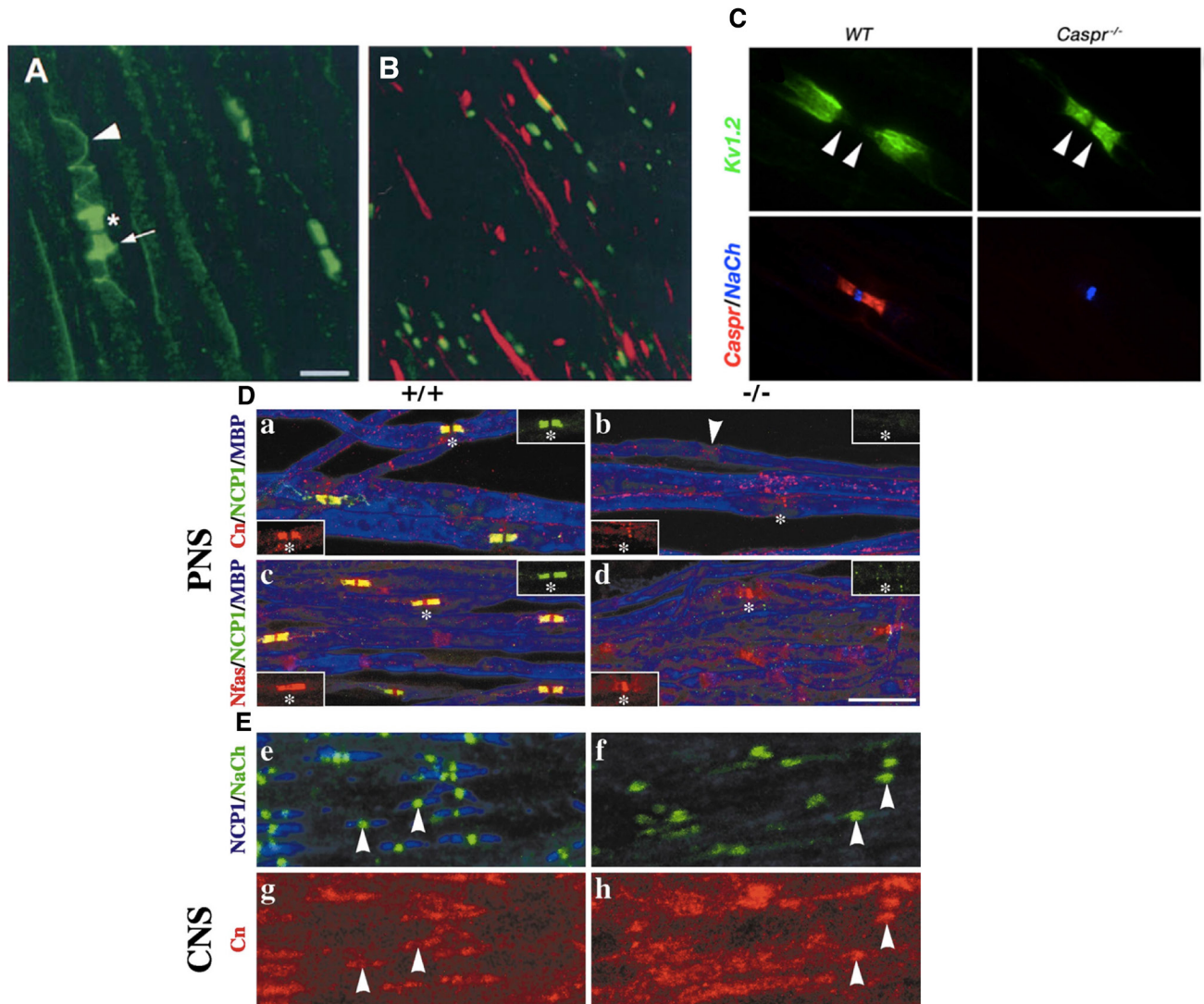


Figure 15: Caspr is a molecular marker for paranodal junction formation. **(A)** PNS clustering of Caspr (green) at the paranodes in sciatic nerve. Asterisk is the putative node of Ranvier. The arrowhead denotes restriction of Caspr to the periaxonal line and the full arrow represents the internal mesaxon. **(B)** CNS clustering of Caspr (green) along myelinated axons stained with MBP (red) in the corpus callosum. Adapted from Menegoz *et al.*, 1997. **(C)** Loss of Caspr (right column) leads to diffusion of Kv1.2 to the paranodes in teased sciatic nerves. Adapted from Horresh *et al.*, 2010. **(D)** Caspr mutants (right column) display aberrant clustering of the paranodal components (red, **Db**) and Nfasc155 (red, **Dd**) in the PNS. Insets are zoomed images of the paranode and nodes of Ranvier (asterisks). Arrowhead denotes contactin-negative nodes of Ranvier. **(E)** Loss of Caspr disrupts paranodal contactin, but neither Na_v (green, **Ef**) nor contactin (red, **Eh**) at CNS nodes of Ranvier (arrowheads). Adapted from Bhat *et al.*, 2001.

junctions at the paranodes, where it is well known for being the bona fide marker for paranodal junction formation (Einheber *et al.*, 1997; Menegoz *et al.*, 1997). Neuronal interactions of Caspr include contactin (Peles *et al.*, 1997), protein 4.1B (Menegoz *et al.*, 1997; Denisenko-Nehrbass *et al.*, 2003), and possibly Nfasc155 (Charles *et al.*, 2002; Gollan *et al.*, 2003).

Rat CNS expression of Caspr protein is observed at P7 and increases until it reaches adult levels by P30 (Poliak *et al.*, 1999). Immunolabeling for clustered Caspr at CNS paranodes can be observed as early as P7 in the rodent optic nerve on the edges of oligodendroglial myelinating segments, which coincides with the very earliest stages of myelination (Fig. 15B; Rasband *et al.*, 1999). Caspr localization at paranodes, which begin to flank clusters of nodal components, continues further over the developmental time course of myelination and into the adult (Rasband *et al.*, 1999). Similar to contactin, Caspr is diffuse along unmyelinated PNS axons, and its localization to rodent sciatic nerve paranodes begins at P2, followed by mostly all paranodes being Caspr⁺ two days later (Fig. 15A; Rios *et al.*, 2000).

Loss of Caspr at the paranodes results in severe disruption of the paranodal domains (Fig. 15D and E; Bhat *et al.*, 2001). Mice lacking Caspr die within the first month of life due to reduction in conduction velocity, which is most likely related to the diffusion of juxtaparanodal K_v1 to the paranodes (Fig. 15C; Bhat *et al.*, 2001). Localization of Caspr to the paranodal junction requires the interaction of its cytoplasmic domain with the adaptor protein 4.1B (Gollan *et al.*, 2002; Horresh *et al.*, 2010). Extracellularly, the FNIII domain of contactin is necessary in order to transport Caspr (Faivre-Sarrailh *et al.*, 2000), and furthermore, trafficking of Caspr, in complex with contactin, to the neuronal membrane surface is mediated through a Golgi-independent pathway (Bonnon *et al.*, 2003).

Caspr2

A second member of the neurexin family, Caspr2, is clustered at the mammalian AIS and juxtaparanode (Fig. 16A; Inda *et al.*, 2006; Ogawa *et al.*, 2008;

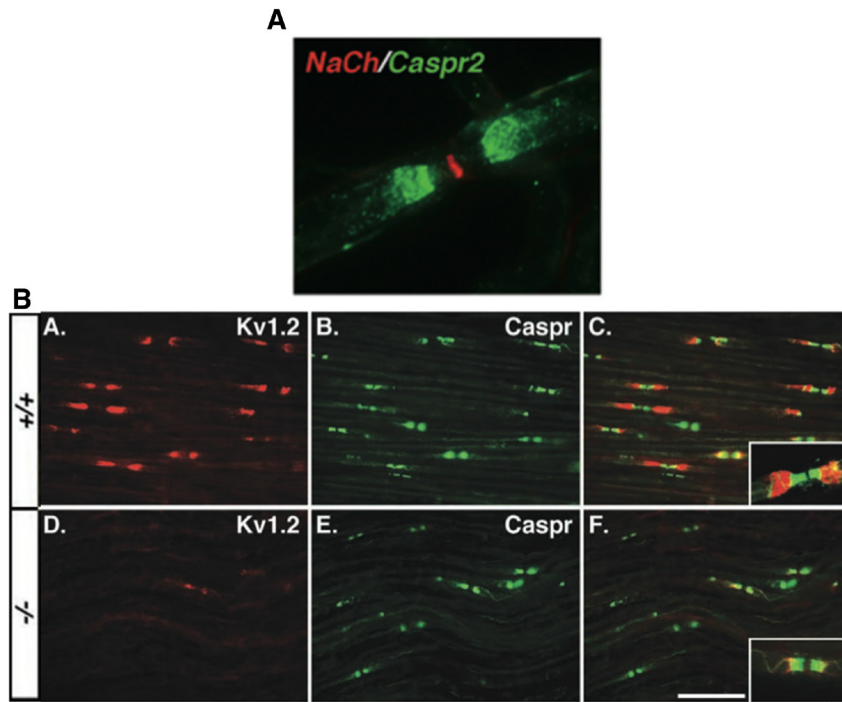


Figure 16: Expression of Caspr2 and the juxtaparanodes. **(A)** Juxtaparanodal Caspr2 (green) is separated from Pan-Nav (red) by paranodal junctions. **(B)** Caspr2 mutant mice (lower three panels) show reduction in juxtaparanodal Kv1.2 (red). **(A)** and **(B)** adapted from Poliak *et al.*, 2003.

Poliak *et al.*, 1999). In relation to Caspr, the amino acid sequence of human Caspr2 protein exhibits 45% identity to that of Caspr (Poliak *et al.*, 1999).

Caspr2 protein is detected embryonically (E15) in the CNS and is continuously expressed into the adult (Poliak *et al.*, 1999). Juxtaparanodal expression of Caspr2, together with Kv1, TAG-1, and 4.1B is observed in adult stages in rat optic nerve (Poliak *et al.*, 1999; Traka *et al.*, 2003; Denisenko-Nehrbass *et al.*, 2003), while PNS juxtaparanodal clustering of Caspr2 coincides with that of TAG-1 (Traka *et al.*, 2003)

Similar to TAG-1, Caspr2 plays an important role in clustering Kv1 to the juxtaparanode (Fig. 16B; Poliak *et al.*, 2003; Gordon *et al.*, 2014). Interestingly, Caspr2 localization to the juxtaparanode is dependent on the expression of TAG-1 (Poliak *et al.*, 2003; Traka *et al.*, 2003). *TAG-1*-null mice result in mislocalization of Caspr2; however, overall protein levels of Caspr2 are unchanged, suggesting that TAG-1 is implicated in proper targeting of Caspr2 to the juxtaparanodal domain. Results gleaned from both *TAG-1* and *Caspr2*-null mice point to the necessity of a stable ternary juxtaparanodal complex in order to target TAG-1, Caspr2, or Kv1.

1.3.3 Cytoskeletal Scaffolding Proteins

Cytoskeletal scaffolding proteins play important structural and membrane patterning roles in various cells where they tether membrane-spanning proteins to the underlying actin cytoskeleton. In regards to our discussion, two families of skeletal proteins are observed to be involved with nervous system cellular plasma membrane patterning: spectrins and ankyrins.

Spectrins form tetramers composed of heterodimerized α and β -subunits in antiparallel orientation, which are then able to tether to actin filaments through multiple accessory proteins (Bennett and Lorenzo, 2013). The mammalian α -spectrin family is comprised of two gene products (α I and α II), while β -spectrin is comprised of five (β I- β V) (Fig. 17; Bennett and Lorenzo, 2013). Expressed by neurons, α - and β -spectrins localize to various axonal domains including the AIS,

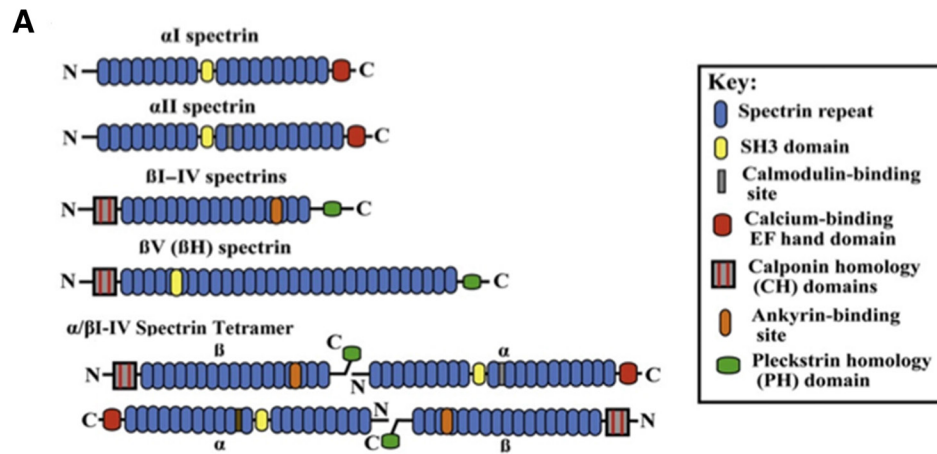


Figure 17: General structure of the spectrin family of scaffolding proteins. Adapted from Bennett and Lorenzo, 2013.

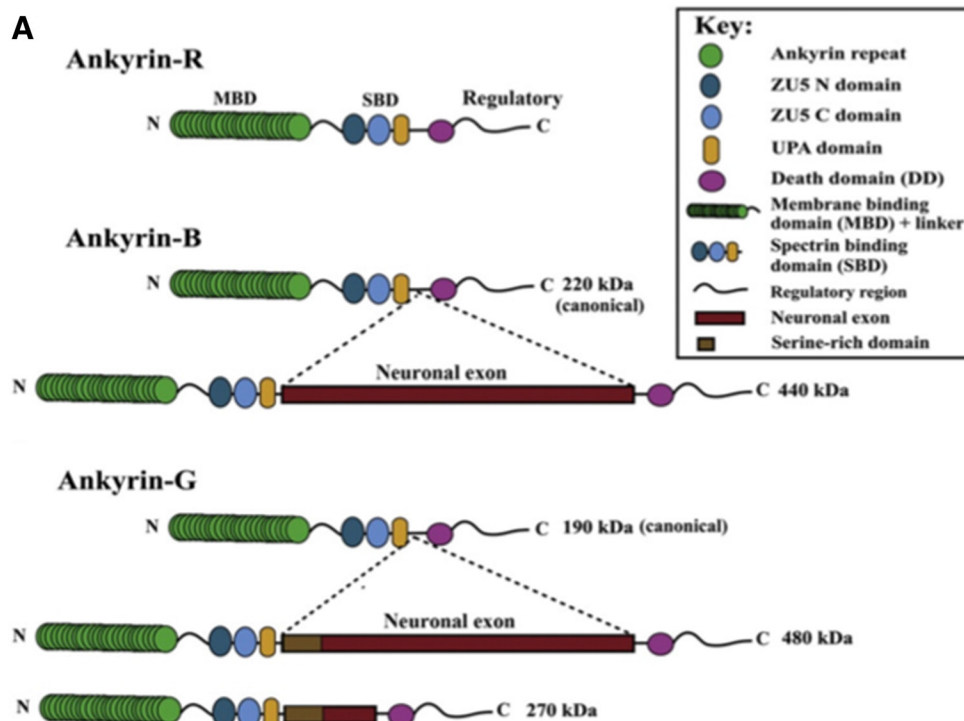


Figure 18: General structure of the ankyrin family of scaffolding proteins. Adapted from Bennett and Lorenzo, 2013.

nodes of Ranvier, and paranodes (Berghs *et al.*, 2000; Komada and Soriano, 2002; Yang *et al.*, 2004; Uemoto *et al.*, 2007; Yang *et al.*, 2007; Ho *et al.*, 2014).

Ankyrins are monomeric proteins that interact with membrane-spanning proteins through its ANK repeats and link to β -spectrins via its first ZU5 domain (Bennett and Lorenzo, 2013). As ankyrins have multiple ANK membrane binding domains (24 in total), ankyrins are able to interact with several partners and thereby allow them to form large macromolecular complexes (Bennett and Lorenzo, 2013). The ankyrin family is comprised of three *ANK* genes that encode for ankyrinR (*ANK1*), ankyrinB (*ANK2*), and ankyrinG (*ANK3*) (Fig. 18). AnkyrinG and AnkyrinB are expressed by myelinating glia and neurons at the AIS, nodes of Ranvier, and paranodes (Zhang and Bennett, 1998; Kordeli *et al.*, 2001; Ogawa *et al.*, 2006; Chang *et al.*, 2014), but recently neuronal ankyrinR, which is well described as an erythrocytic ankyrin, has also been observed to be expressed early in development at nodes of Ranvier (Ho *et al.*, 2014).

Interestingly, there appears to be specific relationships between spectrins and ankyrins in nervous system excitable domains. Typically, ankyrinR interacts with β I-spectrin, ankyrinB interacts with β II-spectrin, and ankyrinG interacts with β IV-spectrin (Bennett and Lorenzo, 2013). Together, this suggests that ankyrins and spectrins form intimately specific scaffolding complexes that ultimately aid in patterning plasma membrane domains.

1.3.3.1 Spectrins

β IV-spectrin, with its six isoforms ranging from β IV Σ 1- β IV Σ 6, is the primary spectrin associated to the AIS and nodes of Ranvier (Fig. 19A and B; Berghs *et al.*, 2000; Komada and Soriano, 2002). At the AISs of neurons in multiple mammalian brain regions, β IV-spectrin, and more specifically β IV Σ 1 and β IV Σ 6, is observed to colocalize with other AIS components such as ankyrinG, ion channels, and CAMs (Berghs *et al.*, 2000; Jenkins and Bennett, 2001; Komada and Soriano, 2002; Lacas-Gervias *et al.*, 2004; Pan *et al.*, 2006; Ogawa *et al.*, 2007). Similar to the AIS, β IV-

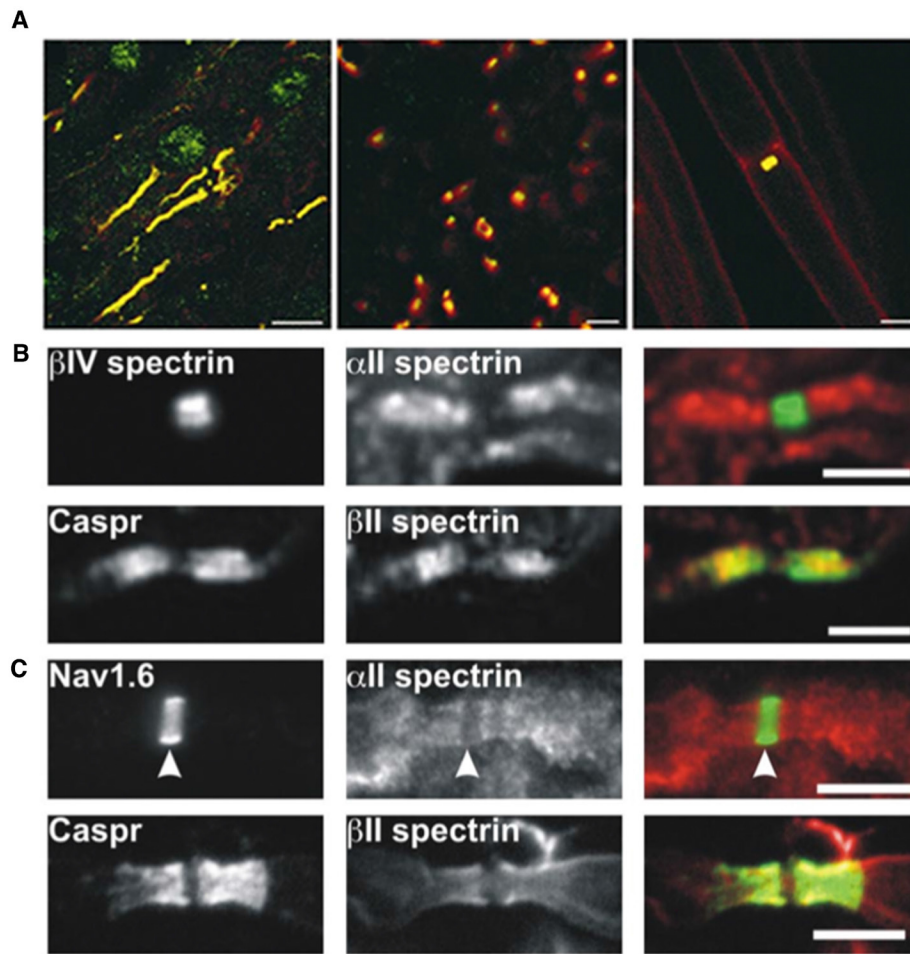


Figure 19: Immunolocalization of spectrin scaffolding proteins at excitable and perinodal domains. **(A)** β IV-spectrin (green) colocalizes with ankyrinG at the AIS (first panel) and at CNS (second panel) and PNS (third panel) nodes of Ranvier. Adapted from Berghs *et al.*, 2000. B and C: α II and β II-spectrin (red) localize to the paranodes of CNS **(B)** and PNS **(C)** axons. Adapted from Ogawa *et al.*, 2006.

spectrin colocalizes with various nodal components in rodent PNS and CNS fibers (Berghs *et al.*, 2000; Komada and Soriano, 2002).

β IV-spectrin-null, *SPNB4^{qv3J/qv3J}* (a β IV-spectrin mutant called “quivering” or “qv^{3J}”, which has a mutation in the C-terminal domain of β IV-spectrin splice variants), and *β IV Σ 1-spectrin*-null mice exhibit neuromuscular defects and disintegration of AIS components, suggesting that β IV-spectrin plays an important role at the AIS (Komada and Soriano, 2002; Parkinson *et al.*, 2001; Yang *et al.*, 2004; Lacas-Gervias *et al.*, 2004). Yet, its localization to the AIS and nodes of Ranvier depends on ankyrinG (Yang *et al.*, 2007; Jenkins *et al.*, 2015), and more specifically serine 2417 of ankyrinG to localize to the AIS (Jenkins *et al.*, 2015).

A complex of α II-spectrin and β II-spectrin form a functional tetramer that is expressed at the paranodes in adult rodent PNS and CNS fibers (Fig. 19C; Bennett and Baines, 2001; Ogawa *et al.*, 2006). Rodent PNS expression of this complex along with other paranodal components starts at P2 and becomes clustered at further more sites throughout the myelination process (Ogawa *et al.*, 2006). CNS paranodal clustering of α II-spectrin and β II-spectrin in rodent optic nerve appear at P8 and also become further clustered at later time points (Ogawa *et al.*, 2006). Additionally, α II-spectrin/ β II-spectrin coclusters with other paranodal components such as 4.1B and Caspr (Ogawa *et al.*, 2006). At the paranodes, β II-spectrin maintains the restriction barrier between juxtaparanodal K_v1 and nodal Na_v (Zhang *et al.*, 2013).

Recently, super-resolution imaging of rat hippocampal axons has revealed that rod-like α II-spectrin/ β II-spectrin tetramers link to regularly spaced rings of actin to form a cylindrically caged structure (Xu *et al.*, 2013). Lastly, and in association with the AIS, α II-spectrin and β II-spectrin (along with ankyrinB) are also involved in AIS assembly. Here, these scaffolding proteins form a distal submembraneous axonal boundary that restricts ankyrinG to the proximal axon, which ultimately plays a role in maintaining neuronal polarity (Galiano *et al.*, 2012; for a review, see Chang and Rasband, 2013).

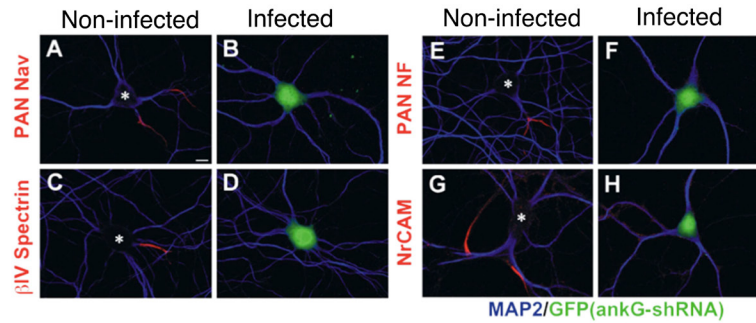


Figure 20: AnkyrinG maintains AIS components. (A) Infection of hippocampal cultures with an ankyrinG shRNA lentivirus reduces clustering of AIS components. Asterisks denote the cell body. Adapted from Hedstrom *et al.*, 2008

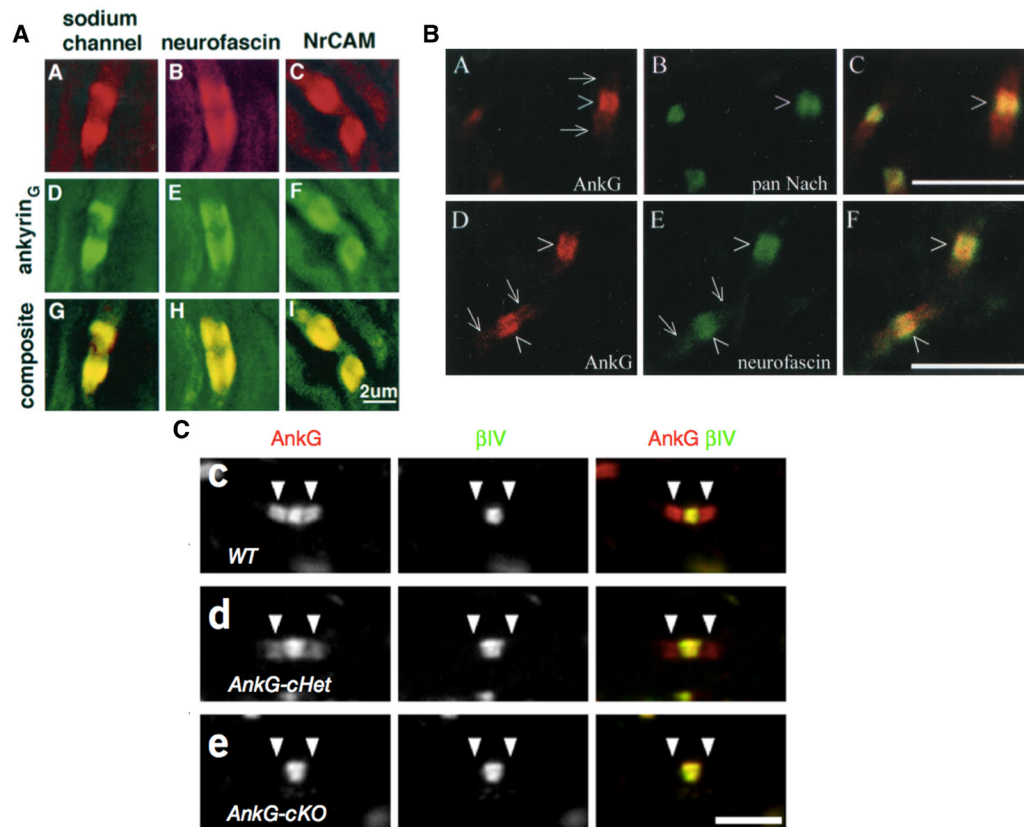


Figure 21: AnkyrinG is a nodal and paranodal component. (A) AnkyrinG coclusters with nodal components in PNS nodes of Ranvier. Adapted from Lambert *et al.*, 1997. (B) CNS nodes of Ranvier contain nodal and paranodal ankyrinG. Adapted from Jenkins and Bennett, 2002. (C) Knockout of ankyrinG in glial cells shows that ankyrinG is a glial component of the CNS paranodes. Adapted from Chang *et al.*, 2014.

1.3.3.2 Ankyrins

AnkyrinG

In the mammalian nervous system, AnkyrinG is the predominant ankyrin subtype that is present at excitable domains. AnkyrinG has several splice isoforms: 480-kDa, 270-kDa, and 190-kDa. 480-kDa ankyrinG is expressed only in neurons (Kordeli *et al.*, 1995; Jenkins *et al.*, 2015), 270 kDa-ankyrinG is expressed in both neurons and oligodendrocytes (Kordeli *et al.*, 1995; Chang *et al.*, 2014; Jenkins *et al.*, 2015), and 190-kDa ankyrinG is expressed primarily in oligodendrocytes and possibly in neurons (Chang *et al.*, 2014; Jenkins *et al.*, 2015). Through raising antibodies against the serine-rich and spectrin binding domains of ankyrinG, Kordeli (1995) observed that both 480-kDa and 270-kDa ankyrinGs were immunolocalized to the AISs of several brain regions including the spinal cord and hippocampus. Subsequent studies have shown that ankyrinG is enriched in various other regions of the mammalian brain where it interacts with AIS components such Nfasc186, NrCAM, Na_v channels, K_v channels, and β IV spectrin (Zhou *et al.*, 1998; Jenkins and Bennett, 2001; Garrido *et al.*, 2003; Lemaillet *et al.*, 2003; Pan *et al.*, 2006; Dzhashiashvili *et al.*, 2007; Hedstrom *et al.*, 2007, 2008; Gasser *et al.*, 2012; Sánchez-Ponce *et al.*, 2012; Le Bras *et al.*, 2014); however, the timing of which components arrives first to the AIS is only partially understood. However, what we clearly do know though is that ankyrinG plays important roles at the AIS including neuronal excitability (Zhou *et al.*, 1998), AIS construction and maintenance (Fig. 20; Zhou *et al.*, 1998; Jenkins and Bennett, 2001; Dzhashiashvili *et al.*, 2007; Hedstrom *et al.*, 2007, 2008; Yang *et al.*, 2007; Galiano *et al.*, 2012; Le Bras *et al.*, 2014; Jenkins *et al.*, 2014), and maintenance of neuronal polarity (Hedstrom *et al.*, 2008; Sobotzik *et al.*, 2009).

Further along the axon, ankyrinG also clusters at PNS and CNS nodes of Ranvier, and at CNS paranodes (Fig. 21A-C; Kordeli *et al.*, 1995; Lambert *et al.*, 1997; Rasband *et al.*, 1999; Jenkins and Bennett, 2001, 2002; Chang *et al.*, 2014). Prior to myelination in the PNS, ankyrinG (480-kDa and 270-kDa) is expressed in a continuous distribution along the axon (Fig. 21A; Lambert *et al.*, 1997). As

myelination begins around P2 in the sciatic nerve, ankyrinG can be observed as clusters alongside MAG⁺ Schwann cell segments (Lambert *et al.*, 1997). Importantly, the clustering of ankyrinG is typically after Nfasc186 and NrCAM in the sciatic nerve (Lambert *et al.*, 1997), and further confirms that PNS nodal assembly begins with the recruitment of axonal CAMs, followed by that of ankyrinG and Na_v (see section on PNS nodal assembly).

AnkyrinG clustering in the rodent optic nerve begins as early as P9 and continues into adult stages (Fig. 21B; Jenkins and Bennett, 2001). Additionally, ankyrinG is observed to cluster at the nodes in several regions and in various cell types of the mammalian brain. At the nodes of Ranvier, ankyrinG interacts with several nodal components such as Na_v, Nfasc186, NrCAM, K_v and β IV spectrin (Jenkins and Bennett, 2001; Malholtra *et al.*, 2002; Garrido *et al.*, 2003; Barry *et al.*, 2014; Davis *et al.*, 1996; Pan *et al.*, 2006; Xu *et al.*, 2010; Yang *et al.*, 2007).

Paranodal ankyrinG is observed in the CNS contrary to the PNS where it is expressed by oligodendrocytes as the 190-kDa isoform (Fig. 21C; Rasband *et al.*, 1999; Jenkins and Bennett, 2001; Chang *et al.*, 2014). This paranodal oligodendroglial ankyrinG isoform appears at P7 in the optic nerve and continues to remain at the paranodes until at least P22 (Chang *et al.*, 2014). Loss of glial ankyrinG results in a delay in paranodal junction formation (Chang *et al.*, 2014). As ankyrinG interacts with Nfasc155, paranodal ankyrinG is most likely involved in the early assembly of CNS paranodes (Chang *et al.*, 2014).

AnkyrinB

Similar to ankyrinG, ankyrinB also has several splice isoforms of 440-kDa and 220-kDa sizes. Along unmyelinated axons, ankyrinB is expressed diffusely similar to that of ankyrinG (Chan *et al.*, 1993; Kunitomo, 1995). Expression of ankyrinB appears to be well restricted to developing and adult PNS paranodes and occasionally to adult CNS paranodes (Ogawa *et al.*, 2006; Chang *et al.*, 2014). During development, clustering of ankyrinB appears after that of Caspr in the PNS where it is only partially colocalized (Ogawa *et al.*, 2006). AnkyrinB

immunocolocalizes and interacts with α II-spectrin/ β II-spectrin and protein 4.1B, where it most likely forms a paranodal cytoskeletal complex (Ogawa *et al.*, 2006).

Even though ankyrinB is primarily observed in PNS paranodes, ankyrinB has been observed to become enriched at CNS paranodal junctions in glial *Ank3*-deficient mice. Here, ankyrinB compensates for ankyrinG loss, and provides, although minimal, improvement in CNS paranodal junction formation (Chang *et al.*, 2014).

AnkyrinR

The most recent ankyrin to be observed at the node of Ranvier is the erythrocyte ankyrin, ankyrinR. AnkyrinR is immunolocalized during the first two weeks at sciatic nerve nodes of Ranvier, but the amount of ankyrinR⁺ nodes declines precipitously by P30 (Ho *et al.*, 2014). In contrast, there are very few ankyrinR⁺ nodes of Ranvier in the CNS (Ho *et al.*, 2014). While ankyrinR immunoreactivity declines at adult PNS or CNS nodes, the level of ankyrinR mRNA remains the same in the adult (Ho *et al.*, 2014). Interestingly, ankyrinR, together with its scaffolding partner β I-spectrin, become highly colocalized to adult PNS and CNS nodes of Ranvier when ankyrinG is completely lost, and may likely play a role in rescuing the nodal complex (see chapter III; Ho *et al.*, 2014).

1.3.4 Other scaffolding molecules

Protein 4.1

The protein 4.1 family consists of five members (4.1B, 4.1G, 4.1N, 4.1O, 4.1R) that contain a spectrin/actin binding domain and a CAM-interacting FERM domain (Baines *et al.*, 2014). Axonal 4.1B is enriched at paranodes and juxtaparanodes (Poliak *et al.*, 2001; Gollan *et al.*, 2002; Denisenko-Nehrbass *et al.*, 2003), while Schwann cell 4.1G is enriched in the internodes (Ohno *et al.*, 2006; Ivanovic *et al.*, 2012).

Loss of 4.1G results in mislocation of juxtaparanodal proteins (Ivanovic *et al.*, 2012). *4.1B*-deficient mice have rather normal paranodes, but have severely affected

juxtaparanodes (Horresh *et al.*, 2010; Cifuentes-Diaz *et al.*, 2011; Einheber *et al.*, 2013). While controversial (Buttermore *et al.*, 2011), there appears to be an upregulation of 4.1R, the erythrocyte protein 4.1, at paranodes in the absence of 4.1B (Horresh *et al.*, 2010; Einheber *et al.*, 2013). This upregulation of erythrocytic cytoskeletal components in neurons appears to be an interesting redundancy mechanism by which they may partially rescue the loss of neuronal cytoskeletal molecules. It would be interesting to see the timing of 4.1R expression in developing PNS paranodes to see if may be highly expressed early on and decline thereafter, similar to that of ankyrinR at nodes of Ranvier (Ho *et al.*, 2014).

1.3.5 Schwann Cell Microvilli and Extracellular Matrix (ECM) Proteins

The intimate location of Schwann cell microvilli in relation to the nodal axolemma suggests that they are involved in molecular interactions with the PNS nodes of Ranvier. Indeed, several proteins secreted by the Schwann cell microvilli or proteins associated to the Schwann cell microvilli plasma membrane are observed to be coimmunolocalized with PNS nodal components. Proteins of the ezrin/radixin/moesin (ERM) and olfactomedin families can be restricted to or secreted from microvillar processes, respectively. Because CNS nodes lack Schwann cells and microvilli, these proteins are not found at the CNS nodes, and therefore highlight how PNS and CNS ultrastructural differences ultimately impact the molecular structure of the nodes of Ranvier.

However, shared between both PNS and CNS nodes of Ranvier is an extracellular matrix (ECM) that acts as a cation reservoir through the negative charges located on sulfate proteoglycans enriched at the nodal ECM. Several families of ECM molecules have been observed to cluster at PNS and CNS nodes, particularly sulfated proteoglycans, tenascins, and link proteins.

1.3.5.1 Schwann Cell Microvilli

ERM Family

The ERM proteins are plasma membrane associated proteins that are enriched in the microvilli of several cell types such as epithelial cells and Schwann

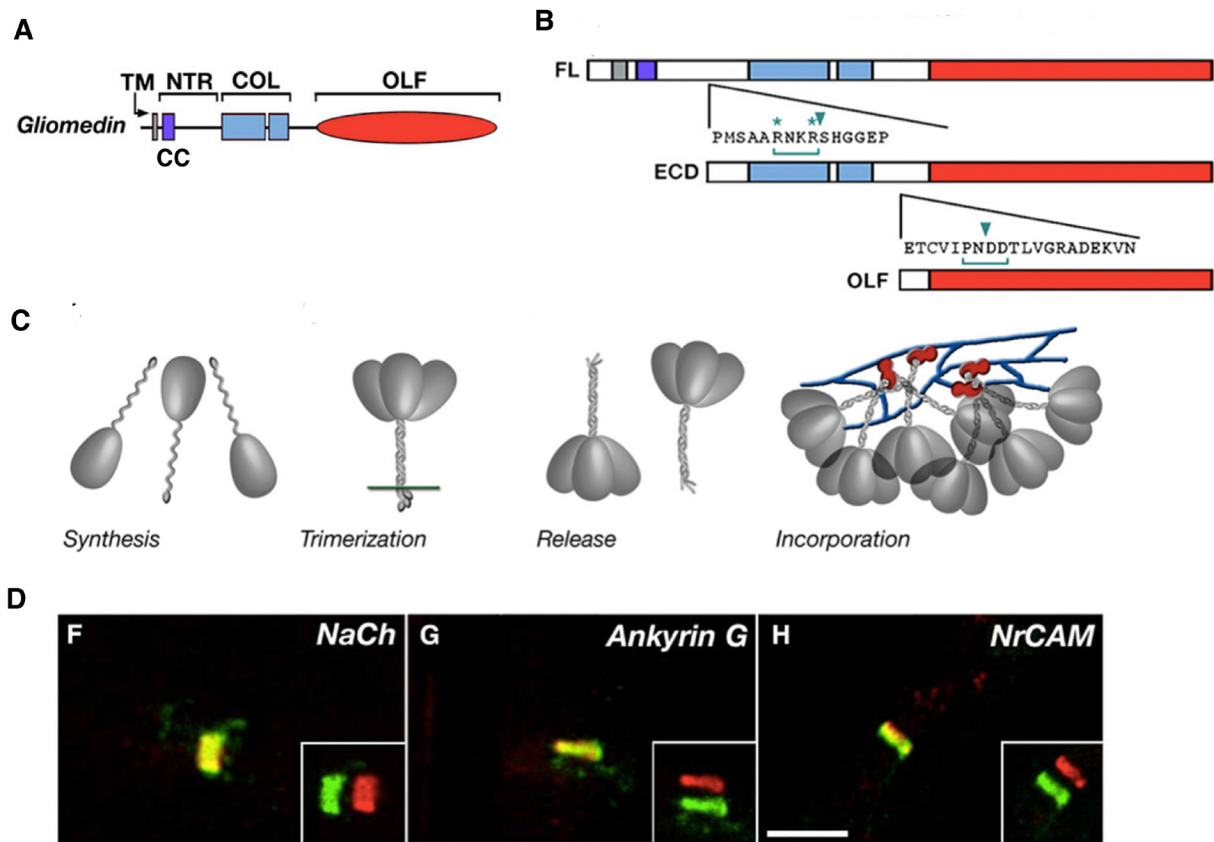


Figure 22: Gliomedin structure, cleavage sites, and immunolocalization in the PNS. **(A)** Gliomedin contains and extracellular olfactomedin (OLF) and interrupted collagen repeats (COL), followed by an N-terminal region (NTR), coiled-coiled domain (CC), and transmembrane domain (TM). **(B)** Cleavage of gliomedin produces a fragment lacking the CC and TM (ECD) and another lacking the interrupted collagen repeats (OLF). Arrowheads represent cleavage sites. **(C)** Model for gliomedin accumulation at the nodes of Ranvier in the PNS. **(A-C)** Adapted from Eshed *et al.*, 2007. **(D)** Colocalization of gliomedin (green) with various nodal components (red). Adapted from Eshed *et al.*, 2005.

cells (Berryman *et al.*, 2003). In Schwann cells, ERM proteins, and the ERM binding protein EBP50, are in association with actin and cluster at developing and adult rodent PNS nodes of Ranvier (Melendez-Vasquez *et al.*, 2001; Gunn-Moore *et al.*, 2006; Scherer *et al.*, 2001). Further roles of ERM proteins in relation to PNS nodes of Ranvier have yet to be elucidated.

Olfactomedin Family

The olfactomedin family of proteins is structurally characterized by an extracellular olfactomedin domain, followed by a coiled-coil sequence that allows for oligomerization (Anholt *et al.*, 2014). Two secreted Schwann cell olfactomedin family members, gliomedin and myocilin, have been reported to cluster at PNS nodes of Ranvier (Eshed *et al.*, 2005; Kwon *et al.*, 2013).

The expression of gliomedin is exclusive to the PNS node of Ranvier and it is strictly glial (Eshed *et al.*, 2005). In the developing PNS node, gliomedin is observed at the edges of each myelinating Schwann cell segment where it colocalizes with other nodal components (Fig. 22D) prior to paranodal Caspr clustering (Eshed *et al.*, 2005). Interestingly, in P1 rat sciatic nerve, gliomedin is occasionally observed to cluster prior to Na_v, but it is always coclustered with Nfasc186 (Eshed *et al.*, 2005). This suggests that gliomedin, in addition to Nfasc and NrCAM, is one of the first nodal components in the PNS.

Gliomedin is found in a transmembrane and a 91-kDa secreted form (Fig. 22B) mediated via furin-dependent proteolytic cleavage [note: a 45-kDa secreted fragment also exists, where it is cleaved bone morphogenic protein/Tolloid-like metalloproteinases, but this form is much less understood; (Maertens *et al.*, 2007; Eshed *et al.*, 2007)]. Prior to proteolytic cleavage, gliomedin trimerizes through its collagen domain on the extracellular surface (Fig. 22C; Eshed *et al.*, 2007). Following trimerization, furin cleavage liberates the trimer in order to be incorporated to the ECM by binding heparan sulfate proteoglycans (HSPGs) (Fig. 22C; Eshed *et al.*, 2007). While incorporated to the perinodal space, gliomedin can

then interact with various nodal molecules such as NrCAM and Nfasc186 through its olfactomedin domain (Eshed *et al.*, 2005). Stabilization of gliomedin to the Schwann cell microvilli depends on NrCAM (Feinberg *et al.*, 2010). The functional roles of gliomedin will be greatly discussed in chapter III.

Like gliomedin, myocilin is expressed in Schwann cell microvilli and is localized to adult rodent PNS nodes of Ranvier where it colocalizes with gliomedin (Kwon *et al.*, 2013). Indeed, the N-terminal non-olfactomedin containing fragment of myocilin is able to physically interact with gliomedin, and additionally with NrCAM and Nfasc186 (Kwon *et al.*, 2013). Further interactions and roles of myocilin and other proteins of olfactomedin family with respect to the nodes of Ranvier remain elusive.

1.3.5.2 ECM

Sulfated Proteoglycans: HSPGs, CSPGs, and mixed HSPG/CSPGs

Proteoglycans are a family of proteins with a structural proteinaceous core comprised of N-terminal Ig-domains, FNIII-domains, and EGF-like domains. Additionally, the core contains covalently attached sulfated glycosaminoglycan side chains made of repeating disaccharide units. Differentiating these proteoglycans depends on the type of sulfated sidechain (Margolis and Margolis, 1994). In the nervous system, three classes of proteoglycans have been observed at excitable domains: HSPGs, chondroitin sulfate proteoglycans (CSPGs), and mixed HSPG/CSPGs.

The HSPGs located at early and adult rodent PNS nodes of Ranvier include agrin (Colombelli *et al.*, 2015), syndecan-3 (along with its ligand Collagen-V; Goutebroze *et al.*, 2003; Melendez-Vasquez *et al.*, 2005) and syndecan-4 (Goutebroze *et al.*, 2003). Agrin is recruited by the nodal-enriched transmembrane glycoprotein dystroglycan (Colombelli *et al.*, 2015; Saito *et al.*, 2003; Occhi *et al.*, 2005), while syndecan-3 and -4 are most likely linked through ezrin (Tkachenko *et al.*, 2005). Versican-V1 and NG2, members of the CSPG family, are located at early rodent PNS nodes (Melendez-Vasquez *et al.*, 2005; Martin *et al.*, 2001). Recently, the

gliomedin-binding mixed HSPG/CSPG (note: “mixed” HSPG/CSPG means that the protein can have both or either sulfated glycosaminoglycan side chains) Perlecan has been observed to cluster at rodent PNS nodes of Ranvier by recruitment via dystroglycan (Oochi *et al.*, 2005; Colombelli *et al.*, 2015).

In the CNS, the CSPGs NG2, Versican-V2, Phosphacan, and the lectin family CSPGs Brevican and Neurocan are clustered at rodent nodes of Ranvier (Melendez-Vasquez *et al.*, 2005; Weber *et al.*, 2009; Dours-Zimmerman *et al.*, 2009; Bekku *et al.*, 2009; Bekku *et al.*, 2010; Susuki *et al.*, 2013). The CNS ECM molecules phosphacan and tenascin-R are both aberrantly localized to smaller-diameter axons in Brevican-deficient mice, wherein they normally are found in association with larger diameter axons (Bekku *et al.*, 2009).

AIS enrichment of the CSPGs Versican, Brevican, Neurocan, and Aggrecan has also been observed in perineuronal nets surrounding GABAergic interneurons (John *et al.*, 2006, Hedstrom *et al.*, 2007). Particularly, knockdown of Nfasc186 in rat hippocampal cultures results in loss of Brevican at the AIS (Hedstrom *et al.*, 2007), implying that NF186 is important in setting up certain components of the AIS ECM.

Tenascins

The structure of the tenascin family of ECM proteins is comprised of a signal sequence and a cysteine-rich region on the aminoterminal end, followed by EGF repeats, FNIII-repeats, and lastly fibrinogen-like repeats (Chiquet-Ehrismann *et al.*, 1994). Of the five members of the tenascin family, only two have been reported to be enriched in PNS and CNS nodes of Ranvier. Interactions of tenascins with nodal components include contactin, β 2Nav, and Nfasc186 (Pesheva *et al.*, 1993; Srinivasan *et al.*, 1998; Volkmer *et al.*, 1998).

Schwann cells secrete tenascin-C/Cytotactin, which ultimately clusters at PNS nodes of Ranvier (Reiger *et al.*, 1986). On the other hand, tenascin-R (otherwise called J1-160/180), which is secreted by oligodendrocytes during myelination (Bartsch *et al.*, 1993), is clustered at the CNS nodes of Ranvier (Ffrench-Constant *et al.*, 1986), and is enriched in perineuronal nets at the AIS of

GABAergic interneurons (Brückner *et al.*, 2006). Mice deficient in tenascin-R result in the loss of the phosphacan and altered axonal conduction velocity (Weber *et al.*, 1999).

Link Proteins

Link proteins are hyaluronan-binding proteins that play a role in stabilizing hyaluronan complexes. One link protein in particular, Brain-specific hyaluronan-binding link protein (Bral1), has been observed to be clustered at developing and adult rodent CNS nodes of Ranvier in conjunction with negatively charged ECM components (Oohashi *et al.*, 2002; Bekku *et al.*, 2010). Bral1 also interacts with Nfasc186 (Susuki *et al.*, 2013). Importantly, *Bral1*^{-/-} mice display a loss of various other ECM molecules such as Versican-V2, Brevican, tenascin-R, Hyaluronan, and Neurocan (Bekku *et al.*, 2010; Susuki *et al.*, 2013). However, there is a strong reduction of Bral1 in Versican-deficient and Versican/Brevican-deficient mice (Susuki *et al.*, 2013). Ultimately, these results shed light on an important role of a ternary complex of Bral1, Versican, and Brevican in linking and stabilizing the components of the nodal ECM.

1.3.6 Signaling Molecules

One interesting signaling molecule in particular that has been observed at the AIS and nodes of Ranvier is CK2. CK2 is a serine/threonine kinase tetramer that is composed of two catalytic α -subunits and two regulatory β -subunits (Meggio and Pena, 2003). *In vivo*, CK2 restricts to the AIS in a majority of cells of various brain regions, and also to PNS and CNS nodes of Ranvier (Bréchet *et al.*, 2008). CK2 functions to phosphorylate serine residues on Na_v channels, and thereby allow Na_v to interact with ankyrinG. Yet, Na_v1 also has a reciprocal relationship with CK2, in that Na_v1 is necessary in order for CK2 to be enriched at the AIS (Hien *et al.*, 2014). Furthermore, interaction of ankyrinG with IQCJ-SCHIP-1 (IQ Motif Containing J-Schwannomin Interacting Protein 1) is permitted through CK2 phosphorylation, where this association is implicated in AIS maintenance (Papandréou *et al.*, 2015).

Protein	Location	Extracellular Domain	Function
Na _v 1.1	AIS, PNS & CNS noR	Yes	Ion Channel Subunit
Na _v 1.2	AIS, PNS & CNS noR	Yes	Ion Channel Subunit
Na _v 1.6	AIS, PNS & CNS noR	Yes	Ion Channel Subunit
β1Na _v	AIS, PNS & CNS noR	Yes	Ion Channel Subunit
β2Na _v	AIS, PNS & CNS noR	Yes	Ion Channel Subunit
β4Na _v	AIS, PNS & CNS noR	Yes	Ion Channel Subunit
K _v 1.1/K _v 1.2	AIS, PNS & CNS JXP	Yes	Ion Channel Subunit
K _v 3.1	PNS & CNS noR	Yes	Ion Channel Subunit
K _v 7.2/K _v 7.3	AIS, PNS & CNS noR	Yes	Ion Channel Subunit
Neurofascin140		Yes	CAM
Neurofascin155	PNS & CNS PN	Yes	CAM
Neurofascin186	AIS, PNS & CNS noR	Yes	CAM
NrCAM	AIS, PNS & CNS noR	Yes	CAM
Contactin	PNS & CNS PN and CNS noR	Yes	CAM
TAG-1 (Contactin2)	AIS, PNS & CNS JXP	Yes	CAM
Caspr/Paranodin	AIS, PNS & CNS PN	Yes	CAM
Caspr2	AIS, PNS & CNS JXP	Yes	CAM
αII-Spectrin	AIS, PNS & CNS PN	No	Scaffolding Protein
βII-Spectrin	AIS, PNS & CNS PN	No	Scaffolding Protein
βIV-Spectrin	AIS, PNS & CNS noR	No	Scaffolding Protein
AnkyrinG	AIS, PNS & CNS noR, CNS PN	No	Scaffolding Protein
AnkyrinB	CNS & PNS PN	No	Scaffolding Protein
AnkyrinR	PNS & CNS noR	No	Scaffolding Protein
Protein4.1B	PNS & CNS PN & JXP	No	Scaffolding Protein
ERM	PNS noR	No	Scaffolding Protein
Gliomedin	PNS noR	Yes	ECM Protein
Myocilin	PNS noR	Yes	ECM Protein
Syndecan-3 and 4	PNS noR	Yes	ECM Protein
Versican V1	PNS noR	Yes	ECM Protein
Versican V2	CNS noR	Yes	ECM Protein
NG2 proteoglycan	CNS noR	Yes	ECM Protein
Perlecan	PNS noR	Yes	ECM Protein
Brevican	AIS & CNS noR	Yes	ECM Protein
Neurocan	CNS noR	Yes	ECM Protein
Phosphacan	CNS noR	Yes	ECM Protein
Aggrecan	CNS noR	Yes	ECM Protein
Tenascin-R	AIS & CNS noR	Yes	ECM Protein
Tenascin-C	PNS noR	Yes	ECM Protein
Agrin	PNS noR	Yes	ECM Protein
Dystroglycan	PNS noR	Yes	ECM Protein
Brall	CNS noR	Yes	ECM Link Protein
CK2	AIS, PNS and CNS noR	No	Signaling Molecule

Figure 23: Summary of ion channels, cellular-adhesion molecules (CAMs), cytoskeletal scaffolding proteins, extracellular matrix (ECM) molecules, and signaling molecules and their subcellular distribution along axons in the PNS and CNS. Abbreviations: AIS = axon initial segment; noR = nodes of Ranvier; PN = Paranode; JXP = juxtaparanode; PNS = peripheral nervous system; CNS = central nervous system.

In conclusion, the extraordinary advances that have been made since the first descriptions by Ranvier and those of his contemporaries in regards to the myelinated nerve are staggering. The various physical and functional interactions between the myelinating glial cell and the axon, coupled with the large repertoire of proteins shared between the AIS, and the nodal and perinodal regions lends itself to an incredible degree of complexity (for a summary see the table in Figure 23). Indeed, these complex interactions give rise to important functions, in particular action potential conduction. Having taken a *bottom-up* approach to the description of the ultrastructural components and molecular composition of the nodes Ranvier, we will now take our discussion towards the role of the nodes of Ranvier in electrogenic conduction.

Chapter II: Action Potential Conduction Along Myelinated Fibers in Healthy and Diseased States

The rapid and efficient propagation of action potentials along nervous fibers is an important necessity to animals since they need to interact with and react to the environment with timeliness and precision. If the proper signals are not relayed quickly or systematically, especially in a life or death or predator and prey situation, the resultant could present the animal with the scales tipped out of its favor. Therefore, it is of the upmost importance that nervous signals be fast and reliable.

Our understanding of how the nervous signal is propagated along axonal fibers primarily comes from experiments performed on unmyelinated axons, which ultimately lends itself to better understanding of conduction timing along myelinated axons. Hence, this chapter will begin with how APs are propagated along unmyelinated fibers, which will then be followed by conduction along myelinated axons. Lastly, the discussion will move towards conduction along axons in the demyelinated state, particularly that of a detrimental demyelinating disease in the CNS, multiple sclerosis.

2.1 Signal Conduction Along Unmyelinated Axons

The propagation of the action potential in both the CNS and PNS occurs along the axons of neurons. Its initiation occurs at the AIS through Na_v permitting entry of depolarizing current in the form of Na^+ ions that will then spread passively along to the next segment of axonal membrane leading the active region (Hodgkin and Huxley, 1952; Palmer and Stuart, 2006). The following region reaches threshold, and Na_v channels open to allow for rapid inward Na^+ current that will then continue to charge adjacent membrane to threshold (Fig. 24A and B; Debanne *et al.*, 2011). In the regions trailing the AP, there is an efflux of K^+ from the

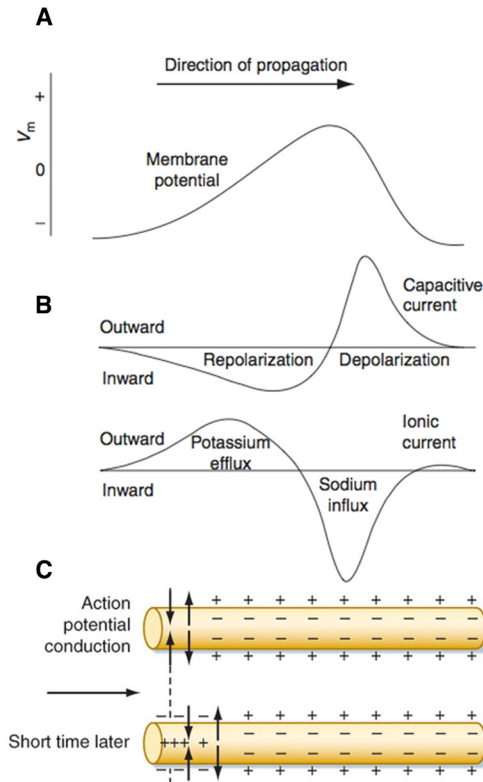


Figure 24: Action potential conduction along unmyelinated fibers. **(A)** Changes in the membrane potential during the upstroke and repolarizing phases of the action potential. **(B)** Capacitive and ionic currents underlying the action potential. Adapted from Caldwell, 2009. **(C)** Action potential conduction along unmyelinated axons is slow due to the leaking of ionic current and high membrane capacitance. Adapted from Berne and Levy Physiology 6th edition, 2008.

activation of K_v channels with concurrent Na_v inactivation (Fig. 24B). The action of K_v channels will actually hyperpolarize the membrane and then slowly deactivate bringing the patch of axonal membrane back to its resting potential (Fig. 24A and B; Debanne *et al.*, 2011). At this state, Na_v are deinactivated and then become deactivated, where they will then be ready to reengage in depolarizing the axonal membrane and propagating the nervous signal (Bean, 2007). Once the nerve signal is propagated it regenerates continuously along the axonal membrane (Fig. 24C) and then reaches the synaptic terminals where it releases neurotransmitters to transfer information to the following neuron.

Above describes a general overview of how the AP is spread from its initiation at the AIS down its length to the synaptic terminals. However, we should look more closely at the biophysical characteristics as to how the action potential spreads from its initiation point to the following region of axonal membrane. In order for this adjacent region to reach threshold and regenerate the AP, the regeneration is dependent on how fast the membrane is able to charge, which is determined by the membrane capacitance (how much charge is stored on the axonal membrane per unit area) and the axial resistance (how resistant the exterior medium and interior axonal medium are to the flow of electrical current). If the charging is quick, then the AP will be rapidly regenerated, but the inverse will occur if charging is slow. What governs how quickly the membrane will be able to charge?

Factors involved in how quickly the membrane will charge in unmyelinated axons are characterized by either a reduction in the membrane capacitance or a reduction in the internal axial resistance (Hartline and Colman, 2007). In the case of the unmyelinated axon, the only physiological means for increasing how fast the membrane will charge, and consequentially increasing conduction velocity, is through reducing the internal axial resistance (Hartline and Colman, 2007). This reduction in the internal axial resistance is achieved through increasing the diameter of the axon. Here, an increase in the axonal diameter reduces the resistivity Na^+ ions must face as they passively spread through the axoplasm. Indeed, it has been experimentally shown that insertion of an axial wire electrode

in squid giant axons increases conduction velocity by short-circuiting the axonal longitudinal resistance (Castillo and Moore, 1959). Accordingly, the action potential conduction velocity in unmyelinated axons is generally described from theoretical calculations to be proportional to the square root of the axonal diameter (Hursh, 1939; Rushton, 1951; Hodgkin, 1954); however, this is not a hard and fast rule since this value varies in several species (Pumphrey and Young, 1938; Abbot *et al.*, 1958; Gasser, 1950) and conduction velocity can be altered by several other means (see below).

Several factors may also change the speed by which the nervous signal is propagated along unmyelinated axons (note: the following factors also play a role in conduction velocity along myelinated neurons, but many other factors untranslatable to the unmyelinated axon affect the myelinated nerve, see below). For example, decrease in temperature will slow the rate in which Na_v will open or close and can result in conduction failure, while an increase in temperature would reduce the half width of the action potential and thus speed up conduction (Hodgkin and Katz, 1949; Franz and Iggo, 1968; Swadlow *et al.*, 1981). Blockage of Na_v through pharmacological drugs, such as tetrodotoxin (Colquhoun and Ritchie, 1972), will obviously reduce conduction velocity since less current will be available to enter and charge the axonal membrane. Furthermore, a decrease in extracellular ion concentration will decrease conduction velocity (Katz, 1947). Increase of voltage-gated ion channels will improve conduction speeds, but there is a limit on sodium channel density since too high of a Na_v channel density will add to the membrane capacitance (Hodgkin, 1975).

Conduction velocity measurements along unmyelinated vertebrate CNS axons has only until recently been achieved through electrophysiological means. Dual soma-axon patch clamp recordings where investigators patch both the soma and the cut end of the axon in slice cultures (called an axon “bleb”) show that orthodromic (direction of the AP from the AIS toward axon terminals) conduction velocity along these axons is quite slow (for review see Kress and Mennerick, 2009). Rat mossy-fiber axons, dentate granule neurons, and Schaffer collaterals propagate

APs around 0.25 ms^{-1} (Andersen *et al.*, 2000; Kress *et al.*, 2007, 2008; Schmidt-Hieber *et al.*, 2008), layer 5 pyramidal neurons propagate APs at $\sim 0.4 \text{ ms}^{-1}$, and CA3 pyramidal neurons between 0.2 and 0.3 ms^{-1} (Soleng *et al.*, 2003; Meeks and Mennerick, 2007). All together, these experimental results suggest that in the CNS unmyelinated fibers propagate action potentials at relatively low speeds.

2.2 Signal Conduction Along Myelinated Axons

While increasing axonal diameter is a viable solution for rapid axonal conduction, it also comes at a price in terms of space constraints and energetics. For vertebrates, it appears as though this particular option would be insufficient. Vertebrates are limited in space due to their CNS being enclosed inside the skull and vertebral column, and the increased diameter without decreased capacitance increases the concentration of ions flowing in and out of the axon. Maintaining the extracellular Na^+ and intracellular K^+ ion gradient, mediated through the action of Na^+/K^+ pumps, is energetically costly and would be inefficient (Arancibia-Carcamo and Attwell, 2014). Therefore, what is the mechanism by which vertebrates overcome these challenges for rapidly propagation?

Myelination is the alternative solution in vertebrates permitting rapid AP propagation. The sheath works by increasing the local resistance of the region covered by myelin wrapping and also reduces the capacitance of the axonal membrane in conjunction with nodes of Ranvier (Hartline and Colman, 2007). The increase in transverse resistance is mediated by the fact that myelin is lipid-rich structure with several layers of compacted membrane that are more or less non-conductive since Na^+ ions are not flowing into or out of the highly resistant region (Hartline and Colman, 2007). Instead, Na^+ enters via the nodes of Ranvier between myelinating glial sheaths through highly concentrated Na_v channels (Fig. 25). As described in the previous chapter, nodes of Ranvier are highly enriched in Na_v to the order of $1200 \text{ channels}/\mu\text{m}^2$ (Rosenbluth, 1976), while internodes contain $\sim 20\text{-}25 \text{ channels}/\mu\text{m}^2$ (Richie and Rogart, 1977). This asymmetrical concentration of Na_v is important for the reduction in the axonal capacitance since the axonal membrane

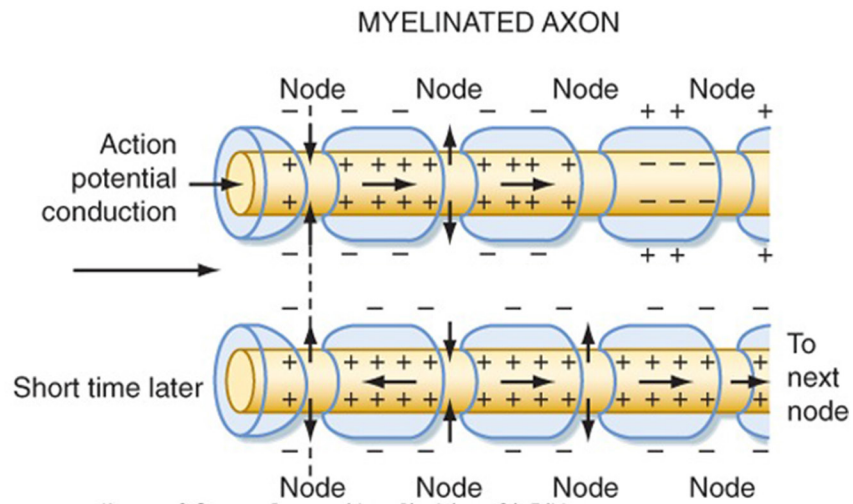


Figure 25: Action potential conduction along myelinated fibers. Myelin increases transverse resistance and reduces axonal capacitance through clustering of voltage-gated sodium channels at the nodes of Ranvier. Adapted from Berne and Levy Physiology 6th edition, 2008.

that is exposed to the extracellular space is confined to the nodes of Ranvier, thus allowing for a restricted area for current flow to occur. Importantly, the confinement of Na_v to the nodes of Ranvier reduces the amount of Na^+ necessary to regenerate the action potential, and furthermore results in the neuron using less energy and being incredibly energy efficient (Arancibia-Carcamo and Attwell, 2014). Lastly, this restriction of Na_v permits high-fidelity impulse conduction since the ratio of current available to stimulate the node to the current necessary to depolarize the node, otherwise called the safety factor, is very high (in the order of 5 to 7). A safety factor less than 1 would result in conduction failure (see below).

With these biophysical parameters in mind, the pathway for AP conduction in the myelinated axon is therefore quite different from that of the non-myelinated axon. Here, initiation of the action potential occurs at the AIS with an influx of Na^+ current. Myelin prevents the leakage of Na^+ current that flows down the axon (i.e. increase in transverse axial resistance) and reduces the cost of charging the internodal regions of the axolemma (i.e. reduction in axonal capacitance). A significant amount of the original depolarizing current will then be able to spread to the densely packed Na_v channels at the node of Ranvier, which will then depolarize and permit an influx of Na^+ current. This current will then flow down the axon where AP regeneration will occur only at the nodes of Ranvier. Due to the manner in which the AP is regenerated, this type of nervous conduction is labeled as “saltatory” (derived from the Latin word “saltare”, to hop or jump), since it appears to “jump” from node to node (Fig. 25).

This type of conduction was first postulated by Lille nearly 90 years ago (1925) and then further confirmed by seminal work from Tasaki (1939) and Huxley and Stämpfli (1949). In the case of Huxley and Stämpfli (1949), they measured the currents at both nodes of Ranvier and internodes and observed that the nodes of Ranvier displayed large amounts of inward current, while the internodes did not, suggesting that the nodes are the regions where APs are regenerated. This fact is important because saltatory conduction allows for great increases in the axon potential conduction. Instead of varying by the square root of the axonal diameter,

the speed of nervous conduction in myelinated axons is linearly proportional to the axonal diameter (Rushton, 1951). However, myelination is generally beneficial in increasing conduction velocity compared to the unmyelinated nerve when the axonal diameter is above $0.2\ \mu\text{m}$ (Waxman and Bennett, 1972). Indeed, this fact correlates well with the finding that only axons with a diameter $> 0.2\ \mu\text{m}$ can be myelinated in the CNS (Waxman and Bennett, 1972).

Conduction timing along myelinated neurons in the CNS ranges from modestly fast to rapidly conducting (Kress and Mennerick, 2009). Utilizing the dual patch soma-bleb technique or rapid acquisition of voltage changes through voltage-sensitive dyes, reports of conduction speeds in pyramidal neurons of the cortex range from ~ 0.5 to $3\ \text{ms}^{-1}$ (Palmer and Stuart, 2006; Kole *et al.*, 2007; Shu *et al.*, 2007). These values are not greatly improved compared to that of the unmyelinated nerve in the brain, but the differences are most likely related to the small diameters of these axons. In larger diameter axons, such as in motoneurons, action potential conduction can reach up to $80\ \text{ms}^{-1}$ (Gogan *et al.*, 1983).

Besides axonal diameter, a number of factors also affect the speed of AP conduction, which includes the thickness of the myelin sheath, paranodal junctions, and the nodes of Ranvier (Waxman, 1980). Interestingly, theoretical and experimental evidence shows that internodal distance does not greatly impact conduction velocity since myelinated axons have an optimal internodal length for maximal conduction and changes to that distance produces very little change in conduction velocity (Rushton, 1951; Moore *et al.*, 1978; Huxley and Stämpfli, 1949; Simpson *et al.*, 2013).

Several great studies and reviews have highlighted the roles of axonal diameter and myelin thickness in regulating conduction velocity (Waxman and Bennett, 1972; Waxman, 1980; Li, 2015); however, further discussion will be lent towards the paranodal junctions and the nodes of Ranvier.

2.3 Factors Affecting Conduction Velocity in Myelinated Axons

2.3.1 Paranodal Junctions

The paranodal junctions are key determinants in maintaining rapid axonal conduction through their barrier-like junctions formed between the myelinating glial cell and the axolemma. These junctions are important for restricting the short-circuiting of the nodes of Ranvier (Rosenbluth, 2009). Simplistically, if the paranodal junctions were not tightly formed, current that should normally flow through the node of Ranvier would instead flow in a low resistance manner to the internodal periaxonal space underneath the myelin sheath (Fig. 26A and B). This would reduce the amount of current going through the node and in turn reduce the amount of current reaching the neighboring nodes of Ranvier, thereby short-circuiting the beneficial gains of the myelin sheath (Rosenbluth, 2009).

As mentioned in the previous chapter, paranodal junctions are necessary to restrict K_v1 to the juxtaparanodal regions (Bhat *et al.*, 2001; Boyle *et al.*, 2001; Zonta *et al.*, 2008). Therefore, current that flows to the periaxonal space would activate these channels, which may dampen excitability and hamper action potential conduction (i.e. conduction block; Koles and Rasinsky, 1972; Hirano and Dembitzer, 1978). This has implications in demyelinating disease, which will be touched on in the subsection on conduction velocity in the diseased state.

This paranodal junction is not 100% restrictive since it does allow diffusion of some molecular tracers (Mierzwa *et al.*, 2010). This may be beneficial for exchange of solutes or excitation of the juxtaparanodal K_v1 channels (Rosenbluth, 2009).

2.3.2 Nodes of Ranvier

Several nodal properties affect axonal conduction along myelinated axons. The first component is through nodal capacitance, since the nodal capacitance is related to the membrane area occupied by the node of Ranvier. Therefore, increasing the size of the nodes of Ranvier can alter conduction velocity (Fig. 26B). An increase in nodal length can alter the conduction velocity due to increased nodal capacitance, resulting in slowing of the action potential being regenerated at the

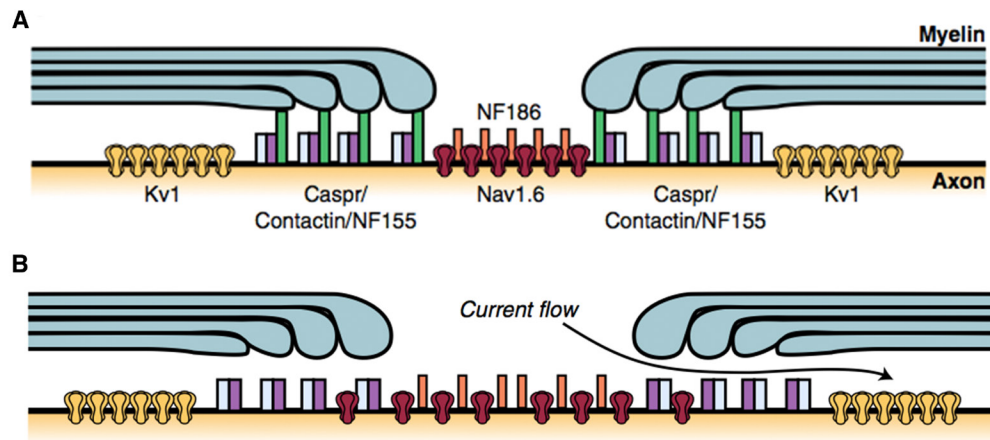


Figure 26: Conduction is altered when the paranodes and nodes of Ranvier are disturbed. **(A)** Normal ultrastructural and molecular architecture of the nodal and paranodal domains. **(B)** The loss of the paranodal junctions allows for a low resistance pathway for current to flow underneath the myelin sheath to the internodes. Sodium channels (red) disperse along the axon, followed by increases in nodal capacitance and slowing of action potential conduction. Adapted from Arancibia-Carcamo and Attwell, 2014.

adjacent node (Arancibia-Carcamo and Attwell, 2014). A theoretical argument proposed by Moore *et al.*, (1978) shows that changes in the nodal area only contributes to relatively modest changes in action potential conduction; although, Moore *et al.*, (1978) also described that this increase in nodal area can be counterbalanced by increase in sodium channels. Yet, experimental evidence in the electric organ of *Sternarchus* showed that large nodes of Ranvier have delayed conduction compared to smaller nodes of Ranvier (Waxman *et al.*, 1972). A more recent theoretical study demonstrated that conduction velocity decreases when increasing the nodal width (Babbs and Shi, 2013). Additionally, increase in the size of the nodes of Ranvier is also observed in demyelinating disease, either large Na_v aggregates persisting along demyelinated fibers, or abnormally large nodal aggregates within areas where remyelination takes place (see below). Further experimental studies should be performed to study the increase in nodal surface area and its role in altering AP conduction.

The relative contribution of the various nodal ion channels on axonal conduction is relatively unknown. Since there are several different types of Na_v channels clustered at the nodes of Ranvier at differing developmental time points, there is no surprise that few studies have been able to decipher their particular roles in axonal conduction by electrophysiological means. At present, many studies have characterized the various biophysical gating properties of the Na_v subunits. Na_v1.2 needs large depolarizing current to fire and inactivates during high frequency firing (Rush *et al.*, 2005). Na_v1.6 and Na_v1.1 participate in persistent sodium current (a type of current that slowly inactivates; Rush *et al.*, 2005; Catterall *et al.*, 2005), which may therefore drive faster conduction through the increase of axoplasmic Na⁺. Interestingly, this type of current may be implicated in axonal damage during in demyelinating conditions (see below; Craner *et al.*, 2004). Nevertheless, further tools need to be developed in order to understand the different contributions of each nodal Na_v isoform on AP conduction.

Recent studies looking at nodal potassium channel K_v7.2/3 identified their contributions to AP conduction. Importantly, both K_v7.2 and K_v7.3 form functional

K⁺ channel complexes that underlie M current (Wang *et al.*, 1998). This M current from heteromeric K_v7.2 and K_v7.3 channels restricted at nodes of Ranvier in rat central L5 axons has been described to play an important role in enhancing short-term axonal excitability through stabilizing the membrane potential (Battefeld *et al.*, 2014). Specifically, these channels reduce the steady-state inactivation of Na_v that are coclustered with K_v7.2 and K_v7.3 at nodes, thus increasing action potential amplitude and augmenting action potential conduction (Battefeld *et al.*, 2014). These interesting results point to an important functional aspect of K_v channels, particularly KCNQ, in relation to axonal conduction.

2.4 The Transition to Saltatory Conduction Along Myelinated Axons

One interesting question arises when the unmyelinated axon becomes a myelinated axon: How does the neuron transition from continuous to saltatory conduction? Lillie (1925) suggested from his experiments that such a transition occurs physiologically, and recently modeling experiments have shed light on this transition from continuous to saltatory conduction. During the myelination process with a large periaxonal gap, conduction remains continuous (Young *et al.*, 2013). At the onset of myelin compaction, the conduction velocity speed actually decreases from that of the continuous nature (Young *et al.*, 2013). However, Young *et al.* (2013) showed that once further compaction occurs, the conduction velocity rapidly rises to saltatory levels (saltatory conduction in this study was a node downstream firing before arrival of the impulse underneath the myelin sheath).

One last finding is that saltatory-like conduction may occur on small-diameter axons prior to myelination. Waxman *et al.* (1989) originally postulated a type of conduction called “micro-saltatory” conduction along neonatal rat optic nerves because these nerves had low densities of Na_v, estimated from measurements of the binding of [³H]-saxitoxin, spaced nearly 1 μm apart. More recently, Pristerà *et al.* (2012) showed that small clusters of Na_v1.8 were associated to lipid raft domains in unmyelinated group-C nerve fibers. Following this report, Neishabouri and Faisal (2014) modeled the observations in the Pristerà (2012)

study and showed that indeed these clusters of $\text{Na}_v1.8$ permitted micro-saltatory conduction, but they found that this type of conduction is metabolically costly due to the inactivation properties of $\text{Na}_v1.8$. Together, these results suggest that small cluster like Na_v channels may permit faster AP conduction along not yet and non-myelinated fibers.

2.5 Action Potential Conduction in the Diseased State

As previously outlined, several factors may affect AP conduction along axons, and in particular loss of the myelinating sheath can have major consequences in terms of rapid and faithful conduction. Several diseases result in such a loss of the myelin sheath and they are categorized as demyelinating diseases. In the context of our laboratory, this section will outline one specific demyelinating disease in the CNS: multiple sclerosis.

2.5.1 Multiple Sclerosis (MS)

Even if the anatomical lesions were identified almost simultaneously by Jean Cruveilhier (1791-1874) in France and Robert Carswell (1793-1857) in England between 1835 and 1838, the identification of the clinic-pathological disease was made by the French neurologist Jean-Martin Charcot (1825-1893) at the Salpêtrière hospital in Paris. In his famous neurology lesson, Charcot named it multiple sclerosis (1868). MS is described as an inflammatory demyelinating and degenerative disease characterized by demyelinating lesions that can manifest in various regions of the CNS. Patients afflicted by the disease early on present clinical symptoms such as blurred vision, numbness, loss of sensation, vertigo, and disequilibrium, that lasts several days or weeks, yet recover during the remittent phase of the disease (Waxman, 2006). Some patients do not present with these relapsing-remitting phases and continue to decline in neurological ability after the initial onset of the disease (primary progressive), yet other patients after the relapsing-remitting phases progress into a phase of continual neurological handicap (secondary progressive; Waxman, 2006). Patients suffering from MS have a slightly decreased life span and a tremendous decline in their quality of life.

The etiology of MS is still poorly characterized, but several factors such as environmental factors, autoimmunity, infections, and genetic susceptibility have been proposed as potential candidates for triggering the disease. In regards to autoimmunity, the antigenic target(s) remain unknown, with many suspected then non-confirmed candidates. Recently an immune response against paranodal and juxtaparanodal proteins such as Nfasc155 (Mathey *et al.*, 2007) and Contactin-2 (Derfuss *et al.*, 2009), respectively, has been reported in MS patients, suggesting that these constituents might represent targets of the pathological process. These data, however, need confirmation. In this context, disruption of these domains, especially the paranodal junctions, might have severe consequences in regards to AP conduction.

2.5.2 Disruption to the nodal architecture alters axonal conduction

In post-mortem tissue samples from MS lesions, the nodal and perinodal domains are severely altered (Coman *et al.*, 2006; Howell *et al.*, 2006; review by Desmazières *et al.*, 2012). Previously clustered Na_v are either diffusely redistributed, or remain as loose (large) aggregates along the denuded axon (Coman *et al.*, 2006). In addition, juxtaparanodal K_v mis-localization at nodes has been reported (Howell *et al.*, 2006). The loss of the myelin sheath, combined with the diffusion of voltage-gated ion channels has several consequences. The first is that loss of myelin and dispersal of Na_v will increase the area by which sodium current needs to travel. This in turn will drive the secondary consequence of a significant increase in the membrane capacitance. More current will now be required in order to drive depolarization of the axolemma, and raise the metabolic cost of maintaining the Na^+/K^+ gradient. Furthermore, disruption of the localization of K_v and exposing them to more current exacerbates axonal conduction since they can dampen excitability. Together, these changes lower the safety factor by a notable amount (near 1), and can thereby lead to conduction failures (Fig. 26B) that manifest into substantial neurological deficits in MS patients. Many other factors can result in conduction block such as the time since demyelination onset, temperature and

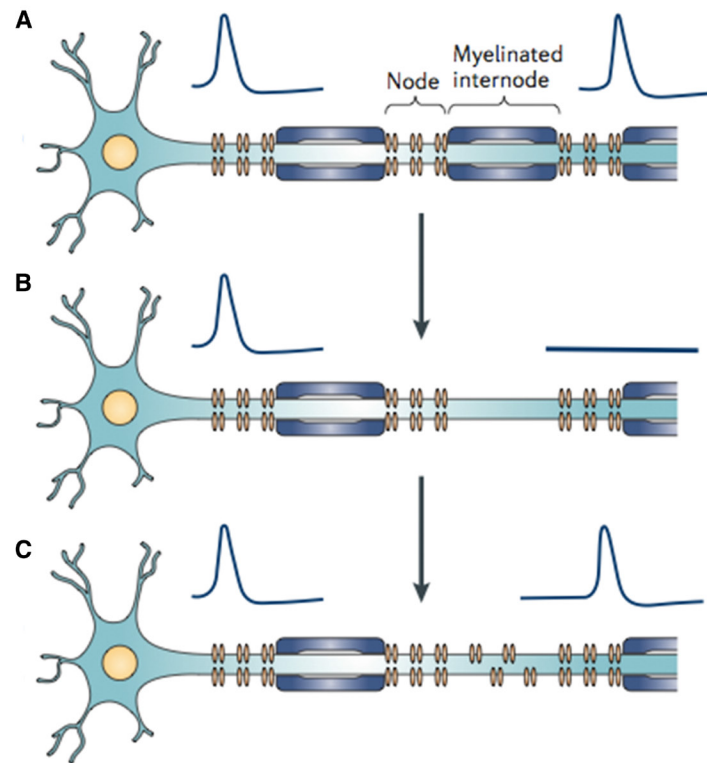


Figure 26: Changes in nodal architecture during demyelination. **(A)** Normal saltatory conduction occurs along the myelinated fiber. **(B)** Once a demyelinating event occurs, acutely denuded axons may display a conduction block due to the reduction in the safety factor. **(C)** To overcome conduction block and to restore AP conduction, some axons display upregulation of sodium channels at the demyelinated regions of the axon. Adapted from Waxman, 2006.

axonal geometry; however, readers interested in a more fundamental or clinical account can refer to Smith *et al.* (1994) for further details.

Several molecular changes also occur during demyelination. The first is that there is an upregulation of Na_v channels in demyelinated MS lesions (Moll *et al.*, 1991). This upregulation is most likely a counterbalance to the changes in capacitance and reduction in transverse axial resistance. One other unique observation on demyelinated axons is that there is diffusion of $\text{Na}_v1.2$ along axons (Fig. 26C), which is normally expressed in immature nodes of Ranvier and unmyelinated axons (Craner *et al.*, 2004; Boiko *et al.*, 2001). Expression of $\text{Na}_v1.2$ is thought to be adaptive in restoring conduction velocity since the threshold of activation is high for this isoform and it displays deactivation at high-frequency firing (Fig. 26C). In contrast, $\text{Na}_v1.6$ is thought to be detrimental in this case because the persistent sodium current from this isoform drives the activity of the $\text{Na}^+/\text{Ca}^{2+}$ exchanger (Craner *et al.*, 2004). Activity of this exchanger will pump Na^+ out of the axoplasm while permitting influx of Ca^{2+} , and can therefore lead to activation of several Ca^{2+} -induced secondary cascades that can cause neuronal injury (Waxman, 2006).

Lastly, for the restoration of conduction velocity to speeds prior to the demyelinating event, remyelination must occur at the denuded regions. Interestingly, it has been shown that Na_v clusters could be found on non-remyelinated axons within partially remyelinated zones in post-mortem tissue from MS patients (Coman *et al.*, 2006). These Na_v aggregates could either be beneficial for directing remyelination or they could be transient structures that may allow for improved AP conduction in a micro-saltatory manner along the demyelinated regions of the axon.

In summary, several factors regulate the timing of axonal conduction in both the unmyelinated and myelinated neuron, and the continual investigation of these parameters will allow us to shed light on how to augment and hopefully improve rapid action potential conduction in pathological conditions. Furthermore, having

described the molecular architecture of the myelinated nerve and the fundamentals of how action potentials are propagated along myelinated axons, the following chapter will delve into the mechanisms of nodes of Ranvier assembly.

Chapter III: Mechanisms of Nodes of Ranvier

Assembly and Transport of Nodal Components in the PNS and CNS

Even though PNS and CNS nodes of Ranvier are by and large similar in their molecular composition, the mechanisms underlying the formation of the nodes of Ranvier in the PNS and CNS are not identical. This dissimilarity between the two nervous systems mainly stems from the differences in cell types producing the myelin sheath, which give rise to differing nodal ultrastructure and slight changes in molecular composition that ultimately govern the neuron-glia interactions necessary to form the nodes of Ranvier. To date, the mechanisms underlying PNS nodal assembly are well characterized, but our understanding of how CNS nodes of Ranvier form appear to be more complicated since there are multiple layers of redundancy via several extrinsic (glial) and intrinsic (neuronal) factors.

This section will first outline the mechanisms governing PNS nodal formation, which will then be followed by a section on CNS nodes of Ranvier formation. The CNS section will be broken into one section dedicated to extrinsic factors and the other to intrinsic factors. Lastly, this section will end with trafficking and targeting of nodal components.

3.1 Mechanisms of PNS nodes of Ranvier assembly

During initial myelination of the axon by the Schwann cell between P0-P1, components of the nodal complex cluster to regions adjacent to the myelinating segment called heminodes (Vabnick *et al.*, 1996). Next, as the length of the myelin segment elongates throughout the first postnatal week, two heminodes adjacent separate myelinating segments fuse to form a full mature node of Ranvier (Vabnick *et al.*, 1996). Either before or during heminodal fusion, clustering of paranodal

components occurs (Eshed *et al.*, 2005), which is in turn followed by the clustering of K_v1 and CAMs at the juxtaparanodal region (Rasband *et al.*, 2004). This time course of PNS nodal formation appears to be the standard—yet, looking more deeply into this time course begs two related questions: Does following this strict pattern ultimately predict the formation of the PNS nodes of Ranvier? And if not, are there multiple mechanisms regulating PNS nodal assembly? Several reports suggest that there are two complementary axoglial mechanisms by which PNS nodes of Ranvier form.

3.1.1 Heminodal Clustering Mechanism

As alluded to in the previous chapter on molecular composition of nodes of Ranvier, several proteins appear first at the nodes of Ranvier and act as pioneer molecules in clustering PNS nodal components. The proteins Nfasc186, NrCAM, and gliomedin are the first constituents to cluster at the PNS nodes (Lambert *et al.*, 1997; Custer *et al.*, 2003; Eshed *et al.*, 2005; Schafer *et al.*, 2006; Koticha *et al.*, 2005; Feinberg *et al.*, 2010; Thaxton *et al.*, 2011), and clustering of these proteins at heminodes precede that of nodal ankyrinG, β IV-spectrin/ Na_v and paranodal Nfasc155/Caspr/contactin (Lambert *et al.*, 1997; Lustig *et al.*, 2001; Thaxton *et al.*, 2011; Schafer *et al.*, 2006; Yang *et al.*, 2007). Accordingly, the initial steps of heminodal formation, which ultimately gives rise to mature nodes, depend on axonal Nfasc186 and glial gliomedin and NrCAM.

First, Nfasc186 is involved in incorporating axonal nodal components to the developing PNS nodes of Ranvier. Nfasc186 interacts with ankyrinG, which in turn is able to recruit Na_v and its scaffolding partner β IV-spectrin (Bennett and Baines, 2001; Dzhashiashvili *et al.*, 2007; Yang *et al.*, 2007; Zhang *et al.*, 2012). Several reports suggest that this is the proper timing of events on the axonal surface of PNS fibers. Two studies utilizing either Nfasc-Fc or NrCAM-Fc fusion proteins in Schwann cell-DRG neuron cocultures observed an inhibition of ankyrinG, β IV-spectrin, and Na_v clustering at developing heminodes (Koticha *et al.*, 2005; Lustig *et*

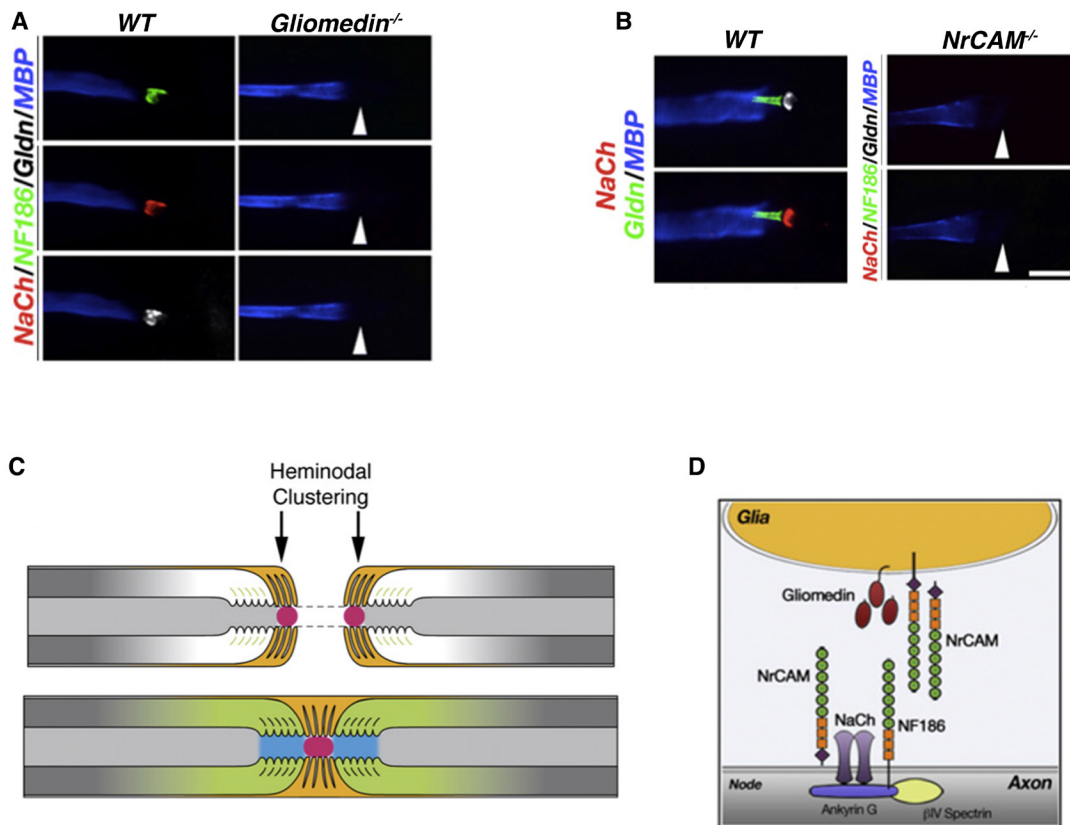


Figure 27: Heminodal clustering mechanism in the PNS. **(A)** Nfasc186 (green) and Na_v (red) fail to cluster (arrowheads) at heminodes in the absence of gliomedin in DRG Schwann cell cocultures. **(B)** Na_v, Nfasc186, and gliomedin (rightside panel) fail to form (arrowheads) at heminodes in the absence of NrCAM. **(C)** and **(D)** PNS heminodal clustering is mediated by the interaction of Nfasc186 with gliomedin and NrCAM tethered to the Schwann cell microvilli. Two heminodes then merge together to form a full node of Ranvier. **A-D** adapted from Feinberg *et al.*, 2010.

et al., 2001). Loss of function experiments by suppressing *Nfasc186* or knocking out neuronal *Nfasc186* altogether show that Na_v and ankyrinG fail to cluster at nodes in Schwann cell-DRG neuron cocultures and *in vivo* (Dzhashiashvili *et al.*, 2007; Feinberg *et al.*, 2010; Thaxton *et al.*, 2011). Zonta *et al.* (2008) selectively expressed transgenic *Nfasc186* in *Nfasc*-null mice and showed that it rescued the nodal complex in sciatic nerves (using a similar strategy, this has also been observed with *Nfasc140* in teased quadriceps; Zhang *et al.*, 2015). Lastly, by modifying only the ankyrin binding domain in the cytoplasmic region of *Nfasc186* but leaving the extracellular domains intact, Dzhashiashvili *et al.* (2007) reported that *Nfasc186* clustered normally to developing heminodes, yet lacked ankyrinG and Na_v . Together, these data confirm that *Nfasc186* acts as the axonal pioneer molecule in recruitment of PNS nodal components.

Yet, in order to cluster *Nfasc186* (initially diffusely expressed along the internode) to heminodes, the extracellular domains of *Nfasc186* must interact with the gliomedin/NrCAM complex (Dzhashiashvili *et al.*, 2007; Zhang *et al.*, 2012; Labasque *et al.*, 2011; Eshed *et al.*, 2005, 2007; Feinberg *et al.*, 2010). This cooperative interaction is highlighted by the fact that *Nfasc186* fails to properly localize to heminodes in both *NrCAM*- and *Gliomedin*-deficient mice (Fig. 27A and B; Custer *et al.*, 2003; Feinberg *et al.*, 2010). Here, gliomedin traps *Nfasc186* to developing heminodes, while glial NrCAM stabilizes secreted trimerized gliomedin to the microvilli for increased interaction with *Nfasc186* (Eshed *et al.*, 2007; Feinberg *et al.*, 2010). Therefore, glial expression of both gliomedin and glial NrCAM are crucial for PNS heminode formation (Fig. 27C and D).

The expression of certain molecules of the basal lamina, microvilli, and ECM appear to be involved in promoting the heminodal clustering mechanism. Ablation of laminins 211 and 511, which are enriched at nodes at the basal lamina, result in abnormal microvilli and reduced density of nodal Na_v clustering in sciatic nerves (Oochi *et al.*, 2005). In line with this report, loss of the microvillar enriched laminin receptor dystroglycan results in mislocalized Schwann cell microvilli and a 20% reduction in the amount of heminodal Na_v clustering (Saito *et al.*, 2003; Colombelli

et al., 2015). Perlecan, which interacts with dystroglycan and binds gliomedin to improve its multimerization, is lost at PNS nodes in dystroglycan mutant mice, suggesting that perlecan may account for the reduction in heminodal Na_v clustering (Colombelli *et al.*, 2015). However, in perlecan mutant mice, clustering of gliomedin and Na_v is unaltered (Colombelli *et al.*, 2015). Knockout mice for syndecan-3, another PNS nodal HSPG that is not lost in dystroglycan mutants (Colombelli *et al.*, 2015), also appear to have normal PNS nodes of Ranvier (Melendez-Vasquez *et al.*, 2005). These two latter results suggest that ECM HSPGs may act in a redundant manner in the absence of one another, and therefore it would be interesting to test double knockout mutants for these various HSPGs to see their impact on PNS nodes of Ranvier assembly.

3.1.2 Paranodal-Junction Dependent Mechanism

Although nodal components do not cluster to heminodes in *NrCAM*-null and *Gliomedin*-null mice, they nevertheless ultimately cluster at mature nodes (Fig. 28A; Custer *et al.*, 2003; Feinberg *et al.*, 2010). Indeed, when the heminodal assembly mechanism fails, there appears to be a secondary, yet complementary, paranodal-junction dependent pathway in order to cluster PNS nodes of Ranvier.

The use of double mutant mice has helped shed light on this particular mechanism. Single paranodal mutant mice (*Caspr*^{-/-}, *Contactin*^{-/-}, *Nfasc155*^{-/-}), which have severely disrupted paranodal junctions, appear to have only minimally affected PNS nodes of Ranvier (Bhat *et al.*, 2001; Boyle *et al.*, 2001; Pillai *et al.*, 2009; Feinberg *et al.*, 2010), suggesting that they properly cluster through the heminodal mechanism. Conversely, *Gliomedin*^{-/-}/*Caspr*^{-/-} or *NrCAM*^{-/-}/*Caspr*^{-/-} mice show a significant reduction in the amount of Na_v clusters along sciatic nerves, a dramatic increase in the nodal length, and a significant decrease in nerve conduction (Feinberg *et al.*, 2010). Using an *in vitro* coculture system of *Nfasc*-null DRG neurons and myelinating wild-type Schwann cells (i.e. *Nfasc155*⁺ and functional paranodal domains), Feinberg *et al.* (2010) showed that nodal components cluster at mature nodes, but not at heminodes (Fig. 28A). What these

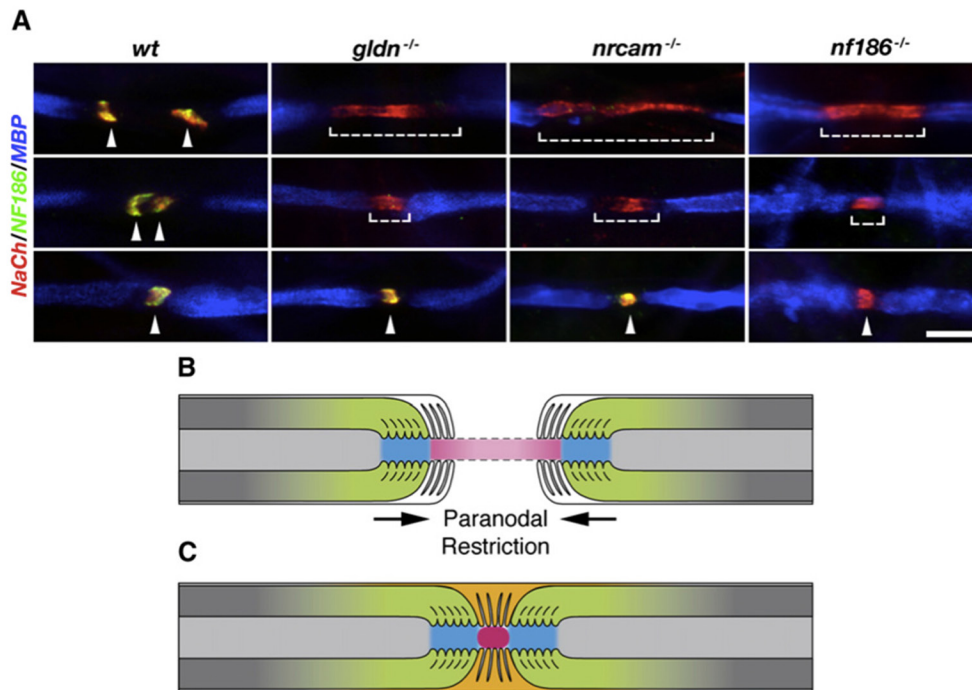


Figure 28: Role of paranodal junctions in forming PNS nodes of Ranvier. **(A)** While Na_v (red) does not cluster to heminodes (top panels excluding the *wt*), it is restricted between the paranodal junctions in Gliomedin-, NrCAM-, and Nfasc186-null DRG Schwann cell cocultures. Overtime as the myelinating segments (blue) move towards each other and Na_v clusters at PNS nodes (lower panels). **(B)** and **(C)** Overview of the model for paranodal restriction of PNS nodes of Ranvier. Adapted from Feinberg *et al.*, 2010.

results suggest is that paranodal junctions may act as a back-up mechanism in organizing the PNS nodes of Ranvier when heminodes fail to form (Fig. 28 B and C).

In spite of that, several reports seem to counter this secondary model. Selectively expressing transgenic Nfasc155 lacking the cytoplasmic domain in *Nfasc*-null mice effectively rescues the paranodal junction (i.e. axonal Caspr and Contactin), but fails to cluster the PNS nodal components in sciatic nerves (Sherman *et al.*, 2005; Zonta *et al.* 2008). Furthermore, nodal molecules fail to cluster at mature nodes when neuronal Nfasc186 is ablated in mouse sciatic nerves with normal paranodal junctions (Thaxton *et al.*, 2011). These *in vivo* reports, in contrast to the *in vitro* studies by Feinberg *et al.* (2010), would thusly suggest that the paranodal back-up system does not compensate for the lack of a Nfasc186-mediated assembly mechanism in the PNS.

With these discrepancies, one should therefore ask: Do paranodal junctions truly act as a secondary mechanism to cluster PNS nodes of Ranvier? This answer is that they may very well likely act as backups to heminodal clustering, and that the inconsistencies of these studies are probably linked to the different models used. For example, the neuronal Nfasc186 mutant mouse model used in Thaxton *et al.* (2011) is only partial—and looking more closely at their quantification on P11 mouse sciatic nerve it appears as though ~15-20% of the nodes lacking Nfasc186 were still positive for ankyrinG and Na_v. This could suggest that either paranodal junctions are functional secondary back-ups to heminodal clustering or that another mechanism besides the paranodal junctions, such as ankyrins, could be implicated in assembling PNS nodes of Ranvier.

In line with the latter hypothesis, mice lacking β IV-spectrin and Caspr (*qv^{3J} Caspr^{-/-}* mice) have normal PNS nodes enriched in ankyrinG (Susuki *et al.*, 2013), which can target and localize to nodes in the absence of β IV-spectrin (Ogawa *et al.*, 2007). One should keep in mind though that the results from Susuki *et al.* (2013) do not rule out the possibility that interaction of ECM components (i.e. Gliomedin and NrCAM) with Nfasc186 clustered PNS nodes. In this context, a recent study showed that both ankyrinG and ankyrinR together are necessary in order to form Na_v

clusters in P3 mouse dorsal roots (Ho *et al.*, 2014), thereby giving a supporting role for ankyrins. Here, PNS nodes most likely fail to assemble because ankyrins are sufficient for transporting and localizing Nav (Barry *et al.*, 2014; Gasser *et al.*, 2012), or it could be that loss of ankyrins fail to stabilize Nfasc186 (Dzhashiashvili *et al.*, 2007). In regards to Feinberg *et al.* (2010), it could be possible that mature nodal clustering in the *Nfasc*-null DRG neurons wild-type Schwann cells cocultures might have been rescued through an ankyrin mechanism that targets Nav to nodes in conjunction with (or in absence of) the paranodal-junction pathway; or, another possibility could be that redistributed Nav, independent of ankyrins, is clustered through paranodal restriction. Going forward, it would be interesting to look at the interactions of these two mechanisms by utilizing a combinatorial loss of function approach of various pan-ankyrin and paranodal components in order to study their complementarity in secondary PNS nodes of Ranvier assembly.

3.2 Mechanisms of CNS nodes of Ranvier assembly

In contrast to PNS nodes of Ranvier, there are a number of overlapping mechanisms to cluster CNS nodes of Ranvier. These include ECM components, paranodal junctions, cellular adhesion molecules, oligodendroglial secreted proteins, and cytoskeletal scaffolding proteins. The four former mechanisms are related to extrinsic axo-glia interactions, while the latter is regulated by the axon.

3.2.1 Extrinsic mechanisms of CNS nodes of Ranvier formation

3.2.1.1 Paranodal Junctions

The order of nodal domain formation in the CNS appears to be different from that of the PNS. In the rodent optic nerve, Caspr⁺ paranodal junctions are the first domains to be formed, followed by the nodal components, and then the nodal ECM (Rasband *et al.*, 1999; Susuki *et al.*, 2013). This sequential order of axonal domain formation suggests that paranodes act as lateral diffusion barriers or sieves, and might be the primary components that cluster CNS nodes of Ranvier. Support of

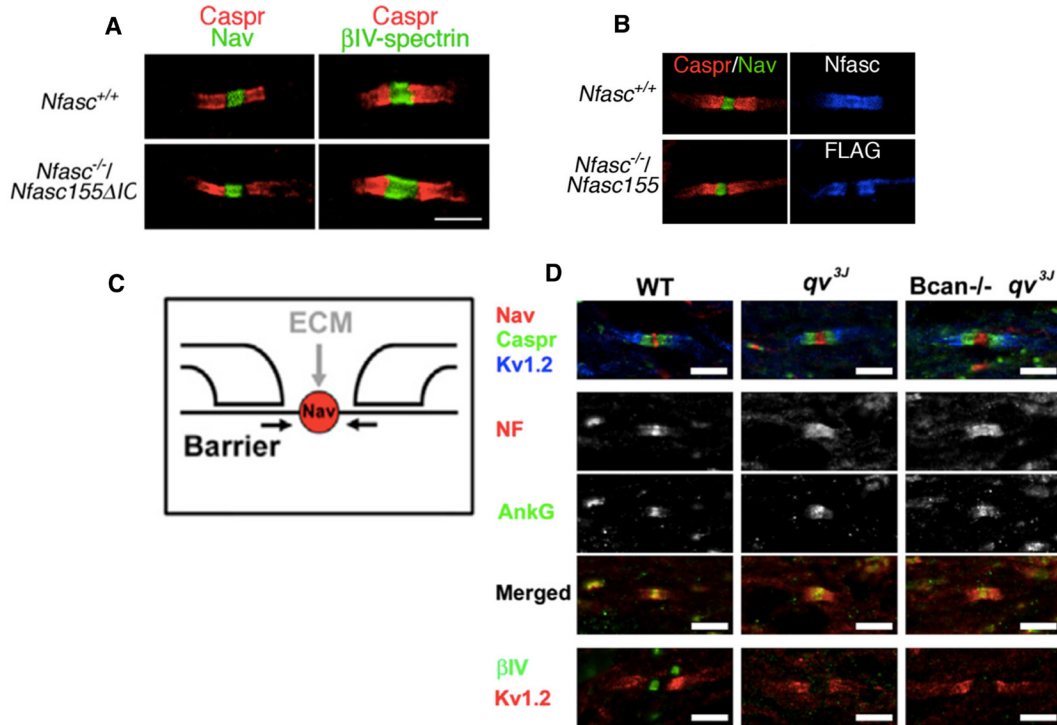


Figure 29: Role of paranodal junctions in forming CNS nodes of Ranvier. **(A)** and **(B)** Transgenic expression of full length **(B)** *Nfasc155* full-length or *Nfasc* 155 lacking its cytoplasmic region **(A)** in *Nfasc*-null mice rescues the paranodal junctions (red) and restores clustering of nodal components (green) in the CNS. **(A)** and **(B)** adapted from Zonta *et al.*, 2008. **(C)** Genetic strategy used in Susuki *et al.* (2013) to decipher the contribution of paranodal junctions in CNS nodal assembly. **(D)** Combined loss of β IV-spectrin and the ECM molecule brevican alters the number of nodes of Ranvier formed in the optic nerve, but nodes of Ranvier still form, confirming that paranodal junctions can assemble CNS nodes of Ranvier. **(C)** and **(D)** adapted from Susuki *et al.*, 2013.

this conclusion is highlighted by several studies. Using the hypomyelinating *shiverer* mutant mice that display abnormal paranodal junctions, Rasband *et al.* (1999) reported irregular optic nerve nodes of Ranvier with elongated Na_v immunostaining and lack of clustered ankyrinG. Another study, using a paranodal rescue approach by expressing the *Nfasc155ΔIC* transgene (i.e. lacks the intracellular portion of Nfasc155) in *Nfasc*-null mice, showed that Na_v clusters formed along spinal cord ventral funicular axons, suggesting that reformation of the paranodal junction is sufficient to cluster Na_v in the absence of Nfasc186 (Fig. 29A and B; Zonta *et al.*, 2008). Recently, Çolakoglu *et al.* (2014) reported that loss of glial Contactin impaired paranodal junctions, which therefore resulted in a significant decrease in Na_v clustering along optic nerve axons.

In contrast to these studies, however, *Caspr*^{-/-} (Bhat *et al.*, 2001; Rios *et al.*, 2003) mutant mice have disrupted paranodal junctions but have properly assembled CNS nodes of Ranvier. Moreover, *CGT*^{-/-} and *CST*^{-/-} mice, both of which have disrupted paranodal junctions and mislocalized K_v1 to the paranodes, have only mildly affected nodes of Ranvier (Dupree *et al.*, 1999; Ishibashi *et al.*, 2002). Overall, what these studies tell us is that other mechanisms work in conjunction with the paranodes in order to form CNS nodes of Ranvier.

In this context, Susuki *et al.* (2013) looked at the proportion of Na_v clustering in mutants lacking both ECM components (Brevican or Versican) and βIV-spectrin (using a βIV spectrin mutant referred to as *qv3J*). While these *qv3J Brevican*^{-/-} and *qv3J Versican*^{-/-} mice had less Na_v clustering than wild-type and single knockout mice, when compared to other double knock out mutants (disruption of paranodal junctions and scaffold proteins or disruption of ECM and paranodal junctions) their Na_v clustering ability was the least affected (Fig. 29D; Susuki *et al.*, 2013). This suggests that paranodal junctions have the ability to cluster CNS nodes of Ranvier and that they function in the absence of the ECM and scaffolding components.

3.2.1.2 ECM

The interactions of Nfasc186 with the PNS ECM components would suggest that there most likely is a similar nodal assembly mechanism in the CNS. However, Schwann cell-produced gliomedin is undetectable on CNS axons and oligodendroglial cells (Eshed *et al.*, 2005), and the ECM composition of the PNS and CNS is different from one another. Thus, are there other ECM molecules by which Nfasc186 may interact and cluster CNS nodes of Ranvier? The response to this question is difficult because there are several members of the proteoglycan family enriched at CNS nodes that indeed interact with Nfasc186, yet the appearance of ECM molecules at CNS nodes appears to be later than that of Nfasc186 (Susuki *et al.*, 2013). Therefore, while this section will try and untether the assembly versus stabilization role of ECM/Nfasc186 interactions in regards to the nodes of Ranvier, one must be cautious in interpretation. As the line between these two processes is blurry, determining whether their ultimate roles are linked to assembly rather than stabilization is hard to distinguish.

In this context, mice lacking Brevican (Bekku *et al.*, 2009), Versican (Dours-Zimmermann *et al.*, 2009; Susuki *et al.*, 2013), Brevican/Versican (Susuki *et al.*, 2013), Tenascin-R (Weber *et al.*, 1999), NrCAM (Susuki *et al.*, 2013) and Bral1 (Bekku *et al.*, 2010; Susuki *et al.*, 2013), which can all interact with Nfasc186, have normal CNS nodes of Ranvier. Only Bral1 and Tenascin-R deficient mice produce an alteration in nerve conduction (Bekku *et al.*, 2010; Weber *et al.*, 1999), which is probably linked to disruption of other ECM molecules and thus reducing the ion buffering capacity at the axonodal space. Interestingly, NrCAM- and Brevican-Fcs can induce node-like clusters of HA-Nfasc186 in DRG cultures (Susuki *et al.*, 2013), suggesting that these two nodal ECM components at least may have “clustering” ability on DRG axons.

In light of these single and double ECM knock out mouse studies, important experiments performed by Susuki *et al.* (2013) should be further discussed. The authors observed that mice with disrupted ECM and paranodal junction components or disrupted ECM and cytoskeletal components displayed motor

handicap and reduced Na_v clusters compared to single mutants lacking only a single mechanism (Susuki *et al.*, 2013). This could suggest that either ECM molecules are involved in initiation of Na_v clustering or that they may be involved in CNS maintenance. But again, it is difficult to uncouple the two processes based on the investigators last experiment with the *qv^{3J} Caspr^{-/-}* mice that enabled them to look solely at the function of the ECM. Here, Susuki *et al.* (2013) showed that CNS nodes could assemble when lacking cytoskeletal scaffolds and paranodal junctions, suggesting that ECM molecules cluster CNS nodes. Yet, two important points should be noted regarding this knockout: 1.) The strongest neurological phenotype and severest nodal disruption out of all of the combinatorial loss of function mechanisms tested was observed with *qv^{3J} Caspr^{-/-}* mice; and 2.) *qv^{3J} Caspr^{-/-}* mice fail to live past P18, which is a time point where the developmental expression of ECM components at nodes is all together quite low in wild-type mice. Thus, it is unlikely that ECM molecules play a critical role in assembling CNS nodes of Ranvier *in vivo*. Further studies must be performed in order to untether the role of the ECM in either assembly or maintenance of CNS nodes of Ranvier.

3.2.1.3 Oligodendroglial Secreted Proteins

Oligodendrocytes, similar to many other cells, are secretory cells that can release macromolecular substances that provide trophic support and modulate various neuronal functions. In the context of CNS nodes of Ranvier assembly, work from Kaplan *et al.* (1997, 2001) reported that oligodendrocytes were able to induce the clustering of Na_v in the absence of paranodal junctions *in vitro*.

Using a purified retinal ganglion cell (RGC) culture system void of glial cells, Kaplan *et al.* (1997) showed that Na_v immunoreactivity was diffuse along the axons, while the AIS had strong and restricted Na_v immunoreactivity (Fig. 30A). However, when they added purified RGCs directly with or suspended over a conditioning layer of optic nerve glia, they strikingly observed Na_v immunoreactivity in evenly-spaced clusters along the axons (Fig. 30A). AnkyrinG was also observed in these clusters, suggesting that they were stabilized to the actin cytoskeleton. Further

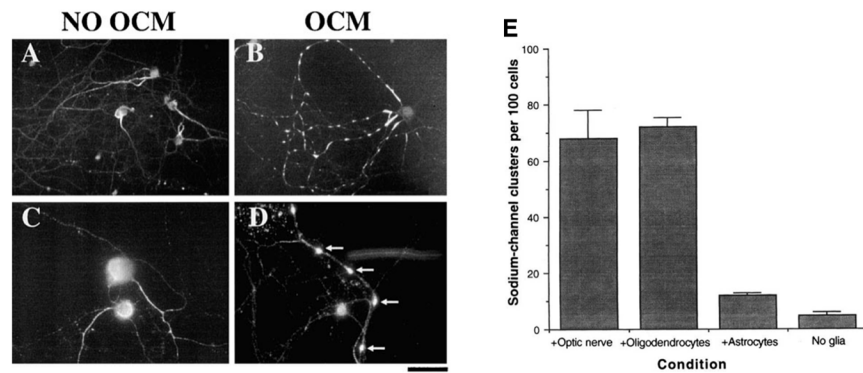


Figure 30: Oligodendrocyte secreted factors induces node-like clustering in the CNS. **(A)** Na_v clustering is induced along retinal ganglion cell axons **(B and D)** after treatment with concentrated oligodendrocyte conditioned medium (OCM). Adapted from Kaplan *et al.*, 2001. **(E)** Optic nerve or oligodendrocytes can induce this clustering, but lack of glia or addition of astrocytes does not permit Na_v clustering. Adapted from Kaplan *et al.*, 1997.

experiments showed that only oligodendroglial conditioned media (OCM) added to the RGC cultures, and not other glial conditioned media, induced the Na_v clustering (Fig. 30B). Additional analysis of the OCM suggested that the cluster-inducing factor was a protein, and they also observed that these clusters persisted after changing the media to non-conditioned media. These results put forward several important conclusions: 1.) Nodal components could form in regularly spaced clusters in the absence of paranodal junctions, suggesting that nodal domains are pre-specified by the axon; 2.) Oligodendroglial secreted proteins, and not other glial secreted factors, are necessary in order to form these node-like clusters; and 3) Na_v remains persistently clustered along axons two weeks after removal of the conditioned media, which may have direct implications in axonal conduction.

A following report by the same group shortly thereafter showed through several experiments that blocking protein synthesis and vesicular trafficking or depolymerizing the actin cytoskeleton prevented the formation but not the maintenance of node-like clusters along RGC axons (Kaplan *et al.*, 2001). Furthermore, they observed that the OCM did not increase the levels of surface or cellular sodium channels, suggesting that the action of OCM is to induce clustering of sodium channels already on the membrane. These results are interesting considering that the OCM factor(s) can induce clustering very rapidly (within a day; Kaplan *et al.*, 2001), so either OCM acts by rapidly upregulating the synthesis and trafficking of a protein that induces Na_v clustering, or OCM interacts with a molecule (or molecules) on the axonal surface, which then recruits Na_v , and further stabilized by ankyrins to the actin cytoskeleton.

Looking to further characterize the biochemical nature of the OCM, Kaplan *et al.* (2001) first tested the clustering ability of several candidate proteins such as agrin, a protein fragment of Tenascin-R, and Tenascin-C, but did not observe any clustering activity. By using spin concentrators with different molecular weight cutoffs, they also observed that clustering activity was preserved between the ranges of 30 and 50-kDa (Kaplan *et al.*, 2001).

While these reports presented an interesting case for a combination of extrinsic and intrinsic mechanisms necessary for CNS nodal assembly, further analysis of the extrinsic oligodendroglial secreted factor has yet to be reported.

3.2.1.4 Nodal CAMs and Na_vβ-Subunits

As one of the key players in the assembly of PNS nodes of Ranvier (Feinberg *et al.*, 2010), Nfasc186 also greatly contributes to nodes of Ranvier formation in the CNS. In this context, it has been reported that *Nfasc186*-null mice fail to cluster CNS nodes of Ranvier (Thaxton *et al.*, 2011). Furthermore, by expressing transgenic Nfasc186-FLAG in *Nfasc*-null mice, Zonta *et al.* (2008) reported that FLAG-tagged Nfasc186 was able to rescue Na_v, CAMs and cytoskeletal components of the CNS nodes of Ranvier, and also increased the viability of *Nfasc*-null mice by 11-12 days (*Nfasc*-null mice fail to survive past P7; Sherman *et al.*, 2005; Zonta *et al.*, 2008). By utilizing a similar transgenic rescue approach, an embryonic neuronal isoform of Neurofascin Nfasc140, has also been observed to reconstitute CNS nodes of Ranvier (Zhang *et al.*, 2015). Even though these mice display significant motor problems, they are, nevertheless, viable up to 9 months of age (Zhang *et al.*, 2015). Together, these reports confirm an important developmental and functional role for neuronal neurofascins in CNS nodes of Ranvier assembly.

A further role for Nfasc186 resides in maintaining the nodes of Ranvier and paranodal junctions in the CNS. Conditional ablation of Nfasc186 results in the loss of various nodal components and disruption of the paranodal junctions (Desmazières *et al.*, 2014). This latter result has also been reported during development in mice lacking Nfasc186 (Thaxton *et al.*, 2011). Together, these results point to an important role of Nfasc186 in the maintenance of the nodes of Ranvier and paranodal junctions.

Contactin is enriched solely in CNS nodes of Ranvier, yet it is expressed in both PNS and CNS paranodes (Rios *et al.*, 2003). The fact that it is expressed in both the nodes and paranodes presents a challenge in trying to determine specific roles of nodal Contactin. Indeed, Çolakoğlu *et al.* (2014) recently reported that

Contactin-1 mutant mice have disrupted nodes of Ranvier; however, this disruption may be attributed to either nodal, paranodal, or glial Contactin. What can be gleaned from several previous experiments is that Contactin interacts with nodal components such as Nfasc186 (Volkmer *et al.*, 1998), NrCAM (Morales *et al.*, 1993), phosphacan (Peles *et al.*, 1995), Tenascin-R (Volkmer *et al.*, 1998), and $\beta 1Na_v$ (McEwen *et al.* 2004), thereby placing it as a possible associative partner in other mechanisms that are thought to cluster CNS nodes of Ranvier. In this light, it has been reported that Contactin can increase the cellular surface expression of Na_v , suggesting that Contactin is involved in distributing Na_v in axons (Kazarinova-Noyes *et al.*, 2001).

The auxiliary CAM-like Na_v β -subunits are also enriched at CNS nodes of Ranvier where they are observed to interact with several nodal CAMs, cytoskeletal components, and ECM molecules (see O'Malley and Isom, 2015). Both $\beta 1Na_v^{-/-}$ and $\beta 2Na_v^{-/-}$ mice have normally formed CNS nodes of Ranvier (Chen *et al.*, 2002, 2004); however, optic nerves from $\beta 1Na_v^{-/-}$ mice display fewer mature nodes of Ranvier and slower axonal conduction compared to wild-type mice, all of which may be linked to the observation that 30% of the paranodal junctions are altered in the $\beta 1Na_v^{-/-}$ mice (Chen *et al.*, 2004). $\beta 2Na_v^{-/-}$ mice display no reduction in $Na_v1.6$ at the nodes of Ranvier (Chen *et al.*, 2012). $\beta 4Na_v$ is also enriched at CNS nodes (Buffington and Rasband, 2014), but its role in their assembly has yet to be explored.

3.2.2 Intrinsic mechanisms of CNS nodes of Ranvier formation

3.2.2.1 Cytoskeletal Scaffolds

As we saw in the first chapter, cytoskeletal scaffolding proteins are highly implicated in the patterning and establishment of specialized cell membranes. Particularly in the context of our discussion, these intrinsic neuronal membrane organizers have also been observed to play a key role in assembling CNS nodes of Ranvier. Kordeli and colleagues (1995) first put forth the hypothesis of an intrinsic cytoskeletal clustering mechanism 20 years ago with the observation of ankyrinG at nodes of Ranvier in central myelinated fibers. Later work by the same laboratory

showed that ankyrinG was located at P9 optic nerve nodes prior to other nodal components such as β IV-spectrin, Na_v and Nfasc186, but overlapped with or was bordered by Caspr (Jenkins and Bennett, 2002). Another report observed that ankyrinG formed in nodal clusters prior to paranodal aggregates of Caspr in P7 mouse corpus callosum (Mathis *et al.*, 2001), suggesting that ankyrinG could cluster CNS nodal components prior to paranodal junction formation. Therefore, to understand the role of ankyrinG with respect to the paranodal junctions, both Mathis *et al.* (2001) and Jenkins and Bennett (2002) utilized *jimpy* mice, a dysmyelinating mutant that does not have intact paranodal junctions and thus non-clustered Caspr, and reported that corpus callosum and optic nerve nodes of Ranvier, respectively, were unimpaired. Ultimately, these two independent reports suggested an important role for ankyrinG in CNS nodes of Ranvier assembly.

Yet, as seen above in this section, we now know that multiple mechanisms are able to assemble CNS nodes of Ranvier. With that in mind, Susuki *et al.* (2013) utilized a genetic ablation approach of the paranodal junctions and ECM components to understand the role of the cytoskeletal scaffolds in CNS nodes of Ranvier formation. By combining *Caspr*^{-/-} mice with *Brevican*^{-/-}, *Versican*^{-/-}, *Bral*^{-/-}, or *Brevican*^{-/-} and *Versican*^{-/-} mice (thereby disrupting the paranodal junctions and most of the ECM components), Susuki *et al.* (2013) observed that in the optic nerve of each of these mice there was a significant reduction in the amount of nodes of Ranvier formed compared to single knockouts and controls, but there was no apparent disruption in the nodal molecular organization in the double or triple paranodal junction/ECM mutants. Together, these results confirm that cytoskeletal components are sufficient to cluster CNS nodes of Ranvier. But, as the nodal scaffolding components are comprised of ankyrins and spectrins, what is the contribution of each scaffolding component regarding CNS nodes of Ranvier assembly?

β IV-spectrin links the nodal complex to the actin cytoskeleton, so therefore it could be possible that β IV-spectrin is involved in its initial clustering. Recent results would suggest that this is not the case considering that *qv^{3J}*-null mice

display no difference in the percentage of nodes of Ranvier in the optic nerve at early post-natal time points compared to controls (Susuki *et al.*, 2013). In contrast, at 1.5 months and 6 months of age in qv^{3J} -null mice (Yang *et al.*, 2004, 2007) and at 3 months in the βIV -spectrin-null mice (Komada and Soriano, 2002) there is decreased nodal immunoreactivity of ankyrinG and Na_v compared to controls, and the clusters are widely dispersed (Yang *et al.*, 2004, 2007; Komada and Soriano, 2002). These results suggest that βIV -spectrin is most likely not involved in assembly of CNS nodes of Ranvier but rather their maintenance.

Therefore, as it appears that βIV -spectrin is mainly important for CNS nodes of Ranvier maintenance, what is the role of ankyrinG in their formation? A loss of function approach would most likely shed light on the subtle roles of ankyrinG in this process, but utilizing mutant ankyrinG mice in this context is incredibly challenging due to the fact that ankyrinG is present in multiple tissues (Kordeli *et al.*, 1995). Therefore, this necessitated a strategy for region specific loss of function. In looking to use region specific ankyrinG ablation, Zhou *et al.* (1998) observed through *in situ* hybridization that exon1b of ankyrinG (one of the five first alternative exons of ankyrinG) was expressed only in the cerebellum, and thus was able to generate a cerebellum-specific ankyrinG mutant mouse. While ankyrinG's role in clustering AIS components using this mouse is widely accepted (Zhou *et al.*, 1998; Jenkins and Bennett, 2001), reports regarding ankyrinG's role in assembling CNS nodes of Ranvier using the cerebellum-specific mutant mouse are inconsistent. Barry *et al.* (2014) showed that loss of ankyrinG in Purkinje neurons showed a marked reduction of Na_v immunostaining at nodes of Ranvier, while Jenkins and Bennett (2002) observed clustering of ankyrinG at Purkinje neuron nodes of Ranvier, suggesting that ankyrinG can remain in cerebellar Purkinje neuron nodes of Ranvier. Lastly, Ho *et al.* (2014) reported robust cerebellar immunolabeling of Na_v at nodes of Ranvier. Consequently, results from this model do not provide a clear picture of the role of ankyrinG in CNS nodes of Ranvier assembly.

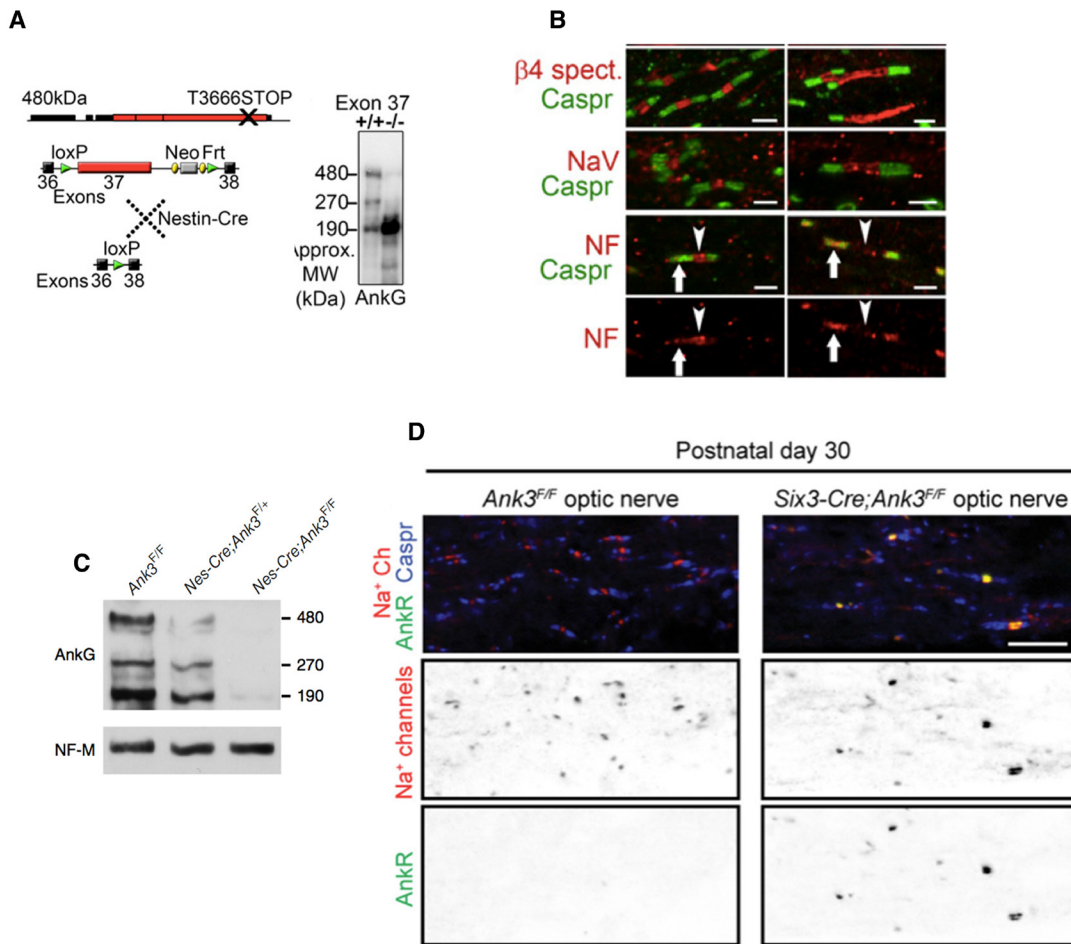


Figure 31: Cre-lox systems utilized to study the roles of ankyrinG in CNS nodes of Ranvier assembly. **(A)** Giant-ankyrin specific knockout by excising exon 37. 480-kDa and 270-kDa ankyrinG isoforms are lost, while 190-kDa remains (western blot, right). **(B)** Loss of exon 37 results in significant alterations to CNS nodal components (red). Both **(A)** and **(B)** adapted from Jenkins *et al.*, 2015. **(C)** *Ank3^{F/F}* mice lack all isoforms of ankyrinG. **(D)** Optic nerve specific loss of ankyrinG results in the rescue of CNS nodes of Ranvier by ankyrinR (green). Adapted from Ho *et al.*, 2014.

Several recent reports utilizing the Cre-Lox recombination system on other ankyrinG exons suggest further intricacies of its role in clustering CNS nodes. Using nestin-Cre recombination of the giant exon from ankyrinG (Fig. 31A; results in the loss of both 480-kDa and 270-kDa ankyrinG isoforms in neurons and glial cells), Jenkins *et al.* (2015) reported in P20 corpus callosum that nodes of Ranvier were significantly altered, wherein the number of nodal clusters was diminished by 80% compared to controls (Fig. 31B). The remaining 20% of nodes had diffuse expression of nodal components between paranodal flanking clusters of Caspr (Fig. 31B), suggesting that the nodal clustering process stalled but the remaining clustering could be due to 190-kDa ankyrinG or other known CNS clustering mechanisms (Jenkins *et al.*, 2015).

A recent study from Ho *et al.* (2014) reported that nodes of Ranvier form normally in mice lacking ankyrinG specifically in the optic nerve (Fig. 31C and D; *Six3-Cre;Ank3^{F/F}*, these mice lack exon 23 and 24 of ankyrinG in retinal ganglion cells, resulting in the loss of all ankyrinG isoforms). Surprisingly, with this optic nerve specific loss of ankyrinG, Ho *et al.* (2014) also reported that there was clustering of ankyrinR at nodes of Ranvier (Fig. 31D), which could also rescue CNS nodes of Ranvier in absence of ankyrinG. Moreover, ankyrinR expression was observed to be colocalized with its scaffolding binding partner β 1-spectrin, but loss of ankyrinR by itself did not disrupt CNS nodes (Ho *et al.*, 2014). While the study from Ho *et al.* (2014) did not detail the CNS nodes of Ranvier clustering in the double ankyrinG/ankyrinR knockout (*Avil-Cre;Ank3^{F/F}; Ank1^{pale/pale}*), they did observe in DRG sensory neurons that there was a strong decrease in nodes of Ranvier formation, suggesting that these two ankyrins are necessary to form nodes of Ranvier.

These two last studies provide an interesting, yet complex role for ankyrins. It is challenging to resolve the individual contributions of ankyrins in these multiple reports since the giant 270-kDa and 480-kDa ankyrinG isoforms appear to play a role in CNS nodes of Ranvier formation, while ankyrinR can substitute for ankyrinG when ankyrinG is completely lost. The different models used give rise to

divergent conclusions; yet, what is apparent in taking these results together is a supportive conclusion of ankyrins as a scaffolding protein family are able to initiate the clustering of Na_v and assemble CNS nodes of Ranvier.

3.2 Trafficking and Targeting of Neuronal Nodal Components

The polarization and length of axons presents a veritable challenge to the select patterning of excitable and non-excitable domains along the axon. While nodal assembly requires neuron-glia interactions, neurons must first transport nodal components in order to be clustered at the developing nodes of Ranvier, and therefore neurons require distinctive mechanisms for protein delivery to these highly excitable domains that can extend far away from the cell body. Several questions come to light in regards to the selective transport of the nodal components: 1) How do nodal components arrive to the developing nodes of Ranvier? 2) Do sodium channels, CAMs and cytoskeletal components share the similar targeting mechanisms? 3) Are these mechanisms similar between the CNS and PNS? and 4) What are the mechanisms by which sodium channel isoforms are differentially targeted to the nodes of Ranvier?

Several models have been proposed as to how proteins are targeted to specialized domains. The first model is through select targeting of the nodal component through vesicles to the developing nodes; the second is through random insertion of the nodal component in the neuronal membrane of somatodendritic regions or the distal axon followed by endocytosis and targeting to the proper domain (i.e. transcytosis); the last is selective retention mediated either by diffusion trapping or by association with scaffolding proteins to sequester nodal components to these specific sites while they are internalized in other regions destined for lysosomal degradation (Fig. 32; Lasiecka and Winckler, 2011). Na_v channels appear

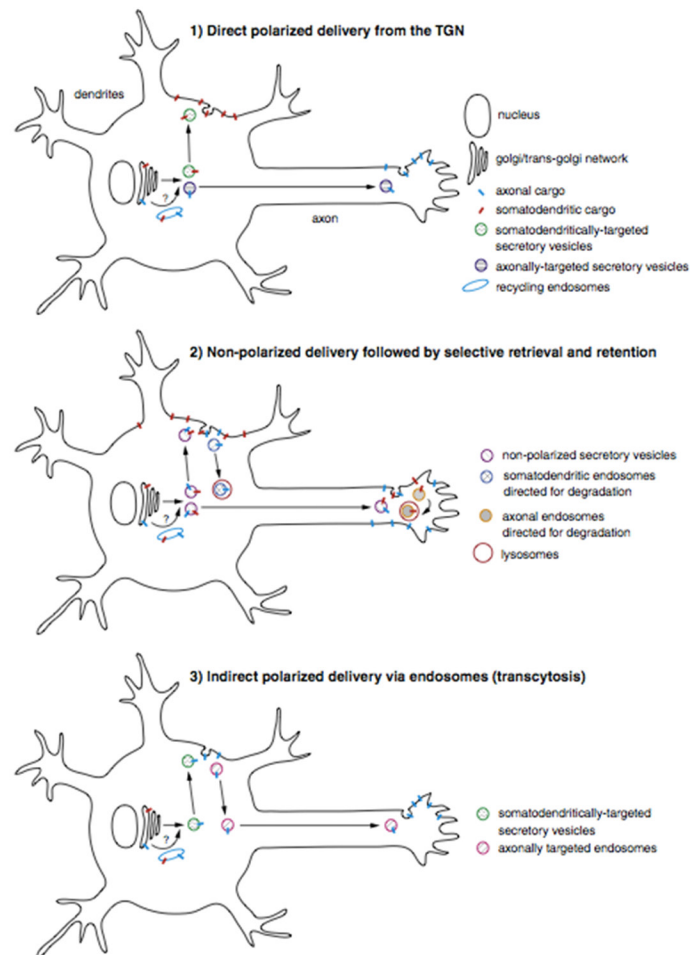


Figure 32: Overview of the trafficking pathways axonal proteins to be delivered to specific axonal domains. From Lasiecka and Winckler, 2011.

to follow a selective retention model for axonal localization that is ankyrinG dependent (Leterrier *et al.*, 2011; Barry *et al.*, 2014). Na_v channels are first unsystematically localized to the somatodendritic compartment and distal axon (Leterrier *et al.*, 2011). At this step Na_v can be harnessed by ankyrins through a 9 amino acid sequence in the cytoplasmic loop between II and III of Na_v that interact with the membrane-binding domain of ankyrin (Garrido *et al.*, 2003; Lemaillet *et al.*, 2003; Pan *et al.*, 2006), or the unbound Na_v is selectively endocytosed via two endocytosis signals located in the C-terminal tail and proximal region of the Na_v II-III loop (Garrido *et al.*, 2001; Fache *et al.*, 2004; Leterrier *et al.*, 2011). Importantly, the affinity for this interaction between Na_v and ankyrinG is highly mediated by CK2 (Brechet *et al.*, 2008; Hien *et al.*, 2014), where CK2 is involved in phosphorylation of several serine residues residing in the Na_v ankyrin-binding motif (Brechet *et al.*, 2008; Hien *et al.*, 2014). This CK2-mediated phosphorylation is important for localizing Na_v to the AIS (Brechet *et al.*, 2008; Hien *et al.*, 2014), but it appears as though it is not an absolute requirement for Na_v localization to the nodes of Ranvier (Gasser *et al.*, 2012), where at the nodes CK2 most likely facilitates greater affinity of ankyrinG for Na_v channels. In the PNS, vesicular transport is necessary in order for Na_v to reach the developing node of Ranvier (Zhang *et al.*, 2012).

Continuing on the targeting of Na_v through Na_v-ankyrinG interaction, trafficking of Na_v can also be mediated through an indirect interaction with kinesins via ankyrinG. Kinesins are anterograde molecular motors that move along microtubule tracks and transport various types of cargoes (Hirokawa *et al.*, 2010). The II-III cytoplasmic loop of Na_v interacts with the ankyrin-repeats of ankyrinG (Bouzidi *et al.*, 2002), but these ankyrin-repeats also interact with the tail domains of conventional kinesin-1 (Barry *et al.*, 2014). Overexpression of the mutated tail domain of kinesin-1 disrupts trafficking of the Na_v II-III loop and reduction in the axonal targeting of Na_v to the nodes of Ranvier (Barry *et al.*, 2014). Taken together, these results point to an important interaction between ankyrinG and Na_v, where

ankyrinG restricts Na_v to the proper subcompartmentalized domains along the axon and participates in the transport of Na_v through kinesin-1.

Nodal potassium channels can interact with cytoskeletal scaffolding proteins in order to localize to excitable domains. K_v7 can interact with ankyrinG through a motif analogous to the Na_v ankyrin-binding motif that is required for its localization at the AIS (Cooper, 2011). The localization of K_v7.2 to the nodes of Ranvier is dependent on the presence of the C-terminal domain of β IV-spectrin (Devaux *et al.*, 2010). As for K_v3.1b, it can directly bind with the tail domain of kinesin-1 (Xu *et al.*, 2010).

The accumulation of nodal scaffolding components seems to be dependent on vesicular transport from the neuronal cell body. Inhibiting vesicular transport through Brefeldin A treatment blocks the clustering of ankyrinG at developing CNS and PNS nodes of Ranvier (Kaplan *et al.* 2001; Zhang *et al.*, 2012). PNS nodes have also been observed to be devoid of ankyrinG and β IV-spectrin clusters when axons were mechanically separated from the neuronal cell body in and kept from undergoing Wallerian degeneration (Zhang *et al.*, 2012), further suggesting that ankyrinG must be trafficked to the developing node in vesicles from the soma. Additionally, overexpression of kinesin-1 with a mutation in the ankyrin-binding domain reduces the axonal level of ankyrinG at nodes of Ranvier in the CNS (Barry *et al.*, 2014). In *Drosophila* S2 cells, extracellular *trans* homophilic interactions of β 1Na_v have been shown to increase the recruitment of ankyrinG at points of cell-cell contact (Malhotra *et al.*, 2000). Nevertheless, the recruitment of ankyrinG requires phosphorylation of the residue Tyr¹⁸¹ in the intracellular region of β 1Na_v (Malhotra *et al.*, 2002). Furthermore, palmitoylation of ankyrinG at Cys⁷⁰ permits its targeting to excitable domains (He *et al.*, 2012). Together, these reports confirm that ankyrinG transport is mediated through vesicular trafficking, and can be recruited to the membrane via interactions with Na_v β -subunits. Whether ankyrinG goes through transcytosis or is directly targeted to nodes of Ranvier remains to be observed.

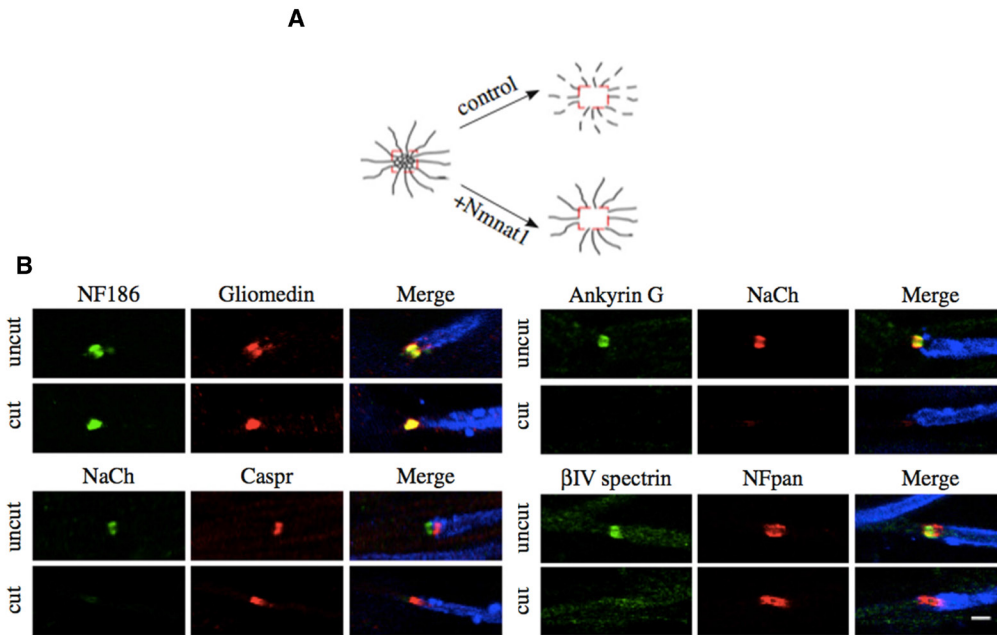


Figure 33: Neurofascin186 is selectively retained at PNS nodes of Ranvier. **(A)** Schematic of mechanically separated axons kept from degeneration through *Nmnat1*. **(B)** Nfasc186 (green top left panels) is able to cluster at nodes of Ranvier in cut axons, while the other nodal components fail to cluster. Adapted from Zhang *et al.*, 2012.

Nfasc186 appears sequestered to the nodes of Ranvier in the PNS through selective retention from a mobile surface pool of Nfasc186 molecules (Fig. 33). Zhang *et al.* (2012) showed through several important experiments that Nfasc186 was able to cluster to PNS nodes in culture and *in vivo* through diffusion trapping via interactions of its extracellular domain with gliomedin and NrCAM on Schwann cell microvilli (Fig. 33). This extracellular Nfasc186 domain is also important for its clearance from the internode (Dzhashiashvili *et al.*, 2007), but the FIGQY cytoplasmic domain of nodal Nfasc186 is ultimately necessary for replenishing vesicular transported Nfasc186 to the AIS and mature PNS nodes of Ranvier (Dzhashiashvili *et al.*, 2007; Zhang *et al.*, 2012). Modulation of the surface expression of Nfasc186 is mediated through its interaction with doublecortin, since it increases endocytosis from the somatodendritic regions of the neuron (Yap *et al.*, 2012). In primary cultured hippocampal neurons, Nfasc186 is enriched to the distal axon independently of ankyrinG, yet it becomes clustered to the AIS based on ankyrinG interactions (Boiko *et al.*, 2007). Furthermore, in the CNS, Nfasc186 can localize to the nodes through its extracellular and intracellular domains (Susuki *et al.*, 2013), but it remains to be seen whether its targeting to the developing node is mainly dependent on selective retention through the paranodal junctions or ankyrinG, or via direct transport.

3.2.1 Mechanisms for the Transition of Voltage-Gated Channels at Nodes of Ranvier

The immature and mature nodes of Ranvier display an interesting switch in their voltage-gated sodium channels and auxiliary β -subunit isoforms in both the PNS and CNS. The developing CNS nodes of Ranvier display a high concentration of Na_v1.2 as early as P9 in the optic nerve either absent of or flanked by paranodal Caspr clustering (Boiko *et al.*, 2001). Concentration of Na_v1.2 subsequently declines at mature optic nerve nodes of Ranvier and is eventually replaced by Na_v1.6 (Fig. 34; Boiko *et al.*, 2001), but Na_v1.1 is observed to be continually expressed in the spinal cord (Duflocq *et al.* 2008). In the PNS, sciatic nerve nodes of Ranvier are

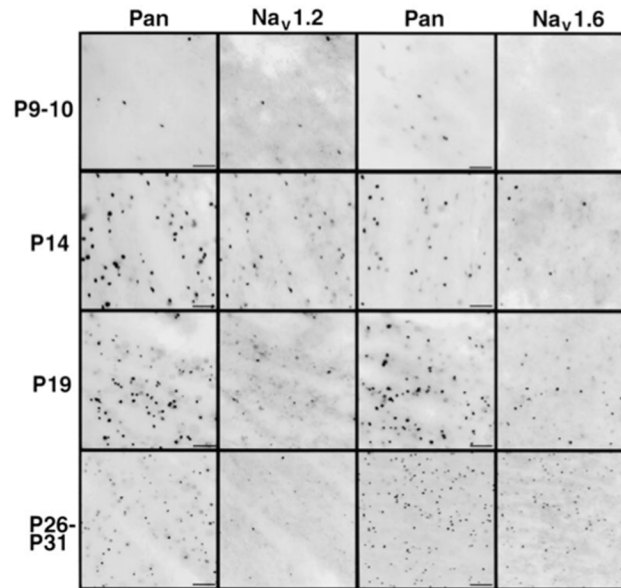


Figure 34: Developing optic nerve nodes of Ranvier are enriched in Na_v1.2, but overtime Na_v1.2 is replaced at mature nodes by Na_v1.6. From Boiko *et al.*, 2001.

enriched in both $\text{Na}_v1.2$ and $\text{Na}_v1.6$, but then transition to $\text{Na}_v1.6$ only (Schafer *et al.*, 2006). This developmental switch of Na_v isoforms may be functionally relevant in altering action potential conduction, which in turn, as described earlier, has implications in demyelinating diseases (Craner *et al.*, 2004); yet, what are the targeting mechanisms behind such a transition and are these changes different between the PNS and CNS? While answers to these questions have been partly fulfilled through several reports, the mechanism of this transition has yet to be fully understood.

Interestingly, in the PNS, the targeting of $\text{Na}_v1.6$ at nodes of Ranvier and the $\text{Na}_v1.2$ to $\text{Na}_v1.6$ isoform switch has been suggested to not depend on a signaling role via paranodal junctions and myelination. Mutant mice with altered axoglial junctions do not appear to have a defect in the $\text{Na}_v1.6$ isoform switch in PNS nodes (Rios *et al.*, 2003; Rasband *et al.*, 2003; Suzuki *et al.*, 2004). More recently, it has been described that this transition in the PNS is pre-programmed regardless of myelination (Luo *et al.*, 2014). By using transgenic mice ($\text{Oct6}^{\Delta\text{SCE}/\beta_{\text{geo}}}$) that display delayed PNS myelination during the first postnatal week but returns to normal thereafter, Luo *et al.* (2014) observed that there was a delay in nodal clustering between all PNS sodium channel isoforms. Yet, during this delayed myelination, $\text{Na}_v1.6$ gene and protein expression were observed to increase while the other Na_v isoforms remained constant or decreased, suggesting that isoform expression is preprogrammed and the myelination process clusters nodes from existing pools of sodium channel isoforms instead of signaling $\text{Na}_v1.6$ to the developing nodes to promote a sodium channel isoform switch (Luo *et al.*, 2014).

In the CNS, the regulation of the Na_v isoform switch may be dependent on a combination of compact myelin, axo-glial junctions, and ankyrins. By using the dysmyelinating *Shiverer* mouse, Boiko *et al.* (2001) showed that $\text{Na}_v1.6$ was severely disrupted in optic nerve nodes of Ranvier, suggesting that $\text{Na}_v1.6$ targeting and the $\text{Na}_v1.2$ to $\text{Na}_v1.6$ isoform switch in the CNS is mediated by tight axoglial contact. Additionally, $\text{Na}_v1.6$ is normally clustered in mice expressing *Nfasc186* in a *Nfasc*-null background (Zonta *et al.*, 2008), which is similar to that observed in *jimpy* mice

that have disrupted paranodal junctions (Jenkins and Bennett, 2002). Na_v1.6 initial localization appears to be normal in the galactolipid-deficient *CGT*-null and *CST*-null mice that display disrupted transverse bands but normally compacted myelin (Rasband *et al.*, 2003; Suzuki *et al.*, 2004). In these mice Na_v1.6 is critically disrupted over time, suggesting an important role for transverse bands in maintaining the long-term restriction of this Na_v isoform to CNS nodes of Ranvier. On the other hand, support for strict axoglial junction-mediated targeting of nodal Na_v1.6 has been reported in both *Caspr*^{-/-} and *Contactin*^{-/-} mice, where there is a strong reduction in the amount of Na_v1.6⁺ optic nerve nodes of Ranvier (Rios *et al.*, 2003; Çolakoğlu *et al.*, 2014). Lastly, and unlike Na_v1.2, Na_v1.6 is not observed in node-like clusters along rat retinal ganglion cell axons when treated with oligodendrocyte conditioned medium (Kaplan *et al.*, 2001), further supporting the role of axoglial contacts in targeting Na_v1.6 to CNS nodes of Ranvier and promoting the switch between these two sodium channel isoforms.

In this process, it also appears as though ankyrins may be necessary for targeting Na_v1.6. Gasser *et al.* (2012) reported that the ankyrinG-binding motif of Na_v1.6 was necessary to target it to CNS nodes of Ranvier; yet, it has been recently published that ankyrinG exon1b knockout mice display robust clustering of Na_v1.6 in the cerebellum (Ho *et al.*, 2014). It is tempting to speculate in this case that Na_v1.6 may interact with ankyrinR in order to be clustered at mature CNS nodes of Ranvier. AnkyrinG could preferentially target Na_v1.6 to normal mature CNS nodes since it may likely have a higher affinity for Na_v1.6 than ankyrinR, similar to that of ankyrinG and ankyrinR with Nfasc186 (Ho *et al.*, 2014). Additionally, Gasser *et al.* (2012) mutated a glutamic acid residue within the ankyrinG-binding motif of Na_v1.6, which may have also removed any possible interaction with ankyrinR and thereby resulted in a lack of Na_v1.6 at the nodes of Ranvier in this report.

What could be the interaction between compact myelin and ankyrins in the transition from Na_v1.2 to Na_v1.6 in CNS nodes of Ranvier? It has been reported that phosphorylation of axonal cytoskeletal proteins and neuronal gene expression are altered in the optic nerve of *shiverer* mice, suggesting that compact myelin can

sufficiently regulate important cytoskeletal components (Brady *et al.*, 1999). Ankyrins, which are cytoskeletal scaffolding components that can interact with Na_v1.6 (Garrido *et al.*, 2003; Lemailet *et al.*, 2003; Pan *et al.*, 2006; Akin *et al.*, 2015), could be involved in its trafficking, similar to that observed with the interactions of Na_v1.2 and ankyrinG to KIF5 (Barry *et al.* 2014). Accordingly, one could conceivably speculate that the altered compact myelin observed in *shiverer* mice may impact the level of ankyrin expression, thus altering the trafficking and stabilization of Na_v1.6 at mature CNS nodes.

In contrast to the α -subunits, our knowledge regarding a transition of Na_v β -subunits in developing and mature nodes of Ranvier is quite limited. At present, it appears that the time course of CNS β 1Na_v nodal clustering is seen to follow the myelination time course. Indeed, β 1Na_v is absent from node-like clusters (while β 2Na_v is present) along purified rat RGC axons when treated with oligodendrocyte conditioned medium (Kaplan *et al.*, 2001), supporting the conclusion that myelin (or axo-glial contact) is required for β 1Na_v nodal clustering and most likely localizes to mature nodes of Ranvier, while β 2Na_v is able to cluster to the developing nodes without paranodal junctions being formed. Interestingly, the disulfide linkage between β 2Na_v and α -subunits through the Cys-26 residue is necessary for targeting β 2Na_v to both the AIS and the nodes of Ranvier, and additionally Cys-26 is necessary for rendering β 2Na_v resistant to detergent extraction (Chen *et al.*, 2012), suggesting that this residue is highly important for its stabilization on the axon. Whether β 2Na_v is slowly replaced by β 1Na_v similarly to that of Na_v1.2 by Na_v1.6, or whether Na_v β -subunits are involved in the Na_v1.2 to Na_v1.6 isoform transition remain to be seen.

3.3 Aim of the Dissertation

Considering that there are several mechanisms sufficient to assemble CNS nodes of Ranvier, we set out to further understand the overlapping mechanisms necessary for these complex domains to form. The first aim of my dissertation was to characterize the extrinsic and intrinsic factors governing nodal protein clustering

in an *in vitro* hippocampal culture system, and additionally to explore the functional consequences of these clusters, which we called “prenodes”, prior to myelin ensheathment through electrophysiological recordings. The results of this work are published (Freeman *et al.*, 2015) and inserted in page 139. As detailed in the previous section, our understanding of how nodal molecules are trafficked and sequestered to the developing CNS nodes of Ranvier have yet to be well described. The model system that we have used in the first part of my dissertation is a particularly useful system since the clusters of nodal proteins form quickly and prior to myelination. Therefore, the second aim of my dissertation was to study the trafficking of several fluorescently—tagged nodal constructs through live imaging in hippocampal cultures. This is a current work in progress and is detailed starting on page 153.

Part II: Results

Article I

Acceleration of conduction velocity linked to clustering of nodal components precedes myelination

Sean A. Freeman, Anne Desmazières, Jean Simonnet, Marie Gatta, Friederike Pfeiffer, Marie Stéphane Aigrot, Quentin Rappeneau, Serge Guerreiro, Patrick Pierre Michel, Yuchio Yanagawa, Gilles Barbin, Peter J. Brophy, Desdemona Fricker, Catherine Lubetzki, and Nathalie Sol-Foulon

PNAS, 2015, 112 : E321-E328

Summary

The clustering of voltage-gated sodium channels (Na_v) at the nodes of Ranvier is an important step in permitting saltatory conduction along myelinated axons. Along with Na_v , nodes of Ranvier are concentrated with cellular-adhesion molecules such as neurofascin186 (Nfasc186), NrCAM and contactin, and cytoskeletal molecules such as ankyrinG and β IV-spectrin. These molecules, which interact with Na_v , have been observed to play a role in either the clustering or stabilization of the nodes of Ranvier (Chang and Rasband, 2013).

Formation of the nodes of Ranvier is neuron-glia dependent. Myelinating cells of the CNS (oligodendrocytes) and PNS (Schwann cells) form tight septate-like paranodal junctions that flank the nodes of Ranvier or secrete several molecules that incorporate into the extracellular matrix. The mechanisms governing nodes of Ranvier formation in the PNS are well described and depend either on the interaction of ECM molecules with Nfasc186 or the paranodal junctions (Eshed *et al.*, 2005, 2007; Feinberg *et al.*, 2010). Yet, formation of CNS nodes of Ranvier appears to be more complex since there are several overlapping assembly mechanisms that can override when one of them fails (Susuki *et al.*, 2013).

Therefore, the objective of this study was to look at the mechanisms of nodes of Ranvier formation in the CNS using a dissociated hippocampal culture system in order to tease apart the individual contributions of several mechanisms implicated in CNS nodes of Ranvier assembly. This study further allowed us the unique opportunity to explore the functional consequences of node-like clusters in the absence of myelination.

In order to study mechanisms of CNS nodal assembly, we utilized dissociated mixed hippocampal cultures from embryonic day 18 (E18) rats as an *in vitro* model system. These cultures contain neurons such as glutamatergic neurons and GABAergic interneurons, and glial cells such as microglia, astrocytes and oligodendrocytes. During the first week of culture, all neurons formed AISs as expected; yet, at 14 days *in vitro* (DIV) we observed that discrete node-like clusters of Na_v , ankyrinG, and Nfasc186 formed along some axons. Importantly, these

clusters formed in the absence of myelination and axoglial junctions. Since these canonical nodal components clustered in the absence of myelin and axoglial junctions, we named these pre-myelinating nodal clusters “prenodes”.

Because prenodes were not observed in all neurons, we questioned whether there might be a subpopulation of neurons permissive to prenodal assembly. Indeed, 70% of glutamate decarboxylase isoform of 67 kDa (GAD) immunolabeled GABAergic interneurons formed these clusters, while prenodal clustering was absent on calmodulin kinase II (CaMKII) immunolabeled glutamatergic neurons. Furthermore, prenodal clustering was majorly restricted to parvalbumin- and somatostatin-positive interneurons.

Our *in vitro* system is also useful in that over several weeks in culture oligodendrocytes will eventually myelinate axons with the help of a myelinating medium. When adding myelination medium to these mixed hippocampal cultures we observed robust PLP⁺ myelinating segments on the axons of both CaMKII and GABAergic neurons, and clustering of nodal and paranodal components in both neuronal populations. Taken together, these results suggest that hippocampal glutamatergic neurons form nodes of Ranvier concomitantly with myelination, while GABAergic interneurons form nodes of Ranvier prior to myelin ensheathment.

To address the role of glial cells in prenodal formation, we created nearly purified dissociated hippocampal neuronal cultures through anti-mitotic treatment to eliminate glial cells. Prenodal clustering along the axons of all neurons was rare. However, when purified oligodendrocyte lineage cells or conditioned media (OCM) prepared from these oligodendroglial cultures were added to the purified neuronal cultures, restoration of prenodal clustering was observed specifically on GABAergic interneurons. These results suggest that prenodal assembly is driven through oligodendroglial secreted factor(s) that interact(s) only with GABAergic interneurons.

As hippocampal GABAergic neurons express Na_v1.1, Na_v1.2, and Na_v1.6 at the nodes of Ranvier (Duflocq *et al.*, 2008), we analyzed the presence of these Na_v isoforms in prenodal clusters over time. Na_v1.1 remained constant during the

entirety of our analysis, while $\text{Na}_v1.2$ diminished in expression over time in culture. Much to our surprise at 17 DIV, $\text{Na}_v1.6$ began to appear at clusters in the absence of myelination, eventually replacing $\text{Na}_v1.2$ at prenodes. In purified neuronal cultures treated with OCM, $\text{Na}_v1.6$ was never present and $\text{Na}_v1.2$ persisted until the latest culture time point. These results suggest that targeting of $\text{Na}_v1.6$ to prenodal clusters does not rely on axoglial junctions and myelination, but instead on the physical presence of glial cells.

We then investigated the roles of intrinsic factors governing prenodal clustering. Because neurofascin is highly important for CNS nodes of Ranvier assembly (Sherman *et al.*, 2005; Zonta *et al.*, 2008), we addressed whether this family of CAMs is necessary for prenodal formation by preparing mixed hippocampal cultures from *Nfasc*-null mice. These cultures showed no difference in prenodal formation compared to wild-type cultures, suggesting that neurofascins are not necessary to form prenodes. Cytoskeletal scaffolding proteins are additionally well described to be essential for CNS nodes of Ranvier formation (Jenkins and Bennett, 2002; Susuki *et al.*, 2013), therefore we transfected mixed hippocampal cultures with either ankyrinG miRNA or scrambled miRNA. Here, we observed abolishment of pre-nodal clustering in cultures transfected with ankyrinG miRNA. Ultimately, these results confirm that ankyrinG is the intrinsic organizer of prenodes.

This model system also presented us with a unique opportunity to study the functional roles of Na_v aggregates in the absence of myelination. First, we looked to explore the intrinsic differences of GABAergic neurons with and without clusters by preparing hippocampal cultures from *GAD67-GFP* knockin mice and performing whole-cell electrophysiological recordings on GFP⁺ cells. We observed from post-hoc immunocytochemical analysis that GABAergic neurons with prenodes had a significantly lower input resistance than GABAergic neurons without. As input resistance is linked to neuronal maturity, we concluded that the neurons with prenodes were more mature. To determine if prenodal clusters could increase axonal conduction velocity along GABAergic neurons prior to myelination, we

prepared mixed hippocampal cultures from *VGAT* (*Vesicular glutamate transporter*)-*Venus* rats and labeled axons prior to simultaneous soma-axon cell attached recordings with an antibody conjugated to Alexa-594 that targets the extracellular domain of Nfasc186. This labeling allowed us to discriminate between GABAergic neurons with and without prenodes during live recordings. Analysis of the simultaneous soma-axon cell attached recordings showed that GABAergic neurons with clusters had faster conduction velocities than GABAergic neurons without. Post-hoc analysis of the data further concluded that this increase was independent of axonal diameter. Taken together, these results strongly confirm that prenodal clustering acts as another means to increase axonal conduction velocity in the prior to myelination and independently of axonal diameter.

Finally, in order to expand upon the functional relevance of prenodes, we investigated whether these clusters formed *in vivo*. To test this, we used hippocampal tissue sections from *GAD67-GFP* mice and observed that axonal clusters of ankyrinG could be observed prior to myelination in the CA1 region of the hippocampus at P12. These results confirm that prenodal formation can occur during development prior to myelination.

This study sheds light on several key aspects of CNS nodes of Ranvier assembly. Extending previously described mechanisms, we reported that clusters of nodal components formed in the absence of myelination on GABAergic neurons *in vitro* and *in vivo*, and prenodal clustering is dependent on oligodendroglial secreted factors and the cytoskeletal scaffolding protein ankyrinG. Taken together, these results suggest that there are indeed overlapping, yet cooperative mechanisms by which CNS nodes of Ranvier form. The differential targeting of Na_v1.6 prior to myelination in mixed and purified hippocampal cultures was a novel finding, and illustrates the importance of glial cells in the targeting of this Na_v isoform. Finally, the fact that prenodes, independent of both myelin and axonal diameter, can accelerate conduction velocity puts forth another mechanism by which axons may increase conduction velocity, and it suggests that this may be functionally relevant during development.



Acceleration of conduction velocity linked to clustering of nodal components precedes myelination

Sean A. Freeman^{a,b,c,1}, Anne Desmazières^{a,b,c,1}, Jean Simonnet^{a,b,c}, Marie Gatta^{a,b,c}, Friederike Pfeiffer^{a,b,c}, Marie Stéphane Aigrot^{a,b,c}, Quentin Rappeneau^{a,b,c}, Serge Guerreiro^{a,b,c}, Patrick Pierre Michel^{a,b,c}, Yuchio Yanagawa^{d,e}, Gilles Barbin^{a,b,c}, Peter J. Brophy^f, Desdemona Fricker^{a,b,c}, Catherine Lubetzki^{a,b,c,g,1,2}, and Nathalie Sol-Foulon^{a,b,c,1,2}

^aSorbonne Universités Université Pierre et Marie Curie University of Paris 06, UMR_S 1127, Institut du Cerveau et de la Moelle–Groupe Hospitalo-Universitaire Pitié-Salpêtrière, F-75013, Paris, France; ^bINSERM U1127, F-75013, Paris, France; ^cCNRS UMR7225, F-75013, Paris, France; ^dDepartment of Genetic and Behavioral Neuroscience, Gunma University Graduate School of Medicine, Maebashi 371-8511, Japan; ^eJapan Science and Technology Agency, Tokyo 102-8666, Japan; ^fCentre for Neuroregeneration, University of Edinburgh, Edinburgh EH16 4SB, United Kingdom; and ^gAssistance Publique–Hôpitaux de Paris, Hôpital Pitié-Salpêtrière, 75013, Paris, France

Edited by William A. Catterall, University of Washington School of Medicine, Seattle, WA, and approved December 16, 2014 (received for review October 6, 2014)

High-density accumulation of voltage-gated sodium (Na_v) channels at nodes of Ranvier ensures rapid saltatory conduction along myelinated axons. To gain insight into mechanisms of node assembly in the CNS, we focused on early steps of nodal protein clustering. We show in hippocampal cultures that prenodos (i.e., clusters of Na_v channels colocalizing with the scaffold protein ankyrinG and nodal cell adhesion molecules) are detected before myelin deposition along axons. These clusters can be induced on purified neurons by addition of oligodendroglial-secreted factor(s), whereas ankyrinG silencing prevents their formation. The Na_v isoforms Na_v1.1, Na_v1.2, and Na_v1.6 are detected at prenodos, with Na_v1.6 progressively replacing Na_v1.2 over time in hippocampal neurons cultured with oligodendrocytes and astrocytes. However, the oligodendrocyte-secreted factor(s) can induce the clustering of Na_v1.1 and Na_v1.2 but not of Na_v1.6 on purified neurons. We observed that prenodos are restricted to GABAergic neurons, whereas clustering of nodal proteins only occurs concomitantly with myelin ensheathment on pyramidal neurons, implying separate mechanisms of assembly among different neuronal subpopulations. To address the functional significance of these early clusters, we used single-axon electrophysiological recordings in vitro and showed that prenodule formation is sufficient to accelerate the speed of axonal conduction before myelination. Finally, we provide evidence that prenodal clusters are also detected in vivo before myelination, further strengthening their physiological relevance.

node of Ranvier | sodium channel | myelination | GABAergic neuron | conduction velocity

Voltage-gated sodium (Na_v) channels are highly enriched at the axon initial segment (AIS) and the node of Ranvier, allowing generation and rapid propagation of action potentials by saltatory conduction in myelinated fibers. These axonal domains also contain cell adhesion molecules [e.g., neurofascin 186 (Nfasc186)] and the scaffolding proteins ankyrinG (AnkG) and β IV spectrin, which provide a potential link with the actin cytoskeleton (1). Flanking the nodes are the paranodes, where axoglial junctions between paranodal myelin loops and the axon are formed through interactions between axonal contactin-associated protein (Caspr)/contactin and glial Nfasc155 (2, 3). Although the mechanisms of nodal assembly are best characterized in the peripheral nervous system (4–9), less is known about the cellular and molecular mechanisms underlying node assembly in the CNS. ECM proteins, adhesion molecules, such as Nfasc186, and also, axoglial paranodal junctions have been shown to trigger CNS nodal clustering, although their respective roles remain uncertain (10–19). Moreover, axonal clustering of Na_v channels before myelin deposition and oligodendroglial contact has been shown to occur in retinal ganglion cell (RGC) cultures, where these clusters were induced by oligodendroglial-secreted factor(s) (20, 21).

Here, we have investigated the cellular and molecular mechanisms underlying nodal protein assembly in hippocampal neuron cultures. We first showed that evenly spaced clusters of Na_v channels, colocalizing with Nfasc186 and AnkG, are detected along axons before myelination. Strikingly, this prenodule assembly is restricted to GABAergic interneurons, suggesting the existence of different mechanisms of nodal assembly. The prenodule clustering can be induced on purified neurons by the addition of oligodendroglial-secreted factor(s) and also depends on intrinsic cues, such as AnkG. Furthermore, we also provide evidence that these clusters are detected in vivo before myelination on hippocampal tissue sections. Finally, to gain insight into their functional significance, we performed in vitro simultaneous somatic and axonal recordings and showed that the presence of prenodos increases the speed of action potential propagation along axons before myelination.

Results

Clusters of Nodal Proteins Are Detected Before Myelination on Hippocampal GABAergic Axons. To gain insight into the chronology of axonal domain assembly, we first analyzed the distribution of Na_v channels in mixed hippocampal cultures (i.e., neurons with oligodendrocytes and astrocytes) from embryonic day 18 (E18) rat embryos at different time points before myelination.

Significance

Cellular and molecular mechanisms underlying the assembly of nodes of Ranvier of myelinated axons in the CNS are still only partly understood. Our study shows the influence of intrinsic cues and glial extrinsic factors for nodal protein clustering before myelination on specific hippocampal neuronal subpopulations and extends to electrophysiological understandings and in vivo relevance. Although conduction velocity along axons has long been thought to mostly rely on the insulating properties of myelin, we here show that nodal protein aggregation can increase this speed in the absence of such insulation. These results highlight the role of nodal clusters per se on conduction velocity by uncoupling it from myelination.

Author contributions: S.A.F., A.D., J.S., G.B., D.F., C.L., and N.S.-F. designed research; S.A.F., A.D., J.S., M.G., F.P., M.S.A., Q.R., S.G., and N.S.-F. performed research; P.P.M., Y.Y., and P.J.B. contributed new reagents/analytic tools; S.A.F., A.D., J.S., D.F., C.L., and N.S.-F. analyzed data; and S.A.F., A.D., C.L., and N.S.-F. wrote the paper.

The authors declare no conflict of interest.

This article is a PNAS Direct Submission.

¹S.A.F., A.D., C.L., and N.S.-F. contributed equally to this work.

²To whom correspondence may be addressed. Email: catherine.lubetzki@psl.aphp.fr or nathalie.sol-foulon@upmc.fr.

This article contains supporting information online at www.pnas.org/lookup/suppl/doi:10.1073/pnas.1419099112/-DCSupplemental.

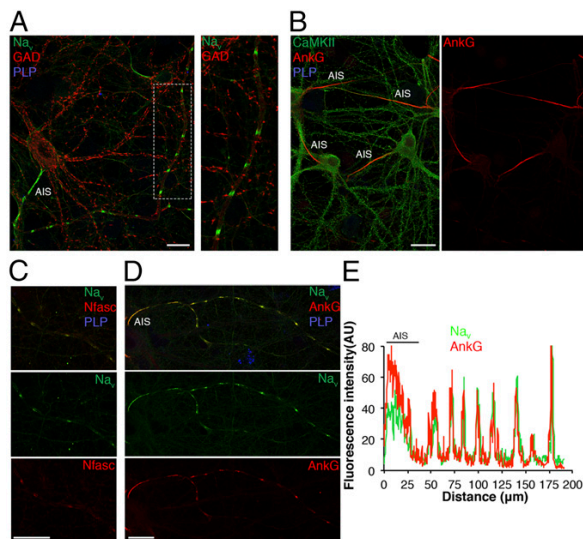


Fig. 1. Prenodes are formed before myelination on hippocampal GABAergic neurons in culture. Immunostaining of mixed hippocampal rat cultures at 17 DIV. (A) Clustering of Na_v (green) in the absence of myelin (PLP⁻; blue) along a GABAergic axon (GAD67⁺; red), (B) contrasting with the absence of prenodal clusters (AnkG; red) on the axons of pyramidal cells Ca²⁺/calmodulin-dependent protein kinase II⁺ (CaMKII⁺; green). Na_v clusters (green) colocalized with (C) Nfasc186 (Nfasc) and (D) AnkG (plot profile is in E) in red along unmyelinated axons (PLP⁻; blue). (Scale bars: 25 μm.)

Hippocampal neuronal cultures contain both glutamatergic pyramidal cells, identified by Ca²⁺/calmodulin-dependent protein kinase II immunolabeling (75% ± 5% of neurons), and GABA releasing interneurons, identified by glutamate decarboxylase isoform of 67 kDa (GAD67) expression (24.5% ± 3.9% of neurons). As might be predicted, Na_v channel accumulation was detected at the AIS of all neurons during the first week of culture and colocalized with AnkG and Nfasc186, whereas expression along the axon was diffuse and barely visible. Surprisingly, in contrast, at 17 days in vitro (DIV), evenly spaced clusters of Na_v channels AnkG and Nfasc186 were found exclusively localized on GABAergic neurons (67% ± 15% of total GAD67⁺ neurons) (Fig. 1 and Fig. S1). These clusters, which were formed in the absence of myelin ensheathment as indicated by the lack of proteolipid protein (PLP) immunostaining (Fig. 1 A, C, and D), were named prenodes. The percentage of hippocampal axons with prenodes increased as a function of time in vitro from 4.1% ± 3.1% at 14 DIV to 15.8% ± 3.5% and 17.1% ± 7.1% at 17 and 21 DIV, respectively. We also observed that the number of prenodes distributed along each axon increased from 14 to 21 DIV (Fig. S1B).

Because hippocampal interneurons are highly diverse (22), we further investigated whether neurons with prenodes are restricted to a particular interneuron subtype by characterizing calcium-binding protein (i.e., calbindin, calretinin, and parvalbumin) and somatostatin expression. Most neurons with prenodes were somatostatin⁺ and/or parvalbumin⁺ (81.3% ± 6.8% and 57.5% ± 3.5, respectively) (Fig. S2), suggesting an overlap in prenodal formation between varying interneuron subtypes, particularly those that express both somatostatin and parvalbumin together (23).

Prenode Assembly Requires Oligodendroglial Cues. To gain insight into the role of glial cells in prenode formation, we used purified hippocampal neuronal cultures through elimination of dividing

cells by antimetabolic treatment, which were virtually devoid of oligodendrocytes and contained a small percentage of astrocytes (less than 5%). We observed that purified neurons with nodal protein clusters along axons were rare (1.1% ± 0.7%) (Fig. 2 A and F). However, when we prepared highly purified populations of oligodendroglial lineage cells and added oligodendrocytes or oligodendroglial-conditioned medium (OCM) to purified neuronal cultures, the percentage of axons with prenodes increased, respectively from 1.1% ± 0.7% to 10.8% ± 3.3% and 11.9% ± 3.9% (Fig. 2F). Under these conditions, Na_v was observed to colocalize with AnkG and Nfasc186 in prenodes (Fig. 2 B and D). Furthermore, similar to mixed cultures, prenodes were restricted to GAD67⁺ neurons (Fig. 2C). The number of prenodes along each axon was decreased compared with mixed cultures (Fig. S1C), and the spacing between clusters was shorter in OCM-treated purified neurons compared with neurons in mixed cultures (9.6 ± 1.1 and 15.8 ± 1.8 μm, respectively; *P* = 0.028) (Fig. 2E). In addition, nodal protein clustering occurred preferentially along axons with highly phosphorylated neurofilaments, suggesting an association with neuronal maturity (Fig. 2D). Altogether, our results show that glial cues are necessary and that a diffusible oligodendroglial factor(s) participate(s) in prenode formation along GABAergic axons.

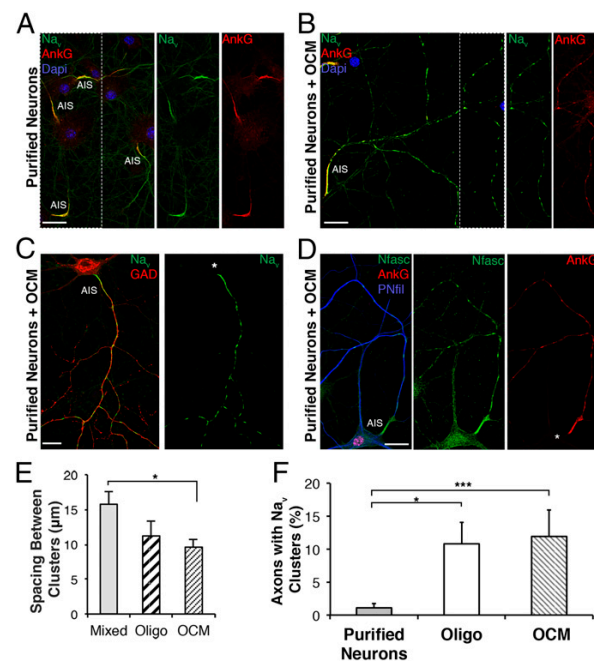


Fig. 2. A secreted oligodendroglial factor promotes nodal protein clustering. Immunostaining of purified hippocampal neurons cultured in the (A) absence or (B–D) presence of OCM. (A–D) The AIS is detected in all conditions, but (B–D) clusters of Na_v (green), AnkG (red), and Nfasc (green) are only detected in the presence of OCM. (C) Prenodes are formed on GAD67⁺ neurons treated with OCM. (D) Neuronal cell body and neurites stained with an Ab targeting phosphorylated neurofilaments (PNfil; blue). (Scale bars: 25 μm.) (E) Distance between prenodes measured on axons in mixed culture or purified neurons cocultured with oligodendrocytes (oligo) or OCM. Mean spacing between clusters (micrometers) ± SEM of four independent experiments is shown. **P* = 0.028 (Mann-Whitney test). (F) Percentage of axons (AIS⁺) having at least two Na_v clusters at 21 DIV in purified neuron cultures, purified neurons cocultured with oligodendrocytes (oligo), or OCM. The means ± SDs of 4 (for oligo) and 10 (for OCM) independent experiments are shown. For each experiment, at least 100 neurons were analyzed. **P* = 0.0187; ****P* = 0.0003 (Mann-Whitney test).

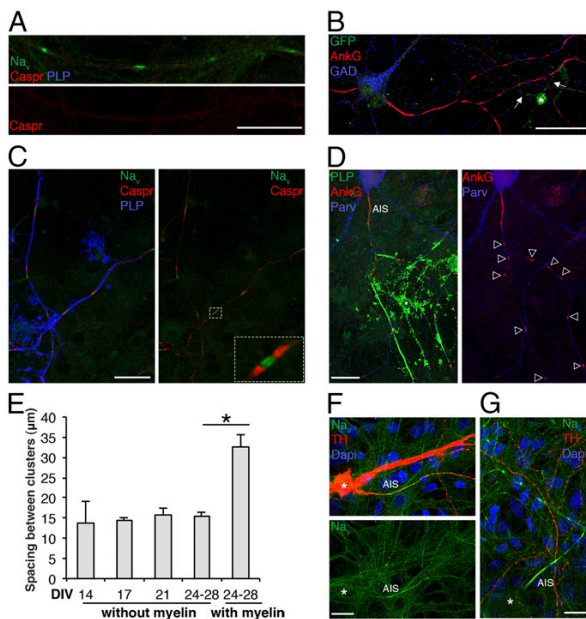


Fig. 3. Prenodes are formed on myelin-competent GABAergic neurons. (A and B) Immunostaining of mixed hippocampal culture at 17 DIV. (A) Na_v clusters (green) observed in the absence of Caspr aggregation (red) and the absence of myelin (PLP⁺; blue). (B) Hippocampal culture from *CNP-EGFP* embryos shows an oligodendrocyte (asterisk) stained with an anti-GFP Ab with processes contacting the axon (arrows). Numerous AnkG clusters (red) are observed at a distance from these processes on a GAD67⁺ neuron (blue). (C and D) Immunostaining of mixed hippocampal culture at 24 DIV. (C) Myelinated axons (PLP⁺; blue) with nodes (Na_v; green) and paranodes (Caspr; red). A higher magnification of a node with flanking paranodes is shown. (D) Myelinated segments (PLP⁺; green) with nodes (AnkG⁺; red) on GABAergic axons [Parvalbumin⁺ (Parv); blue]. (Scale bars: 25 μm.) (E) Measure of the distance between prenodes on unmyelinated axons and between nodes of Ranvier on myelinated axons at different time points. Values are the mean spaces between clusters (micrometers) ± SEMs of four independent experiments. **P* = 0.028 (Mann–Whitney test). (F and G) Immunostaining of mesencephalic cultures at 21 DIV. (F) Dopaminergic neurons tyrosine hydroxylase (TH⁺; red) do not form Na_v clusters downstream of the AIS (Na_v⁺; green), whereas (G) Na_v clusters are formed on a nondopaminergic (TH⁻) axon. *Neuronal cell body. (Scale bars: 25 μm.)

Hippocampal GABAergic and Pyramidal Neurons Assemble Nodal Proteins by Different Mechanisms. To further examine if oligodendrocytes were contacting prenodes, we used mixed hippocampal cultures from *CNP-EGFP* embryos, in which all cells in the oligodendrocyte lineage express EGFP (24). Although oligodendrocyte processes contacted some axons with prenodes, most clusters were not (Fig. 3B), suggesting that nodal protein clustering on GABAergic interneurons does not depend on strict oligodendroglial contact. In addition, prenodes were formed independently of paranodal aggregation as indicated by the diffuse Caspr expression (Fig. 3A).

We also examined, at later time points (24–28 DIV), whether neurons were eventually myelinated by analyzing mixed hippocampal cultures treated with differentiation medium to enhance the myelination process. Myelinated axons were detected with Na_v channel clusters flanked by paranodal Caspr clusters, forming either heminodes or nodes of Ranvier at the tips of myelinated internodes (Fig. 3C). Myelinated internodes were detected on both GABAergic and pyramidal neurons (Fig. 3D and Fig. S3), suggesting that clustering at the node on glutamatergic axons coincides with myelin deposition, in contrast to GABAergic

axons. Within GABAergic myelinated axons, internodal length was $32.7 \pm 3.1 \mu\text{m}$ (i.e., twofold longer than the distance between clusters observed in nonmyelinated GABAergic axons present at the same time point in the same cultures) (Fig. 3E). To determine if prenodal clustering is restricted to neurons destined to be myelinated, we used dopaminergic neurons in culture, which are known to remain unmyelinated *in vivo*. These neurons exhibited Na_v clustering at the AIS but not along axons (Fig. 3F and G).

Taken together, our results suggest that the mechanisms of nodal assembly differ between neuron subtypes. Indeed, whereas most GABAergic neurons assemble prenodes before myelination, hippocampal pyramidal cells initiate nodal clustering concomitantly to myelination.

Na_v Channel Isoforms Are Differentially Regulated in Prenodes over Time *in Vitro*. Because CNS nodes of Ranvier express different Na_v α-subunits (25, 26), we also analyzed prenodal expression of Na_v α-subunits before myelination. Na_v1.1 was detected in more than 90% of AnkG⁺ clusters at all time points analyzed (Fig. 4D), whereas Na_v1.2 was mainly detected at 14 DIV (Fig. 4) and progressively disappeared at later time points. Na_v1.6, which

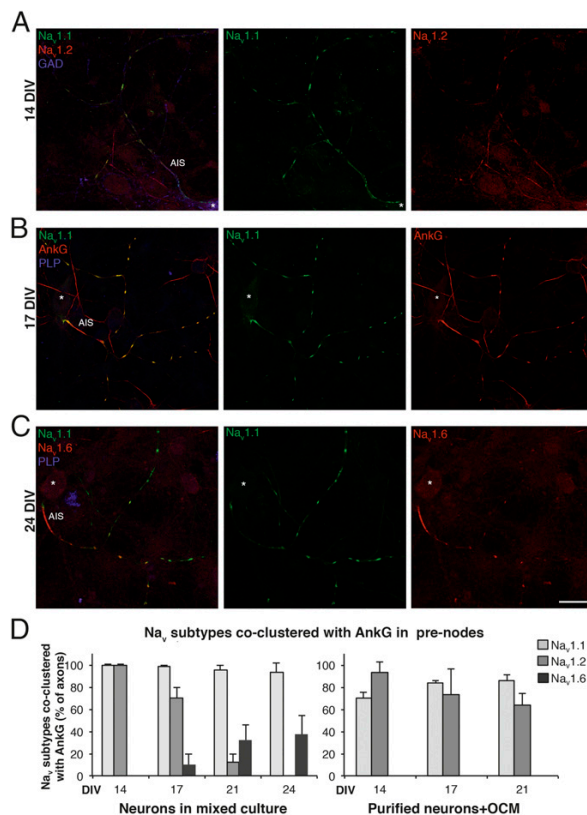


Fig. 4. Prenodes express different Na_v isoforms. (A–C) Hippocampal neuron cultures at (A) 14, (B) 17, or (C) 24 DIV immunostained for Na_v1.1, Na_v1.2, Na_v1.6, AnkG, GAD, and/or PLP as indicated, illustrating the different Na_v α-subunit isoform expression in prenodes at different time points. *Neuronal cell body. (Scale bar: 25 μm.) (D) Percentage of axons with clusters of AnkG, which are colocalized with Na_v1.1, Na_v1.2, or Na_v1.6 at different DIVs. Quantifications were performed in mixed cultures and cultures of purified neurons with OCM. The means ± SDs of three independent experiments are shown. For each experiment, at least 100 neurons were analyzed.

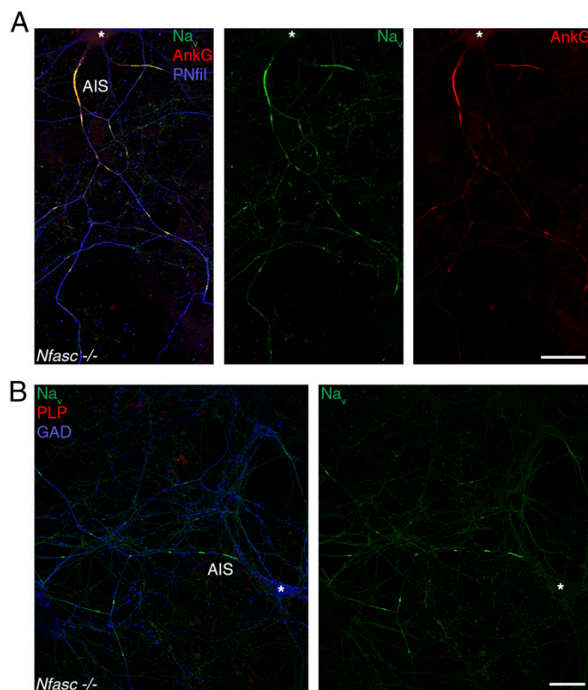


Fig. 5. Prenodes are formed in the absence of Nfasc expression. Immunostaining of hippocampal neuron cultures of *Nfasc*^{-/-} mice at 20 DIV showing clusters of Na_v (green) and AnkG (red) along an axon with phosphorylated neurofilaments (PNfil; blue) in A and in the absence of myelin (PLP; red) on a GAD67⁺ neuron (blue) in B. *Neuronal cell body. (Scale bars: 25 μ m.)

appeared at 17 DIV, was detected at 21 DIV before myelination on $32.2\% \pm 13.3\%$ of axons with prenodes (Fig. 4 B and D). In contrast, in pure hippocampal neuronal cultures treated with OCM, whereas Na_v1.1 and/or Na_v1.2 were expressed in prenodes, Na_v1.6 was not detected (Fig. 4D). These results show that Na_v channel isoforms described at nodes of Ranvier in myelinated fibers (26) are expressed in prenodal clusters on unmyelinated fibers in hippocampal cultures. Moreover, oligodendrocyte-secreted factors can induce the clustering of Na_v1.1 and Na_v1.2 but not Na_v1.6 isoforms in prenodes.

Nfasc Is Not Necessary for Prenode Assembly. In the CNS, Nfasc186 can induce nodal clustering of Na_v channels in the absence of intact paranodal junctions (19), and it has been proposed recently that Nfasc186 participates in nodal protein clustering in the presence of nodal ECM molecules (12). To address the role of Nfasc186 as the neuronal organizer of prenodes, we prepared mixed hippocampal cultures from *Nfasc*^{-/-} or WT mice. There were no differences at 17 and 21 DIV in prenode (i.e., Na_v and AnkG) clustering between *Nfasc*^{-/-} and WT cultures (Fig. 5 and Fig. S4 A and B). Furthermore, when purified *Nfasc*^{-/-} hippocampal neurons were cultured and treated with OCM, prenodal clustering was induced on GAD67⁺ neurons as in WT cultures (Fig. S4C). Therefore, the neuronal neurofascin isoform is not necessary for prenode assembly, and clustering of prenodes by OCM does not rely on an Nfasc186-based mechanism.

Prenode Assembly Requires AnkG. The cytoskeletal architecture has been seen to play an important role in the maintenance and possible clustering of the nodal complex (12, 18). We then addressed whether prenodal formation was dependent on AnkG by silencing AnkG expression within hippocampal cultures. Be-

cause AnkG is required for assembly and maintenance of the AIS (27, 28), transfection with either AnkG miRNA or control miRNA plasmids coexpressing GFP was performed at 6 DIV (i.e., after AIS assembly). In neurons expressing AnkG miRNA (GFP⁺), AnkG was weakly detectable at the AIS, illustrating the efficiency of the miRNA (Fig. 6 B and C). Because AnkG removal may alter neuronal polarity (21), we analyzed Na_v clustering at a time point when microtubule associated protein 2 (MAP2) immunostaining was still restricted to the somatodendritic domain (Fig. 6B). In AnkG knockdown, GAD67⁺ neurons, some Na_v and Nfasc immunoreactivity was detected at the AIS, but Na_v clustering along the axon was completely prevented (Fig. 6 A, C, and E and Fig. S5). In contrast, in neurons transfected with the control plasmid, axonal clusters of AnkG, Na_v (Fig. 6 D and E), and Nfasc were formed.

Taken together, these results show that premyelination clustering of Na_v channels and Nfasc along axons of hippocampal neurons depends on AnkG.

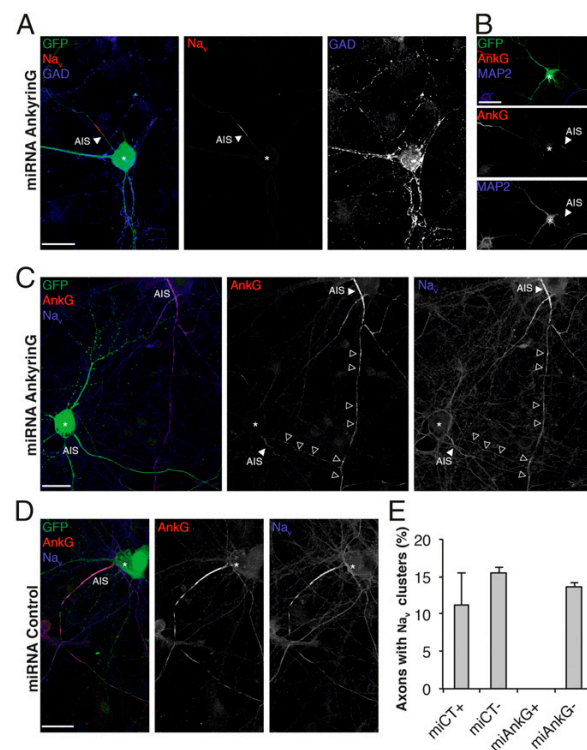


Fig. 6. Prenode assembly requires AnkG expression. (A–C) Immunostaining of hippocampal cell cultures transfected at 6 DIV with AnkG miRNA and fixed at 18 DIV. Transfected neurons are GFP⁺ (green). (A) Representative image of a transfected GAD67⁺ neuron (blue); Na_v expression (red) is weak at the AIS (arrowheads), and no prenodes are observed. (B) Transfected AnkG miRNA GFP⁺ neuron with somatodendritic expression of MAP2 (blue) and a weak AnkG (red) staining of the AIS (arrowheads). (C) Transfected AnkG miRNA GFP⁺ neuron with weak expression of AnkG (red) and Na_v (blue) at the AIS and no prenodes, whereas prenodes are observed in the neighboring nontransfected neuron (arrowheads). *Neuronal cell body. (D) Image of a neuron transfected with control miRNA showing AnkG (red) and Na_v (blue) expression at the AIS and prenodes. (E) Quantification of axons forming Na_v clusters in hippocampal cell cultures transfected (+) or not (–) with control miRNA (miCT) or AnkG miRNA (miAnkG). The means \pm SDs of three independent experiments are shown. For each experiment, at least 50 neurons were analyzed. (Scale bars: 25 μ m.)

Conduction Velocity Is Increased on Axons with Prenodes in the Absence of Myelination. We first investigated whether unmyelinated interneurons with and without prenodes had different intrinsic electrophysiological properties by performing somatic whole-cell patch-clamp recordings on mixed hippocampal cultures from *GAD67-GFP* knockin mice (29) (Fig. S64). We observed no significant difference between the mean resting membrane potential, action potential (AP) threshold, AP rise time, AP half-width, and AP decay in cells with prenodes and those without (Fig. S6B). However, we observed that neurons with prenodes tended to exhibit a significantly lower input resistance compared to neurons without [with prenodes = 67.5 ± 24.5 M Ω ; without prenodes = 175.1 ± 74.4 M Ω ; $n = 7$ (each group); $P = 0.01$].

We then examined whether prenodal aggregates might accelerate axonal conduction velocity before myelination. Therefore, we compared electrical conduction on cultured rat mixed hippocampal GABAergic interneurons with and without prenodes using simultaneous recordings from the soma and axon of the same neuron from 10 to 19 DIV. AIS and prenodes were identified using live staining with an Ab targeting the extracellular domain of Nfasc (Fig. 7A and B). Cell-attached patch-clamp recordings of action currents from the soma and axon were made during spontaneous firing of neurons at a minimum distance of 150 μ m between the two recording electrodes (Fig. 7C and D). At longer intervals between the somatic and axonal recording electrodes, we observed that the latencies between spikes recorded in the axon and at the soma increased in both neurons with and without prenodes (Fig. 7E). Interestingly, the mean apparent conduction velocity was significantly higher in neurons with prenodes compared to neurons without prenodes (Fig. 7F) (1.23 ± 0.09 m/s, $n = 10$; 0.72 ± 0.05 m/s, $n = 8$, respectively; $P = 0.0002$). Because the mean axonal diameter was significantly larger in neurons with prenodes compared to neurons without prenodes (1.96 ± 0.18 μ m, $n = 10$; 1.26 ± 0.12 μ m, $n = 8$, respectively; $P = 0.008$), one possibility might have been that increased conduction velocity was caused by larger axonal diameter. To test this alternative hypothesis, we selected neurons with and without prenodes having similar mean axonal diameters (1.71 ± 0.10 μ m, $n = 3$; 1.68 ± 0.05 μ m, $n = 3$, respectively) and showed that the mean conduction velocity was significantly higher in neurons with prenodes (1.24 ± 0.12 m/s, $n = 3$) compared to neurons without prenodes (0.74 ± 0.03 m/s, $n = 3$; $P = 0.016$). Taken together, these results show that clusters of nodal proteins increase axonal conduction velocity in hippocampal GABAergic neurons before myelination.

Prenodes Are Detected on Some Hippocampal GABAergic Neurons Before Myelination in Vivo. Using hippocampal tissue sections from vesicular GABA transporter (*VGAT*)-*venus* rat and *GAD67-GFP* mice (29, 30), we then addressed if this prenodal clustering occurred in vivo. We first showed that, in both rat and mouse CNS, some GABAergic neurons (GFP⁺), mostly located in the stratum oriens of CA1 and CA3 and the subiculum (Fig. 8A), were myelinated as previously reported (31, 32). We then assessed whether prenodal clustering occurred at different premyelination time points. Indeed, axonal clusters of AnkG and Na_v channels were detected just before myelination (postnatal days P12 and P13) on some GABAergic neurons in the absence of myelin and paranodal accumulation of Caspr (Fig. 8B–E). They had an intercluster interval ranging from 5 to 25 μ m (seen in the plot profiles in Fig. 8B', C', and E'), which is consistent with prenodes spacing measured on unmyelinated axons in vitro. These results show that prenodule formation can occur before myelination in the hippocampus in vivo.

Discussion

Prenodal Clustering Occurs on GABAergic Interneurons in Vitro and in Vivo. Here, we report that discrete clusters of Na_v channels, colocalizing with AnkG and Nfasc, are detected before myelina-

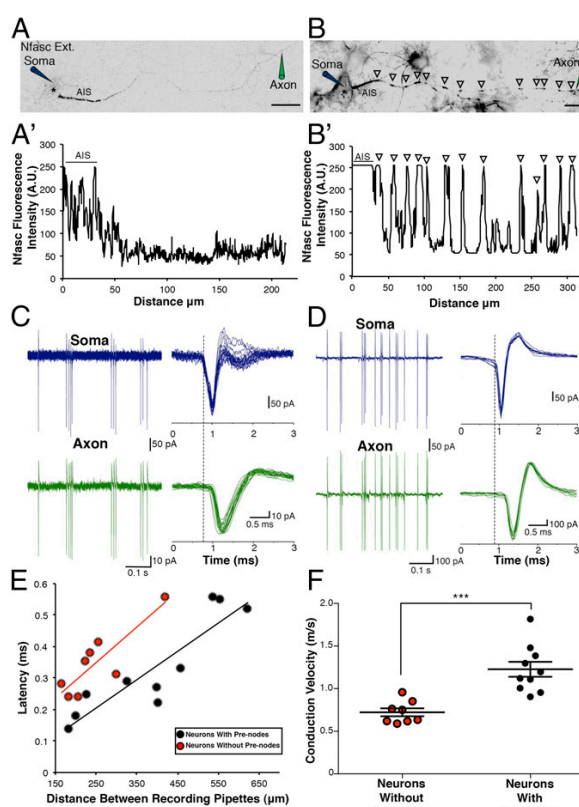


Fig. 7. Prenodes influence conduction velocity of unmyelinated neurons. (A and B) Live immunostaining of the AIS and prenodes (arrowheads) with an Ab recognizing the external domain of Nfasc and coupled to Alexa 594 during simultaneous recordings from the soma (blue-colored electrode) and axon (green-colored electrode) of neurons (B) with prenodes and (A) without prenodes in *VGAT-venus* rat hippocampal cultures. (Scale bar: 25 μ m.) *Neuronal cell body. (A' and B') Fluorescence intensity profiles corresponding to axonal Nfasc immunolabeling in A and B; individual peaks in B' correspond to prenodes (arrowheads), and fluorescence intensity is expressed in arbitrary units. (C and D) Spontaneous action currents recorded from the soma and axon from A and B, respectively. (E) Latencies plotted against recording distances (red points represent neurons without prenodes, and black points represent neurons with prenodes) show that latencies increase with recording distance ($R^2 = 0.737$, red line for neurons without prenodes; $R^2 = 0.801$, black line for neurons with prenodes). (F) Mean conduction velocity (CV) of neurons with prenodes is significantly increased compared with neurons without prenodes. CV for neuron in A = 0.85 m/s; CV for neuron in B = 1.12 m/s. *** $P = 0.0002$ (Student's *t* test).

tion along axons of hippocampal neurons in culture and during postnatal development in vivo. Notably, these clusters were detected on GABAergic neurons only and not on glutamatergic neurons, which constitute the other major subtype of hippocampal neurons. In the latter, nodal protein clustering coincides with myelination and paranodal junction formation. This result suggests that, depending on neuronal subtype, mechanisms of node of Ranvier formation can differ in the hippocampus and therefore, highlights the diversity of neuronal responses during development.

Interestingly, this restriction to a specific subtype was also seen when clustering was induced on purified hippocampal neurons by oligodendrocyte-conditioned media, strengthening the hypothesis that only neurons responsive to an oligodendroglial soluble signal form prenodes. What distinguishes neurons responsive and non-responsive to this clustering signal is unknown. In this context, it is

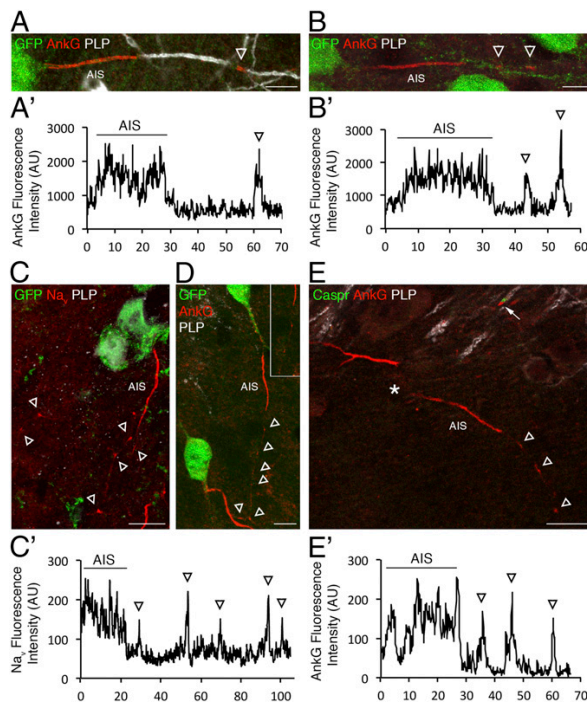


Fig. 8. Prenodes can be detected in vivo during postnatal development in both mouse and rat. (A and B) Immunostaining of sagittal sections of P13 VGAT-venus rat hippocampus shows the presence of AnkG⁺ nodes of Ranvier on myelinated fibers (PLP⁺) in A as well as AnkG axonal clusters in absence of myelin (PLP⁻) in B on some GABAergic neurons stained with an anti-GFP Ab. (Scale bars: 10 μ m.) Intensity profiles corresponding to AnkG expression in (A') myelinated and (B') nonmyelinated fibers. Arrowheads indicate AnkG axonal clusters. (C and D) Immunostaining of sagittal sections of P12 GAD-GFP mouse hippocampus shows the presence of (C) Na_v and (D) AnkG clusters (arrowheads) in the absence of myelin (PLP⁻). In D, the boxed area is shown as a zoomed-in view. (Scale bars: 10 μ m.) (E) Immunostaining of P12 GAD-GFP hippocampus shows that Caspr is not clustered around prenodal AnkG before myelination (arrowheads), whereas it is accumulated at hemiparanodes flanking nodal AnkG in myelinated fibers (arrow). *Neuronal cell body. (Scale bar: 20 μ m.) (C' and E') Intensity profiles corresponding to (C) Na_v staining and (D) AnkG show isolated peaks corresponding to prenodes (arrowheads).

of note that the induction of Na_v clustering by a soluble oligodendroglial factor has been identified previously by Kaplan et al. (20, 21) on RGCs, which are glutamatergic neurons, suggesting that the clustering permissivity does not depend on the type of neurotransmitter. An attractive hypothesis is that prenodal formation might be associated with the need for early establishment of neuronal connections during development on axons with long trajectories. In favor of this hypothesis, these two types of axons with prenodes are known to be characterized by long-range projecting axons: RGC axons extend from the retina to the superior colliculus, and our results reveal that most axons with clusters in vivo extended from the CA1 region of the hippocampus, which has been found to project to farther interregional areas, such as the medial septum, the subiculum, or the retrosplenial cortex (31, 33, 34).

Lastly, whether these nodal protein clusters disappear or fuse to form nodes of Ranvier when oligodendrocyte processes contact the axon, such as described for heminodes (35, 36), remains to be determined. Indeed, the increase in the spacing of nodal clusters upon myelination in vitro and in vivo along GABAergic axons suggests that spatial rearrangements could occur.

Oligodendrocyte-Secreted Factor Induces Prenodal Clustering. Our results on purified hippocampal neurons extend previous data that a proteinaceous factor(s) secreted by oligodendroglia induces clustering of nodal proteins (20, 21). Whether this factor(s) induces Na_v clustering through interactions with the axonal membrane or stimulation of neuronal protein synthesis has yet to be fully understood. Gliomedin expressed by Schwann cells is known to induce nodal clustering in the peripheral nervous system (7). However, not only has CNS expression of gliomedin not been reported, but also, we found that gliomedin was undetectable both in oligodendroglial cultures and at prenodes. The various ECM proteins enriched at the CNS nodes mainly play a role in buffering nodal environment and stabilizing the nodes (10–12). Whether they participate in the induction of prenodal assembly remains to be seen. However, our results provide that clustering of prenodes through OCM is not mediated through an Nfasc-based mechanism, implying that other cell adhesion molecules may interact with the oligodendroglial-secreted factor. Furthermore, we addressed whether this oligodendroglial clustering effect might be related to oligodendrocyte-induced neuronal maturation and survival (37). This hypothesis was partly supported by the facts that clusters were mostly detected in vitro on large-diameter axons with highly phosphorylated neurofilaments, a hallmark of maturation, that also, in vivo, prenodes were found more frequently at P12 and P13 compared with earlier time points, and lastly, that neurons with prenodes exhibited a lower input resistance compared to neurons without clusters. In accordance with these findings, it has been observed that there is a significant decrease in the input resistance as mice matured from P9–P11 to P12–P16 (38). However, addition of maturation/growth factors [glial cell derived neurotrophic factor (GDNF), BDNF, ciliary neurotrophic factor (CNTF), leukemia inhibitory factor (LIF), or NGF] to pure neuron cultures while inducing neurofilament phosphorylation did not trigger Na_v clustering, suggesting that axonal maturation is not sufficient to induce nodal protein clustering. We also addressed the role of electrical activity by using tetrodotoxin or veratridine (blocker and activator of Na_v channels, respectively), which did not affect prenode formation.

AnkG Is Essential for Prenodal Formation, Whereas Nfasc Is Dispensable.

In the CNS, several mechanisms are involved in nodal assembly: clustering of Nfasc186 through interactions with ECM, restriction of diffusion through paranodal junctions, and stabilization by the cytoskeletal scaffold. Numerous studies suggest that these three mechanisms are alternative or complementary to induce nodal assembly (8, 9). Direct axoglial contacts established at the paranodal junctions have been suggested to induce nodal protein clustering through restriction of their diffusion (12, 13). Nevertheless, other studies have indicated that, when paranode assembly is impaired by inactivation of genes coding for the paranodal proteins (Caspr, contactin, or Nfasc155) or the myelin proteins, the timing and number of developing nodes occur normally, suggesting that formation of paranodal junctions may be sufficient but not necessary for nodal assembly (14–19). Recently, by using a genetic strategy to determine their requirement, Susuki et al. (12) have shown that disruption of at least two of these three mechanisms is necessary to affect node formation. We show here that Na_v clusters can be formed without direct axoglial contact, which has been previously found (20, 21). We also show that AnkG is required for the formation of Na_v and Nfasc186 clusters along unmyelinated axons. AnkG, which likely provides a link by establishing interactions with the intracellular domains of Nfasc186 and Na_v α -subunit as well as β IV spectrin and kinesin motors (39, 40), may either initiate or stabilize prenodal protein clustering before myelination. In contrast, Nfasc is not necessary for Na_v and AnkG prenodal clustering. This result suggests that Nfasc186 plays a role in late rather than early stages of node of Ranvier assembly.

Na_v Clustering Is Differentially Regulated in Prenodes. We observed that distinct Na_v channel isoforms are targeted differentially in prenodes along different time points in vitro. Whereas the Na_v1.1 isoform is found at all time points, the immature isoform Na_v1.2 progressively disappears, and Na_v1.6 is recruited in ~35% of neurons with prenodes in mixed culture. One noteworthy finding is that Na_v1.6 was found in the absence of myelination, but Na_v1.6 does not appear in axonal clusters on purified hippocampal neurons treated with OCM, the latter of which are similar to those previously reported on purified RGCs treated with OCM (21). Interestingly, the timing of Na_v1.6 expression at prenodes coincided with late in vitro culture time points, wherein its first appearance started at 17 DIV and gradually increased up to 24 DIV. These results may implicate either the transition of immature to mature oligodendrocytes in culture and/or that neuronal maturation is necessary to synthesize and recruit Na_v1.6 to prenodes. Although these results differ from a previous report of Na_v1.6 recruitment requiring myelin compaction during optic nerve development (25), these results nevertheless point to an important role for the physical presence of oligodendrocytes to target Na_v1.6 at prenodes. Because we did observe some CNP-EGFP⁺ oligodendrocytes contacting prenodal clusters, it would be interesting to investigate the role of oligodendroglial contact and their influence on the distribution of sodium channel subtypes, which may shed light onto additional cues necessary for Na_v1.6 targeting in the CNS.

What Are the Functional Roles of Prenodes? What is the functional gain provided by axonal Na_v clusters in the absence of myelin? Axonal propagation velocity of the action potential is known to depend on the axon diameter and the presence of a myelin sheath (41). Here, our whole-cell patch-clamp recordings and single-axon electrophysiological results strongly suggest that the presence of regularly spaced Na_v clusters increases action potential propagation in the absence of myelination independent of axonal caliber, and these data suggest another level of influence by oligodendrocytes on the regulation of conduction velocity beyond the production of a myelin sheath. In addition, the shorter interval between prenodes compared with mature nodes of Ranvier could compensate for a lack of insulation in the absence of myelin. Of note, on GABAergic neurons with prenodal clusters, recorded apparent conduction velocities were in a similar range to those reported for myelinated axons of cortical pyramidal neurons (42, 43). Prenodes with high-density sodium channel clusters could serve as acceleration points, which was predicted by theoretical modeling calculations (44, 45). It is tempting to speculate that optimization of propagation of electrical signaling at a given developmental stage will be especially crucial for highly connected GABAergic hub neurons, which have a widespread axonal arborization, and for long-range projection neurons, and provides a means to impact network activities (33). Moreover, Na_v clustering may help to overcome axonal branch point failures and maintain reliable propagation of action potentials (41).

In multiple sclerosis, within lesions undergoing remyelination, clustering of Na_v channels has been observed on PLP⁺ (i.e., non-remyelinated) fibers (46), suggesting that, such as for developmental myelination, nodal protein clustering might precede myelin repair. Although the mechanisms of axonal domain reassembly during remyelination are still poorly understood, it can be hypothesized that, similar to early nodal clustering during developmental myelination, these clusters accelerate conduction velocity before remyelination and therefore, participate in functional recovery.

Materials and Methods

Animals. The care and use of rats and mice in all experiments conformed to institutional policies and guidelines (UPMC, INSERM, and European Community Council Directive 86/609/EEC). The following rat and mouse strains were used in this study: Sprague-Dawley or Wistar rats (Janvier Breeding Center), VGAT-venus Wistar rats (30), *Nfasc*^{-/-} mice (1), *GAD67-GFP* knockin mice (29), *CNP-EGFP* mice (24), and C57Bl/6 WT mice.

Cell Cultures. Mixed hippocampal cultures (containing neurons and glial cells) at E18 were prepared according to procedures described previously (47) with modifications. Briefly, pooled hippocampi were dissociated enzymatically by trypsin (0.1%; Worthington) treatment for 20 min with DNase (50 µg/mL). After trypsin neutralization, cells were centrifuged at 400 × g for 5 min, resuspended, and then seeded on polyethylenimine precoated glass coverslips at a density of 5.0 × 10⁴ cells/35 mm². Cultures were maintained for 24 h in a 1:1 mixture of DMEM (11880; Gibco) with 10% FCS (100 IU/mL), penicillin-streptomycin (100 IU/mL), and neuron culture medium (NCM). Culture medium was replaced by a 1:1 mixture of Bottenstein-Sato (BS) medium with PDGF-A (0.5%) and NCM, and then, one-half of the medium was changed every 3 d and replaced by NCM. To increase myelination in cultures maintained until 24–28 DIV, differentiation medium was added at 18 DIV. Compositions of NCM, BS medium, and differentiation medium are detailed in *SI Materials and Methods*. Purified hippocampal neuronal cultures were obtained by adding (24 h after isolation) the antimitotic agents uridine and 5-fluorodeoxyuridine (5 µM; Sigma) to the NCM for 36 h. Cultures of dopaminergic neurons were prepared from Wistar rats at E15.5 according to procedures described previously (48). Glial cell cultures were prepared using cerebral cortices from P2 Wistar rats dissected free of meninges, then incubated for 45 min in papain (30 U/mL; Worthington) supplemented with L-cysteine (0.24 mg/mL) and DNase (50 µg/mL) in DMEM at 37 °C, and mechanically homogenized. Cells were resuspended in DMEM with 10% FCS and penicillin-streptomycin and dispensed into T175 culture flasks at a density of 10⁵ cells/cm². After 12–15 d in culture, flasks were shaken for 1 h at 180 rpm to remove microglial cells, medium was replaced, and flasks were shaken on a rotary shaker overnight at 230 rpm at 37 °C. Detached cells were used for immunopanning (*SI Materials and Methods*) to isolate oligodendrocytes. All cultures were maintained at 37 °C and 5% CO₂.

Preparation of OCM. Oligodendrocytes were cultured for 24 h in BS medium, and then, medium was replaced with NCM and collected after 48 h. OCM was filtered through a 0.22-µm filter. Protein concentration (4.1 ± 2.4 µg/µL, mean ± SD of four OCMs) was measured using the bicinchoninic acid (BCA) protein assay (Pierce).

Purified Hippocampal Neurons Cultured with OCM or Oligodendrocytes. OCM (500 µL/well) or oligodendrocytes (2.5 × 10⁴ cells/well) were added to purified hippocampal neuronal cultures at 3 DIV after removal of antimitotic agents. Then, one-half of the medium was changed with NCM every 5 d. Percentages of neurons (AnkG⁺ cells), astrocytes (GFAP⁺ cells), and oligodendrocytes (O4⁺ and PLP⁺ cells) were determined at 21 DIV. Mixed hippocampal cultures contained 43.7% ± 2.7% of neurons, 42.5% ± 5.4% of astrocytes, and 11.2% ± 2.7% of oligodendrocytes, whereas purified neuronal cultures contained 94.2% ± 2.2% of neurons, 3.6% ± 1.7% of astrocytes, and 0.4% ± 0.6% of oligodendrocytes; purified neurons cultured with OCM contained 92% ± 2.6% of neurons, 4.3% ± 3.4% of astrocytes, and 0.5% ± 0.5% of oligodendrocytes; and purified neurons cocultured with oligodendrocytes contained 77.5% ± 3.5% of neurons, 4.5% ± 4.2% of astrocytes, and 17.3% ± 0.4% of oligodendrocytes (mean ± SD; *n* = 3, 150 cells at least were counted for each experiment).

Tissue Sections. *GAD67-GFP* mice and *VGAT-venus* rats were anesthetized at P12 and P13 with lethal doses of Imalgene 500 (Merial) combined with 2% Rompun (Bayer). They were transcardially perfused with 1% or 4% paraformaldehyde (PFA), and brains were dissected and postfixed in 1% or 4% PFA followed by PBS washes and subsequent equilibration in sucrose (5–30%) solution overnight at 4 °C for cryostat sectioning. The next day, brains were embedded in OCT (Tissue-Tek), frozen, and then cryosectioned (CM 3050; Leica) at 35 µm. Serial sectioning of the hippocampus was in the sagittal plane.

Abs and Immunofluorescence. All Abs used can be found listed in *SI Materials and Methods*. Cell cultures were fixed with 4% PFA for 10 min or for Na_v channel staining, 1% PFA for 10 min at room temperature (RT) and then incubated with methanol for 10 min at −20 °C. Coverslips were then washed with PBS one time. After fixation, cells were incubated with blocking buffer (BB; 1× PBS, 5% normal goat serum, 0.1% Triton) for 15 min and then primary Ab (diluted in BB) for 2 h at RT or 4 °C overnight. Coverslips were then washed and incubated with secondary Ab at RT for 1 h. After last wash, Hoechst stain (1 mM) was placed on cells at RT for 5 min. Floating brain cryostat sections were pretreated with ethanol at −20 °C for 10 min and then washed with PBS. They were then treated with BB with 0.2% Triton for 1 h at RT before incubation with Ab overnight at 4 °C. Sections were then washed, and secondary Abs were added for 2 h at RT. Coverslips and sections were mounted on superfrost glass slides with Fluoromount G (Southern Biotech).

Image Acquisition and Analysis. Slides from hippocampal cultures and cryostat sections were visualized using an Olympus FV-1000 Upright Confocal Microscope or a Zeiss AxioImager-Apoptome. Z series of optical sections was performed at 0.3- μ m increments for qualitative analysis. Blue, green, red, and far-red fluorescence was acquired sequentially. Maximum orthogonal projection of images and plot profiles of immunofluorescence intensity were carried out using ImageJ software (NIH).

Quantification of Neurons with Clusters, Sizes of Clusters, Intervals, and Myelination. At least 100 neurons per coverslip, identified by the presence of an AIS, were counted, and the percentage of neurons with Na_v/AnkG clusters was determined for at least two coverslips per condition. Results were expressed as means \pm SDs of at least three independent experiments. An Na_v cluster was defined by its size and mean intensity of area (i.e., size of clusters varied from 1 to 8 μ m, and mean value of cluster area was at least 2.5 that of the adjacent part of the axon). Intervals between clusters were measured on acquired images by using ImageJ software. The mean intervals were calculated for one neuron; then, the mean of all neurons for one experiment was determined, and results were expressed as means \pm SEMs of four independent experiments. Myelination was assessed at 24 DIV and identified as bright PLP⁺ double lines interrupted at nodes of Ranvier. Statistical analyses were performed using the Mann-Whitney test or Student's *t* test with Prism software (GraphPad software).

Design and Transfection of miRNA. To generate AnkG miRNA constructs, we used the Block-it PolII miR RNAi Expression Vector Kits (K4936-00) (*SI Materials and Methods*). Hippocampal cells in 24-well plates were transfected at 6 DIV

with 0.5 μ g DNA/well using the lipofectamine 2000 reagent according to the manufacturer's protocol (11668-019; Invitrogen). Transfected cells were fixed at 18 or 20 DIV. The two miRNAs used gave similar results.

Electrophysiology: Simultaneous Soma/Axon Recordings. Rat hippocampal cultures were used between 10 and 19 DIV for electrophysiological recordings. Nfasc external Ab (cloneA12/18; Neuromab) was coupled to Alexa 594 according to the manufacturer's protocol (A10474; Invitrogen) and then incubated on hippocampal cultures for 30 min at 37 °C with a 1:15 dilution in culture medium. Labeled cultures were transferred to the recording chamber on the stage of an Axioskop 2 FS plus microscope (Zeiss) and continuously superfused with artificial cerebrospinal fluid. Simultaneous patch recordings were performed with a Multiclamp 700B amplifier (Molecular Devices) and digitized with pClamp10 software (Axon; Molecular Devices). Spontaneous action currents were recorded in cell-attached mode from both the somatic and axonal electrodes (*SI Materials and Methods*).

ACKNOWLEDGMENTS. We thank François Couraud, Rock Levinson, and Elior Peles for the gift of Abs. We also thank Bernard Zalc, Charles-Felix Calvo, and members of the laboratory of C.L. for discussions and critical reading of the manuscript. We thank Plate-forme d'Imagerie Cellulaire de la Pitié-Salpêtrière for support with image acquisition. This work was supported by INSERM, French Multiple Sclerosis Research Foundation association pour la recherche sur la sclérose en plaques (ARSEP) Program "Investissements d'avenir" ANR-10-AIHU-06, and the Bouvet-Labruyère prize (to N.S.-F.). S.A.F. and A.D. were supported by the French Medical Research Foundation, and C.L. was supported by the Sobeck Prize. P.J.B. was supported by the Wellcome Trust.

- Sherman DL, Brophy PJ (2005) Mechanisms of axon ensheathment and myelin growth. *Nat Rev Neurosci* 6(9):683–690.
- Charles P, et al. (2002) Neurofascin is a glial receptor for the paranodin/Caspr-contactin axonal complex at the axoglial junction. *Curr Biol* 12(3):217–220.
- Sherman DL, et al. (2005) Neurofascins are required to establish axonal domains for saltatory conduction. *Neuron* 48(5):737–742.
- Lustig M, et al. (2001) Nr-CAM and neurofascin interactions regulate ankyrin G and sodium channel clustering at the node of Ranvier. *Curr Biol* 11(23):1864–1869.
- Zhang Y, et al. (2012) Assembly and maintenance of nodes of ranvier rely on distinct sources of proteins and targeting mechanisms. *Neuron* 73(1):92–107.
- Feinberg K, et al. (2010) A glial signal consisting of gliomedin and NrCAM clusters axonal Na⁺ channels during the formation of nodes of Ranvier. *Neuron* 65(4):490–502.
- Eshed Y, et al. (2005) Gliomedin mediates Schwann cell-axon interaction and the molecular assembly of the nodes of Ranvier. *Neuron* 47(2):215–229.
- Chang KJ, Rasband MN (2003) Excitable domains of myelinated nerves: Axon initial segments and nodes of Ranvier. *Curr Top Membr* 72(2013):159–192.
- Leterrier C, Brachet A, Dargent B, Vacher H (2011) Determinants of voltage-gated sodium channel clustering in neurons. *Semin Cell Dev Biol* 22(2):171–177.
- Dours-Zimmermann MT, et al. (2009) Versican V2 assembles the extracellular matrix surrounding the nodes of ranvier in the CNS. *J Neurosci* 29(24):7731–7742.
- Bekku Y, Rauch U, Ninomiya Y, Ohashi T (2009) Brevican distinctively assembles extracellular components at the large diameter nodes of Ranvier in the CNS. *J Neurochem* 108(5):1266–1276.
- Susuki K, et al. (2013) Three mechanisms assemble central nervous system nodes of Ranvier. *Neuron* 78(3):469–482.
- Rasband MN, et al. (1999) Dependence of nodal sodium channel clustering on paranodal axoglial contact in the developing CNS. *J Neurosci* 19(17):7516–7528.
- Mathis C, Denisenko-Nehrbass N, Girault JA, Borrelli E (2001) Essential role of oligodendrocytes in the formation and maintenance of central nervous system nodal regions. *Development* 128(23):4881–4890.
- Bhat MA, et al. (2001) Axon-glia interactions and the domain organization of myelinated axons requires neurexin IV/Caspr/Paranodin. *Neuron* 30(2):369–383.
- Boyle ME, et al. (2001) Contactin orchestrates assembly of the septate-like junctions at the paranode in myelinated peripheral nerve. *Neuron* 30(2):385–397.
- Ishibashi T, et al. (2002) A myelin galactolipid, sulfatide, is essential for maintenance of ion channels on myelinated axon but not essential for initial cluster formation. *J Neurosci* 22(15):6507–6514.
- Jenkins SM, Bennett V (2002) Developing nodes of Ranvier are defined by ankyrin-G clustering and are independent of paranodal axoglial adhesion. *Proc Natl Acad Sci USA* 99(4):2303–2308.
- Zonta B, et al. (2008) Glial and neuronal isoforms of Neurofascin have distinct roles in the assembly of nodes of Ranvier in the central nervous system. *J Cell Biol* 181(7):1169–1177.
- Kaplan MR, et al. (1997) Induction of sodium channel clustering by oligodendrocytes. *Nature* 386(6626):724–728.
- Kaplan MR, et al. (2001) Differential control of clustering of the sodium channels Na(v)1.2 and Na(v)1.6 at developing CNS nodes of Ranvier. *Neuron* 30(1):105–119.
- Freund TF, Buzsáki G (1996) Interneurons of the hippocampus. *Hippocampus* 6(4):347–470.
- Jinno S, Kosaka T (2000) Colocalization of parvalbumin and somatostatin-like immunoreactivity in the mouse hippocampus: Quantitative analysis with optical disector. *J Comp Neurol* 428(3):377–388.
- Yuan X, et al. (2002) Expression of the green fluorescent protein in the oligodendrocyte lineage: A transgenic mouse for developmental and physiological studies. *J Neurosci Res* 70(4):529–545.
- Boiko T, et al. (2001) Compact myelin dictates the differential targeting of two sodium channel isoforms in the same axon. *Neuron* 30(1):91–104.
- Duflocq A, Le Bras B, Bullier E, Couraud F, Davenne M (2008) Nav1.1 is predominantly expressed in nodes of Ranvier and axon initial segments. *Mol Cell Neurosci* 39(2):180–192.
- Hedstrom KL, et al. (2007) Neurofascin assembles a specialized extracellular matrix at the axon initial segment. *J Cell Biol* 178(5):875–886.
- Hedstrom KL, Ogawa Y, Rasband MN (2008) AnkyrinG is required for maintenance of the axon initial segment and neuronal polarity. *J Cell Biol* 183(4):635–640.
- Tamamaki N, et al. (2003) Green fluorescent protein expression and colocalization with calretinin, parvalbumin, and somatostatin in the GAD67-GFP knock-in mouse. *J Comp Neurol* 467(1):60–79.
- Uematsu M, et al. (2008) Quantitative chemical composition of cortical GABAergic neurons revealed in transgenic venus-expressing rats. *Cereb Cortex* 18(2):315–330.
- Jinno S, et al. (2007) Neuronal diversity in GABAergic long-range projections from the hippocampus. *J Neurosci* 27(33):8790–8804.
- Meier S, Bräuer AU, Heimrich B, Nitsch R, Savaskan NE (2004) Myelination in the hippocampus during development and following lesion. *Cell Mol Life Sci* 61(9):1082–1094.
- Picardo MA, et al. (2011) Pioneer GABA cells comprise a subpopulation of hub neurons in the developing hippocampus. *Neuron* 71(4):695–709.
- Melzer S, et al. (2012) Long-range-projecting GABAergic neurons modulate inhibition in hippocampus and entorhinal cortex. *Science* 335(6075):1506–1510.
- Vabnick I, Novaković SD, Levinson SR, Schachner M, Shrager P (1996) The clustering of axonal sodium channels during development of the peripheral nervous system. *J Neurosci* 16(16):4914–4922.
- Custer AW, et al. (2003) The role of the ankyrin-binding protein NrCAM in node of Ranvier formation. *J Neurosci* 23(31):10032–10039.
- Du Y, Dreyfus CF (2002) Oligodendrocytes as providers of growth factors. *J Neurosci Res* 68(6):647–654.
- Holter NI, Zuber N, Bruehl C, Draguhn A (2007) Functional maturation of developing interneurons in the molecular layer of mouse dentate gyrus. *Brain Res* 1186:56–64.
- Bennett V, Baines AJ (2001) Spectrin and ankyrin-based pathways: Metazoan inventions for integrating cells into tissues. *Physiol Rev* 81(3):1353–1392.
- Barry J, et al. (2014) Ankyrin-G directly binds to kinesin-1 to transport voltage-gated Na⁺ channels into axons. *Dev Cell* 28(2):117–131.
- Debanne D, Campanac E, Bialowas A, Carlier E, Alcaraz G (2011) Axon physiology. *Physiol Rev* 91(2):555–602.
- Palmer LM, Stuart GJ (2006) Site of action potential initiation in layer 5 pyramidal neurons. *J Neurosci* 26(6):1854–1863.
- Popovic MA, Foust AJ, McCormick DA, Zecevic D (2011) The spatio-temporal characteristics of action potential initiation in layer 5 pyramidal neurons: A voltage imaging study. *J Physiol* 589(Pt 17):4167–4187.
- Johnston WL, Dyer JR, Castellucci VF, Dunn RJ (1996) Clustered voltage-gated Na⁺ channels in Aplysia axons. *J Neurosci* 16(5):1730–1739.
- Zeng S, Tang Y (2009) Effect of clustered ion channels along an unmyelinated axon. *Phys Rev E Stat Nonlin Soft Matter Phys* 80(2 Pt 1):021917.
- Coman I, et al. (2006) Nodal, paranodal and juxtaparanodal axonal proteins during demyelination and remyelination in multiple sclerosis. *Brain* 129(Pt 12):3186–3195.
- Banker GA, Cowan WM (1977) Rat hippocampal neurons in dispersed cell culture. *Brain Res* 126(3):397–445.
- Toulorge D, et al. (2011) Neuroprotection of midbrain dopamine neurons by nicotine is gated by cytoplasmic Ca²⁺. *FASEB J* 25(8):2563–2573.

Supporting Information

Freeman et al. 10.1073/pnas.1419099112

SI Materials and Methods

Culture Media. NCM: neurobasal medium (21103-049; Gibco) supplemented with 0.5 mM L-glutamine, B27 (1×; Invitrogen), and penicillin-streptomycin (100 IU/mL each). BS medium: DMEM Glutamax supplemented with transferrin (50 µg/mL), albumin (50 µg/mL), insulin (5 µg/mL), progesterone (20 nM), putrescine (16 µg/mL), sodium selenite (5 ng/mL), T3 (40 ng/mL), and T4 (40 ng/mL). Differentiation medium: DMEM Glutamax supplemented with transferrin (50 µg/mL), albumin (50 µg/mL), insulin (5 µg/mL), putrescine (16 µg/mL), sodium selenite (5 ng/mL), T3 (40 ng/mL), T4 (40 ng/mL), biotin (10 ng/mL), vitamin B12 (27.2 ng/mL), ceruloplasmin (100 ng/mL), hydrocortisone (0.05 µM), CNTF (0.1 ng/mL), and sodium pyruvate (1 mM).

Immunopanning. The procedure was modified from ref. 1. Petri dishes were incubated overnight at 4 °C with anti-mouse IgG or anti-mouse IgM in 50 mM Tris-HCl (7.2 µg/mL; Jackson ImmunoResearch Laboratories) and then washed with L-15 (GIBCO) supplemented with 0.3% BSA before the addition of 10–20 µg/mL hybridoma RAN-2 (IgG; #TIB-119; ATCC) or hybridoma O4 (in L-15 BSA) to the IgG or IgM dishes, respectively. Selection plates were incubated for 1.5 or 2 h at RT and then washed two times with L-15 BSA. Cells collected from the flasks that were previously shaken overnight were resuspended in L-15 BSA and then incubated in the RAN-2 selection dishes for 35 min at RT. Nonadherent cells from the RAN-2 dishes were then transferred to the O4 selection dishes and incubated for 45 min at RT. Nonadherent cells were removed, and plates were washed with PBS. To detach cells, O4 selection plates were incubated with 0.25% trypsin for 3 min at 37 °C. After neutralization with FCS, cells were centrifuged in DMEM for 5 min at 1,500 rpm, resuspended, and seeded on polyethylenimine-coated T25 flasks at a density of $1.5 \times 10^5/\text{cm}^2$ in BS medium with 0.5% PDGF.

Analyses of different markers' expressions indicated that oligodendrocyte cultures were mostly immature oligodendrocyte lineage cells [90% ± 4% of cells were O4⁺, 85% ± 7% of cells were NG2 proteoglycan NG2⁺, 4.7% ± 2.1% of cells were PLP⁺, and 7.2% ± 2.5% of cells were GFAP⁺ astrocytes (mean ± SD; $n = 3$)].

Abs. The following primary Abs were used for immunolabeling. Mouse mAbs included anti-AnkG (clone N106/36; 1:100), Nfasc (pan, external; clone A12/18), and Nav1.1 (clone K74/71; 1:400) from Antibodies Incorporated (Neuromab). Na_v (pan; clone K58/35; 1:250) and Parvalbumin (clone Parv-19; 1:1,000) were from Sigma. GAD67 (clone 1610.2; 1:400) was from Millipore, Ca²⁺/calmodulin-dependent protein kinase II (clone 6G9; 1:1,000) was from Abcam, MAP2 (clone AP20; 1:100) was from Chemicon, phosphorylated neurofilament marker Ab (SMI31) (1:1,000) was from Covance, and Calretinin (6B3; 1:400) was from Swant. Anti-O4 (IgM; 1:5 hybridoma) was also used. Rabbit polyclonal Abs included anti-NG2 (1:500; Chemicon), Neurofilament M (1:400; Millipore), Calbindin (1:1,000; Swant), Caspr (1:500; Abcam), Nfasc (pan; 1:100; Abcam), AnkG (1:500; provided by François Couraud INSERM, UMR5952, Paris), and Na_v1.2 and Na_v1.6

(1:100; provided by Rock Levinson, University of Colorado School of Medicine, Aurora, CO). We also used chicken anti-GFP (1:400; Millipore) and rat antisomatostatin (1:200; Millipore) and anti-PLP (1:10; hybridoma). Secondary Abs were Alexa Fluor 488, 594, or 647 goat anti-rabbit or anti-mouse IgG_{2a}, IgG₁, or IgM, anti-chicken, or anti-rat from Invitrogen (1:1,000).

Design of miRNA. Two different miRNA sequences were designed to knock down the expression of AnkG: CATAGTGACAGCCCACATGGAGTTTTGGCCACTGACTGACTCCATGTGCTGTCACTATG and TTTGGAAGCAAGATGGAGTGCGTTTTGGCCACTGA CTGACGCACTCCATTGCTTCAAA. They were then cloned into the supplied vector (pcDNA 6.2-GW/EmGFP-miR). A plasmid-expressing miRNA predicted not to target any known vertebrate gene was used as a control. A GFP marker was coexpressed to identify transfected cells.

Electrophysiology. Simultaneous patch recordings were performed with a Multiclamp 700B Amplifier (Molecular Devices) and digitized with pClamp10 software (Axon; Molecular Devices). Artificial cerebrospinal fluid was continuously superfused and contained 124 mM NaCl, 2.5 mM KCl, 26 mM NaHCO₃, 1 mM NaH₂PO₄, 2 mM CaCl₂, 2 mM MgCl₂, and 11 mM D-glucose gently bubbled with 5% CO₂ in O₂ (pH 7.3; 305–315 mOsm/L). For the somatic electrode, pipettes were pulled with a resistance of 3–6 MΩ, whereas pipettes for the axonal electrode were pulled with a resistance of 8–15 MΩ. Both somatic and axonal pipettes were made from borosilicate glass with a 1.5-mm external diameter using a Brown–Flaming electrode puller (Sutter Instruments). The internal solution for whole-cell recordings contained 130 mM K-gluconate, 5 mM KCl, 10 mM Hepes, 10 mM ethylene glycol tetraacetic acid, 2 mM MgCl₂, 4 mM MgATP, 0.4 mM Tris-GTP, and 10 mM Na₂-phosphocreatine (2), whereas artificial cerebrospinal fluid was used to fill the cell-attached recording pipettes. All recordings were made at 35 °C. Of note, Alexa 594-conjugated Nfasc Ab colocalized with AnkG and Na_v without interfering with AP initiation or AP propagation. Spontaneous action currents were recorded in cell-attached mode from both the somatic and axonal electrodes (3). Somatic recordings were made as close as possible to the AIS to minimize latency caused by backpropagation. ImageJ tracing software was used to calculate the distances between electrodes and diameter measurements. AxoGraph X was used to detect action currents in both somatic and axonal recordings followed by an averaging of 10–50 aligned action currents. Action currents were aligned at the peak of the somatic action current and averaged to calculate latencies. Fluorescent and differential interference contrast images were taken with a 40× water-immersion lens (Zeiss) to calculate the distances between electrodes and analyze nodal clustering. The latency was calculated as the difference between the peaks of the somatic- and axonal-averaged action current recordings. Conduction velocities were calculated by dividing the axonal distance between the somatic and axonal electrodes by the latency.

- Caporaso GL, Chao MV (2001) Telomerase and oligodendrocyte differentiation. *J Neurobiol* 49(3):224–234.
- Simonnet J, Eugène E, Cohen I, Miles R, Fricker D (2013) Cellular neuroanatomy of rat presubiculum. *Eur J Neurosci* 37(4):583–597.

- Fricker D, Verheugen JA, Miles R (1999) Cell-attached measurements of the firing threshold of rat hippocampal neurones. *J Physiol* 517(Pt 3):791–804.

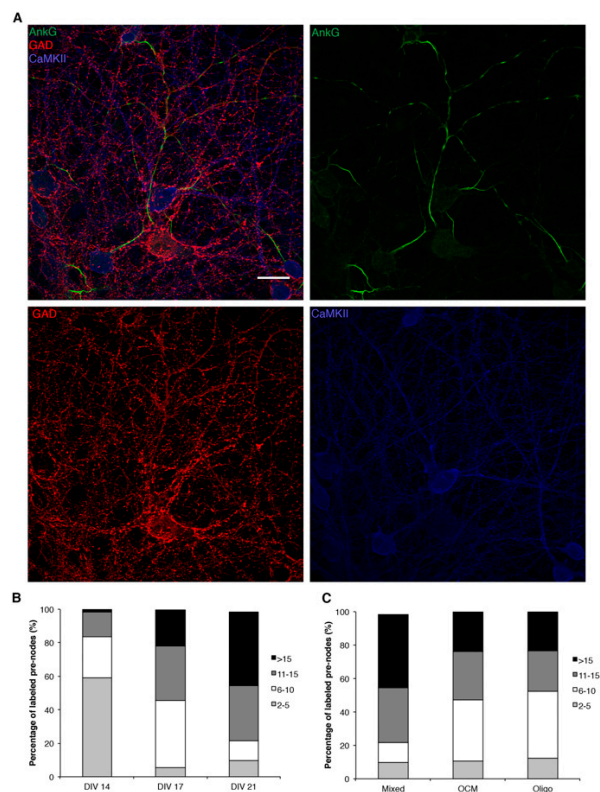


Fig. S1. Prenodes are formed on GAD67⁺ Ca²⁺/calmodulin-dependent protein kinase II⁻ (CaMKII⁻) neurons. (A) Immunostaining of mixed hippocampal rat culture at 17 DIV. Clustering of AnkG (green) along a GABAergic axon (GAD67⁺; red) contrasting with the absence of prenodal clusters on pyramidal cells axons (CaMKII⁺; blue). (Scale bar: 25 μm .) (B) Quantification of the percentage of labeled prenodes binned into numbered categories (2–5, 5–10, 10–15, and 15+) from mixed hippocampal cultures at 14, 17, and 21 DIV. Mean percentages \pm SDs of three independent experiments for each time point are shown. (C) Quantification of the percentage of labeled prenodes on DIV 21 mixed hippocampal cultures or purified neuronal hippocampal cultures treated with OCM or oligodendrocytes (oligo). The numbers of prenodes were binned into numbered ranges (2–5, 5–10, 10–15, and 15+). Mean percentages \pm SDs of three independent experiments for each condition are shown.

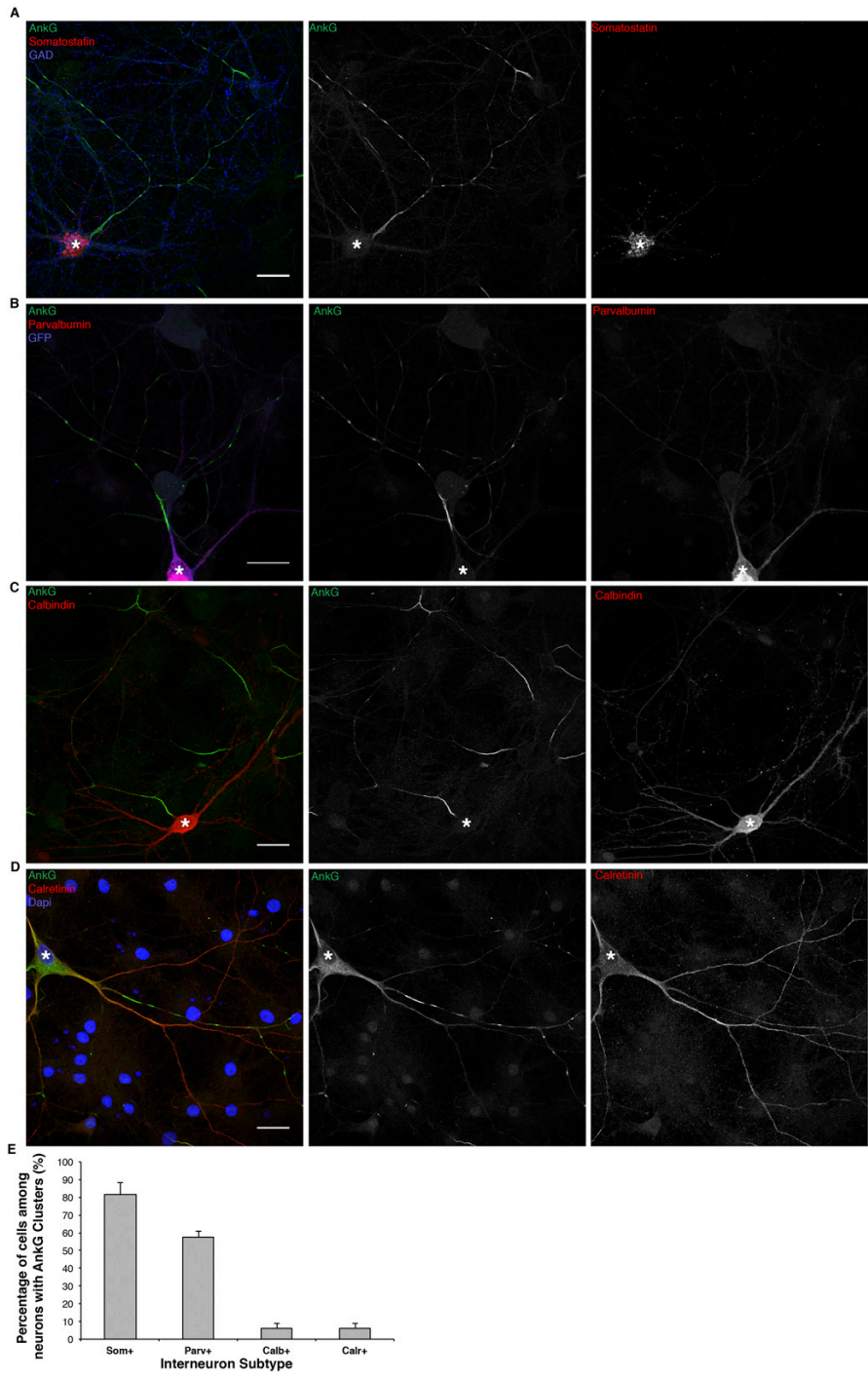


Fig. S2. Multiple interneuron subtypes form prenodal clusters. (A–D) Prenodal clusters of AnkiG were found at 21 DIV along rat hippocampal axons of (A) Somatostatin⁺ (Som+), (C) Calbindin⁺ (Calb+), and (D) Calretinin⁺ (Calr+) interneurons and (B) mouse GAD-GFP⁺ hippocampal axons of Parvalbumin⁺ (Parv+) interneurons. (E) Quantification of the percentage of neurons with clusters among GAD⁺ cells with respect to interneuron subtype. The means \pm SEMs of three independent experiments are shown. At least 100 axons were analyzed in each experiment. (Scale bars: 25 μ m.) *Neuronal cell body.

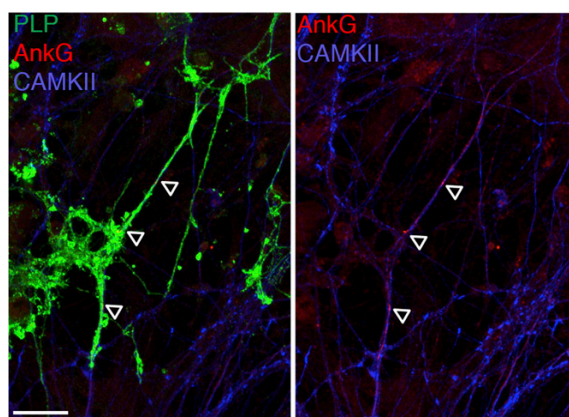


Fig. S3. Immunostaining of mixed hippocampal cultures at 24 DIV showing myelinated segments (PLP⁺; green) with nodes of Ranvier (AnkG⁺; red) on axons of pyramidal cells Ca²⁺/calmodulin-dependent protein kinase I⁺ (CaMKII⁺; blue). (Scale bar: 25 μm.)

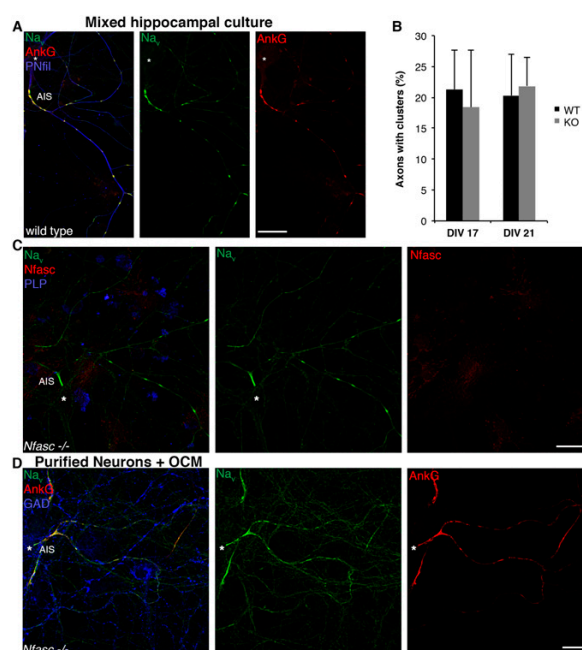


Fig. S4. Prenodes are formed in the absence of Nfasc expression on GABAergic neurons. (A) Immunostaining of mixed hippocampal culture of WT mice at 17 DIV showing Na_v clusters (green) colocalized with AnkG (red) along axons with phosphorylated neurofilaments (PNfil; blue). (B) Quantification of the number of axons with prenodal clusters in both WT and *Nfasc*^{-/-} cultures at DIV 17 and 21. The means ± SEMs of three (*Nfasc*^{-/-}) or four (WT) independent experiments are shown. At least 100 axons were analyzed in each experiment per each condition. (C) Mixed hippocampal culture of *Nfasc*^{-/-} mice at 17 DIV. Na_v clusters (green) observed in the absence of Nfasc expression (red) on unmyelinated neurons (PLP⁻; blue). (D) Purified hippocampal neurons of *Nfasc*^{-/-} mice cultured with OCM. Images show Na_v (green) and AnkG (red) prenodal clusters on a GAD⁺ neuron (blue). (Scale bars: 25 μm.) *Neuronal cell body.

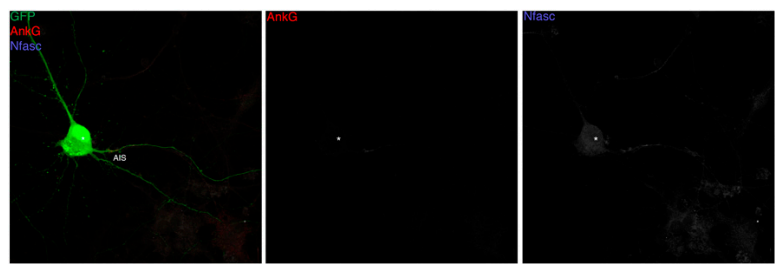


Fig. S5. Immunostaining of hippocampal cell cultures transfected at 6 DIV with AnkG miRNA and fixed at 18 DIV. Transfected neurons are GFP⁺ (green). Representative image of a transfected neuron (GFP⁺). AnkG (red) and Nfasc (blue) expression is weak at the AIS (arrowhead), and no prenodes are observed. (Scale bar: 25 μ m.) *Neuronal cell body.

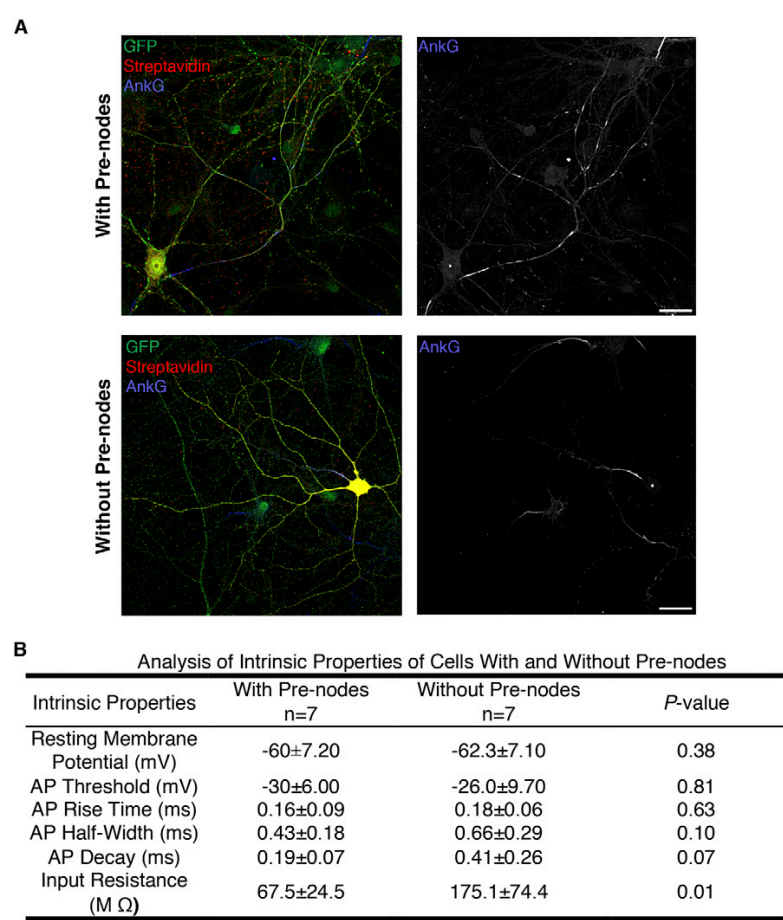


Fig. S6. Electrophysiological properties characterizing unmyelinated interneurons with and without prenodal clusters. (A) Representative immunostaining after somatic whole-cell recordings in *in vitro* hippocampal GAD-GFP-expressing neurons with and without prenodes at 21 and 17 DIV, respectively. (Scale bar: 25 μ m.) (B) The intrinsic properties of hippocampal GAD-GFP-expressing neurons with and without prenodes were analyzed as previously described (1, 2). A lower-input resistance was the only significantly observable difference in neurons with prenodes compared with those without.

1. Simonnet J, Eugène E, Cohen I, Miles R, Fricker D (2013) Cellular neuroanatomy of rat presubiculum. *Eur J Neurosci* 37(4):583–597.
2. Fricker D, Verheugen JA, Miles R (1999) Cell-attached measurements of the firing threshold of rat hippocampal neurones. *J Physiol* 517(Pt 3):791–804.

Chapter II: Work in Progress

Study of the trafficking of nodal components by live imaging in dissociated hippocampal culture

Study of the trafficking of nodal components by live imaging in dissociated hippocampal cultures

Introduction

Neurons are highly polarized cells that can be compartmentalized into a somatodendritic region that receives synaptic input and integrates the coded signal, and an axon that initiates and propagates electrical signals necessary to relay information to the next neuron. These regions can be further subcompartmentalized into areas with discrete functions, which would necessitate precise localization of the domain constituents by distinct mechanisms. For the axon, the proper trafficking and targeting of voltage-gated sodium channels (Na_v) to excitable domains along the axonal membrane is an important step in neuronal excitability (see chapter 3.2). Hence, axonal trafficking must be finely regulated throughout development for proper neuronal function, and its impairment in disease, such as the case for multiple sclerosis, can induce extensive axonal dysfunction and dystrophy (Sorbara *et al.*, 2014).

One particular domain along myelinated axon, called the node of Ranvier, allows for rapid action potential regeneration and propagation. Responsible for the regeneration of electrical activity at the nodes of Ranvier is the high concentration of Na_v , which consists of a pore-forming Na_v alpha subunit together with auxiliary β -subunits that play critical roles in modulating the expression, targeting, and regulation in the rate of alpha subunit activation and inactivation (Patton *et al.*, 1994; Kazen-Gillespie *et al.*, 2000; Chen *et al.*, 2002; Schmidt and Catterall, 2002). Further enriched at this excitable domain are cellular-adhesion molecules (CAMs) such as neurofascin186 (Nfasc186), NrCAM and contactin, and cytoskeletal scaffolding proteins such as ankyrinG and β IV-spectrin, which together act in concert to target, traffic, and stabilize Na_v at the nodes of Ranvier (Zonta *et al.*, 2008; Zhang *et al.*, 2012; Boyle *et al.*, 2001; Çolakoğlu *et al.*, 2014; Davis *et al.*, 1996; Jenkins and Bennett, 2002; Dzhashiashvili *et al.*, 2007; Jenkins *et al.*, 2015; Yang *et al.*, 2004). While the mechanisms involved in nodal formation are best characterized

in the peripheral nervous system (Eshed *et al.*, 2005, 2007; Feinberg *et al.*, 2010; Zhang *et al.*, 2012), the assembly mechanisms governing nodes of Ranvier clustering in the central nervous system (CNS) have yet to reach consensus. There appear to be several overlapping and redundant mechanisms that converge on the fact that neuron-glia interactions are necessary for CNS nodal assembly (Susuki *et al.*, 2013; Chang and Rasband, 2013).

While these recent publications have advanced our understanding of the neuron-glia interactions involved in CNS nodes of Ranvier assembly (see chapter 3.1), an even more open question is in regards to the intrinsic neuronal properties governing the trafficking and compartmentalization of nodes of Ranvier components to the nodal axolemma. Several studies have greatly detailed the trafficking and targeting mechanisms to the axon initial segment (for review see Leterrier and Dargent, 2014), a region with a similar macromolecular composition to the nodes of Ranvier; however, few studies have detailed how these components are trafficked and targeted over time to the CNS nodes of Ranvier. Recent work by Barry *et al.* (2014) reported that KIF5B, an anterograde molecular motor of the kinesin-1 family, is able to transport Na_v1.2 to the CNS nodes of Ranvier through associative linkage via ankyrinG. Yet, the trafficking dynamics and targeting of various other nodal CAMs and auxiliary Na_v β -subunits to the CNS nodes of Ranvier remain relatively unknown. Because the mammalian kinesin-1 family has two other neuron-specific isoforms (KIF5A and KIF5C; Kanai *et al.*, 2000), it is also unclear as to whether KIF5B is solely responsible for the trafficking of Na_v channels or if redundancy exists through KIF5A and KIF5C. Finally, as the nodes of Ranvier are large and heterogenous macromolecular structures, it is uncertain whether the nodal constituents are co-transported together along the axon and if the trafficking dynamics change for nodal vesicles over the developmental formation of nodes of Ranvier, which may present regions of steric hindrance for the passage for these vesicles.

Our laboratory recently reported that evenly spaced clusters of canonical nodal components, called prenodes, cluster along hippocampal GABAergic axons in

the absence of myelination *in vitro* (Freeman *et al.*, 2015). This dissociated hippocampal culture system produces prenodal clusters in the span of two weeks, and is therefore a unique and practical tool in order to study the dynamics of nodal protein trafficking in the CNS.

In the present study, we set out to gain further insight into the intrinsic dynamics of CNS nodal clustering by using time-lapse imaging of fluorescently tagged nodal markers along axons in dissociated mixed hippocampal neuron glia cell cultures. We first showed that $\beta 1$ and $\beta 2\text{Na}_v$ subunits are clustered at prenodes along GABAergic axons prior to myelination and that the various fluorescently tagged nodal markers that we generated restrict to axons similarly to the corresponding endogenous proteins. Time-lapse imaging studies showed that axonal transport of $\beta 2\text{Na}_v$ and NF186 is dynamic and moves in anterograde, bidirectional, and retrograde motions. Anterograde movements are fast, and reach speeds similar to those reported for kinesin-1, while retrograde movements are significantly slower. Knockdown of two neuronal motor proteins of the kinesin-1 family, KIF5A and KIF5C, reduces the speed of anterograde transport of NF186, and knockdown of KIF5C appears to increase the fraction of retrograde moving NF186 vesicles. Together, these studies help shed light on the trafficking patterns of various nodal components and key molecular motors that could be involved in prenodal formation.

Materials and Methods

Reagents

Antibodies and immunofluorescence

The following primary antibodies were used for immunolabeling: Mouse monoclonal antibodies included anti-ankyrinG (clone N106/36, 1:200), anti-Pan Nfasc (external, clone A12/18, 1:500) from Antibodies Incorporated (Neuromab), and anti-MAP2 (clone AP20; 1:1000) was from Chemicon. Rabbit polyclonal antibodies included anti- $\beta 1\text{Na}_v$ (1:100, kind gift from Dr. Peter Brophy, described in Desmazières *et al.*, 2015), anti- $\beta 2\text{Na}_v$ (1:200) from Millipore, anti-kinesin 5A (1:1000, Abcam), anti-kinesin 5B (1:400, Abcam), anti-kinesin 5C (1:1000, Abcam) anti-Pan Nfasc (1:100,

Abcam), anti-ankyrinG (1:2000, kindly provided by Prof. François Couraud, UPMC, Paris, France; described in Le Bras *et al.*, 2014). We also used chicken anti-GFP (1:400, Millipore) and anti-mCherry (1:2000, EnCor). Secondary antibodies were Alexa Fluor 488, 594 or 647 goat anti-rabbit or anti-mouse IgG_{2a}, or IgG₁, or anti-chicken from Invitrogen (1:1000). The procedures of immunocytochemistry have been previously described (Freeman *et al.*, 2015).

Plasmids

pCMVAnkG270-GFP was a kind gift from Prof. François Couraud. pEGFPN₁, and pmCherry-N1 were acquired from Clontech. pdAnkG190-EYFP-N₁ was acquired from BioValley. mCherry driven by the neuronal promoter synapsin (syn) promoter (pTripSynmCherry) was kindly provided by Dr. Phillippe Ravassard (ICM-University Paris Pierre and Marie Curie). Nfasc186-mCherry driven by the CMV promoter (pCMVNfasc186-mCherry) was kindly provided by Prof. Peter Brophy (University of Edinburgh).

Generation of pTRIPSynNfasc186-mCherry: Briefly, the Nfasc186-mcherry encoding sequence was retrieved from the pCMV Nfasc186-mCherry plasmid using EcoRI/SalI restrictions sites (restriction enzymes and buffers from New England Biolabs) and ligated into the pENTR vector using a rapid ligation kit from Roche. pENTRNfasc186-mCherry was then recombined into the pTrip Syn RFA Delta U3 plasmid kindly provided by Dr. Philippe Ravassard using the LR recombination kit. pTRIPSynNfasc186-mCherry was further used to generate lentiviral particles (ICM vectorology platform).

Generation of pTripSyn β 1Na_v-mCherry and pTripSyn β 2Na_v-mCherry: PCR fragments of the β 1 and β 2 Na_v encoding sequence from the pCMV6-AC- β 1Na_v-GFP and pd β 2Na_v-EYFP-N₁ (BioValley), respectively, were subcloned into the pENTRNfasc186-mCherry vector using EcoRI/HindIII restriction sites to replace the Nfasc186 encoding sequence. pENTR β 1Na_v-mCherry and pENTR β 2Na_v-

mCherry were then recombined into the pTrip Syn RFA Delta U3 plasmid as previously described.

Generation of miR RNA Constructs: Single-strand DNA oligos encoding the miR RNA of interest were designed using the Life Technologies online tool. The corresponding oligos were then annealed and inserted into the pcDNA 6.2W/EmGFP linearised plasmid using the Block-it Pol II miR RNAi expression vector kits (K4936-00). All constructs were confirmed by sequencing of the miR RNA encoding sequences.

Hippocampal Cultures

Mixed hippocampal cultures (containing neurons and glial cells) from embryonic day (E) 18 rats were prepared according to procedures previously described (Freeman *et al.*, 2015) with slight modification. Briefly, pooled hippocampi were dissociated enzymatically by trypsin (0.1%; Worthington) treatment for 20 min with DNase (50 µg/mL). After trypsin neutralization, cells were centrifuged at 400 x g for 5 min, resuspended, and then seeded on polyethylenimine precoated glass coverslips or 60 mm glass-bottom dishes (Ibidi) at a density of 5.0×10^4 cells/35 mm². Cultures were maintained for 24 h in a 1:1 mixture of Dulbecco's modified Eagle's medium with Glutamax (11880;Gibco) with 10% fetal calf serum (100 IU/mL), penicillin-streptomycin (100 IU/mL) and neuron conditioned medium [NCM; neurobasal medium supplemented with 0.5 mM L-glutamine, B27 (1X; Invitrogen), and penicillin-streptomycin (100 IU/mL)]. Culture medium following the 24 hr incubation period was replaced by a 1:1 mixture of Bottenstein-Sato medium (Freeman *et al.*, 2015) with PDGF- α (0.5%) and NCM. Medium was changed every 3 days and replaced by NCM. The care and use of rats in all experiments conformed to institutional policies and guidelines (UPMC, INSERM and European Community Council Directive 86/609/EEC). For this study we used Sprague Dawley, Wistar, (Janvier Breeding Center) and *VGAT-Venus* (Uematsu *et al.*, 2008) rats.

Transfections and Lentiviral Infection

Two hours prior to transfection, media was removed from wells and kept at 4°C to be used after transfection. After this step, 500 uL (24-well plates and slide dishes) or 1.0 mL (round glass bottom imaging dishes) of NCM without penicillin-streptomycin was then added to wells or dishes. Hippocampal cultures in 24-well plates were transfected at either 5 or 6 days *in vitro* with a 0.5 µg plasmid and 1.0 uL Lipofectamine 2000 reagent (11668-019; Life Technologies) diluted in Opti-MEM reduced serum medium (31985-062; Life Technologies) according to the manufacturer's protocol. The quantity of plasmid and Lipofectamine 2000 reagent was doubled for 35 mm glass-bottom dishes. After 1 ½ hour transfection at 37°C, transfection media was removed from wells and replaced with a pre-warmed 1:1 mixture of mixed culture conditioned media recuperated from wells prior to transfection and fresh NCM media. Hippocampal cultures in 24-well plates were fixed at either 9 or 10 DIV with either 1% or 4% paraformaldehyde for immunocytochemical analysis, while round bottom glass dishes were utilized from either 8-10 or 17-18 DIV for video microscopy studies.

Hippocampal cultures from VGAT-Venus rats in 24-well were infected at 5 DIV in half-culture volume and then fed with a mix of fresh culture media with NCM two hours later. Cultures were fixed and immunolabeled at the indicated time points.

Imaging

Confocal microscopy

High-magnification confocal images of slides from hippocampal cultures were captured with an Olympus FV-1000 Upright Confocal Microscope using a 63x oil immersion objective (numerical aperture = 1.35). Z-series of optical sections were performed at 0.3 µm increments. Green, red and far-red fluorescence were acquired sequentially. Maximum orthogonal projection of images and adjustment for brightness and contrast were carried out using ImageJ software (NIH, Bethesda, Maryland).

Live-Cell Imaging

For single-color live imaging, cells were grown on 35 mm glass-bottom dishes and transfected with either Nfasc186-mCherry, β 2Na_v-mCherry, or mCherry plasmids. Cells used in dual-color live imaging were transfected with Nfasc186-mCherry with either control, KIF5A, or KIF5C miRNA coexpressing GFP for transfected cell identification. Five to thirteen days after transfection, dishes were mounted in a temperature controlled imaging chamber stabilized at 37° under 5% CO₂ for live-cell time-lapse imaging. Single and dual live imaging were performed on a AxioVert200 inverted Zeiss microscope using a 63x PlanApo oil objective (numerical aperture = 1.4), and captured using a Photometrics DualCam2 Evolve camera through GFP, mCherry, or GFP/mCherry filter sets. Time-lapse imaging was taken in continuous streaming mode with a 250 ms exposure time for 201 frames using Metamorph software (Molecular Devices) on a Dell Precision T5500 computer. Axons were distinguished morphologically by the lack of dendritic spines or by either the enrichment of the fluorescently tagged protein at the AIS or identification of the axon growth cone.

Live-cell Image Analysis

For analysis of single-color live imaging, time-lapse sequences were saved as TIF files and exported to FIJI. Generation of kymographs was performed using the FIJI software plugin KymoToolBox (designed by Dr. Fabrice Cordelière of University of Bordeaux 2), which were then further analyzed by manually following the trajectories of individual vesicles. Moving vesicles in either the anterograde or retrograde direction were defined as having speeds above 0.1 μ m/s while in movement and a total distance of more than 3 μ m in a given direction. Our quantifications assessed the mean total velocity, defined as the Δ displacement of the trajectory/ Δ time, and the mean moving transport velocity of puncta, which excluded all non-moving segments in the analysis. This latter velocity was the mean of summed weights of a manually drawn segment on the trajectory, which can be defined by the equation: moving velocity = $t^{-1} \sum_i v_i t_i$, where i = the segment, v =

individual segment velocity, and t = time. We also calculated the proportion of anterograde, retrograde, bidirectional and stationary vesicles, and mean percentage of time in movement in both the anterograde and retrograde directions. Group analysis of the trajectories was performed using a homemade Excel macro by Dr. Julien Tailleur (University of Paris Diderot). Statistical analysis was performed using Prism (GraphPad software). Two groups were compared by unpaired t -test, while multiple groups were compared by repeated measures one-way analysis of variance (ANOVA) test, with a Tukey's post-test. The criterion for statistical significance was set at *, $p < 0.05$; **, $p < 0.01$; and ***, $p < 0.001$.

Results

Fluorescently-tagged nodal markers are localized to the axon of neurons in mixed hippocampal cultures

In our mixed hippocampal culture system, the formation of the AIS occurs during the first week in culture, followed several days later with clustering of nodal components at sites called prenodes that form in the absence of myelination (Freeman *et al.*, 2015). Both the AIS and prenodes display clustering of Nfasc186, Na_v (including Na_v1.1, Na_v1.2, and Na_v1.6), and ankyrinG (Freeman *et al.*, 2015); however, it was uncertain as to whether other nodal components cluster at these regions in our model system. Because it has been previously described that Na_v β -subunits are involved in modulating the expression and targeting of Na_v α -subunits (Patton *et al.*, 1994; Kazen-Gillespie *et al.*, 2000), we therefore immunolabeled mixed hippocampal cultures with antibodies against β 1Na_v and β 2Na_v at time points during AIS formation and during prenodal assembly. During the first week of culture, β 1Na_v immunolabeling was observed to be clustered at the AIS (not shown). Surprisingly, and in contrast to a previous report (Kaplan *et al.*, 2001), β 1Na_v was enriched at prenodal clusters in the absence of myelination at 17 DIV (Fig. 1A). β 2Na_v accumulation was observed at the AIS at 10 DIV (not shown), and also at prenodal clusters that were restricted to GABAergic neurons at 17 DIV (Fig. 1B). This antibody also showed non-specific nuclear labeling that overlapped with DAPI

(not shown). Together, this suggests that Na_v α - and β -subunits, along with CAMs and cytoskeletal proteins are coclustered at the AIS and prenodes in mixed hippocampal cultures in the absence of myelination in GABAergic interneurons.

Having further characterized the endogenous proteins expressed at the AIS and in prenodes in our model system, we then developed several fluorescently-tagged nodal constructs in order to investigate the dynamics of nodal protein trafficking in the CNS. We first transfected, β 2Na_v-mCherry, β 2Na_v-GFP, Nfasc186-mCherry, and ankyrinG270-GFP constructs into mixed hippocampal cultures from 5-6 DIV in order to verify that they mimicked endogenous expression of the protein by restricting to the axon. Indeed, at 10 DIV all constructs, similar to their respective endogenous expression (Fig. 2A), were able to restrict to the AIS and axon (Fig. 2B). This was confirmed by the absence of the somatodendritic marker MAP2 in axons (Fig. 2B), and furthermore the specificity of the tagged nodal constructs was confirmed by the colocalization of antibodies recognizing the nodal protein (Fig. 2B).

In order to verify that these fluorescently-tagged nodal markers also restricted to prenodes in GABAergic neurons, we infected dissociated mixed hippocampal cultures from *VGAT-Venus* rats at DIV5 with lentiviral-delivered Nfasc186-mCherry. At 21 DIV, we were able to observe strong restriction of Nfasc186-mCherry to the AIS of both VGAT-Venus positive and negative axons. We also observed tight restriction of Nfasc186-mCherry to prenodes along VGAT-Venus positive axons (Fig. 2C). Taken together, fluorescently-tagged nodal markers are highly restricted to the axon through both transfection and transduction methods, and also puts forth two different systems in order to study the early dynamics of nodal protein trafficking and another to study long-term formation of nodal clusters in GABAergic interneurons.

Nodal markers exhibit dynamic transport

Having established that nodal markers are able to restrict to the axon of hippocampal neurons, we then focused on the trafficking patterns of two prenodal components, Nfasc186-mCherry and $\beta 2Na_v$ -mCherry, by transfecting these constructs in dissociated mixed hippocampal cultures between 4-6 DIV and performed live time-lapse imaging along axons between 8-10 DIV. These constructs were furthermore compared against mCherry control that is not restricted to the axonal compartment (not shown). Axons in culture were defined by either identifying the axonal growth cone or by identifying the cell body of the transfected neuron and discriminating the axon by the lack of dendritic spines and enrichment at the AIS. Importantly, this type of axonal identification allowed us to establish directionality for vesicular transport for further analysis. We then analyzed the time-lapse images of each construct by generating kymographs (Fig. 3A'-C') that display the displacement of vesicles (x-axis) over the time of the recording (y-axis). Vesicles from each construct were then manually traced on the kymographs (Fig. 3A''-C'') to calculate several parameters such as the mean velocities for each construct, their mean fraction of time in movement, and the distribution of vesicular movements.

While a subset of vesicles was stationary in all cultures (defined as displacement $< 3\mu m$, see materials and methods), we also observed that vesicles of each transfected construct exhibited dynamic anterograde, retrograde, and bidirectional vesicular transport (Fig. 3A-C). Anterograde vesicles from each construct ranged from dense to faintly expressing vesicles (Fig. 3A'-C'), while retrograde vesicles were qualitatively larger and denser than anterograde vesicles (Fig. 3A'-C'). Anterograde movements of vesicles from each construct were fast and reached speeds of approximately $1.0 \mu m/s$ (Fig. 3D). Conversely, retrograde vesicular movements of all constructs were significantly slower than anterograde movements, which ranged from $0.5-0.7 \mu m/s$ (Fig. 3D). Additionally, anterograde vesicles from each construct spent a larger fraction of their time in movement compared to their retrograde counterpart (Fig. 3D; $p < 0.001$), suggesting that

retrograde vesicles tend to spend more of their time paused rather than moving (Fig. 3E). Even though we did not observe significant differences in the velocity of axonal vesicular transport in anterograde or retrograde directions between control mCherry and Nfasc186-mCherry or $\beta 2\text{Na}_v$ -mCherry (Fig. 3D), Nfasc186-mCherry and $\beta 2\text{Na}_v$ -mCherry vesicles spent a significantly larger fraction of time moving in both anterograde and retrograde directions than mCherry vesicles (Fig. 3E; $p < 0.001$). Analysis of the distribution of all vesicles analyzed from each construct showed that the majority of vesicles analyzed were anterograde, while bidirectional vesicles represented the minority of vesicles observed (Fig. 3F). Interestingly, there was a larger proportion of stationary and bidirectional mCherry vesicles compared to Nfasc186-mCherry and $\beta 2\text{Na}_v$ -mCherry vesicles (Fig. 3F), suggesting that axonal transport of mCherry vesicles may be more uncoordinated. Thus, our results show that Nfasc186-mCherry and $\beta 2\text{Na}_v$ -mCherry exhibit dynamic vesicular axonal transport, wherein anterograde vesicles move by continuous fast axonal transport while retrograde vesicles are slower and tend to pause more often.

Knockdown of KIF5A and KIF5C disrupts Nfasc186-mCherry transport

The conventional kinesin, kinesin-1 or KIF5, is a fast, plus-end-directed microtubule motor that is able to bind several different types of cargoes including mitochondria (Tanaka *et al.*, 1998), vesicles (Colin *et al.*, 2008; Kamal *et al.*, 2000), retrograde motor proteins (Kamada *et al.*, 2010), and mRNA complexes (Kanai *et al.*, 2004). Recently, by expressing dominant-negative KIF5B in hippocampal neurons, Barry *et al.* (2014) reported that there is a reduction of axonal ankyrinG and Na_v , suggesting that this molecular motor is implicated in ankyrinG and Na_v trafficking. Because the mammalian KIF5 family includes three neuronal isoforms (KIF5A, KIF5B, and KIF5C; Kanai *et al.*, 2000) that are able to form heterodimers and may have overlapping functions in axonal transport (Hirokawa *et al.*, 2010), we first addressed whether KIF5A or KIF5C could similarly be implicated in expression of nodal components by specifically silencing their expression through miRNA plasmids coexpressing GFP within hippocampal neurons. At 17 DIV,

neurons expressing KIF5A miRNA (GFP⁺) had a marked reduction in somatic and axonal expression of KIF5A when compared to neurons expressing control miRNA (Fig. 4A and C). A more drastic suppression of KIF5C was observed in neurons expressing KIF5C miRNA compared to control at 17 DIV (Fig. 4B and D). KIF5C immunolabeling was all but absent in KIF5C miRNA transfected neurons, except for dense nuclear labeling (Fig. 4B and D). Therefore, axonal or complete neuronal suppression of either KIF5A or KIF5C illustrates the efficiency of the miRNAs and presents a useful tool in further understanding their roles in axonal transport of nodal markers.

In addition to the KIF5A and KIF5C immunolabelings, we performed in conjunction immunostainings of axonal Nfasc in these preparations with an antibody recognizing its extracellular epitope. We observed no clear difference in Nfasc AIS surface expression between KIF5A miRNA or KIF5C miRNA treated with control miRNA (Fig. 4A and B). Similarly, we observed no reduction in ankyrinG immunolabeling at the AIS in comparing neurons transfected KIF5A miRNA or KIF5C miRNA with control miRNA (Fig. 4C and D).

Because we did not observe drastic changes in the axonal expression of Nfasc186 or ankyrinG through immunolabeling, we then investigated whether silencing of KIF5A or KIF5C could impair the trafficking of Nfasc186 by cotransfecting KIF5A or KIF5C miRNAs with Nfasc186-mCherry in mixed hippocampal cultures from DIV4-6 followed by two color time-lapse imaging between DIV 17-18 (Fig. 5A-C). Similar to that observed for Nfasc186-mCherry trafficking at DIV 10, transport speeds at these later time points were significantly faster in the anterograde direction than the retrograde direction in all conditions (Fig. 4D; $p < 0.001$). Strikingly, Nfasc186-mCherry transport speeds were significantly slower in the anterograde direction when comparing KIF5A with controls (Fig. 4D; $p < 0.001$). While Nfasc186-mCherry anterograde speed decreased when treated with KIF5C miRNA compared to control (Fig. 4D; $p < 0.01$), retrograde transport of Nfasc186-mCherry was also slightly faster in neurons treated with KIF5C miRNA compared to those treated with control, and

significantly faster compared to KIF5A miRNA (Fig. 4D; $p < 0.01$). The fraction of time spent moving between Nfasc186-mCherry anterograde and retrograde vesicles when treated with control miRNA was significantly different (Fig. 4E); however, this difference was lost when transfected with KIF5A or KIF5C miRNA (Fig. 4E). Lastly, the proportion of retrograde moving Nfasc186-mCherry vesicles was elevated when KIF5C was suppressed (Fig. 4F). Together, these results suggest that silencing KIF5A and KIF5C expression impairs the trafficking of Nfasc186 and positively augments the fraction of time retrograde vesicles are in movement, and that reducing KIF5C changes the balance between anterograde and retrograde movement and alters the speed of moving vesicles.

Discussion and Perspectives

In this study, we further characterized the molecules restricted to prenodes, and also outlined a potentially useful model system for studying the dynamic trafficking of nodal molecules and the long-term visualization of prenodal assembly in GABAergic neurons. By investigating two nodal markers, we were able to show that Nfasc186 and $\beta 2\text{Na}_v$ exhibit dynamic anterograde, retrograde or bidirectional movements. However, suppressing the expression of neuronal microtubule motors KIF5A and KIF5C disrupted the anterograde trafficking velocity of Nfasc186, suggesting that these two motors could be implicated in its transport.

$\beta 1$ and $\beta 2\text{Na}_v$ are components of the prenodal complex

While the expression of $\beta 1$ and $\beta 2\text{Na}_v$ have been observed at CNS nodes of Ranvier (Chen *et al.*, 2002; Desmazières *et al.*, 2014; Wimmer *et al.*, 2015) and that node-like clusters express $\beta 2\text{Na}_v$ and not $\beta 1\text{Na}_v$ in the absence of myelination (Kaplan *et al.*, 2001), it was unknown whether prenodes in our model system would express one or both of these β -subunit subtypes. One intriguing finding that we report here is that both $\beta 1$ and $\beta 2\text{Na}_v$ are expressed at the same time point and colocalized with Na_v in prenodal clusters (Fig. 1A and B). Additionally, we observed clusters of these two β -subunits in the absence of myelination and along GABAergic

axons (Fig. 1A and B), which is in line with our previous results that clusters of canonical nodal components can form prior to myelination on GABAergic neurons (Freeman *et al.*, 2015). As it has been suggested that $\beta 1\text{Na}_v$ is associated to $\text{Na}_v 1.6$ (Kaplan *et al.*, 2001), and that we previously observed clusters of $\text{Na}_v 1.6$ at beginning at 17 DIV (Freeman *et al.*, 2015), it is possible that the expression of $\beta 1\text{Na}_v$ could correspond to an overlap with $\text{Na}_v 1.6$ at prenodes. No developmental analyses of the expression of either $\beta 1$ or $\beta 2\text{Na}_v$ in conjunction with Na_v α -subunits were performed since the β -subunit and α -subunit antibodies are of the same isotype. Further tools will need to be generated in order to facilitate the analysis of developmental regulation of β -subunits and their interaction with α -subunits in prenodal clusters.

Dynamic movement of nodal markers

Our live time-lapse imaging of Nfasc186-mCherry and $\beta 2\text{Na}_v$ -mCherry showed that they exhibited several types of trafficking patterns: anterograde, retrograde, and bidirectional. Anterograde movements were highly motile and reached speeds of approximately $\sim 1.0 \mu\text{m/s}$, while retrograde movements were punctuated by longer periods of pausing, which is illustrated in the significant difference in the fraction of time moving between anterograde and retrograde vesicles for all constructs. In comparing a non-axonal specific mCherry with axonal restricted Nfasc186-mCherry and $\beta 2\text{Na}_v$ -mCherry we observed that mCherry spent a lower fraction of time moving in both anterograde and retrograde directions their Nfasc186-mCherry and $\beta 2\text{Na}_v$ -mCherry counterparts. Furthermore, a larger proportion of bidirectional and stationary mCherry vesicles were observed compared to Nfasc186-mCherry and $\beta 2\text{Na}_v$ -mCherry. This latter result could suggest that mCherry bidirectional vesicles are destined for lysosomal degradation since bidirectional movement is characteristic of late endosomes/lysosomes (Hendricks *et al.*, 2010), while stationary vesicles may be untethered from either kinesin or dynein motors.

Although we were able to show dynamic trafficking of two nodal components, it is of high importance to explore the trafficking patterns of other nodal markers one by one and also together to further understand their co-transport. Because we were able to express $\beta 2\text{Na}_v\text{-GFP}$ and ankyrinG270-GFP in hippocampal cultures, we could potentially co-transfect either one of these two constructs together with Nfasc186-mCherry or $\beta 2\text{Na}_v\text{-mCherry}$ to investigate the co-transport of these nodal markers through dual color time-lapse imaging. This could potentially help shed light on understanding whether the nodal components are preassembled as a complex from the Golgi apparatus or if they are transported separately and then form clusters through diffusion trapping.

It is also worthwhile to understand the trafficking patterns of nodal markers over time in order to see if there are dynamic changes in vesicular transport during development, especially during prenodal formation. Transfecting hippocampal cultures with our fluorescently-labeled constructs appeared to delay the formation of prenodal clusters. Therefore, our system combining mixed hippocampal cultures from VGAT-Venus rats with lentiviral-mediated infection nodal constructs will help us elucidate the long-term formation of prenodes and the trafficking patterns of vesicles as they approach these regions.

KIF5A and KIF5C may be implicated in Nfasc186 transport

Dual time-lapse imaging of hippocampal cultures co-transfected with miRNAs directed against KIF5A and KIF5C with Nfasc186-mCherry showed that Nfasc186 trafficking was impaired when reducing these kinesins. A significant reduction in Nfasc186 transport speeds may correspond to a lack of ATP available to power fast axonal transport since KIF5A is able to transport mitochondria (Hirokawa *et al.*, 2010). However, glycolytic enzymes are also localized on vesicles and can propel fast axonal transport in the absence of mitochondria ATP production (Zala *et al.*, 2013). Because we did not observe complete reduction in either Nfasc or ankyrinG immunoreactivity, and that Nfasc186-mCherry still maintained anterograde vesicular transport in our live imaging studies, these results also

indirectly suggest that other kinesin motors are able to compensate for the loss of KIF5A or KIF5C. Continual studies using a combinatorial knockdown strategy will help us further elucidate the overlapping redundancies of kinesin motors.

Our results may also fit in the proposed “tug-of-war” model of vesicular trafficking, wherein both kinesin and dynein motors attach to the cargo and oppose one another in anterograde and retrograde directions (Fig. 6; Müller *et al.*, 2008; Hendricks *et al.*, 2010). As we did not observe a difference in fraction of time in movement in the anterograde and retrograde directions for Nfasc186-mCherry vesicles when treated with KIF5A and KIF5C miRNA, this reduction of KIF5A or KIF5C anterograde motors may have positively augmented of the fraction of time retrograde Nfasc186 vesicles spent moving. Additionally, suppression of KIF5C may have shifted the proportion of anterograde vesicles to retrograde and bidirectional movements.

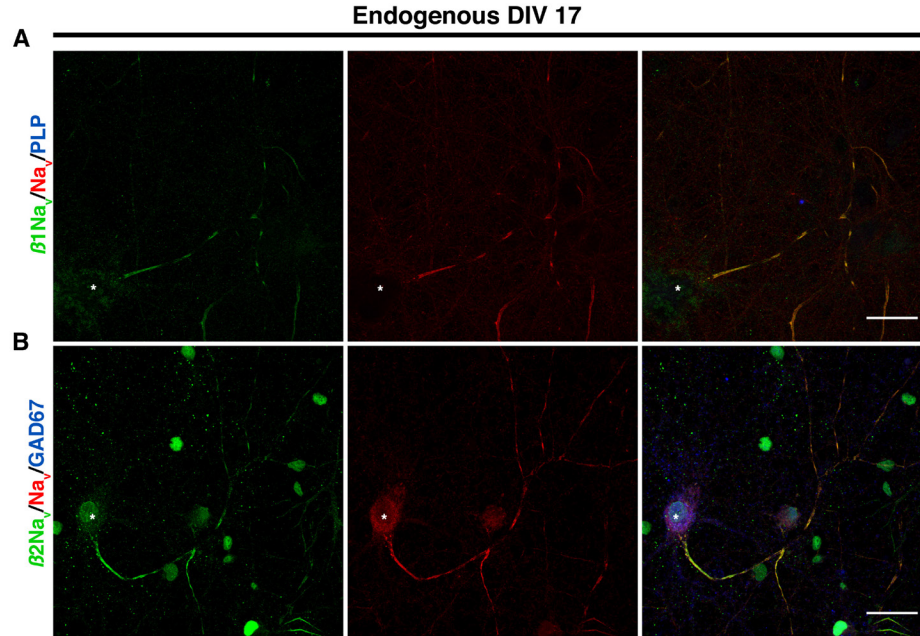


Figure 1: $\beta 1$ and $\beta 2\text{Na}_v$ are restricted to prenodes in mixed hippocampal cultures at 17 DIV. **(A)** Immunolabeling of mixed hippocampal cultures show that $\beta 1\text{Na}_v$ (green) colocalizes with Na_v (red) at prenodes in the absence of myelination (blue) at 17 DIV. **(B)** $\beta 2\text{Na}_v$ (green) colocalizes with Na_v (red) at prenodes along axons expressing the GABAergic marker GAD67 (blue) at 17 DIV. Asterisks denote the neuronal cell body. Scale bars = 25 μm .

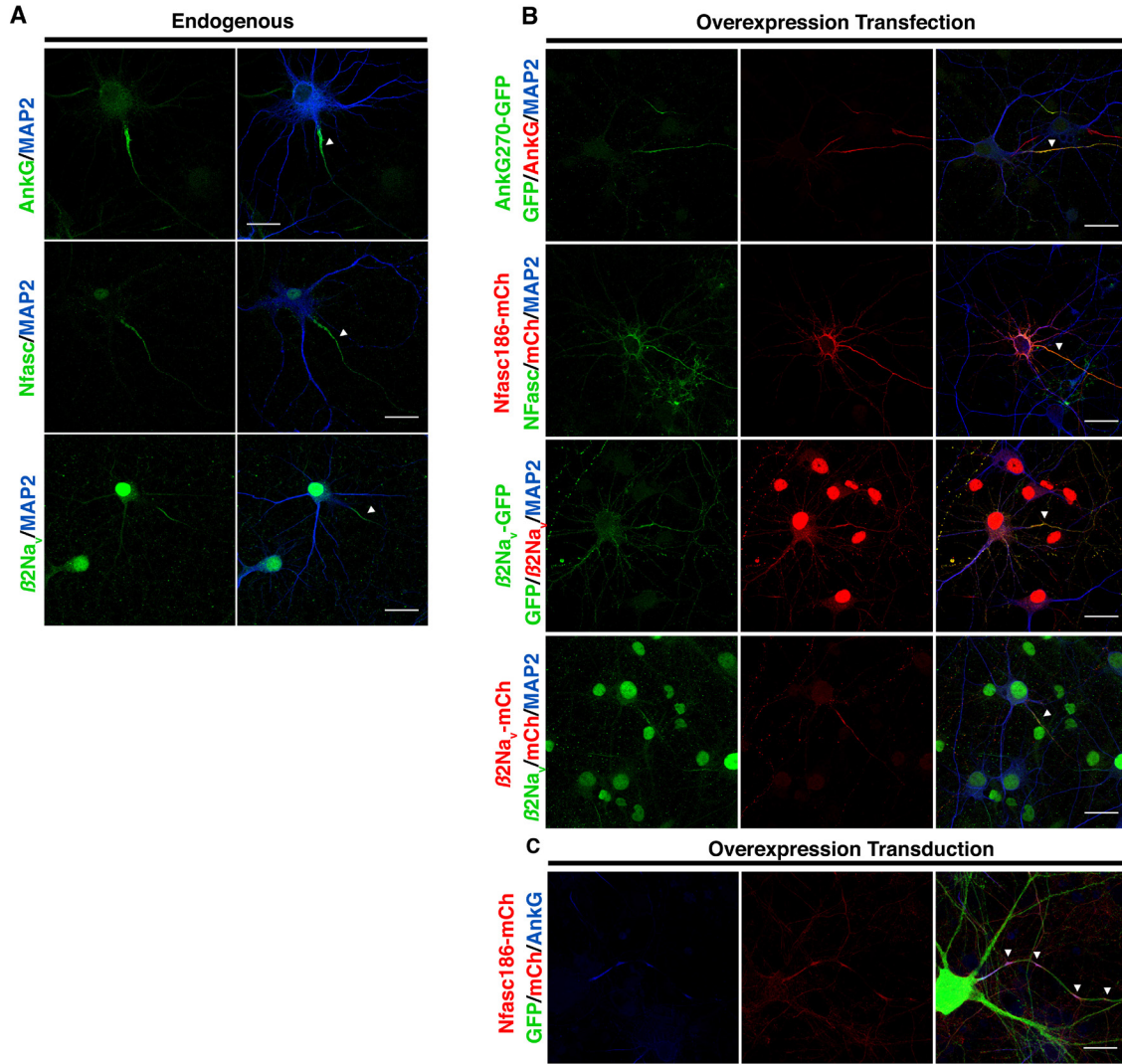


Figure 2: Overexpression of fluorescent constructs mimics endogenous expression and restricts to the axon. **(A)** At 10 DIV, endogenous ankyrinG (green, top panel), Nfasc (green, middle panel), and $\beta 2Na_v$ (green, lower panel) restrict to the AIS, which is devoid of the somatodendritic marker MAP2 (blue). White arrowheads denote the AIS **(B)** Overexpression of ankyrinG270-GFP (green, top panel), Nfasc186-mCherry (red, second panel), $\beta 2Na_v$ -GFP (green, third panel), $\beta 2Na_v$ -mCherry (red, bottom panel) all restricted to the axon (absence of MAP2 labeling, blue) when transfected in mixed hippocampal cultures. White arrowheads denote the AIS **(C)** Nfasc186-mCherry (red) restricts and colocalizes with ankyrinG at prenodos in VGAT-venus⁺ neurons (green) when transduced. White arrowheads denote prenodal clusters. Scale bars = 25 μ m.

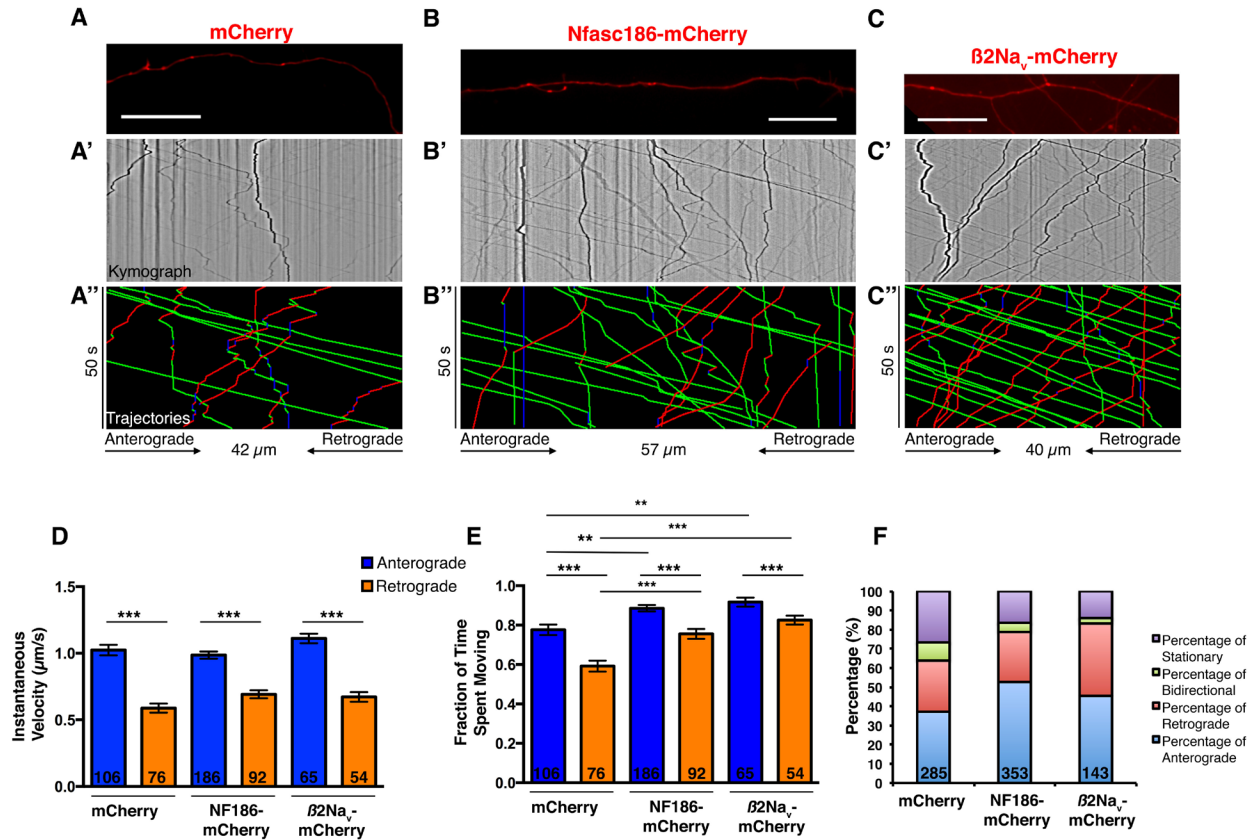


Figure 3: Trafficking of Nfasc186-mCherry and $\beta 2\text{Na}_v$ -mCherry is dynamic. **(A, B, and C)** Live time-lapse imaging was performed on mixed hippocampal cultures between 8-10 DIV transfected with mCherry **(A)**, Nfasc186-mCherry **(B)** or $\beta 2\text{Na}_v$ -mCherry plasmids **(C)**. Kymographs were generated from the time-lapse images **(A', B', C')**, followed by manual tracing of each vesicular trajectory **(A'', B'', C'')**. Anterograde trajectories are denoted in green, retrograde in red, and stationary in blue **(A'', B'', C'')**. Total time of the time-lapse recording and distance of the axon analyzed are denoted to the right and bottom, respectively, of the analyzed kymographs. **(D)** Analysis of the continuous movement in both anterograde and retrograde directions showed that retrograde movements were significantly slower than their anterograde counterpart. **(E)** Anterograde vesicles spent a larger fraction of time moving versus retrograde vesicles for each construct. Similarly, anterograde and retrograde movements of Nfasc186-mCherry and $\beta 2\text{Na}_v$ -mCherry vesicles spent a larger fraction of time moving compared to mCherry. **(F)** Distribution of the types of movements analyzed in each condition. The number of vesicles analyzed is the bolded numbers included in the columns for each condition. The data shown for mCherry include two independent experiments, three independent experiments for Nfasc186-mCherry, and one independent experiment for $\beta 2\text{Na}_v$ -mCherry. Data represent means \pm SEM. *, $p < 0.05$; **, $p < 0.01$; and ***, $p < 0.001$, one-way ANOVA with Tukey's post-test.

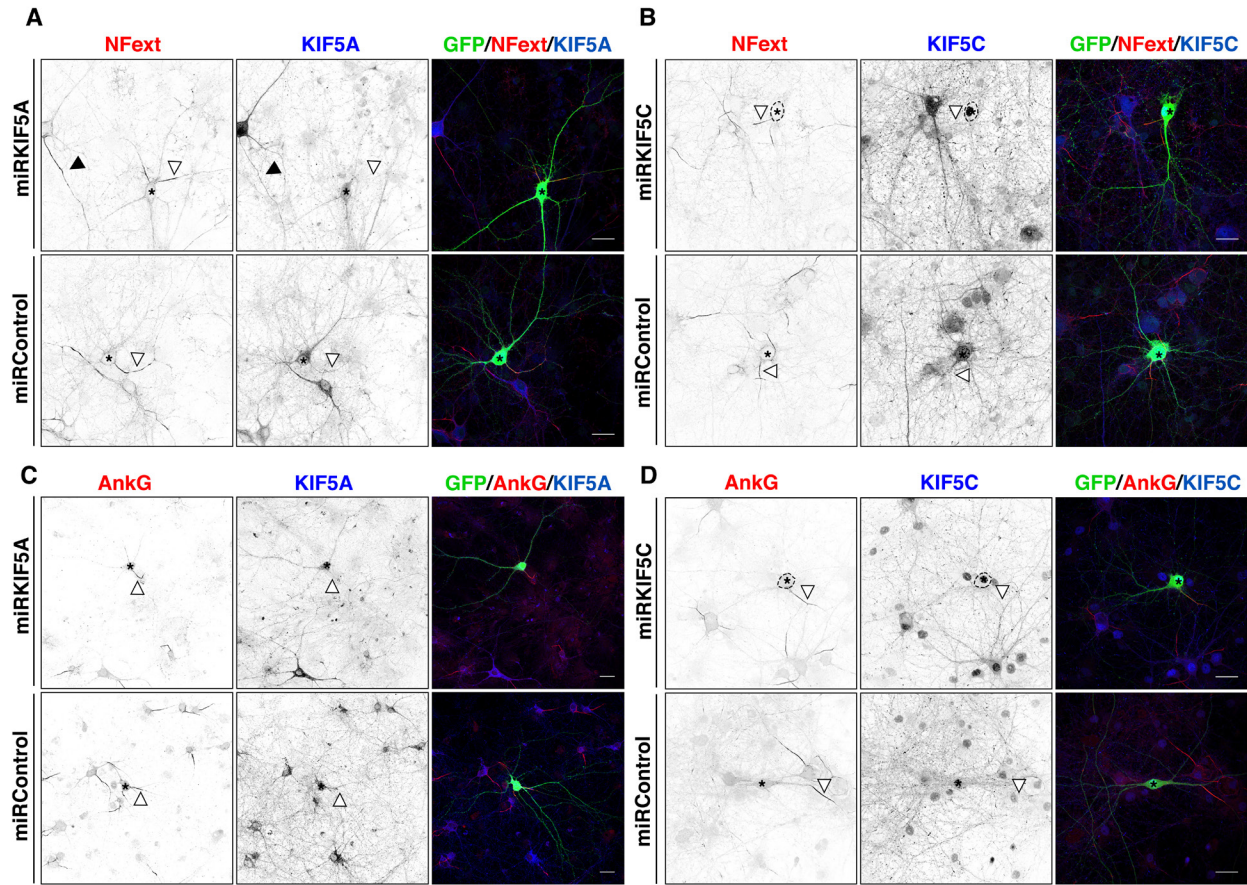


Figure 4: Knockdown of KIF5A and KIF5C in mixed hippocampal cultures at 17 DIV. **(A)** and **(C)** KIF5A (blue) immunolabeling is reduced (white arrowheads) in the axons of transfected KIF5A miRNA positive neurons (green) while non-transfected (black arrowheads) and neurons expressed with control miRNA have KIF5A immunolabeling in the axon (white arrowheads). Surface Nfasc (red, **A**) and ankyrinG (red, **C**) immunolabeling are not reduced at the AIS when KIF5A is silenced. **(B)** and **(D)** KIF5C immunolabeling (blue) is severely decreased in the neuronal cell body and in axons (white arrowheads) when exposed to KIF5C miRNA (green). Only nuclear KIF5C immunolabeling remains in the neuronal cell body (traced with broken black circle). Nfasc external and ankyrinG remain restricted to the AIS when hippocampal cultures are treated with KIF5C miRNA and control miRNA. Asterisks denote neuronal cell body. Scale bars = 25 μm.

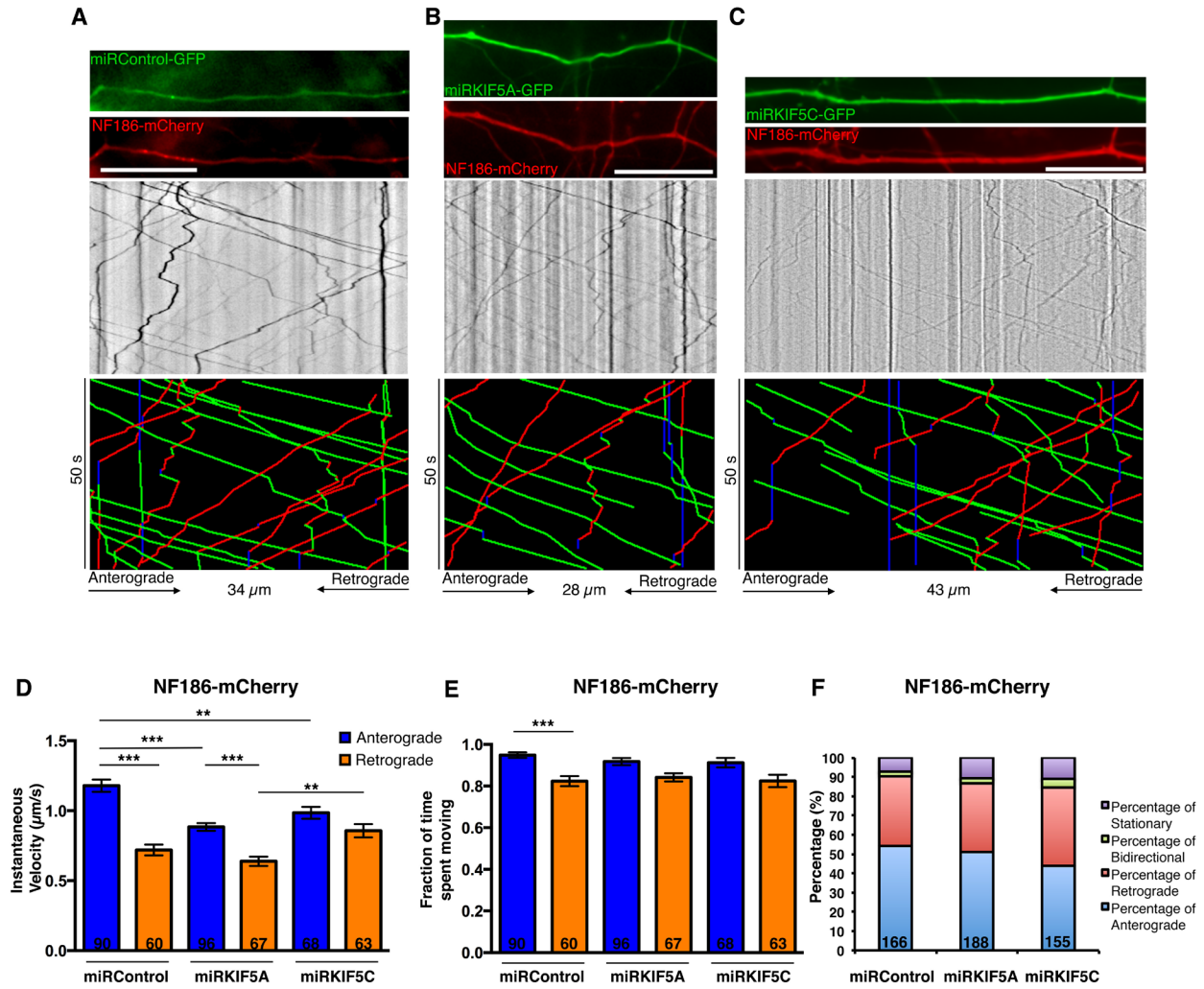


Figure 5: Suppression of KIF5A and KIF5C disrupt the trafficking of Nfasc186. **(A, B, C)** Mixed hippocampal cultures were cotransfected at 5-6 DIV with Nfasc186-mCherry with either control miRNA, KIF5A miRNA, or KIF5C miRNA, followed by two color live imaging at 17-18 DIV. **(D)** The continuous anterograde velocity of Nfasc186-mCherry vesicles is reduced in neurons transfected with KIF5A and KIF5C miRNA compared to controls. Continuous retrograde velocities are increased in axons expressing KIF5C miRNA compared to KIF5A miRNA. **(E)** Calculation of the fraction of time moving in cultures treated with control, KIF5A, and KIF5C miRNA. **(F)** Distribution of the types of movements analyzed in each condition. Of note, the proportion of retrograde moving vesicles is elevated in neurons treated with KIF5C miRNA. The number of vesicles analyzed is the bolded numbers included in the columns for each condition. The data shown for control miRNA include three independent experiments, two independent experiments for KIF5A miRNA, and two independent experiments for KIF5C miRNA. Data represent means \pm SEM. *, $p < 0.05$; **, $p < 0.01$; and ***, $p < 0.001$, one-way ANOVA with Tukey's post-test.

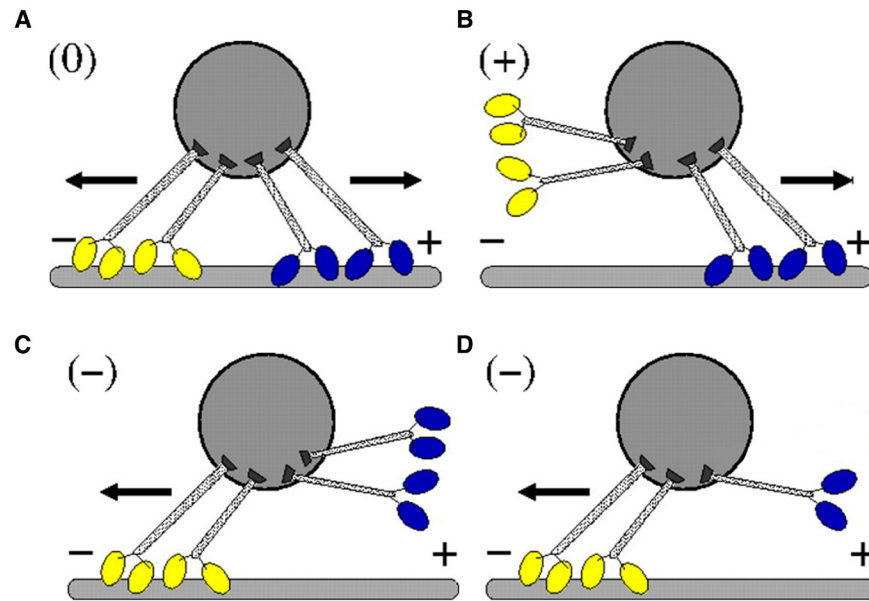


Figure 6: Kinesin and dynein tug-of-war model. **(A)** Both kinesin (blue) and dynein (yellow) microtubule motors are attached to vesicles. The net movement in both directions results may result in stalled movement (0; stationary) or stochastic bidirectional movement. **(B)** Fast-antegrade movement (+) can occur when dynein motors are not attached to the microtubules; **(C)** however, the contrary (-) may occur when dynein motors are attached to the microtubules and kinesins are not. **(D)** Suppressing kinesins motors through miRNAs lifts the antegrade inhibition of movement, which may allow for faster retrograde movement. Adapted from Müller *et al.*, 2008.

Part III: Discussion

Discussion

1.1 Prenodes form Along GABAergic Interneurons in the Absence of Myelination: Developmental Function and Beyond

The first aim of my dissertation was able to demonstrate that canonical nodes of Ranvier components assembled along the axons of hippocampal GABAergic interneurons in culture and *in vivo* in the absence of myelination and paranodal junction formation. We also showed that hippocampal glutamatergic neurons formed nodes of Ranvier concomitantly with myelination. However, Kaplan *et al.* (1997, 2001) reported Na_v clusters along RGC axons, which are glutamatergic in nature. What could underlie the differences observed in our culture system and the one in Kaplan *et al.* (1997, 2001)? The conclusion most likely does not reside in the culture system *per se* but rather the developmental functions of these two cell types in their respective CNS origins.

Some GABAergic, called early-generated interneurons because they are generated during early stages of neurogenesis, are well known to project long-range axons to several interregional areas and to other cortical regions during development (Jinno *et al.*, 2007; Picardo *et al.*, 2011; Melzer *et al.*, 2012). These neurons in particular, which can become myelinated (unpublished observations of Dr. Rosa Cossart), are somatostatin-releasing interneurons (Picardo *et al.*, 2011), similar to our reported observations in looking more closely at the interneuron subpopulations in our hippocampal culture system. These neurons are sparse in the hippocampus, but the role of these cells is to pioneer hippocampal circuits through synapse-driven network synchronizations during early-postnatal stages (Ben-Ari *et al.*, 1989; Garaschuk *et al.*, 1998; Bonifazi *et al.*, 2009; Picardo *et al.*, 2011). In a similar fashion, RGCs project their axons from the retina to the thalamus, pretectum, superior colliculus, and hypothalamus. Prenodal clusters along long-range projecting axons from these two cell types may underlie a developmental strategy for increasing action potential conduction prior to myelination, and thereby

allow these cells to drive network activity in their target regions. In going forward, it would be interesting to use the genetic-fate mapping approach used in the Picardo *et al.* (2011) study and perform immunohistochemical staining for nodal components along the axons of these early-generated interneurons.

While we have detailed that prenodes can form along GABAergic axons in the mouse hippocampus and in the mesencephalon *in vitro*, a number of studies have identified Na_v clusters on unmyelinated fibers in several other species, such as the marine invertebrate *Aplysia* (Johnston *et al.*, 1996) and in zebrafish mutants lacking Schwann cells in peripheral nerves (Voas *et al.*, 2009). Interestingly, in dystrophic mice lacking merosin, a laminin that is involved in Schwann cell migration and mitogenesis, Na_v channels cluster along large-diameter unmyelinated axons with a spacing of ~60 μ m (Deerinck *et al.*, 1997). Moreover, Na_v channels clusters have also been reported along unmyelinated axonal segments in non-pathological human dental pulp (Henry *et al.*, 2012). Taken together, these studies demonstrate that some Na_v clusters can be formed on unmyelinated axons and also maintained as stable structures without myelin.

1.2 Do prenodes determine where myelination takes place?

The fact that prenodes exist in evenly spaced clusters along axons destined to become myelinated could suggest that these domains are axonal determinants that drive the positioning of the myelin sheath. Indeed, by incubating mixed hippocampal cultures with the conjugated Nfasc-Alexa594 antibody (recognizes extracellular epitope), we have also observed through time-lapse imaging that these clusters remain quite stable over time (unpublished observations).

In this respect, we have created cocultures of mixed hippocampal cultures labeled with the Nfasc-Alexa594 antibody together with either FACS-sorted oligodendrocytes from *PLP-GFP* mice in order to examine through time-lapse imaging whether the stabilized clusters direct the myelination process. While we were able to observe many GFP⁺ oligodendrocytes and even robust myelination in these cultures, the time-lapse imaging proved to be quite difficult due to the

photobleaching of the GFP⁺ oligodendrocytes and the challenge of catching the critical time window of oligodendroglial myelination (Czopka *et al.*, 2013). Our experimental design proved to be too ambitious for the optical setup that we currently have, since we were only able to visualize one field of the entire culture, and thus reduced our opportunity of simultaneously visualizing multiple axons undergoing myelination. In spite of these technical issues, the feasibility of this particular experiment is quite high, and would therefore be quite useful in answering this fundamental question. However, a new optical system that reduces the amount of fluorescence, combined with a stage that can observe several fields over the course of the time-lapse study would be of great importance.

In conjunction with this question, another important secondary point raised is whether prenodes disappear or fuse to form mature nodes of Ranvier once myelination takes place. The former hypothesis is not supported by our study since we observed that the internodal distance between prenodal clusters, which was approximately 16 μm prior to myelination, doubled after myelination. The proposed experimental time-lapse microscopy setup could additionally address whether these clusters disappear or fuse together.

2.1 Prenodal Assembly Requires Extrinsic and Intrinsic Factors

The first aim of my dissertation was successfully able to show that both extrinsic and intrinsic factors are necessary in order to govern prenodal assembly in the CNS. Our results fit well within the currently accepted model that several compensation mechanisms are available to cluster CNS nodes of Ranvier and they do so cooperatively (Susuki *et al.*, 2013; Chang and Rasband, 2013). In our model system, paranodal junctions were not immediately formed, so prenodes assembled through the action of the cytoskeletal scaffolds and oligodendrocyte secreted proteins. Loss of the cytoskeletal protein ankyrinG resulted in the abolishment of prenodal clusters, since the oligodendrocyte secreted proteins were insufficient to assemble prenodes in the absence of the paranodal junctions. Similarly, compensation by ankyrinG was insufficient in order to rescue prenodes on neurons

when glial cells were eliminated, thereby losing both paranodal junctions and oligodendrocyte secreted proteins. Together, these results highlight the remarkable complexity necessary to assemble the CNS nodes of Ranvier.

2.1.1 What is the Nature of the Oligodendrocyte Secreted Factor(s)

Similar to Kaplan *et al.*, (1997, 2001), our work confirms that there are proteinaceous oligodendroglial secreted factors able to cluster prenodes along the axons of hippocampal GABAergic interneurons. At present, the factor(s) present in OCM that permits clustering remains to be described. What is clear in our system is that the OCM factor is not gliomedin. However, when incubating purified neuronal cultures with a soluble Fc-fusion protein containing the olfactomedin domain of gliomedin, we were able to observe robust prenodal clustering in GABAergic, and to a lesser extent in glutamatergic neurons (unpublished observations). Since gliomedin is only expressed in the cilia of ependymal cells in the CNS (unpublished observations), we investigated proteins of the olfactomedin family, which share the extracellular olfactomedin domain with gliomedin, and are expressed in several regions of the CNS and also in oligodendrocytes (Cahoy *et al.*, 2007; Anholt *et al.*, 2014). We performed immunocytochemical experiments to see if olfactomedins were present at prenodes; however, no clear results have been yielded from these studies.

It has been speculated that the cluster-inducing factor could be an ECM molecule, since ECM molecules are secreted by oligodendrocytes and can bind Nfasc186 (Bartsch *et al.*, 1993; Hedstrom *et al.*, 2007; Suzuki *et al.*, 2013). These ECM molecules may then be incorporated in perineuronal nets, which surround the neuronal somata, proximal dendrites and at times the AIS, primarily in hippocampal parvalbumin-positive interneurons (Kwok *et al.*, 2011), a second interneuron subpopulation that we found to majorly have prenodes. These nets contain high amounts of hyaluronan and chondroitin sulfate proteoglycans such as tenascin-R, versican, brevican, neurocan and aggrecan, which have been observed to be localized at the AIS and nodes of Ranvier in the CNS (Weber *et al.*, 1999; Bekku *et al.*, 2009; Suzuki *et al.*, 2013). Whether these various proteins, known to be

enriched at the CNS nodes, are present in OCM and participate in the induction of prenodal assembly remains to be seen.

In this context, looking back at the molecular weight cutoffs of clustering activity observed in the Kaplan *et al.* (2001) study and comparing the sizes of the known ECM molecules enriched at CNS nodes of Ranvier, only the small cleaved forms of Brevican and Bral1 would fit their reported 30- to 50-kDa size range. As previously mentioned, Brevican-Fcs induce node-like clusters of HA-Nfasc186 along DRG cultures, which in turn recruit ankyrinG (Susuki *et al.*, 2013)—and furthermore, loss of Bral1 completely disassembles the adult nodal ECM (Susuki *et al.*, 2013). Therefore, in culture, these two molecules could act in concert to induce node-like clusters in the CNS, wherein Brevican first triggers clustering of nodal components followed by its stabilization through Bral1. It would be of great interest to determine the expression profile of these molecules overtime in mixed hippocampal culture and determine if these molecules are present in OCM.

2.1.2 The Action of the Oligodendrocyte Secreted Factor(s)

Our published study presents a number of important findings in relation to the action of OCM; however, it is unclear whether OCM increases synthesis of intrinsic clustering components, such as ankyrinG, or interacts with the extracellular region of a(n) (un)known axonal protein. In regards to the latter, in both mixed hippocampal cultures and purified hippocampal neuronal cultures treated with OCM from *Nfasc*-null mice we observed robust clustering of nodal components along the axons of GABAergic interneurons. This suggests that neurofascins are not entirely responsible for clustering prenodes along GABAergic hippocampal axons, as opposed to their highly important role in assembling and maintaining PNS and CNS nodes of Ranvier (Sherman *et al.* 2005; Zonta *et al.*, 2008; Thaxton *et al.*, 2011; Zhang *et al.*, 2015; Desmazières *et al.*, 2014). Interestingly, we also observed robust prenodal immunolocalization of NrCAM in wild-type mixed hippocampal cultures, and in mixed hippocampal neuronal cultures and purified hippocampal neuronal cultures treated with OCM from *Nfasc*^{-/-} mice

(unpublished observations). However, *NrCAM*-null mice also have normal prenodal clustering (unpublished observations), and NrCAM at CNS nodes of Ranvier is reported to be secreted rather than in its full transmembrane form (Zonta *et al.*, 2008; Susuki *et al.*, 2013). In our case, it has yet to be determined whether NrCAM is expressed in its transmembrane form in hippocampal cultures from *Nfasc*^{-/-} mice, an important fact that should be examined, since a transmembrane isoform of NrCAM may be able to interact with the OCM secreted factor and recruit the nodal components. What we may be observing is redundancy in the single knockouts, and it would be worthwhile to examine prenodal clustering in mixed hippocampal cultures and purified neuronal cultures treated with OCM from *Nfasc*^{-/-};*NrCAM*^{-/-} mice.

In light of our results, we cannot preclude the role of other axonal molecules with Ig domains. Contactin could be a possible ligand for OCM since it is also expressed at the nodes of Ranvier in the CNS (Rios *et al.* 2000; Kazarinova-Noyes *et al.*, 2001; Çolakoğlu *et al.*, 2014). In this respect, we tried to analyze the expression of contactin through immunocytochemistry, but the immunolabeling was without success (unpublished observations). Determining if contactin is located at prenodal clusters is a pertinent question that should be addressed by immunocytochemistry with different antibodies or various fixation methods (Çolakoğlu *et al.*, 2014) and by preparing mixed hippocampal cultures from *Contactin*-null mice. Additionally, $\beta 1$ -Na_v could also be a potential partner for OCM. In contrast to Kaplan *et al.* (2001), we observed that $\beta 1$ -Na_v prenodal clustering prior to myelination (results section II). Therefore, it could be possible that OCM interacts with this protein, and then is able to interact and possibly recruit ankyrinG (Malhotra *et al.*, 2004). Here, mixed hippocampal cultures from *SCN1B*^{-/-} mice would help answer determine the role of $\beta 1$ -Na_v in prenodal clustering.

Kaplan *et al.* (2001) observed that the clustering of nodal components along RGC axons was rapid and in the order of a few days, and therefore it could be possible that OCM may act the level of the nucleus to increase the transcription of nodal components, which then cluster based on intrinsic mechanisms. In our hands,

the action of OCM was not rapid and took more than a week and a half to permit the clustering of prenodes. To investigate this question, it would be interesting to analyze the transcription status of several nodal components in hippocampal neurons freshly incubated with OCM by qRT-PCR. Furthermore, it could also be interesting to utilize microfluidic chambers, which have the neuronal cell bodies and axons in separate compartments, and incubate the neuronal cell body chamber with OCM to see if it acts at locally on the soma.

2.2 The Role of AnkyrinG

These results may also suggest that certain mechanisms could be more influential than others in clustering CNS nodes of Ranvier, especially regarding the cytoskeletal scaffolding proteins. For example, loss of giant ankyrinG results in significant alterations in CNS nodal clustering (Jenkins *et al.*, 2015). In our case, the loss of ankyrinG was highly disruptive, which could be related to disruption in the transport of nodal molecules since they can interact with ankyrinG (Dzhashiashvili *et al.*, 2007; Barry *et al.*, 2014) or the loss of neuronal polarity (Hedstrom *et al.*, 2008). However, in our experimental setup, we did not observe a loss in neuronal polarity when knocking down ankyrinG through miRNA. This would suggest that nodal molecules traffic properly down the axon but may have been unable to properly restrict because of ankyrinG loss, or loss of ankyrinG could be implicated in their trafficking through associations (Dzhashiashvili *et al.*, 2007; Barry *et al.*, 2014). The next crucial step is to understand the trafficking of various nodal proteins and their interactions with ankyrinG. The continual work in the second aim of this dissertation, which looks to understand nodal trafficking dynamics, will help shed light on further interactions of ankyrinG in regards to CNS nodes of Ranvier assembly.

Nevertheless, our results are in contrast with a recent report that ankyrinR rescues nodes of Ranvier in both the PNS and CNS in the loss of ankyrinG (Ho *et al.*, 2014). While we did observe AnkyrinR⁺ prenodes in mixed hippocampal cultures (unpublished observations), no further analysis was performed, such as ankyrinR

immunolabeling after ankyrinG knockdown, to fully understand the role of this protein in prenodal assembly. As we observed nearly a complete disruption of prenodal assembly when ankyrinG levels are reduced, it is unclear as to why we did not observe a similar rescue in our system. This may point to a weak interaction with the axonal clustering molecule with ankyrinR, similar to what Ho *et al.* (2014) observed with ankyrinR's weaker interaction with Nfasc186 compared with ankyrinG. Further studies should be performed in our system to assess the contribution of ankyrinR to prenodal assembly and the status of ankyrinR when ankyrinG is reduced.

Another unique observation detailed in our study was that the spacing of around 16 μm between the prenodal clusters was regular, which may suggest a type of axonal patterning. Work by Xu *et al.* (2013) using stochastic optical reconstruction microscopy reported that actin formed in evenly spaced ring-like structures with a periodicity of nearly 190 nm in the axons of hippocampal neurons, and that spectrins and ankyrinG becomes incorporated into the lattice (Zhong *et al.*, 2014). In the case of prenodes, it would be interesting to look at the actin/spectrin/ankyrin lattice structure through similar types of ultra-resolution imaging to understand what may underlie the periodicity of prenodes.

2.3 The Transition of Ion Channels at Prenodes

One intriguing result that we were able to show, contrary to several published reports (Kaplan *et al.*, 2001; Boiko *et al.*, 2001), was that $\text{Na}_v1.6$ clustered in prenodes in the absence of myelination. Interestingly, clustering of this Na_v isoform at prenodes could not be mimicked in purified neuronal cultures when treated with OCM, but could nevertheless cluster at the AIS. This latter result suggests that, in contrast to Gasser *et al.* (2012), ankyrinG is not the only means by which $\text{Na}_v1.6$ is targeted to nodes of Ranvier. Several different mechanisms could be at play in order to facilitate the switch from $\text{Na}_v1.2$ to $\text{Na}_v1.6$, which give rise to a number of experimental avenues to take in order to decipher the mechanism behind this transition.

The fact that $\text{Na}_v1.6$ could target normally to the AIS and not to prenodes further highlights the fact that assembly of prenodes and nodes of Ranvier require neuron-glia interactions (Chang and Rasband, 2013). As such, an important indirect finding is that the physical presence of glial cells is necessary in order to cluster $\text{Na}_v1.6$ at prenodes prior to myelination. We did observe oligodendroglial contact along axons by immunocytochemistry (Freeman *et al.*, 2015) and by time-lapse imaging visualized through CNPase cultures (unpublished observations), but what could be a potential hypothesis as why oligodendroglial contact could mediate clustering of $\text{Na}_v1.6$ to prenodes? One potential hypothesis could be related to the expression of β -subunits by oligodendrocytes (thesis Dr. Heather O'Malley, 2010), especially $\beta1\text{Na}_v$, which is reported to be associated with $\text{Na}_v1.6$ (Kaplan *et al.*, 2001). Both OPCs and mature oligodendrocytes express $\beta1\text{Na}_v$, and in mature oligodendrocytes this expression is strongly increased in the major processes (thesis Dr. Heather O'Malley, 2010). It is tempting to speculate that increased expression of $\beta1\text{Na}_v$ along mature oligodendrocyte processes may participate in non-covalent interactions with diffuse $\text{Na}_v1.6$ and permit clustering at prenodal clusters at late time points (see below). Further studies should be undertaken to explore the role of oligodendroglial contact in relation to this transition from $\text{Na}_v1.2$ to $\text{Na}_v1.6$.

With this being said, we cannot rule out the possibility that other glial cells in our culture system may be implicated in clustering $\text{Na}_v1.6$. In order to test the varying roles of the physical presence of glial cells, it would be interesting to coculture neurons with either purified oligodendrocytes, astrocytes, or microglia and perform immunocytochemical analysis to see which glial cell may contribute to the clustering of $\text{Na}_v1.6$. Additionally, it is unclear whether the presence of these glial cells contributes to the local synthesis of $\text{Na}_v1.6$ or the clustering of the ion channel on the axonal surface. Quantitative PCR could be utilized in conjunction to examine $\text{Na}_v1.6$ transcription levels and supplement the analysis.

The presence of $\text{Na}_v1.6$ at prenodal clusters was a late rather than early event compared to the clustering of $\text{Na}_v1.1$ and $\text{Na}_v1.2$, which would correlate with other studies that $\text{Na}_v1.6$ targets to a mature node of Ranvier (Kaplan *et al.*, 2001;

Boiko *et al.*, 2001). This could point to several important changes in our culture system such as neuronal and glial (in particular oligodendroglial) maturation. Later time points in culture corresponded to phosphorylated neurofilaments along axons, a hallmark of neuronal maturation. Therefore, it would be interesting to see if inducing neurofilament phosphorylation could upregulate the expression of $\text{Na}_v1.6$ at prenodal clusters, or similarly by adding purified mature oligodendrocytes to purified or mixed cultures to see if there would be an increase in $\text{Na}_v1.6$ clustering.

Furthermore, the clustering of $\text{Na}_v1.6$ was rather peculiar in that clusters were not found ectopically along the distal axon but rather clustered to the proximal axon. This would suggest that the insertion of $\text{Na}_v1.6$ to prenodal clusters follows a specific ordering. It is well established that $\text{Na}_v1.6$ is restricted to the distal compartment of the AIS (Van Wart *et al.*, 2007; Hu *et al.*, 2009), so our observation that $\text{Na}_v1.6$ initially clusters to the proximal regions of the axon past the AIS could represent lateral diffusion of $\text{Na}_v1.6$ molecules to prenodes in the proximal axon from the distal AIS, or it could suggest that the density of $\text{Na}_v1.6$ is surpassed at the distal AIS and then the targeting of newly synthesized $\text{Na}_v1.6$ is restricted to the first prenodes. Recently, a new full length $\text{Na}_v1.6$ construct with a biotinylated extracellular domain has been developed that shows restrictive targeting to the AIS and normal Na^+ currents (Akin *et al.*, 2015). In our case, it would be worthwhile to utilize this construct and assess by time-lapse imaging the clustering of $\text{Na}_v1.6$ to prenodal clusters in mixed hippocampal cultures.

In chapter II of the results section, we were also able to observe the clustering of $\beta1$ - and $\beta2$ - Na_v colocalizing with Pan- Na_v in the absence of myelination and on GABAergic interneurons *in vitro*. It has been suggested that $\beta2$ - Na_v is first clustered at node-like clusters along unmyelinated regions, and upon myelination there is a transition to $\beta1$ - Na_v (Kaplan *et al.*, 2001). However, in our condition we were able to observe both isoforms in prenodes at time points when axons are unmyelinated. These auxiliary β -subunits play critical roles in modulating the expression, targeting, and regulation in the rate of α -subunit activation and inactivation (Patton *et al.*, 1994; Kazen-Gillespie *et al.*, 2000; Chen *et al.*, 2002;

Schmidt and Catterall, 2002), and therefore may be implicated in the transition of Na_v α -subunits, as mentioned above. A potential study in our culture system would be to determine the association of these β -subunits with the corresponding α -subunits to see if there is a link between the transition of α - and β -subunits in prenodes.

3.1 The Roles of Prenodes in Action Potential Conduction

3.1.1 Correcting The Value of Action Potential Conduction

Based on the electrophysiological studies performed during the first aim of my dissertation, we confirm that prenodes along GABAergic interneurons can increase action potential conduction (approximately by 1.5x) in the absence of myelination and independent of the axonal diameter. Interestingly, when comparing our conduction values with the speeds of action potential conduction along myelinated axons in the literature, these values are quite similar (Palmer and Stuart, 2006; Kress and Mennerick, 2009). One important point to address is that the values reported in our study may in fact be lower than the true value since conduction velocities were calculated by taking the distance between the recording pipettes at the soma and the axon over the latency values calculated by comparing the mean peak amplitude of the spike in both recordings. As it is widely accepted that the action potential is initiated at the AIS (Palmer and Stuart, 2006; Khaliq and Raman, 2006; Meeks and Mennerick, 2007; Shu *et al.*, 2007; Hu *et al.*, 2009; Popovic *et al.*, 2011) or at distances past the AIS such as the first node of Ranvier (Zecevic, 1996; Clark *et al.*, 2005;), the backpropagation to the somatic pipette presents a small latency lag that was unaccounted for in our study. Furthermore, recording antidromic APs at the soma takes into account both axonal and somatic sodium channels, which are not recruited synchronously into the somatic AP signal (Meeks and Mennerick, 2007).

In relation to our study, two different types of experiments may overcome this bias. The first would be to determine a normalized action potential initiation site in GABAergic axons with and without prenodes and use this value as a

“distance correction”. The normalized action potential initiation site in both conditions would be determined by performing soma-axon recordings and comparing the second derivative (dV^2/dt^2) of the whole-cell somatic AP waveform to the first derivative (dV/dt) of the extracellular-recorded axonal AP waveform. The second derivative of the somatic recording yields the acceleration of the membrane voltage and can detail the separated recruitment of axonal and somatic channels (Khaliq and Raman, 2006; Meeks and Mennerick, 2007). Here, the first component (or first peak) of this waveform will correspond to contribution of the axonal component, while the second peak will correspond to the recruitment of the somatic sodium channels. The first derivative of the extracellular-recorded axonal AP waveform will also yield the acceleration of the membrane voltage since the extracellular axonal recording is already the first derivative of the intracellular voltage recording (Meeks *et al.*, 2005). By recording sites $<100\text{ }\mu\text{m}$ past the axon hillock along the axon and finding when the first peak of the whole-cell somatic dV^2/dt^2 (axonal component) recording aligns with the maximal acceleration of the axonal recording (largest peak of the axonal recording), we would be able to determine a normalized region along the AIS that initiates in the AP in both conditions. Using this value, we could then perform a “distance correction” in determining AP conduction. For example, if the calculated distance between a somatic and axonal recording pipette is $300\text{ }\mu\text{m}$ and the normalized AP initiation zone is $25\text{ }\mu\text{m}$ past the axon hillock, the corrected distance value used in the numerator for conduction velocity measurement would instead be $275\text{ }\mu\text{m}$.

A second, and more technically challenging, experiment would be to perform simultaneous axon-axon recordings $>150\text{ }\mu\text{m}$ past the axon hillock with a similar separated distance between the two recording electrodes. This would eliminate the contributions of the somatic sodium channels and this recording would only take into account orthodromic conduction. While this experiment was tried and would have been the ideal, two significant challenges emerged when trying to patch two distant regions along the axon. Axonal recordings are sensitive to slight movements and noise from other neurites encompassing the desired recording region, which

therefore cannot be used for further analysis (see below). Additionally, axons with prenodes exhibit elaborate branching. Because AP propagation can be reduced at axonal branch points (Debanne *et al.*, 2011), this highly complex axonal arborization could present delays in axonal conduction when patching along a daughter branch, and may not be a reliable method to compare overall AP conduction velocities. While we speculate that prenodes may help these neurons to overcome branchpoint failures, we cannot preclude that the propagation of the AP from the parent branch will be at the same speed as in the daughter branch.

3.1.2 Would Conduction Speed Increase When Myelination Occurs and Do Prenodes Permit Saltatory Conduction?

As previously mentioned, our mixed hippocampal culture system provides an excellent model system in order to understand the contributions of nodal clusters in the absence of myelination. However, two clear questions arise from this work: 1) What would happen to conduction velocity once myelination occurs? 2) Do prenodes allow for saltatory or micro-saltatory conduction to occur?

To answer the first question experimentally using our dual soma-axon cell attached patch clamp technique would be quite daunting. In our culture system, neurites are quite abundant at later time points *in vitro*, and time and high cellular density allows for prenodal clustering and myelination to occur. With our setup, it would therefore be quite difficult to obtain a clean recording without noise from other axons in the axonal recording pipette. A further challenge presents itself when determining what to patch for the axonal electrode. The myelin segment is not electrically active, and therefore this would necessitate the axonal electrode be placed at a node of Ranvier that has the size of $\sim 2 \mu\text{m}$.

There are several ways to possibly get around these technical issues. One would be to use computational modeling of our experimental system in order to determine the contribution of a myelinating sheath. In order to do this, we would need to determine several essential parameters from our experimental setup, such as the mean axonal diameter, mean number of myelin wrappings, mean sodium

channel density at one prenodel, and the mean amount of myelin segments. The latter of these is quite significant considering that myelination is somewhat patchy in our system. Another possible way to answer this question would be use an experimental setup with voltage-sensitive dyes. Several studies have successfully employed the use of these dyes in slice culture (Zecevic, 1996; Palmer and Stuart, 2006; Kress *et al.* 2007). In our condition, the potential setup would be a marker for the prenodel clusters (conjugated Nfasc-Alex594) combined with the voltage-sensitive dye and acquisition in fluorescence changes through rapid-acquisition microscopy. For the myelinated neurons, it would be necessary to determine which neurons were myelinated, which can be observed through differential interference contrast or through a myelin stain such as fluoromyelin.

Considering the short interval between the prenodel clusters there is a possibility that they may conduct in a saltatory manner. Waxman *et al.* (1989) postulated that the short intervals seen in their study could play a potential role in “micro-saltatory” conduction. Similarly, the theoretical work from Neishabouri and Faisal (2014) may also suggest that the prenodels permit micro-saltatory conduction. Therefore, to test whether prenodels are able to conduct in a saltatory manner, we could similarly use computational modeling and voltage-sensitive dyes. Computational modeling experiments have already been performed regarding clusters of sodium channels along unmyelinated axons (Zeng and Tang, 2009), yet modeling of our setup could also be informative since we have a well described experimental paradigm to which we can base the modeling parameters. Voltage-sensitive dye recordings in this setup would be similar to that described in the previous paragraph.

In looking at these two questions from a theoretical standpoint, it is tempting to speculate that precocious myelination at first may not actually be faster than prenodel clusters. This hypothesis is based on the theoretical work by Young *et al.*, (2013), which showed that the transition from continuous to saltatory conduction results in a decrease in conduction velocity. Once myelin compaction occurs, however, conduction velocity along the myelinated segment would most likely be

faster than prenodal clusters. Experiments using computational modeling and voltage-sensitive dyes would help resolve some of these interesting fundamental questions relating to action potential conduction.

3.1.3 Prenodes in the pathological state

It is also important to look at not only the potential physiological benefits of prenodes, but also the detriments of prenodes in the diseased state. Several reports combining experimental demyelinating animal models and electrophysiology have detailed that ectopic spiking from axons (action potentials generated outside of the AIS) may lead to hyperexcitability, which, in taking into account clinical demyelinating diseases such as MS, may ultimately manifest as cognitive impairment (Felts *et al.*, 1995; Kapoor *et al.*, 1997; Hamada and Kole, 2015). Interestingly, in our electrophysiological axonal recordings, we occasionally observed the generation of ectopic spikes (unpublished observations). Ectopic spike generation in our case, similar to the demyelinating animal models, may be related to the persistent current driven by $\text{Na}_v1.6$ or the low-threshold voltage and rapid recovery of inactivation from this channel (Herzog *et al.*, 2003; Catterall *et al.*, 2005). $\text{Na}_v1.6$ begins to be expressed at the latest time points of our electrophysiological recordings, which may point to the rarity of the occasional ectopic spiking observed. However, the presence of ectopic spiking could also point to another possibility that prenodes may lack dense clusters of known nodal K_v channels ($\text{K}_v3.1b$, $\text{K}_v7.2$, and $\text{K}_v7.3$; Trimmer *et al.*, 2015) that can regulate and dampen AP firing and alter AP conduction (Schwarz *et al.*, 2006; Battefeld *et al.*, 2014). Hence, if similar prenodes reported in our study were observed in demyelinating conditions, it is possible that they could present a potential negative impact along demyelinated axons due to aberrant spike generation.

Another point worth discussing is the potential metabolic cost and benefit of prenodes in healthy and demyelinated axons. Myelination of axons reduces the capacitance of the axonal membrane, which results in fewer Na^+ needed to depolarize the axonal membrane. This in turn reduces the amount of ATP used in

order to drive the Na^+/K^+ -ATPase (Arancibia-Carcamo and Attwell, 2014). However, during demyelination, Na_v is diffusely redistributed along the denuded axon, and action potentials that were once propagated by saltatory conduction will now be propagated in a continuous manner (Waxman, 2006). This type of conduction is hypothesized to result in an increased demand for ATP in order to pump out the increased Na^+ in axons by the Na^+/K^+ -ATPase (Waxman, 2006). A number of studies have reported that mitochondrial volume increases along demyelinated axons in postmortem tissue and in experimentally demyelinated axons in mice (Mahad *et al.*, 2009; Witte *et al.*, 2009; Ohno *et al.*, 2014). Since mitochondria are a major source of axonal ATP production, these results suggest that during demyelination there is an increased energy demand that is met by the increased volume of mitochondria in the demyelinated region. Therefore, continuous distributions of Na_v along the denuded axon are metabolically costly; however, in the case of prenodes, would there be a large metabolic cost of Na_v clustering without myelin or would these clusters be energy efficient and present a potential benefit to the demyelinated axon? Recent theoretical studies would suggest that, along unmyelinated axons, Na_v clusters are more energy efficient than a uniform distribution of Na_v channels (Neishabouri *et al.*, 2012). In performing simulations of thin unmyelinated axons with clustered Na_v in lipid rafts and those with a homogenous density of sodium channels, Neishabouri *et al.* (2012) observed that action potential regeneration was nearly three times more metabolically efficient when channels were clustered. In taking the case of prenodes, which are large aggregates of Na_v without myelin, we could speculate there might be similar metabolic savings. In order to investigate this question experimentally it would be useful to measure energy consumption of axons with prenodes through fluorescent biosensors such as Perceval, which is able to sense changes in the ratio of ATP:ADP in neurons and has been described in several studies (Berg *et al.*, 2009; Zala *et al.*, 2013; Tantama *et al.*, 2013). Furthermore it would be interesting to compare the volume and localization of mitochondria along axons with prenodal clusters and those without. These studies would help shed light on the potential metabolic savings of prenodal clusters and the localization of

mitochondria along axons with prenodes, which in turn may be highly relevant to demyelinating pathology.

Looking at another potential benefit of prenodes in demyelinating disease, it is possible that their presence along axons could serve favorable purpose in terms of remyelination and conduction. Indeed, Coman *et al.* (2006) reported the presence of Na_v aggregates in the regions undergoing remyelination in post-mortem MS tissue. As mentioned in chapter 1.3 of the discussion, if prenodes are able to dictate potential regions of myelination, they could ideally be of benefit in restoring fast conduction through the remyelination process. Furthermore, continued electrical activity along axons with prenodes may permit myelination along denuded axons, since it has been described that electrical activity is able to stimulate myelin induction (Wake *et al.*, 2011; Mensch *et al.*, 2015). In terms of conduction in the demyelinated axon, since the safety factor along demyelinated regions is near 1 (values lower than one would mean conduction failure) and the smallest changes could result in conduction block (Smith, 1994), these clusters could play a potential role in restoring action potential conduction and increasing the safety factor to a more favorable level. Therefore, prenodes could serve a dual purpose in governing where myelination takes place through continued electrical activity and also through restoration of faithful axonal conduction.

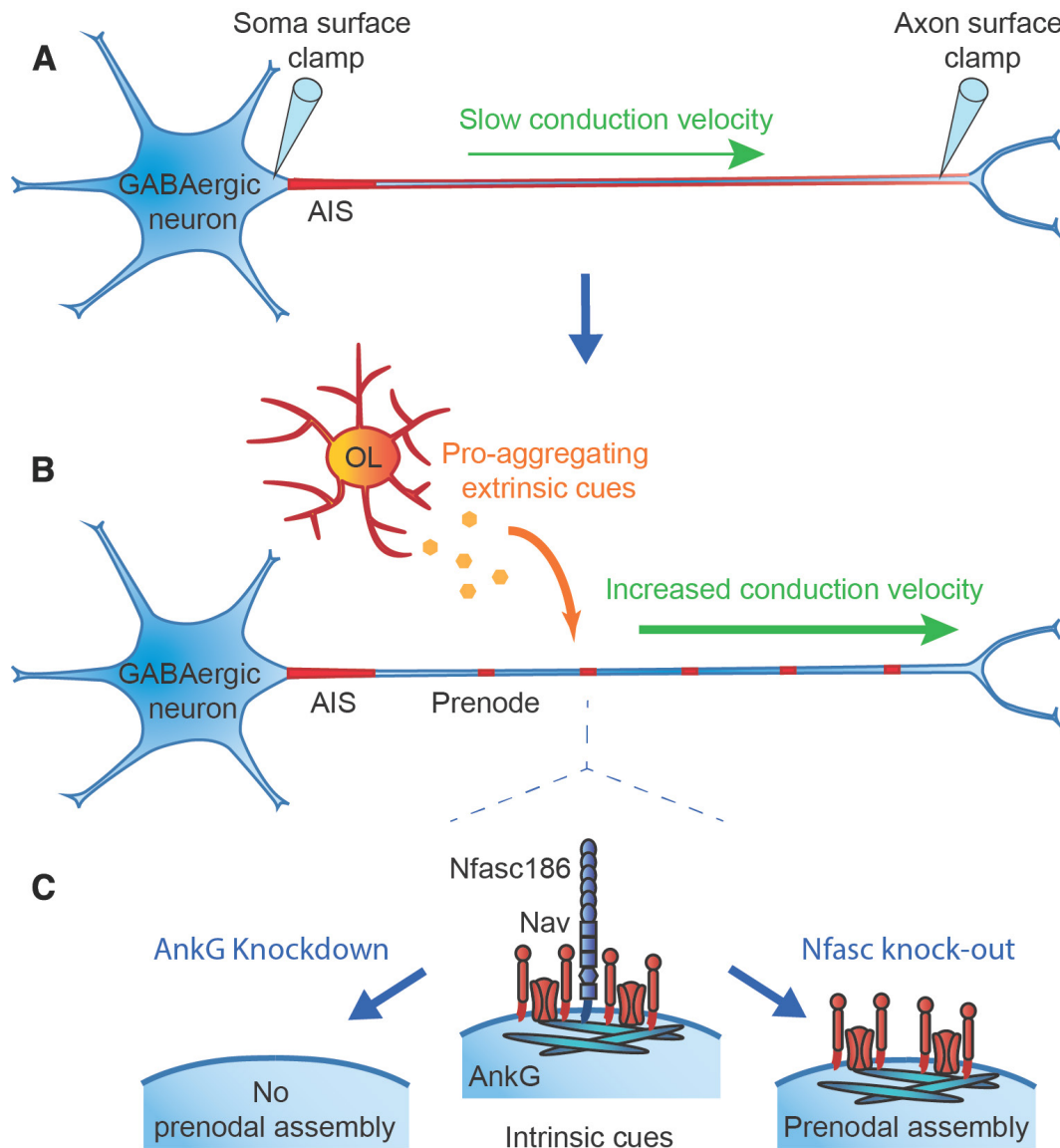


Figure 35: Summary of the assembly mechanisms governing prenodel formation and the functional role of nodal clusters prior to myelination. **(A)** Action potential conduction along GABAergic axons without myelin or nodal aggregates is slow; however, **(B)** formation of prenodels through pro-aggregating extrinsic cues from oligodendroglia can increase action potential propagation by 1.5x prior to myelination. **(C)** While neurofascin is not necessary for prenodel formation, ankyrinG is a required intrinsic cue for prenodel assembly.

Conclusion

The clustering of voltage-gated sodium channels at the nodes of Ranvier is an important developmental step for neuronal excitability by permitting rapid saltatory conduction along myelinated axons. In the central nervous system, several complementary neuron-glia mechanisms exist in order to assemble nodes of Ranvier, which suggests a remarkable level of redundancy in their assembly and highlights the overall importance of forming and maintaining these structures in the CNS. Unraveling the assembly mechanisms central to their formation will not only help us understand nervous system development, but also changes during demyelinating pathology.

In light of these facts, the work presented in this dissertation highlights that oligodendroglial and neuronal factors are necessary in order to form clusters of nodal proteins, called prenodes, along GABAergic axons prior to myelination and paranodal junction formation. Importantly, our results also shed light on a tertiary mechanism by which action potential conduction can be increased along axons through the clustering of voltage-gated sodium channels in the absence of myelination and independently of axon caliber. The next defining step is to further determine how nodal proteins are transported and sequestered at prenodal membrane through the action of microtubule motors and intrinsic neuronal mechanisms, respectively.

Taken together, our results reinforce the current model that CNS nodal clustering requires neuron-glia interactions, and our results also pave the way toward answering previous theoretical questions regarding neuronal excitability and conduction. Tackling these challenging questions experimentally will help us further understand the fundamental aspects of neuronal action potential propagation, and will hopefully allow us to explore further strategic therapeutic avenues in order to restore fast conduction in the diseased state.

References

- Abbott, B.C., Howarth, J.V., and Ritchie, J.M. (1965). The initial heat production associated with the nerve impulse in crustacean and mammalian non-myelinated nerve fibres. *The Journal of Physiology* *178*, 368–383.
- Aggarwal, S., Yurlova, L., and Simons, M. (2011). Central nervous system myelin: structure, synthesis and assembly. *Trends in Cell Biology* *21*, 585–593.
- Akin, E.J., Solé, L., Dib-Hajj, S.D., Waxman, S.G., and Tamkun, M.M. (2015). Preferential Targeting of Nav1.6 Voltage-Gated Na⁺ Channels to the Axon Initial Segment during Development. *PLOS ONE* *10*, e0124397.
- Aman, T.K., Grieco-Calub, T.M., Chen, C., Rusconi, R., Slat, E.A., Isom, L.L., and Raman, I.M. (2009). Regulation of Persistent Na Current by Interactions between Subunits of Voltage-Gated Na Channels. *The Journal of Neuroscience* *29*, 2027–2042.
- Andersen, P., Soleng, A.F., and Raastad, M. (2000). The hippocampal lamella hypothesis revisited. *Brain Research* *886*, 165–171.
- Ango, F., Di Cristo, G., Higashiyama, H., Bennett, V., Wu, P., and Huang, Z.J. (2004). Ankyrin-based subcellular gradient of neurofascin, an immunoglobulin family protein, directs GABAergic innervation at purkinje axon initial segment. *Cell* *119*, 257–272.
- Anholt, R.R.H. (2014). Olfactomedin proteins: central players in development and disease. *Frontiers in Cell and Developmental Biology* *2*.
- Arancibia-Carcamo, I.L., and Attwell, D. (2014). The node of Ranvier in CNS pathology. *Acta Neuropathologica* *128*, 161–175.
- Babbs, C.F., and Shi, R. (2013). Subtle Paranodal Injury Slows Impulse Conduction in a Mathematical Model of Myelinated Axons. *PLoS ONE* *8*, e67767.
- Baines, A.J., Lu, H.-C., and Bennett, P.M. (2014). The Protein 4.1 family: Hub proteins in animals for organizing membrane proteins. *Biochimica et Biophysica Acta (BBA) - Biomembranes* *1838*, 605–619.
- Bansal, R., and Pfeiffer, S.E. (1989). Reversible inhibition of oligodendrocyte progenitor differentiation by a monoclonal antibody against surface galactolipids. *Proceedings of the National Academy of Sciences* *86*, 6181–6185.
- Bansal, R., Gard, A.L., and Pfeiffer, S.E. (1988). Stimulation of Oligodendrocyte

- Differentiation in Culture by Growth in the Presence of a Monoclonal Antibody to Sulfated Glycolipid. *The Journal of Neuroscience Research* *21*, 260–267.
- Barbara, J.-G. (2007). Louis Ranvier (1835–1922): the contribution of microscopy to physiology and the renewal of French general anatomy. *Journal of the History of the Neurosciences* *16*, 413–431.
- Barres, B.A., Hart, I.K., Coles, H.S.R., Burne, J.F., Voyvodic, J.T., Richardson, W.D., and Raff, M.C. (1992). Cell Death and Control of Cell Survival in the Oligodendrocyte Lineage. *Cell* *70*, 31–46.
- Barres, B.A., Schmid, R., Sendtner, M., and Raff, M.C. (1993). Multiple extracellular signals are required for long-term oligodendrocyte survival. *Development* *118*, 283–295.
- Barry, J., Gu, Y., Jukkola, P., O'Neill, B., Gu, H., Mohler, P.J., Rajamani, K.T., and Gu, C. (2014). Ankyrin-G Directly Binds to Kinesin-1 to Transport Voltage-Gated Na⁺ Channels into Axons. *Developmental Cell* *28*, 117–131.
- Basak, S., Raju, K., Babiarz, J., Kane-Goldsmith, N., Koticha, D., and Grumet, M. (2007). Differential expression and functions of neuronal and glial neurofascin isoforms and splice variants during PNS development. *Developmental Biology* *311*, 408–422.
- Battfeld, A., Tran, B.T., Gavrilis, J., Cooper, E.C., and Kole, M.H.P. (2014). Heteromeric K_v7.2/7.3 Channels Differentially Regulate Action Potential Initiation and Conduction in Neocortical Myelinated Axons. *Journal of Neuroscience* *34*, 3719–3732.
- Baumann, N., and Pham-Dinh, D. (2001). Biology of oligodendrocyte and myelin in the mammalian central nervous system. *Physiological Reviews* *81*, 871–927.
- Bean, B.P. (2007). The action potential in mammalian central neurons. *Nature Reviews Neuroscience* *8*, 451–465.
- Beckh, S., Noda, M., Lübbert, H., and Numa, S. (1989). Differential regulation of three sodium channel messenger RNAs in the rat central nervous system during development. *The EMBO Journal* *8*, 3611.
- Bekku, Y., Rauch, U., Ninomiya, Y., and Oohashi, T. (2009). Brevican distinctively assembles extracellular components at the large diameter nodes of Ranvier in the CNS. *Journal of Neurochemistry* *108*, 1266–1276.
- Bekku, Y., Vargova, L., Goto, Y., Vorisek, I., Dmytrenko, L., Narasaki, M., Ohtsuka, A., Fassler, R., Ninomiya, Y., Sykova, E., et al. (2010). Bral1: Its Role in

- Diffusion Barrier Formation and Conduction Velocity in the CNS. *Journal of Neuroscience* *30*, 3113–3123.
- Ben-Ari, Y., Cherubini, E., Corradetti, R., and Gaiarsa, J.L. (1989). Giant synaptic potentials in immature rat CA3 hippocampal neurones. *J. Physiol.* *416*, 303–325.
- Beneski, D.A., and Catterall, W.A. (1980). Covalent labeling of protein components of the sodium channel with a photoactivable derivative of scorpion toxin. *Proceedings of the National Academy of Sciences* *77*, 639–643.
- Bennett, V., and Lorenzo, D.N. (2013). Spectrin- and Ankyrin-Based Membrane Domains and the Evolution of Vertebrates. In *Current Topics in Membranes*, (Elsevier), pp. 1–37.
- Berg, J., Hung, Y.P., and Yellen, G. (2009). A genetically encoded fluorescent reporter of ATP:ADP ratio. *Nature Methods* *6*, 161–166.
- Berghs, S., Aggujaro, D., Dirkx, R., Maksimova, E., Stabach, P., Hermel, J.-M., Zhang, J.-P., Philbrick, W., Slepnev, V., Ort, T., et al. (2000). β IV Spectrin, a New Spectrin Localized at Axon Initial Segments and Nodes of Ranvier in the Central and Peripheral Nervous System. *The Journal of Cell Biology* *151*, 985–1001.
- Berne, R.M., Koeppen, B.M., Stanton, B.A. (2010). *Berne and Levy Physiology*, 6th ed. Elsevier.
- Berthold, C.H. (1986). Ultrastructure of postnatally developing feline peripheral nodes of Ranvier. *Acta Soc. Med. Ups.* *73*, 145–166.
- Bhat, M.A., Rios, J.C., Lu, Y., Garcia-Fresco, G.P., Ching, W., Martin, M.S., Li, J., Einheber, S., Chesler, M., Rosenbluth, J., et al. (2001). Axon-glia interactions and the domain organization of myelinated axons requires neurexin IV/Caspr/Paranodin. *Neuron* *30*, 369–383.
- Bhat, R.V., Axt, K.J., Fosnaugh, J.S., Smith, K.J., Johnson, K.A., Hill, D.E., Kinzler, K.W., and Baraban, J.M. (1996). Expression of the APC Tumor Suppressor Protein in Oligodendroglia. *Glia* *17*, 169–174.
- Black, J.A., Yokoyama, S., Higashida, H., Ransom, B.R., and Waxman, S. (1994). Sodium channel mRNAs I, II and II in the CNS- Cell-specific expression. *Molecular Brain Research* *22*, 275–289.
- Black, J.A., Renganathan, M., and Waxman, S.G. (2002). Sodium channel Na_v1.6 is expressed along nonmyelinated axons and it contributes to conduction. *Molecular Brain Research* *105*, 19–28.

- Boiko, T., Rasband, M.N., Levinson, S.R., Caldwell, J.H., Mandel, G., Trimmer, J.S., and Matthews, G. (2001). Compact myelin dictates the differential targeting of two sodium channel isoforms in the same axon. *Neuron* *30*, 91–104.
- Boiko, T., Van Wart, A., Caldwell, J.H., Levinson, S.R., Trimmer, J.S., and Matthews, G. (2003). Functional specialization of the axon initial segment by isoform-specific sodium channel targeting. *The Journal of Neuroscience* *23*, 2306–2313.
- Boison, D., Büssow, H., D’Urso, D., Müller, H.-W., and Stoffel, W. (1995). Adhesive Properties of Proteolipid Protein Are Responsible for the compaction of CNS Myelin Sheaths. *The Journal of Neuroscience* *15*, 5502–5513.
- Bonifazi, P., Goldin, M., Picardo, M.A., Jorquera, I., Cattani, A., Bianconi, G., Represa, A., Ben-Ari, Y., and Cossart, R. (2009). GABAergic hub neurons orchestrate synchrony in developing hippocampal networks. *Science* *326*, 1419–1424.
- Bonnon, C., Goutebroze, L., Denisenko-Nehrbass, N., Girault, J.-A., and Faivre-Sarrailh, C. (2003). The Paranodal Complex of F3/Contactin and Caspr/Paranodin Traffics to the Cell Surface via a Non-conventional Pathway. *Journal of Biological Chemistry* *278*, 48339–48347.
- Bosio, A., Binczek, E., and Stoffel, W. (1996). Functional breakdown of the lipid bilayer of the myelin membrane in central and peripheral nervous system by disrupted galactocerebroside synthesis. *Proceedings of the National Academy of Sciences* *93*, 13280–13285.
- Bouvier, F., Dogbo, O., and Camara, B. (2003). Biosynthesis of the food and cosmetic plant pigment bixin (annatto). *Science* *300*, 2089–2091.
- Boyle, M.E., Berglund, E.O., Murai, K.K., Weber, L., Peles, E., and Ranscht, B. (2001). Contactin orchestrates assembly of the septate-like junctions at the paranode in myelinated peripheral nerve. *Neuron* *30*, 385–397.
- Brackenbury, W.J., Davis, T.H., Chen, C., Slat, E.A., Detrow, M.J., Dickendesher, T.L., Ranscht, B., and Isom, L.L. (2008). Voltage-Gated Na⁺ Channel 1 Subunit-Mediated Neurite Outgrowth Requires Fyn Kinase and Contributes to Postnatal CNS Development In Vivo. *The Journal of Neuroscience* *28*, 3246–3256.
- Brackenbury, W.J., Calhoun, J.D., Chen, C., Miyazaki, H., Nukina, N., Oyama, F., Ranscht, B., and Isom, L.L. (2010). Functional reciprocity between Na⁺ channel Na_v1.6 and 1 subunits in the coordinated regulation of excitability and neurite outgrowth. *Proceedings of the National Academy of Sciences* *107*, 2283–2288.

- Brady, S.T., Witt, A.S., Kirkpatrick, L.L., de Waegh, S.M., Readhead, C., Tu, P.-H., and Lee, V.M.-Y. (1999). Formation of compact myelin is required for maturation of the axonal cytoskeleton. *The Journal of Neuroscience* *19*, 7278–7288.
- Le Bras, B., Fréal, A., Czarnecki, A., Legendre, P., Bullier, E., Komada, M., Brophy, P.J., Davenne, M., and Couraud, F. (2014). In vivo assembly of the axon initial segment in motor neurons. *Brain Structure and Function* *219*, 1433–1450.
- Bréchet, A., Fache, M.-P., Brachet, A., Ferracci, G., Baude, A., Irondelle, M., Pereira, S., Leterrier, C., and Dargent, B. (2008). Protein kinase CK2 contributes to the organization of sodium channels in axonal membranes by regulating their interactions with ankyrin G. *The Journal of Cell Biology* *183*, 1101–1114.
- Brückner, G., Szeöke, S., Pavlica, S., Grosche, J., and Kacza, J. (2006). Axon initial segment ensheathed by extracellular matrix in perineuronal nets. *Neuroscience* *138*, 365–375.
- Brysch, W., Creutzfeldt, O.D., Lüne, K., Schlingensiepen, R., and Schlingensiepen, K.-H. (1991). Regional and temporal expression of sodium channel messenger RNAs in the rat brain during development. *Experimental Brain Research* *86*, 562–567.
- Buffington, S.A., and Rasband, M.N. (2013). Na⁺ Channel-Dependent Recruitment of Nav 4 to Axon Initial Segments and Nodes of Ranvier. *Journal of Neuroscience* *33*, 6191–6202.
- Buttermore, E.D., Dupree, J.L., Cheng, J., An, X., Tessarollo, L., and Bhat, M.A. (2011). The Cytoskeletal Adaptor Protein Band 4.1B Is Required for the Maintenance of Paranodal Axoglial Septate Junctions in Myelinated Axons. *Journal of Neuroscience* *31*, 8013–8024.
- Buttermore, E.D., Piochon, C., Wallace, M.L., Philpot, B.D., Hansel, C., and Bhat, M.A. (2012). Pinceau Organization in the Cerebellum Requires Distinct Functions of Neurofascin in Purkinje and Basket Neurons during Postnatal Development. *Journal of Neuroscience* *32*, 4724–4742.
- Cahoy, J.D., Emery, B., Kaushal, A., Foo, L.C., Zamanian, J.L., Christopherson, K.S., Xing, Y., Lubischer, J.L., Krieg, P.A., Krupenko, S.A., et al. (2008). A Transcriptome Database for Astrocytes, Neurons, and Oligodendrocytes: A New Resource for Understanding Brain Development and Function. *The Journal of Neuroscience* *28*, 264–278.
- Caldwell, J.H., Schaller, K.L., Lasher, R.S., Peles, E., and Levinson, S.R. (2000).

- Sodium channel Na_v1.6 is localized at nodes of Ranvier, dendrites, and synapses. *Proceedings of the National Academy of Sciences* *97*, 5616–5620.
- Caldwell, J.H. (2009). Action potential initiation and conduction in axons. Elsevier, 23–29.
- Del Castillo, J., and Moore, J.W. (1959). On increasing the velocity of a nerve impulse. *The Journal of Physiology* *148*, 665–670.
- Catterall, W.A., Goldin, A.L., and Waxman, S.G. (2005). International Union of Pharmacology. XLVII. Nomenclature and Structure-Function Relationships of Voltage-Gated Sodium Channels. *Pharmacological Reviews* *57*, 397–409.
- Catterall, W.A. (2012). Voltage-gated sodium channels at 60: structure, function and pathophysiology: Voltage-gated sodium channels. *The Journal of Physiology* *590*, 2577–2589.
- Chan, W., Kordeli, E., and Bennett, V. (1993). 440-kD ankyrinB: structure of the major developmentally regulated domain and selective localization in unmyelinated axons. *The Journal of Cell Biology* *123*, 1463–1473.
- Chang, K.-J., and Rasband, M.N. (2013). Excitable Domains of Myelinated Nerves. In *Current Topics in Membranes*, (Elsevier), pp. 159–192.
- Chang, K.-J., Zollinger, D.R., Susuki, K., Sherman, D.L., Makara, M.A., Brophy, P.J., Cooper, E.C., Bennett, V., Mohler, P.J., and Rasband, M.N. (2014). Glial ankyrins facilitate paranodal axoglial junction assembly. *Nature Neuroscience* *17*, 1673–1681.
- Charles, P., Tait, S., Faivre-Sarrailh, C., Barbin, G., Gunn-Moore, F., Denisenko-Nehrbass, N., Guennoc, A.-M., Girault, J.-A., Brophy, P.J., and Lubetzki, C. (2002). Neurofascin is a glial receptor for the paranodin/Caspr-contactin axonal complex at the axoglial junction. *Current Biology* *12*, 217–220.
- Chen, C. (2004). Mice Lacking Sodium Channel 1 Subunits Display Defects in Neuronal Excitability, Sodium Channel Expression, and Nodal Architecture. *Journal of Neuroscience* *24*, 4030–4042.
- Chen, C., Bharucha, V., Chen, Y., Westenbroek, R.E., Brown, A., Malhotra, J.D., Jones, D., Avery, C., Gillespie, P.J., Kazen-Gillespie, K.A., et al. (2002). Reduced sodium channel density, altered voltage dependence of inactivation, and increased susceptibility to seizures in mice lacking sodium channel β 2-subunits. *Proceedings of the National Academy of Sciences* *99*, 17072–17077.
- Chen, C., Calhoun, J.D., Zhang, Y., Lopez-Santiago, L., Zhou, N., Davis, T.H., Salzer, J.L., and Isom, L.L. (2012). Identification of the Cysteine Residue

- Responsible for Disulfide Linkage of Na⁺ Channel and 2 Subunits. *Journal of Biological Chemistry* **287**, 39061–39069.
- Cifuentes-Diaz, C., Chareyre, F., Garcia, M., Devaux, J., Carnaud, M., Levasseur, G., Niwa-Kawakita, M., Harroch, S., Girault, J.-A., Giovannini, M., et al. (2011). Protein 4.1B Contributes to the Organization of Peripheral Myelinated Axons. *PLoS ONE* **6**, e25043.
- Clark, B.A., Monsivais, P., Branco, T., London, M., & Häusser, M. (2005) The site of action potential initiation in cerebellar Purkinje neurons. *Nature Neuroscience* **8**, 137-139
- Coetzee, T., Fujita, N., Dupree, J., Shi, R., Blight, A., Suzuki, K., Suzuki, K., and Popko, B. (1996). Myelination in the absence of galactocerebroside and sulfatide: normal structure with abnormal function and regional instability. *Cell* **86**, 209–219.
- Çolakoğlu, G., Bergstrom-Tyrberg, U., Berglund, E.O., and Ranscht, B. (2014). Contactin-1 regulates myelination and nodal/paranodal domain organization in the central nervous system. *Proceedings of the National Academy of Sciences* **111**, E394–E403.
- Colin, E., Zala, D., Liot, G., Rangone, H., Borrell-Page`s, M., Li, X.J., Saudou, F., and Humbert, S. (2008). Huntingtin phosphorylation acts as a molecular switch for anterograde/retrograde transport in neurons. *EMBO J.* **27**, 2124–2134.
- Colombelli, C., Palmisano, M., Eshed-Eisenbach, Y., Zambroni, D., Pavoni, E., Ferri, C., Saccucci, S., Nicole, S., Soininen, R., McKee, K.K., et al. (2015). Perlecan is recruited by dystroglycan to nodes of Ranvier and binds the clustering molecule gliomedin. *The Journal of Cell Biology* **208**, 313–329.
- Colquhoun, D., and Ritchie, J.M. (1972). The interaction at equilibrium between tetrodotoxin and mammalian non-myelinated nerve fibres. *The Journal of Physiology* **221**, 533–553.
- Coman, I., Aigrot, M.S., Seilhean, D., Reynolds, R., Girault, J.A., Zalc, B., and Lubetzki, C. (2006). Nodal, paranodal and juxtaparanodal axonal proteins during demyelination and remyelination in multiple sclerosis. *Brain* **129**, 3186–3195.
- Cooper, E.C. (2011). Made for “anchurin”: Kv7.2/7.3 (KCNQ2/KCNQ3) channels and the modulation of neuronal excitability in vertebrate axons. *Seminars in Cell & Developmental Biology* **22**, 185–192.
- Cozza, G., Bonvini, P., Zorzi, E., Poletto, G., Pagano, M.A., Sarno, S., Donella-

- Deana, A., Zagotto, G., Rosolen, A., Pinna, L.A., et al. (2006). Identification of ellagic acid as potent inhibitor of protein kinase CK2: a successful example of a virtual screening application. *Journal of Medicinal Chemistry* *49*, 2363–2366.
- Craner, M.J., Newcombe, J., Black, J.A., Hartle, C., Cuzner, M.L., and Waxman, S.G. (2004). Molecular changes in neurons in multiple sclerosis: altered axonal expression of Na_v1.2 and Na_v1.6 sodium channels and Na⁺/Ca²⁺ exchanger. *Proceedings of the National Academy of Sciences* *101*, 8168–8173.
- Custer, A.W., Kazarinova-Noyes, K., Sakurai, T., Xu, X., Simon, W., Grumet, M., and Shrager, P. (2003). The role of the ankyrin-binding protein NrCAM in node of Ranvier formation. *The Journal of Neuroscience* *23*, 10032–10039.
- Czopka, T., French-Constant, C., and Lyons, D.A. (2013). Individual Oligodendrocytes Have Only a Few Hours in which to Generate New Myelin Sheaths In Vivo. *Developmental Cell* *25*, 599–609.
- Davis, J.Q., and Bennett, V. (1994). Ankyrin binding activity shared by the neurofascin/L1/NrCAM family of nervous system cell adhesion molecules. *Journal of Biological Chemistry* *269*, 27163–27166.
- Davis, J.Q., Lambert, S., and Bennett, V. (1996). Molecular composition of the node of Ranvier: identification of ankyrin-binding cell adhesion molecules neurofascin (mucin+/third FNIII domain-) and NrCAM at nodal axon segments. *The Journal of Cell Biology* *135*, 1355–1367.
- Davis, T.H., Chen, C., and Isom, L.L. (2004). Sodium Channel 1 Subunits Promote Neurite Outgrowth in Cerebellar Granule Neurons. *Journal of Biological Chemistry* *279*, 51424–51432.
- Debanne, D., Campanac, E., Bialowas, A., Carlier, E., and Alcaraz, G. (2011). Axon Physiology. *Physiological Reviews* *91*, 555–602.
- Deerinck, T.J., Levinson, S.R., Bennett, G.V., and Ellisman, M.H. (1997). Clustering of voltage-sensitive sodium channels on axons is independent of direct Schwann cell contact in the dystrophic mouse. *The Journal of Neuroscience* *17*, 5080–5088.
- Denisenko-Nehrbass, N., Oguievetskaia, K., Goutebroze, L., Galvez, T., Yamakawa, H., Ohara, O., Carnaud, M., and Girault, J.-A. (2003). Protein 4.1B associates with both Caspr/paranodin and Caspr2 at paranodes and juxtaparanodes of myelinated fibres. *European Journal of Neuroscience* *17*, 411–416.
- Derfuss, T., Parikh, K., Velhin, S., Braun, M., Mathey, E., Krumbholz, M., Kümpfel, T., Moldenhauer, A., Rader, C., Sonderegger, P., et al. (2009). Contactin-

- 2/TAG-1-directed autoimmunity is identified in multiple sclerosis patients and mediates gray matter pathology in animals. *Proceedings of the National Academy of Sciences* *106*, 8302–8307.
- Desmazières, A., Sol-Foulon, N., and Lubetzki, C. (2012). Changes at the nodal and perinodal axonal domains: a basis for multiple sclerosis pathology? *Multiple Sclerosis Journal* *18*, 133–137.
- Desmazières, A., Zonta, B., Zhang, A., Wu, L.-M.N., Sherman, D.L., and Brophy, P.J. (2014). Differential Stability of PNS and CNS Nodal Complexes When Neuronal Neurofascin Is Lost. *Journal of Neuroscience* *34*, 5083–5088.
- Devaux, J.J., Kleopa, K.A., Cooper, E.C., and Scherer, S.S. (2004). KCNQ2 Is a Nodal K⁺ Channel. *Journal of Neuroscience* *24*, 1236–1244.
- Devaux, J.J. (2010). The C-terminal domain of β IV-spectrin is crucial for KCNQ2 aggregation and excitability at nodes of Ranvier: β IV-spectrin is crucial for axon excitability. *The Journal of Physiology* *588*, 4719–4730.
- Devaux, J., Alcaraz, G., Grinspan, J., Bennett, V., Joho, R., Crest, M., and Scherer, S.S. (2003). Kv3. 1b is a novel component of CNS nodes. *The Journal of Neuroscience* *23*, 4509–4518.
- Dours-Zimmermann, M.T., Maurer, K., Rauch, U., Stoffel, W., Fassler, R., and Zimmermann, D.R. (2009). Versican V2 Assembles the Extracellular Matrix Surrounding the Nodes of Ranvier in the CNS. *The Journal of Neuroscience* *29*, 7731–7742.
- Duflocq, A., Le Bras, B., Bullier, E., Couraud, F., and Davenne, M. (2008). Na_v1.1 is predominantly expressed in nodes of Ranvier and axon initial segments. *Molecular and Cellular Neuroscience* *39*, 180–192.
- Duflocq, A., Chareyre, F., Giovannini, M., Couraud, F., and Davenne, M. (2011). Characterization of the axon initial segment (AIS) of motor neurons and identification of a para-AIS and a juxtapara-AIS, organized by protein 4.1B. *BMC Biology* *9*, 66.
- Dupree, J.L., Coetzee, T., Blight, A., Suzuki, K., and Popko, B. (1998a). Myelin galactolipids are essential for proper node of Ranvier formation in the CNS. *The Journal of Neuroscience* *18*, 1642–1649.
- Dupree, J.L., Suzuki, K., and Popko, B. (1998b). Galactolipids in the formation and function of the myelin sheath. *Microscopy Research and Technique* *41*, 431–440.
- Dzhashiashvili, Y., Zhang, Y., Galinska, J., Lam, I., Grumet, M., and Salzer, J.L.

- (2007). Nodes of Ranvier and axon initial segments are ankyrin G-dependent domains that assemble by distinct mechanisms. *The Journal of Cell Biology* *177*, 857–870.
- Edgar, J.M., McCulloch, M.C., Thomson, C.E., and Griffiths, I.R. (2008). Distribution of mitochondria along small-diameter myelinated central nervous system axons. *Journal of Neuroscience Research* *86*, 2250–2257.
- Einheber, S., Zanazzi, G., Ching, W., Scherer, S., Milner, T.A., Peles, E., and Salzer, J.L. (1997). The axonal membrane protein Caspr, a homologue of neurexin IV, is a component of the septate-like paranodal junctions that assemble during myelination. *The Journal of Cell Biology* *139*, 1495–1506.
- Einheber, S., Bhat, M.A., and Salzer, J.L. (2006). Disrupted axo-glial junctions result in accumulation of abnormal mitochondria at nodes of Ranvier. *Neuron Glia Biology* *2*, 165.
- Einheber, S., Meng, X., Rubin, M., Lam, I., Mohandas, N., An, X., Shrager, P., Kissil, J., Maurel, P., and Salzer, J.L. (2013). The 4.1B cytoskeletal protein regulates the domain organization and sheath thickness of myelinated axons. *Glia* *61*, 240–253.
- Ellisman, M.H., and Levinson, S.R. (1982). Immunocytochemical localization of sodium channel distributions in the excitable membranes of *Electrophorus electricus*. *Proceedings of the National Academy of Sciences* *79*, 6707–6711.
- Eshed, Y., Feinberg, K., Poliak, S., Sabanay, H., Sarig-Nadir, O., Spiegel, I., Bermingham, J.R., and Peles, E. (2005). Gliomedin Mediates Schwann Cell-Axon Interaction and the Molecular Assembly of the Nodes of Ranvier. *Neuron* *47*, 215–229.
- Eshed, Y., Feinberg, K., Carey, D.J., and Peles, E. (2007). Secreted gliomedin is a perinodal matrix component of peripheral nerves. *The Journal of Cell Biology* *177*, 551–562.
- Eshed-Eisenbach, Y., and Peles, E. (2013). The making of a node: a co-production of neurons and glia. *Current Opinion in Neurobiology* *23*, 1049–1056.
- Espinosa, F., McMahon, A., Chan, E., Wang, S., Ho, C.S., Heintz, N., and Joho, R.H. (2001). Alcohol Hypersensitivity, Increased Locomotion, and Spontaneous Myoclonus in Mice Lacking the Potassium Channels K_v3.1 and K_v3.3. *The Journal of Neuroscience* *21*, 6657–6665.
- Fabricius, C., Berthold, C.-H., and Rydmark, M. (1993). Axoplasmic organelles at nodes of Ranvier. II. Occurrence and distribution in large myelinated spinal cord axons of the adult cat. *Journal of Neurocytology* *22*, 941–954.

- Fache, M.-P., Moussif, A., Fernandes, F., Giraud, P., Garrido, J.J., and Dargent, B. (2004). Endocytotic elimination and domain-selective tethering constitute a potential mechanism of protein segregation at the axonal initial segment. *The Journal of Cell Biology* *166*, 571–578.
- Faissner, A. (1997). The tenascin gene family in axon growth and guidance. *Cell and Tissue Research* *290*, 331–341.
- Faivre-Sarrailh, C., Gauthier, F., Denisenko-Nehrbass, N., Le Bivic, A., Rougon, G., and Girault, J.-A. (2000). The glycosylphosphatidyl inositol-anchored adhesion molecule F3/contactin is required for surface transport of paranodin/contactin-associated protein (caspr). *The Journal of Cell Biology* *149*, 491–502.
- Feinberg, K., Eshed-Eisenbach, Y., Frechter, S., Amor, V., Salomon, D., Sabanay, H., Dupree, J.L., Grumet, M., Brophy, P.J., Shrager, P., et al. (2010). A Glial Signal Consisting of Gliomedin and NrCAM Clusters Axonal Na⁺ Channels during the Formation of Nodes of Ranvier. *Neuron* *65*, 490–502.
- Felts, P.A., Kapoor, R., and Smith, K.J. (1995). A mechanism for ectopic firing in central demyelinated axons. *Brain* *118*, 1225–1231.
- Ffrench-Constant, C., Miller, R.H., Kruse, J., Schachner, M., and Raff, M.C. (1986). Molecular specialization of astrocyte processes at nodes of Ranvier in rat optic nerve. *The Journal of Cell Biology* *102*, 844–852.
- Franz, D.N., and Iggo, A. (1968). Conduction failure in myelinated and non-myelinated axons at low temperatures. *The Journal of Physiology* *199*, 319–345.
- Freeman, S.A., Desmazières, A., Simonnet, J., Gatta, M., Pfeiffer, F., Aigrot, M.S., Rappeneau, Q., Guerreiro, S., Michel, P.P., Yanagawa, Y., et al. (2015). Acceleration of conduction velocity linked to clustering of nodal components precedes myelination. *Proceedings of the National Academy of Sciences* *112*, E321–E328.
- Friede, R.L., and Samorajski, T. (1970). Axon caliber related to neurofilaments and microtubules in sciatic nerve fibers of rats and mice. *The Anatomical Record* *167*, 379–387.
- Friese, M.A., Schattling, B., and Fugger, L. (2014). Mechanisms of neurodegeneration and axonal dysfunction in multiple sclerosis. *Nature Reviews Neurology* *10*, 225–238.
- Fünfschilling, U., Supplie, L.M., Mahad, D., Boretius, S., Saab, A.S., Edgar, J., Brinkmann, B.G., Kassmann, C.M., Tzvetanova, I.D., Möbius, W., et al.

- (2012). Glycolytic oligodendrocytes maintain myelin and long-term axonal integrity. *Nature* *485*, 517–522.
- Galiano, M.R., Jha, S., Ho, T.S.-Y., Zhang, C., Ogawa, Y., Chang, K.-J., Stankewich, M.C., Mohler, P.J., and Rasband, M.N. (2012). A Distal Axonal Cytoskeleton Forms an Intra-Axonal Boundary that Controls Axon Initial Segment Assembly. *Cell* *149*, 1125–1139.
- Garaschuk, O., Hanse, E., and Konnerth, A. (1998). Developmental profile and synaptic origin of early network oscillations in the CA1 region of rat neonatal hippocampus. *J. Physiol.* *507*, 219–236.
- Garbern, J.Y., Yool, D.A., Moore, G.A., Wilds, I.B., Faulk, M.W., Klugmann, M., Nave, K.-A., Sistrerians, E.A., van der Knaap, M.S., Bird, T.D., et al. (2002). Patients lacking the major CNS myelin protein, proteolipid protein 1, develop length-dependent axonal degeneration in the absence of demyelination and inflammation. *Brain* *125*, 551–561.
- Gasser, H.S. (1950). Unmyelinated fibers originating in dorsal root ganglia. *The Journal of General Physiology* *33*, 651–690.
- Gasser, A., Ho, T.S.-Y., Cheng, X., Chang, K.-J., Waxman, S.G., Rasband, M.N., and Dib-Hajj, S.D. (2012). An AnkyrinG-Binding Motif Is Necessary and Sufficient for Targeting Nav1.6 Sodium Channels to Axon Initial Segments and Nodes of Ranvier. *The Journal of Neuroscience* *32*, 7232–7243.
- Gerbi, A., Sennoune, S., Pierre, S., Sampol, J., Raccach, D., Vague, P., and Maixent, J.-M. (1999). Localization of Na, K-ATPase α/β Isoforms in Rat Sciatic Nerves: Effect of Diabetes and Fish Oil Treatment. *Journal of Neurochemistry* *73*, 719–726.
- Gilchrist, J., Das, S., Van Petegem, F., and Bosmans, F. (2013). Crystallographic insights into sodium-channel modulation by the 4 subunit. *Proceedings of the National Academy of Sciences* *110*, E5016–E5024.
- Gogan, P., Gueritaud, J.P., and Tyc-Dumont, S. (1983). Comparison of antidromic and orthodromic action potentials of identified motor axons in the cat's brain stem. *The Journal of Physiology* *335*, 205–220.
- Gollan, L., Sabanay, H., Poliak, S., Berglund, E.O., Ranscht, B., and Peles, E. (2002). Retention of a cell adhesion complex at the paranodal junction requires the cytoplasmic region of Caspr. *The Journal of Cell Biology* *157*, 1247–1256.
- Gollan, L., Salomon, D., Salzer, J.L., and Peles, E. (2003). Caspr regulates the processing of contactin and inhibits its binding to neurofascin. *The Journal of*

- Cell Biology *163*, 1213–1218.
- Gong, B., Rhodes, K., Bekele-Arcuri, Z., and Trimmer, J.S. (1999). Type I and type II Na(+) channel alpha-subunit polypeptides exhibit spatial and temporal patterning, and association with auxiliary subunits in rat brain.pdf. The Journal of Comparative Neurology *412*, 342–352.
- Gordon, A., Adamsky, K., Vainshtein, A., Frechter, S., Dupree, J.L., Rosenbluth, J., and Peles, E. (2014). Caspr and Caspr2 Are Required for Both Radial and Longitudinal Organization of Myelinated Axons. Journal of Neuroscience *34*, 14820–14826.
- Gouttebroze, L., Carnaud, M., Denisenko, N., Bouterin, M.-C., and Girault, J.-A. (2003). Syndecan-3 and syndecan-4 are enriched in Schwann cell perinodal processes. BMC Neuroscience *4*, 29.
- Gravel, M., Peterson, J., Yong, V.W., Kottis, V., Trapp, B., and Braun, P.E. (1996). Overexpression of 2', 3'-cyclic nucleotide 3'-phosphodiesterase in transgenic mice alters oligodendrocyte development and produces aberrant myelination. Molecular and Cellular Neuroscience *7*, 453–466.
- Grieco, T.M., Malhotra, J.D., Chen, C., Isom, L.L., and Raman, I.M. (2005). Open-Channel Block by the Cytoplasmic Tail of Sodium Channel $\beta 4$ as a Mechanism for Resurgent Sodium Current. Neuron *45*, 233–244.
- Griffiths, I., Klugmann, M., Anderson, T., Yool, D., Thomson, C., Schwab, M., Schneider, A., Zimmermann, F., McCulloch, M., Nadon, N., et al. (1998). Axonal Swellings and Degeneration in Mice Lacking the Major Proteolipid of Myelin. Science *280*, 1610–1613.
- Grumet, M. (1997). Nr-CAM: a cell adhesion molecule with ligand and receptor functions. Cell and Tissue Research *290*, 423–428.
- Gunn-Moore, F.J., Hill, M., Davey, F., Herron, L.R., Tait, S., Sherman, D., and Brophy, P.J. (2006). A functional FERM domain binding motif in neurofascin. Molecular and Cellular Neuroscience *33*, 441–446.
- Haimovich, B., Bonilla, E., Casadei, J., and Barchi, R. (1984). Immunocytochemical localization of the mammalian voltage-dependent sodium channel using polyclonal antibodies against the purified protein. The Journal of Neuroscience *4*, 2259–2268.
- Hamada, M.S., and Kole, M.H.P. (2015). Myelin Loss and Axonal Ion Channel Adaptations Associated with Gray Matter Neuronal Hyperexcitability. The Journal of Neuroscience *35*, 7272–7286.

- Hartline, D.K., and Colman, D.R. (2007). Rapid Conduction and the Evolution of Giant Axons and Myelinated Fibers. *Current Biology* 17, R29–R35.
- Hartshorne, R.P., and Catterall, W.A. (1984). The sodium channel from rat brain. Purification and subunit composition. *Journal of Biological Chemistry* 259, 1667–1675.
- He, M., Jenkins, P., and Bennett, V. (2012). Cysteine 70 of Ankyrin-G Is S-Palmitoylated and Is Required for Function of Ankyrin-G in Membrane Domain Assembly. *Journal of Biological Chemistry* 287, 43995–44005.
- Hedstrom, K.L., Xu, X., Ogawa, Y., Frischknecht, R., Seidenbecher, C.I., Shrager, P., and Rasband, M.N. (2007). Neurofascin assembles a specialized extracellular matrix at the axon initial segment. *The Journal of Cell Biology* 178, 875–886.
- Hedstrom, K.L., Ogawa, Y., and Rasband, M.N. (2008). AnkyrinG is required for maintenance of the axon initial segment and neuronal polarity. *The Journal of Cell Biology* 183, 635–640.
- Hendricks, A. G., Perlson, E., Ross, J. L., Schroeder, H. W., Tokito, M., and Holzbaur, E. L. F. (2010). Motor Coordination Via Tug-Of-War Mechanism Drives Bidirectional Vesicle Transport. *Current Biology: CB*, 20(8), 697–702.
- Henry, M.A., Luo, S., and Levinson, S.R. (2012). Unmyelinated nerve fibers in the human dental pulp express markers for myelinated fibers and show sodium channel accumulations. *BMC Neuroscience* 13, 29.
- Herzog, R.I., Cummins, T.R., Ghassemi, F., Dib-Hajj, S.D., and Waxman, S.G. (2003). Distinct repriming and closed-state inactivation kinetics of Nav1.6 and Nav1.7 sodium channels in mouse spinal sensory neurons. *The Journal of Physiology* 551, 741–750.
- Hien, Y.E., Montersino, A., Castets, F., Leterrier, C., Filhol, O., Vacher, H., and Dargent, B. (2014). CK2 accumulation at the axon initial segment depends on sodium channel Nav1. *FEBS Letters* 588, 3403–3408.
- Hirano, A., and Dembitzer, H.M. (1978). Morphology of normal central myelinated axons. In “Physiology and Pathobiology of Axons” (S.G. Waxman, ed.), pp. 65–82. Raven, New York.
- Hirokawa, N., Niwa, S., and Tanaka, Y. (2010). Molecular Motors in Neurons: Transport Mechanisms and Roles in Brain Function, Development, and Disease. *Neuron* 68, 610–638.
- Ho, T.S.-Y., Zollinger, D.R., Chang, K.-J., Xu, M., Cooper, E.C., Stankewich, M.C.,

- Bennett, V., and Rasband, M.N. (2014). A hierarchy of ankyrin-spectrin complexes clusters sodium channels at nodes of Ranvier. *Nature Neuroscience* *17*, 1664–1672.
- Hodgkin, A.L. (1975). The optimum density of sodium channels in an unmyelinated nerve. *Philosophical Transactions of the Royal Society of London. Series B, Biological Sciences* 297–300.
- Hodgkin, A.L. (1954). A note on conduction velocity. *The Journal of Physiology* *125*, 221–224.
- Hodgkin, A.L, and Huxley, A.F (1952a). Experiments with relatively brief depolarizations. *The Journal of Physiology* *116*, 473–496.
- Hodgkin, A.L., and Huxley, A.F. (1952b). A quantitative description of membrane current and its application to conduction and excitation in nerve. *The Journal of Physiology* *117*, 500–544.
- Hodgkin, A.L., and Huxley, A.F. (1952c). Currents carried by sodium and potassium ions through the membrane of the giant axon of *Loligo*. *The Journal of Physiology* *116*, 449–472.
- Hodgkin, A.L., and Katz, B. (1949). The effect of temperature on the electrical activity of the giant axon of the squid. *The Journal of Physiology* *109*, 240–249.
- Honke, K., Hirahara, Y., Dupree, J., Suzuki, K., Popko, B., Fukushima, K., Fukushima, J., Nagasawa, T., Yoshida, N., Wada, Y., et al. (2002). Paranodal junction formation and spermatogenesis require sulfoglycolipids. *Proceedings of the National Academy of Sciences* *99*, 4227–4232.
- Horresh, I., Poliak, S., Grant, S., Bredt, D., Rasband, M.N., and Peles, E. (2008). Multiple Molecular Interactions Determine the Clustering of Caspr2 and Kv1 Channels in Myelinated Axons. *The Journal of Neuroscience* *28*, 14213–14222.
- Horresh, I., Bar, V., Kissil, J.L., and Peles, E. (2010). Organization of Myelinated Axons by Caspr and Caspr2 Requires the Cytoskeletal Adapter Protein 4.1B. *The Journal of Neuroscience* *30*, 2480–2489.
- Hortsch, M. (2000). Structural and Functional Evolution of the L1 Family: Are Four Adhesion Molecules Better Than One? *Molecular and Cellular Neuroscience* *15*, 1–10.
- Hortsch, M., Nagaraj, K., and Godenschwege, T. (2009). The interaction between L1-type proteins and ankyrins - a master switch for L1-type CAM function.

Cellular and Molecular Biology Letters 14.

- Howell, O.W., Palser, A., Polito, A., Melrose, S., Zonta, B., Scheiermann, C., Vora, A.J., Brophy, P.J., and Reynolds, R. (2006). Disruption of neurofascin localization reveals early changes preceding demyelination and remyelination in multiple sclerosis. *Brain* 129, 3173–3185.
- Hu, W., Tian, C., Li, T., Yang, M., Hou, H., and Shu, Y. (2009). Distinct contributions of $\text{Na}_v1.6$ and $\text{Na}_v1.2$ in action potential initiation and backpropagation. *Nature Neuroscience* 12, 996–1002.
- Hursh, J.B. (1939). Conduction velocity and diameter of nerve fibers. *The Journal of Physiology* 127, 131–139.
- Huxley, A.F., and Stämpeli, R. (1949). Evidence for saltatory conduction in peripheral myelinated nerve fibres. *The Journal of Physiology* 108, 315–339.
- Inda, M.C., DeFelipe, J., and Muñoz, A. (2006). Voltage-gated ion channels in the axon initial segment of human cortical pyramidal cells and their relationship with chandelier cells. *Proceedings of the National Academy of Sciences* 103, 2920–2925.
- Iozzo, R.V., and Schaefer, L. (2015). Proteoglycan form and function: A comprehensive nomenclature of proteoglycans. *Matrix Biology* 42, 11–55.
- Ishibashi, T., Dupree, J.L., Ikenaka, K., Hirahara, Y., Honke, K., Peles, E., Popko, B., Suzuki, K., Nishino, H., and Baba, H. (2002). A myelin galactolipid, sulfatide, is essential for maintenance of ion channels on myelinated axon but not essential for initial cluster formation. *The Journal of Neuroscience* 22, 6507–6514.
- Isom, L.L., De Jongh, K.S., Patton, D.E., Reber, B.F.X., Offord, J., Charbonneau, H., Walsh, K., Goldin, A.L., and Catterall, W.A. (1992). Primary Structure and Functional Expression of the $\beta 1$ Subunit of the Rat Brain Sodium Channel. *Science* 256, 839–842.
- Isom, L.L., Ragsdale, D.S., De Jongh, K.S., Westenbroek, R.E., Reber, B.F.X., Scheuer, T., and Catterall, W.A. (1995). Structure and Function of the $\beta 2$ subunit of brain sodium channels, a transmembrane glycoprotein with a CAM motif. *Cell* 83, 433–442.
- Ivanovic, A., Horresh, I., Golan, N., Spiegel, I., Sabanay, H., Frechter, S., Ohno, S., Terada, N., Mobius, W., Rosenbluth, J., et al. (2012). The cytoskeletal adapter protein 4.1G organizes the internodes in peripheral myelinated nerves. *The Journal of Cell Biology* 196, 337–344.

- Jenkins, S.M., and Bennett, V. (2001). Ankyrin-G coordinates assembly of the spectrin-based membrane skeleton, voltage-gated sodium channels, and L1 CAMs at Purkinje neuron initial segments. *The Journal of Cell Biology* *155*, 739–746.
- Jenkins, S.M., and Bennett, V. (2002). Developing nodes of Ranvier are defined by ankyrin-G clustering and are independent of paranodal axoglial adhesion. *Proceedings of the National Academy of Sciences* *99*, 2303–2308.
- Jenkins, P.M., Kim, N., Jones, S.L., Tseng, W.C., Svitkina, T.M., Yin, H.H., and Bennett, V. (2015). Giant ankyrin-G: A critical innovation in vertebrate evolution of fast and integrated neuronal signaling. *Proceedings of the National Academy of Sciences* *112*, 957–964.
- John, N., Krügel, H., Frischknecht, R., Smalla, K.-H., Schultz, C., Kreutz, M.R., Gundelfinger, E.D., and Seidenbecher, C.I. (2006). Brevican-containing perineuronal nets of extracellular matrix in dissociated hippocampal primary cultures. *Molecular and Cellular Neuroscience* *31*, 774–784.
- Johnston, W.L., Dyer, J.R., Castellucci, V.F., and Dunn, R.J. (1996). Clustered Voltage-Gated Na⁺ Channels in Aplysia Axons. *The Journal of Neuroscience* *16*, 1730–1739.
- Kalume, F., Yu, F.H., Westenbroek, R.E., Scheuer, T., and Catterall, W.A. (2007). Reduced Sodium Current in Purkinje Neurons from Na_v1.1 Mutant Mice: Implications for Ataxia in Severe Myoclonic Epilepsy in Infancy. *Journal of Neuroscience* *27*, 11065–11074.
- Kamal, A., Stokin, G.B., Yang, Z., Xia, C.H., and Goldstein, L.S. (2000). Axonal transport of amyloid precursor protein is mediated by direct binding to the kinesin light chain subunit of kinesin-I. *Neuron* *28*, 449–459.
- Kanai, Y., Okada, Y., Tanaka, Y., Harada, A., Terada, S., and Hirokawa, N. (2000). KIF5C, a novel neuronal kinesin enriched in motor neurons. *The Journal of Neuroscience* *20*, 6374–6384.
- Kanai, Y., Dohmae, N., and Hirokawa, N. (2004). Kinesin transports RNA: Isolation and characterization of an RNA-transporting granule. *Neuron* *43*, 513–525.
- Kaplan, M.R., Meyer-Franke, A., Lambert, S., Bennett, V., Duncan, I.D., Levinson, S.R., and Barres, B.A. (1997). Induction of Sodium Channel Clustering by Oligodendrocytes. *Nature* *386*, 724–728.
- Kaplan, M.R., Cho, M.-H., Ullian, E.M., Isom, L.L., Levinson, S.R., and Barres, B.A. (2001). Differential control of clustering of the sodium channels Na_v1.2 and Na_v1.6 at developing CNS nodes of Ranvier. *Neuron* *30*, 105–119.

- Kapoor, R., Li, Y.G., and Smith, K.J. (1997). Slow sodium-dependent potential oscillations contribute to ectopic firing in mammalian demyelinated axons. *Brain* *120*, 647–652.
- Katz, B. (1947). The effect of electrolyte deficiency on the rate of conduction in a single nerve fibre. *The Journal of Physiology* *106*, 411–417.
- Kayyem, J.F., Roman, J.M., de la Rosa, E.J., Schwarz, U., and Dreyer, W.J. (1992). Bravo/Nr-CAM is closely related to the cell adhesion molecules L1 and Ng-CAM and has a similar heterodimer structure. *The Journal of Cell Biology* *118*, 1259–1270.
- Kazarinova-Noyes, K., Malhotra, J.D., McEwen, D.P., Mattei, L.N., Berglund, E.O., Ranscht, B., Levinson, S.R., Schachner, M., Shrager, P., Isom, L.L., et al. (2001). Contactin associates with Na⁺ channels and increases their functional expression. *The Journal of Neuroscience* *21*, 7517–7525.
- Kazen-Gillespie, K.A., Ragsdale, D.S., D’Andrea, M.R., Mattei, L.N., Rogers, K.E., and Isom, L.L. (2000). Cloning, localization, and functional expression of sodium channel β 1A subunits. *Journal of Biological Chemistry* *275*, 1079–1088.
- Khaliq, Z.M., and Raman, I.M. (2006). Relative Contributions of Axonal and Somatic Na Channels to Action Potential Initiation in Cerebellar Purkinje Neurons. *The Journal of Neuroscience* *26*, 1935–1944.
- Khaliq, Z.M., Gouwens, N.W., and Raman, I.M. (2003). The contribution of resurgent sodium current to high-frequency firing in Purkinje neurons: an experimental and modeling study. *The Journal of Neuroscience* *23*, 4899–4912.
- Kizhatil, K., Wu, Y.-X., Sen, A., and Bennett, V. (2002). A new activity of doublecortin in recognition of the phospho-FIGQY tyrosine in the cytoplasmic domain of neurofascin. *The Journal of Neuroscience* *22*, 7948–7958.
- Klinger, F., Gould, G., Boehm, S., and Shapiro, M.S. (2011). Distribution of M-channel subunits KCNQ2 and KCNQ3 in rat hippocampus. *NeuroImage* *58*, 761–769.
- Klugmann, M., Schwab, M.H., Pühlhofer, A., Schneider, A., Zimmermann, F., Griffiths, I.R., and Nave, K.-A. (1997). Assembly of CNS myelin in the absence of proteolipid protein. *Neuron* *18*, 59–70.
- Kole, M.H.P., Letzkus, J.J., and Stuart, G.J. (2007). Axon Initial Segment K_v1 Channels Control Axonal Action Potential Waveform and Synaptic Efficacy. *Neuron* *55*, 633–647.

- Kole, M.H.P., Ilshner, S.U., Kampa, B.M., Williams, S.R., Ruben, P.C., and Stuart, G.J. (2008). Action potential generation requires a high sodium channel density in the axon initial segment. *Nature Neuroscience* *11*, 178–186.
- Koles, Z.J., and Rasminsky, M. (1972). A computer simulation of conduction in demyelinated nerve fibres. *The Journal of Physiology* *227*, 351–364.
- Komada, M. (2002). β IV-spectrin regulates sodium channel clustering through ankyrin-G at axon initial segments and nodes of Ranvier. *The Journal of Cell Biology* *156*, 337–348.
- Kordeli, E., and Bennett, V. (1991). Distinct ankyrin isoforms at neuron cell bodies and nodes of Ranvier resolved using erythrocyte ankyrin-deficient mice. *The Journal of Cell Biology* *114*, 1243–1259.
- Kordeli, E., Lambert, S., and Bennett, V. (1995). AnkyrinG: A New Ankyrin Gene with Neural-Specific Isoforms Localized at the AIS and the node of Ranvier.pdf. *The Journal of Biological Chemistry* *270*, 2352–2359.
- Koticha, D., Babiarz, J., Kane-Goldsmith, N., Jacob, J., Raju, K., and Grumet, M. (2005). Cell adhesion and neurite outgrowth are promoted by neurofascin NF155 and inhibited by NF186. *Molecular and Cellular Neuroscience* *30*, 137–148.
- Koticha, D., Maurel, P., Zanazzi, G., Kane-Goldsmith, N., Basak, S., Babiarz, J., Salzer, J., and Grumet, M. (2006). Neurofascin interactions play a critical role in clustering sodium channels, ankyrinG and β IV spectrin at peripheral nodes of Ranvier. *Developmental Biology* *293*, 1–12.
- Kress, G.J., and Mennerick, S. (2009). Action potential initiation and propagation: Upstream influences on neurotransmission. *Neuroscience* *158*, 211–222.
- Kress, G.J., Dowling, M.J., Meeks, J.P., and Mennerick, S. (2008). High Threshold, Proximal Initiation, and Slow Conduction Velocity of Action Potentials in Dentate Granule Neuron Mossy Fibers. *The Journal of Neurophysiology* *100*, 281–291.
- Kriebel, M., Metzger, J., Trinks, S., Chugh, D., Harvey, R.J., Harvey, K., and Volkmer, H. (2011). The Cell Adhesion Molecule Neurofascin Stabilizes Axo-axonic GABAergic Terminals at the Axon Initial Segment. *The Journal of Biological Chemistry* *286*, 24385–24393.
- Kriebel, M., Wuchter, J., Trinks, S., and Volkmer, H. (2012). Neurofascin: A switch between neuronal plasticity and stability. *The International Journal of Biochemistry & Cell Biology* *44*, 694–697.

- Krzemien, D.M., Schaller, K.L., Levinson, S.R., and Caldwell, J.H. (2000). Immunolocalization of sodium channel isoform NaCh6 in the nervous system. *Journal of Comparative Neurology* 420, 70–83.
- Kunimoto, M. (1995). A neuron-specific isoform of brain ankyrin, 440-kD ankyrinB, is targeted to the axons of rat cerebellar neurons. *The Journal of Cell Biology* 131, 1821–1829.
- Kwon, H.S., Johnson, T.V., Joe, M.K., Abu-Asab, M., Zhang, J., Chan, C.C., and Tomarev, S.I. (2013). Myocilin Mediates Myelination in the Peripheral Nervous System through ErbB2/3 Signaling. *The Journal of Biological Chemistry* 288, 26357–26371.
- Labasque, M., and Faivre-Sarrailh, C. (2010). GPI-anchored proteins at the node of Ranvier. *FEBS Letters* 584, 1787–1792.
- Labasque, M., Devaux, J.J., Leveque, C., and Faivre-Sarrailh, C. (2011). Fibronectin Type III-like Domains of Neurofascin-186 Protein Mediate Gliomedin Binding and Its Clustering at the Developing Nodes of Ranvier. *The Journal of Biological Chemistry* 286, 42426–42434.
- Lacas-Gervais, S., Guo, J., Strenzke, N., Scarfone, E., Kolpe, M., Jahkel, M., De Camilli, P., Moser, T., Rasband, M.N., and Solimena, M. (2004). β IV Σ 1 spectrin stabilizes the nodes of Ranvier and axon initial segments. *The Journal of Cell Biology* 166, 983–990.
- Lai, H.C., and Jan, L.Y. (2006). The distribution and targeting of neuronal voltage-gated ion channels. *Nature Reviews Neuroscience* 7, 548–562.
- Lambert, S., Davis, J.Q., and Bennett, V. (1997). Morphogenesis of the node of Ranvier: co-clusters of ankyrin and ankyrin-binding integral proteins define early developmental intermediates. *The Journal of Neuroscience* 17, 7025–7036.
- Landon, D.N., and Hall, S. (1976). The myelinated nerve fiber. In “The Peripheral Nerve”. D.N. Landon, ed, Chapman & Hall, London, 1-105.
- Landon, D.N., and Langley, O.K. (1971). The local chemical environment of nodes of Ranvier: a study of cation binding. *Journal of Anatomy* 108, 419.
- Landon, D.N., and Williams, P.L. (1963). Ultrastructure of the node of Ranvier. *Nature* 199, 575–577.
- Lappe-Siefke, C., Goebbels, S., Gravel, M., Nicksch, E., Lee, J., Braun, P.E., Griffiths, I.R., and Nave, K.-A. (2003). Disruption of Cnp1 uncouples oligodendroglial functions in axonal support and myelination. *Nature*

- Genetics 33, 366–374.
- Lasiecka, Z.M., and Winckler, B. (2011). Mechanisms of polarized membrane trafficking in neurons — Focusing in on endosomes. *Molecular and Cellular Neuroscience* 48, 278–287.
- Lee, Y., Morrison, B.M., Li, Y., Lengacher, S., Farah, M.H., Hoffman, P.N., Liu, Y., Tsingalia, A., Jin, L., Zhang, P.-W., et al. (2012). Oligodendroglia metabolically support axons and contribute to neurodegeneration. *Nature* 487, 443–448.
- Lemaillet, G., Walker, B., and Lambert, S. (2003). Identification of a Conserved Ankyrin-binding Motif in the Family of Sodium Channel Subunits. *The Journal of Biological Chemistry* 278, 27333–27339.
- Leterrier, C., and Dargent, B. (2014). No Pasaran! Role of the axon initial segment in the regulation of protein transport and the maintenance of axonal identity. *Semin. Cell Dev. Biol.* 27, 44–51.
- Leterrier, C., Brachet, A., Dargent, B., and Vacher, H. (2011). Determinants of voltage-gated sodium channel clustering in neurons. *Seminars in Cell & Developmental Biology* 22, 171–177.
- Li, J. (2015). Molecular regulators of nerve conduction — Lessons from inherited neuropathies and rodent genetic models. *Experimental Neurology* 267, 209–218.
- Lien, C.-C., and Jonas, P. (2003). Kv3 potassium conductance is necessary and kinetically optimized for high-frequency action potential generation in hippocampal interneurons. *The Journal of Neuroscience* 23, 2058–2068.
- Lillie, R.S. (1925). Factors affecting transmission and recovery in the passive iron nerve model. *The Journal of General Physiology* 7, 473–507.
- Lorincz, A., and Nusser, Z. (2008). Cell-Type-Dependent Molecular Composition of the Axon Initial Segment. *Journal of Neuroscience* 28, 14329–14340.
- Luo, S., Jaegle, M., Li, R., Ehring, G.R., Meijer, D., and Levinson, S.R. (2014). The sodium channel isoform transition at developing nodes of Ranvier in the peripheral nervous system: Dependence on a Genetic program and myelination-induced cluster formation: Sodium Channel Isoforms at Nodes. *The Journal of Comparative Neurology* 522, 4057–4073.
- Lustig, M., Zanazzi, G., Sakurai, T., Blanco, C., Levinson, S.R., Lambert, S., Grumet, M., and Salzer, J.L. (2001a). Nr-CAM and neurofascin interactions regulate ankyrin G and sodium channel clustering at the node of Ranvier.

- Current Biology *11*, 1864–1869.
- Lustig, M., Erskine, L., Mason, C.A., Grumet, M., and Sakurai, T. (2001b). Nr-CAM expression in the developing mouse nervous system: Ventral midline structures, specific fiber tracts, and neuropilar regions. *The Journal of Comparative Neurology* *434*, 13–28.
- Maertens, B., Hopkins, D., Franzke, C.-W., Keene, D.R., Bruckner-Tuderman, L., Greenspan, D.S., and Koch, M. (2007). Cleavage and Oligomerization of Gliomedin, a Transmembrane Collagen Required for Node of Ranvier Formation. *The Journal of Biological Chemistry* *282*, 10647–10659.
- Malhotra, J.D., Kazen-Gillespie, K.A., Hortsch, M., and Isom, L.L. (2000). Sodium Channel beta Subunits Mediate Homophilic Cell Adhesion and Recruit Ankyrin to Points of Cell-Cell Contact. *The Journal of Biological Chemistry* *275*, 11383–11388.
- Malhotra, J.D., Koopmann, M.C., Kazen-Gillespie, K.A., Fettman, N., Hortsch, M., and Isom, L.L. (2002). Structural Requirements for Interaction of Sodium Channel 1 Subunits with Ankyrin. *The Journal of Biological Chemistry* *277*, 26681–26688.
- Marcus, J., Honigbaum, S., Shroff, S., Honke, K., Rosenbluth, J., and Dupree, J.L. (2006). Sulfatide is essential for the maintenance of CNS myelin and axon structure. *Glia* *53*, 372–381.
- Marionneau, C., Carrasquillo, Y., Norris, A.J., Townsend, R.R., Isom, L.L., Link, A.J., and Nerbonne, J.M. (2012). The Sodium Channel Accessory Subunit Nav1 Regulates Neuronal Excitability through Modulation of Repolarizing Voltage-Gated K⁺ Channels. *The Journal of Neuroscience* *32*, 5716–5727.
- Martin, S., Levine, A.K., Chen, Z.J., Ughrin, Y., and Levine, J.M. (2001). Deposition of the NG2 proteoglycan at nodes of Ranvier in the peripheral nervous system. *The Journal of Neuroscience* *21*, 8119–8128.
- Martini, R., and Schachner, M. (1986). Immunoelectron microscopic localization of neural cell adhesion molecules (L1, N-CAM, and MAG) and their shared carbohydrate epitope and myelin basic protein in developing sciatic nerve. *The Journal of Cell Biology* *103*, 2439–2448.
- Mathey, E.K., Derfuss, T., Storch, M.K., Williams, K.R., Hales, K., Woolley, D.R., Al-Hayani, A., Davies, S.N., Rasband, M.N., Olsson, T., et al. (2007). Neurofascin as a novel target for autoantibody-mediated axonal injury. *Journal of Experimental Medicine* *204*, 2363–2372.
- Mathis, C., Denisenko-Nehrbass, N., Girault, J.-A., and Borrelli, E. (2001).

- Essential role of oligodendrocytes in the formation and maintenance of central nervous system nodal regions. *Development* *128*, 4881–4890.
- McEwen, D.P., and Isom, L.L. (2004). Heterophilic Interactions of Sodium Channel 1 Subunits with Axonal and Glial Cell Adhesion Molecules. *The Journal of Biological Chemistry* *279*, 52744–52752.
- McEwen, D.P., Meadows, L.S., Chen, C., Thyagarajan, V., and Isom, L.L. (2004). Sodium Channel 1 Subunit-mediated Modulation of Na_v1.2 Currents and Cell Surface Density Is Dependent on Interactions with Contactin and Ankyrin. *Journal of Biological Chemistry* *279*, 16044–16049.
- McGrail, K.M., Phillips, J.M., and Sweadner, K.J. (1991). Immunofluorescent localization of three Na, K-ATPase isozymes in the rat central nervous system: both neurons and glia can express more than one Na, K-ATPase. *The Journal of Neuroscience* *11*, 381–391.
- Meeks, J.P., Jiang, X., and Mennerick, S. (2005). Action potential fidelity during normal and epileptiform activity in paired soma-axon recordings from rat hippocampus: Axonal action potential fidelity in hippocampus. *The Journal of Physiology* *566*, 425–441.
- Meeks, J.P., and Mennerick, S. (2007). Action Potential Initiation and Propagation in CA3 Pyramidal Axons. *Journal of Neurophysiology* *97*, 3460–3472.
- Melendez-Vasquez, C., Carey, D.J., Zanazzi, G., Reizes, O., Maurel, P., and Salzer, J.L. (2005). Differential expression of proteoglycans at central and peripheral nodes of Ranvier. *Glia* *52*, 301–308.
- Melendez-Vasquez, C.V., Rios, J.C., Zanazzi, G., Lambert, S., Bretscher, A., and Salzer, J.L. (2001). Nodes of Ranvier form in association with ezrin-radixin-moesin (ERM)-positive Schwann cell processes. *Proceedings of the National Academy of Sciences* *98*, 1235–1240.
- Menegoz, M., Gaspar, P., Le Bert, M., Galvez, T., Burgaya, F., Palfrey, C., Ezan, P., Arnos, F., and Girault, J.-A. (1997). Paranodin, a glycoprotein of neuronal paranodal membranes. *Neuron* *19*, 319–331.
- Mensch, S., Baraban, M., Almeida, R., Czopka, T., Ausborn, J., El Manira, A., and Lyons, D.A. (2015). Synaptic vesicle release regulates myelin sheath number of individual oligodendrocytes in vivo. *Nature Neuroscience* *18*, 628–630.
- Messner, D.J., and Catterall, W.A. (1985). The Sodium Channel from Rat Brain. *The Journal of Biological Chemistry* *260*, 10597–10604.
- Mierzwa, A., Shroff, S., and Rosenbluth, J. (2010). Permeability of the Paranodal

- Junction of Myelinated Nerve Fibers. *The Journal of Neuroscience* *30*, 15962–15968.
- Montag, D., Giese, K.P., Bartsch, U., Martini, R., Lang, Y., Bluethmann, H., Karthigasan, J., Kirschner, D.A., Wintergerst, E.S., Nave, K.-A., et al. (1994). Mice Deficient for the Myelin-Associated Glycoprotein Show Subtle Abnormalities in Myelin. *Neuron* *13*, 229–246.
- Moore, J.W., Joyner, R.W., Brill, M.H., Waxman, S.D., and Najar-Joa, M. (1978). Simulations of conduction in uniform myelinated fibers. Relative sensitivity to changes in nodal and internodal parameters. *Biophysical Journal* *21*, 147–160.
- Morell, P., and Radin, N.S. (1969). Synthesis of cerebroside by brain from uridine diphosphate galactose and ceramide containing hydroxy fatty acid. *Biochemistry* *8*, 506–512.
- Mörtl, M., Sonderegger, P., Diederichs, K., and Welte, W. (2007). The crystal structure of the ligand-binding module of human TAG-1 suggests a new mode of homophilic interaction. *Protein Science* *16*, 2174–2183.
- Müller, M. J. I., Klumpp, S., Lipowsky, R. (2008). Tug-of-war as a cooperative mechanism for bidirectional cargo transport by molecular motors. *Proceedings of the National Academy of Sciences* *105*(12), 4609–4614.
- Nakazawa, E., and Ishikawa, H. (1995). Occurrence of fasciculated microtubules at nodes of Ranvier in rat spinal roots. *Journal of Neurocytology* *24*, 399–407.
- Nave, K.-A. (2010). Myelination and the trophic support of long axons. *Nature Reviews Neuroscience* *11*, 275–283.
- Neishabouri, A., Finn, A., Pristera, A., Okuse, K., and Faisal, A.A. (2012). Stochastic simulations reveal how clustering sodium ion channels in thin axons more than doubles the metabolic efficiency of action potentials. *Front. Comput. Neurosci. Conference Abstract: Bernstein Conference 2012*.
- Neishabouri, A., and Faisal, A.A. (2014). Saltatory conduction in unmyelinated axons: clustering of Na⁺ channels on lipid rafts enables micro-saltatory conduction in C-fibers. *Frontiers in Neuroanatomy* *8*.
- Nguyen, H.M., Miyazaki, H., Hoshi, N., Smith, B.J., Nukina, N., Goldin, A.L., and Chandy, K.G. (2012). Modulation of voltage-gated K⁺ channels by the sodium channel 1 subunit. *Proceedings of the National Academy of Sciences* *109*, 18577–18582.
- Occhi, S., Zambroni, D., Del Carro, U., Amadio, S., Sirkowski, E.E., Scherer, S.S.,

- Campbell, K.P., Moore, S.A., Chen, Z.L., Strickland, S., et al. (2005). Both Laminin and Schwann Cell Dystroglycan Are Necessary for Proper Clustering of Sodium Channels at Nodes of Ranvier. *The Journal of Neuroscience* *25*, 9418–9427.
- Ogawa, Y., Schafer, D.P., Horresh, I., Bar, V., Hales, K., Yang, Y., Susuki, K., Peles, E., Stankewich, M.C., and Rasband, M.N. (2006). Spectrins and AnkyrinB Constitute a Specialized Paranodal Cytoskeleton. *The Journal of Neuroscience* *26*, 5230–5239.
- Ogawa, Y., Horresh, I., Trimmer, J.S., Bredt, D.S., Peles, E., and Rasband, M.N. (2008). Postsynaptic Density-93 Clusters Kv1 Channels at Axon Initial Segments Independently of Caspr2. *The Journal of Neuroscience* *28*, 5731–5739.
- Ogiwara, I., Miyamoto, H., Morita, N., Atapour, N., Mazaki, E., Inoue, I., Takeuchi, T., Itohara, S., Yanagawa, Y., Obata, K., et al. (2007). Na_v1.1 Localizes to Axons of Parvalbumin-Positive Inhibitory Interneurons: A Circuit Basis for Epileptic Seizures in Mice Carrying an Scn1a Gene Mutation. *The Journal of Neuroscience* *27*, 5903–5914.
- Ohno, N., Terada, N., Yamakawa, H., Komada, M., Ohara, O., Trapp, B.D., and Ohno, S. (2006). Expression of protein 4.1G in Schwann cells of the peripheral nervous system. *Journal of Neuroscience Research* *84*, 568–577.
- Ohno, N., Kidd, G.J., Mahad, D., Kiryu-Seo, S., Avishai, A., Komuro, H., and Trapp, B.D. (2011). Myelination and Axonal Electrical Activity Modulate the Distribution and Motility of Mitochondria at CNS Nodes of Ranvier. *The Journal of Neuroscience* *31*, 7249–7258.
- Ohno, N., Chiang, H., Mahad, D.J., Kidd, G.J., Liu, L., Ransohoff, R.M., Sheng, Z.-H., Komuro, H., and Trapp, B.D. (2014). Mitochondrial immobilization mediated by syntaphilin facilitates survival of demyelinated axons. *Proceedings of the National Academy of Sciences* *111*, 9953–9958.
- O'Malley, H.A., and Isom, L.L. (2015). Sodium Channel β Subunits: Emerging Targets in Channelopathies. *Annual Review of Physiology* *77*, 481–504.
- O'Malley, H.A., Shreiner, A.B., Chen, G.-H., Huffnagle, G.B., and Isom, L.L. (2009). Loss of Na⁺ channel β 2 subunits is neuroprotective in a mouse model of multiple sclerosis. *Molecular and Cellular Neuroscience* *40*, 143–155.
- Oohashi, T., Hirakawa, S., Bekku, Y., Rauch, U., Zimmerman, D.R., Su, W.D., Ohtsuka, A., Murakami, T., Ninomiya, Y. (2002). Bral1, a Brain-Specific Link Protein, Colocalizing with the Versican V2 Isoform at the Nodes of Ranvier in Developing and Adult Mouse Central Nervous Systems. *Molecular and*

- Cellular Neuroscience *19*, 43–57.
- Osorio, N., Cathala, L., Meisler, M.H., Crest, M., Magistretti, J., and Delmas, P. (2010). Persistent $\text{Na}_v1.6$ current at axon initial segments tunes spike timing of cerebellar granule cells: $\text{Na}_v1.6$ ensures spike regularity in cerebellar granule cells. *The Journal of Physiology* *588*, 651–670.
- Palmer, L.M. and Stuart, G.J. (2006). Site of Action Potential Initiation in Layer 5 Pyramidal Neurons. *The Journal of Neuroscience* *26*, 1854–1863.
- Papandréou, M.-J., Vacher, H., Fache, M.-P., Klinger, E., Rueda-Boroni, F., Farracci, G., Debarnot, C., Pipérolou, C., Garcia Del Cano, G., Goutebroze, L., and Dargent, B. (2015). CK2-regulated schwannomin-interacting protein IQCJ-SCHIP-1 association with AnkG contributes to the maintenance of the axon initial segment. *Journal of Neurochemistry*, accepted article, doi: 10.1111/jnc.13158.
- Pan, Z., Kao, T., Horvath, Z., Lemos, J., Sul, J.Y., Cranstoun, S.D., Bennett, V., Scherer, S.S., and Cooper, E.C. (2006). A Common Ankyrin-G-Based Mechanism Retains KCNQ and Na_v Channels at Electrically Active Domains of the Axon. *The Journal of Neuroscience* *26*, 2599–2613.
- Pannese, E. (2015). *Neurocytology: Fine structure of neurons, nerve processes, and neuroglial cells*, 2nd ed. London, 45-49.
- Parkinson, N.J., Olsson, C.L., Hallows, J.L., McKee-Johnson, J., Keogh, B.P., Noben-Trauth, K., Kujawa, S.G., and Tempel, B.L. (2001). Mutant β -spectrin 4 causes auditory and motor neuropathies in quivering mice. *Nature Genetics* *29*, 61–65.
- Patton, D.E., Isom, L.L., Catterall, W.A., and Goldin, A.L. (1994). The Adult Rat Brain $\beta 1$ Subunit Modifies Activation and Inactivation of Multiple Sodium Channel α subunits. *The Journal of Biological Chemistry* *269*, 17649–17655.
- Peles, E., Nativ, M., Campbell, P.L., Sakurai, T., Martinez, R., Lev, S., Clary, D.O., Schilling, J., Barnea, G., Plowman, G.D., et al. (1995). The Carbonic Anhydrase Domain of Receptor Tyrosine Phosphatase β Is a Functional Ligand for the Axonal Cell Recognition Molecule Contactin. *Cell* *82*, 251–260.
- Peles, E., Nativ, M., Lustig, M., Grumet, M., Schilling, J., Martinez, R., Plowman, G.D., and Schlessinger, J. (1997). Identification of a novel contactin-associated transmembrane receptor with multiple domains implicated in protein–protein interactions. *The EMBO Journal* *16*, 978–988.
- Perkins, G.A., and Ellisman, M.H. (2011). Mitochondrial configurations in

- peripheral nerve suggest differential ATP production. *Journal of Structural Biology* 173, 117–127.
- Pesheva, P., Gennarini, G., Goridis, C., and Schachner, M. (1993). The F3/11 Cell Adhesion Molecule Mediates the Repulsion of Neurons by the Extracellular Matrix Glycoprotein J1-160/180. *Neuron* 10, 69–82.
- Peters, A., Palay, S.L., and Webster, H. (1976). *The Fine Structure of the Nervous System*. WB Saunders, Philadelphia, p. 215.
- Picardo, M.A., Guigue, P., Bonifazi, P., Batista-Brito, R., Allene, C., Ribas, A., Fishell, G., Baude, A., and Cossart, R. (2011). Pioneer GABA Cells Comprise a Subpopulation of Hub Neurons in the Developing Hippocampus. *Neuron* 71, 695–709.
- Pillai, A.M., Thaxton, C., Pribisko, A.L., Cheng, J.-G., Dupree, J.L., and Bhat, M.A. (2009). Spatiotemporal ablation of myelinating glia-specific *neurofascin* (Nfasc^{NF155}) in mice reveals gradual loss of paranodal axoglial junctions and concomitant disorganization of axonal domains. *The Journal of Neuroscience Research* 87, 1773–1793.
- Planells-Cases, R., Caprini, M., Zhang, J., Rockenstein, E.M., Rivera, R.R., Murre, C., Masliah, E., and Montal, M. (2000). Neuronal Death and Perinatal Lethality in Voltage-Gated Sodium Channel α II-Deficient Mice. *Biophysical Journal* 78, 2878–2891.
- Poliak, S., Salomon, D., Elhanany, H., Sabanay, H., Kiernan, B., Pevny, L., Stewart, C.L., Xu, X., Chiu, S.Y., Shrager, P., Furley, A.J.W., and Peles, E. (2003). Juxtaparanodal clustering of Shaker-like K⁺ channels in myelinated axons depends on Caspr2 and TAG-1. *The Journal of Cell Biology* 162, 1149–1160.
- Poliak, S., and Peles, E. (2003). The local differentiation of myelinated axons at nodes of Ranvier. *Nature Reviews Neuroscience* 4, 968–980.
- Poliak, S., Gollan, L., Martinez, R., Custer, A.W., Einheber, S., Salzer, J.L., Trimmer, J.S., Shrager, P., and Peles, E. (1999). Caspr2, a New Member of the Neurexin Superfamily, Is Localized at the Juxtaparanodes of Myelinated Axons and Associates with K⁺ Channels. *Neuron* 24, 1037–1047.
- Poliak, S., Gollan, L., Salomon, D., Berglund, E.O., Ohara, R., Ranscht, B., and Peles, E. (2001). Localization of Caspr2 in myelinated nerves depends on axon–glia interactions and the generation of barriers along the axon. *The Journal of Neuroscience* 21, 7568–7575.
- Pomictier, A.D., Shroff, S.M., Fuss, B., Sato-Bigbee, C., Brophy, P.J., Rasband, M.N., Bhat, M.A., and Dupree, J.L. (2010). Novel forms of neurofascin 155 in the

- central nervous system: alterations in paranodal disruption models and multiple sclerosis. *Brain* *133*, 389–405.
- Popovic, M.A., Foust, A.J., McCormick, D.A., and Zecevic, D. (2011). The spatio-temporal characteristics of action potential initiation in layer 5 pyramidal neurons: a voltage imaging study. *The Journal of Physiology* *589.17*, 4167–4187.
- Porter, K.R., and Bonneville, M.A. (1973). *Fine structure of Cells and Tissues*, 4th ed. Lea & Febiger, Philadelphia, p. 184.
- Pringle, N.P., and Richardson, W.D. (1993). A singularity of PDGF alpha-receptor expression in the dorsoventral axis of the neural tube may define the origin of the oligodendrocyte lineage. *Development* *117*, 525–533.
- Pristerà, A., Baker, M.D., and Okuse, K. (2012). Association between Tetrodotoxin Resistant Channels and Lipid Rafts Regulates Sensory Neuron Excitability. *PLoS ONE* *7*, e40079.
- Privat, A., Jacque, C., Bourre, J.M., Dupouey, P., and Baumann, N. (1979). Absence of the major dense line in myelin of the mutant mouse “shiverer.” *Neuroscience Letters* *12*, 107–112.
- Pumphrey, R.J., and Young, J.Z. (1938). The rates of conduction of nerve fibres of various diameters in cephalopods. *Journal of Experimental Biology* *15*, 453–466.
- Raff, M.C., Abney, E.R., Cohen, J., Lindsay, R., and Noble, M. (1983). Two types of astrocytes in cultures of developing rat white matter: differences in morphology, surface gangliosides, and growth characteristics. *The Journal of Neuroscience* *3*, 1289–1300.
- Raman, I.M., Sprunger, L.K., Meisler, M.H., and Bean, B.P. (1997). Altered Subthreshold Sodium Currents and Disrupted Firing Patterns in Purkinje Neurons of Scn8a Mutant Mice. *Neuron* *19*, 881–891.
- Ranvier, L.A. (1878). *Leçons sur l’histologie du système nerveux* (F. Savy).
- Rasband, M.N. (2004). It’s “juxta” potassium channel *The Journal of Neuroscience Research* *76*, 749–757.
- Rasband, M.N., and Shrager, P. (2000). Ion Channel Sequestration in CNS Axons. *The Journal of Physiology* *525.1*, 63–73.
- Rasband, M.N., and Trimmer, J.S. (2001). Developmental Clustering of Ion Channels at and near the Node of Ranvier. *Developmental Biology* *236*, 5–16.

- Rasband, M.N., Peles, E., Trimmer, J.S., Levinson, S.R., Lux, S.E., and Shrager, P. (1999). Dependence of nodal sodium channel clustering on paranodal axoglial contact in the developing CNS. *The Journal of Neuroscience* *19*, 7516–7528.
- Rasband, M.N., Taylor, C.M., and Bansal, R. (2003). Paranodal transverse bands are required for maintenance but not initiation of Na_v1.6 sodium channel clustering in CNS optic nerve axons. *Glia* *44*, 173–182.
- Rasband, M.N., Tayler, J., Kaga, Y., Yang, Y., Lappe-Siefke, C., Nave, K.-A., and Bansal, R. (2005). CNP is required for maintenance of axon-glia interactions at nodes of Ranvier in the CNS. *Glia* *50*, 86–90.
- Ratcliffe, C.F., Westenbroek, R.E., Curtis, R., Catterall, W.A. (2001). Sodium channel β 1 and β 3 subunits associate with neurofascin through their extracellular immunoglobulin-like domain. *The Journal of Cell Biology* *154*, 427–434.
- Rathjen, F.G., Wolff, J.M., Chang, S., Bonhoeffer, F., and Raper, J.A. (1987a). Neurofascin-a novel chick cell-surface glycoprotein involved in neurite-neurite interactions. *Cell* *51*, 841–849.
- Rathjen, F.G., Wolff, J.M., Frank, R., Bonhoeffer, F., and Rutishauser, U. (1987b). Membrane glycoproteins involved in neurite fasciculation. *The Journal of Cell Biology* *104*, 343–353.
- Ren, Q., and Bennett, V. (1998). Palmitoylation of Neurofascin at a Site in the Membrane-Spanning Domain Highly Conserved Among the L1 Family of Cell Adhesion Molecules. *Journal of Neurochemistry* *70*, 1839–1849.
- Rios, J.C., Melendez-Vasquez, C.V., Einheber, S., Lustig, M., Grumet, M., Hemperly, J., Peles, E., and Salzer, J.L. (2000). Contactin-associated protein (Caspr) and contactin form a complex that is targeted to the paranodal junctions during myelination. *The Journal of Neuroscience* *20*, 8354–8364.
- Rios, J.C., Rubin, M., Martin, M.S., Downey, R.T., Einheber, S., Rosenbluth, J., Levinson, S.R., Bhat, M., and Salzer, J.L. (2003). Paranodal interactions regulate expression of sodium channel subtypes and provide a diffusion barrier for the node of Ranvier. *The Journal of Neuroscience* *23*, 7001–7011.
- Ritchie, J.M. (1982). On the relation between fibre diameter and conduction velocity in myelinated nerve fibres. *Proceedings of the Royal Society of London. Series B. Biological Sciences* *217*, 29–35.
- Ritchie, J., and Rogart, R.B. (1977). Density of sodium channels in mammalian myelinated nerve fibers and nature of the axonal membrane under the myelin sheath. *Proceedings of the National Academy of Sciences* *74*, 211–215.

- Rosenbluth, J. (1976). Intramembranous particle distribution at the node of Ranvier and adjacent axolemma in myelinated axons of the frog brain. *The Journal of Neurocytology* *5*, 731–745.
- Rosenbluth, J. (2009). Multiple functions of the paranodal junction of myelinated nerve fibers. *The Journal of Neuroscience Research* *87*, 3250–3258.
- Rush, A.M., Dib-Hajj, S.D., and Waxman, S.G. (2005). Electrophysiological properties of two axonal sodium channels, Na_v1.2 and Na_v1.6, expressed in mouse spinal sensory neurones: Sodium channels in sensory neurones. *The Journal of Physiology* *564*, 803–815.
- Rushton, W.A.H. (1951). A theory of the effects of fibre size in medullated nerve. *The Journal of Physiology* *115*, 101–122.
- Saito, F., Moore, S.A., Barresi, R., Henry, M.D., Messing, A., Ross-Barta, S.E., Cohn, R.D., Williamson, R.A., Sluka, K.A., Sherman, D.L., et al. (2003). Unique role of dystroglycan in peripheral nerve myelination, nodal structure, and sodium channel stabilization. *Neuron* *38*, 747–758.
- Sakurai, T. (2012). The role of NrCAM in neural development and disorders—Beyond a simple glue in the brain. *Molecular and Cellular Neuroscience* *49*, 351–363.
- Salzer, J.L. (2003). Polarized domains of myelinated axons. *Neuron* *40*, 297–318.
- Salzer, J.L., Holmes, W.P., and Colman, D.R. (1987). The amino acid sequences of the myelin-associated glycoproteins: homology to the immunoglobulin gene superfamily. *The Journal of Cell Biology* *104*, 957–965.
- Sánchez-Ponce, D., DeFelipe, J., Garrido, J.J., and Muñoz, A. (2012). Developmental Expression of Kv Potassium Channels at the Axon Initial Segment of Cultured Hippocampal Neurons. *PLoS ONE* *7*, e48557.
- Schafer, D.P., Bansal, R., Hedstrom, K.L., Pfeiffer, S.E., and Rasband, M.N. (2004). Does Paranode Formation and Maintenance Require Partitioning of Neurofascin 155 into Lipid Rafts? *The Journal of Neuroscience* *24*, 3176–3185.
- Schafer, D.P., Custer, A.W., Shrager, P., and Rasband, M.N. (2006). Early events in node of Ranvier formation during myelination and remyelination in the PNS. *Neuron Glia Biology* *2*, 69–79.
- Schaller, K.L., Krzemien, D.M., Yarowsky, P.J., Krueger, B.K., and Caldwell, J.H. (1995). A novel, abundant sodium channel expressed in neurons and glia. *The Journal of Neuroscience* *15*, 3231–3242.

- Scherer, S.S., Xu, T., Crino, P., Arroyo, E.J., and Gutmann, D.H. (2001). Ezrin, radixin, and moesin are components of Schwann cell microvilli. *The Journal of Neuroscience Research* 65, 150–164.
- Schmidt-Hieber, C., Jonas, P., and Bischofberger, J. (2008). Action potential initiation and propagation in hippocampal mossy fibre axons: Action potential initiation in granule cell axons. *The Journal of Physiology* 586, 1849–1857.
- Schwarz, J.R., Glassmeier, G., Cooper, E.C., Kao, T.-C., Nodera, H., Tabuena, D., Kaji, R., and Bostock, H. (2006). KCNQ channels mediate I_{Ks} , a slow K^+ current regulating excitability in the rat node of Ranvier: Nodal KCNQ current. *The Journal of Physiology* 573, 17–34.
- Sherman, D.L., and Brophy, P.J. (2005). Mechanisms of axon ensheathment and myelin growth. *Nature Reviews Neuroscience* 6, 683–690.
- Sherman, D.L., Tait, S., Melrose, S., Johnson, R., Zonta, B., Court, F.A., Macklin, W.B., Meek, S., Smith, A.J.H., Cottrell, D.F., et al. (2005). Neurofascins Are Required to Establish Axonal Domains for Saltatory Conduction. *Neuron* 48, 737–742.
- Shrager, P. (1987). The distribution of sodium and potassium channels in single demyelinated axons of the frog. *The Journal of Physiology* 392, 587–602.
- Shu, Y., Duque, A., Yu, Y., Haider, B., and McCormick, D.A. (2007). Properties of Action-Potential Initiation in Neocortical Pyramidal Cells: Evidence From Whole Cell Axon Recordings. *Journal of Neurophysiology* 97, 746–760.
- Smith, K. (1994). Conduction properties of central demyelinated and remyelinated axons, and their relation to symptom production in demyelinating disorders. *Eye* 8, 224–237.
- Sobotzik, J.-M., Sie, J.M., Politi, C., Del Turco, D., Bennett, V., Deller, T., and Schultz, C. (2009). AnkyrinG is required to maintain axo-dendritic polarity in vivo. *Proceedings of the National Academy of Sciences* 106, 17564–17569.
- Soleng, A.F., Raastad, M., and Andersen, P. (2003). Conduction latency along CA3 hippocampal axons from rat. *Hippocampus* 13, 953–961.
- Solly, S.K., Thomas, J.-L., Monge, M., Demerens, C., Lubetzki, C., Gardinier, M.V., Matthieu, J.-M., and Zalc, B. (1996). Myelin/oligodendrocyte glycoprotein (MOG) expression is associated with myelin deposition. *Glia* 18, 39–48.
- Spassky, N., Olivier, C., Cobos, I., Le Bras, B., Goujet-Zalc, C., Martínez, S., Zalc, B., and Thomas, J.-L. (2001). The Early Steps of Oligodendrogenesis: Insights

- from the Study of the plp Lineage in the Brain of Chicks and Rodents. *Developmental Neuroscience* *23*, 318–326.
- Srinivasan, J., Schachner, M., and Catterall, W.A. (1998). Interaction of voltage-gated sodium channels with the extracellular matrix molecules tenascin-C and tenascin-R. *Proceedings of the National Academy of Sciences* *95*, 15753–15757.
- Stathopoulos, P., Alexopoulos, H., and Dalakas, M.C. (2015). Autoimmune antigenic targets at the node of Ranvier in demyelinating disorders. *Nature Reviews Neurology* *11*, 143–156.
- Sugawara, T., Mazaki-Miyazaki, E., Ito, M., Nagafuji, H., Fukuma, G., Mitsudome, A., Wada, K., Kaneko, S., Hirose, S., and Yamakawa, K. (2001). Na_v1.1 mutations cause febrile seizures associated with afebrile partial seizures. *Neurology* *57*, 703–705.
- Susuki, K., Chang, K.-J., Zollinger, D.R., Liu, Y., Ogawa, Y., Eshed-Eisenbach, Y., Dours-Zimmermann, M.T., Osés-Prieto, J.A., Burlingame, A.L., Seidenbecher, C.I., et al. (2013). Three Mechanisms Assemble Central Nervous System Nodes of Ranvier. *Neuron* *78*, 469–482.
- Suzuki, A., Hoshi, T., Ishibashi, T., Hayashi, A., Yamaguchi, Y., and Baba, H. (2004). Paranodal axoglial junction is required for the maintenance of the Na_v1.6-type sodium channel in the node of Ranvier in the optic nerves but not in peripheral nerve fibers in the sulfatide-deficient mice. *Glia* *46*, 274–283.
- Swadlow, H.A., Waxman, S.G., and Weyand, T.G. (1981). Effects of variations in temperature on impulse conduction along nonmyelinated axons in the mammalian brain. *Experimental Neurology* *71*, 383–389.
- Tait, S., Gunn-Moore, F., Collinson, J.M., Huang, J., Lubetzki, C., Pedraza, L., Sherman, D.L., Colman, D.R., and Brophy, P.J. (2000). An oligodendrocyte cell adhesion molecule at the site of assembly of the paranodal axo-glial junction. *The Journal of Cell Biology* *150*, 657–666.
- Tantama, M., Martínez-François, J.R., Mongeon, R., and Yellen, G. (2013). Imaging energy status in live cells with a fluorescent biosensor of the intracellular ATP-to-ADP ratio. *Nature Communications* *4*.
- Tasaki, I. (1939). The electro-saltatory transmission of the nerve impulse and the effect of narcosis upon the nerve fiber. *The American Journal of Physiology* *127*, 211–227.
- Thaxton, C., Pillai, A.M., Pribisko, A.L., Labasque, M., Dupree, J.L., Faivre-Sarrailh, C., and Bhat, M.A. (2010). In Vivo Deletion of Immunoglobulin

- Domains 5 and 6 in Neurofascin (Nfasc) Reveals Domain-Specific Requirements in Myelinated Axons. *The Journal of Neuroscience* *30*, 4868–4876.
- Thaxton, C., Pillai, A.M., Pribisko, A.L., Dupree, J.L., and Bhat, M.A. (2011). Nodes of Ranvier Act as Barriers to Restrict Invasion of Flanking Paranodal Domains in Myelinated Axons. *Neuron* *69*, 244–257.
- Tian, C., Wang, K., Ke, W., Guo, H., and Shu, Y. (2014). Molecular identity of axonal sodium channels in human cortical pyramidal cells. *Frontiers in Cellular Neuroscience* *8*, 1-16.
- Tkachenko, E. (2005). Syndecans: New Kids on the Signaling Block. *Circulation Research* *96*, 488–500.
- Traka, M., Goutebroze, L., Denisenko, N., Bessa, M., Nifli, A., Havaki, S., Iwakura, Y., Fukamauchi, Watanabe, K., Soliven, B., Girault, J.-A., and Karagogeos D. (2003). Association of TAG-1 with Caspr2 is essential for the molecular organization of juxtaparanodal regions of myelinated fibers. *The Journal of Cell Biology* *162*, 1161–1172.
- Traka, M., Dupree, J.L., Popko, B., and Karagogeos, D. (2002). The neuronal adhesion protein TAG-1 is expressed by Schwann cells and oligodendrocytes and is localized to the juxtaparanodal region of myelinated fibers. *The Journal of Neuroscience* *22*, 3016–3024.
- Trimmer, J.S. (2015). Subcellular Localization of K⁺ Channels in Mammalian Brain Neurons: Remarkable Precision in the Midst of Extraordinary Complexity. *Neuron* *85*, 238–256.
- Tuvia, S., Garver, T.D., and Bennett, V. (1997). The phosphorylation state of the FIGQY tyrosine of neurofascin determines ankyrin-binding activity and patterns of cell segregation. *Proceedings of the National Academy of Sciences* *94*, 12957–12962.
- Tzoumaka, E., Tischler, A.C., Sangameswaran, L., Eglen, R.M., Hunter, J.C., and Novaković, S.D. (2000). Differential Distribution of the Tetrodotoxin-Sensitive rPN4/NaCH6/Scn8a Sodium Channel in the Nervous System. *Journal of Neuroscience Research* *60*, 37–44.
- Uemoto, Y., Suzuki, S.-I., Terada, N., Ohno, N., Ohno, S., Yamanaka, S., and Komada, M. (2006). Specific Role of the Truncated β IV-Spectrin Σ 6 in Sodium Channel Clustering at Axon Initial Segments and Nodes of Ranvier. *The Journal of Biological Chemistry* *282*, 6548–6555.
- Vabnick, I., Novaković, S.D., Levinson, S.R., Schachner, M., and Shrager, P. (1996).

- The clustering of axonal sodium channels during development of the peripheral nervous system. *The Journal of Neuroscience* *16*, 4914–4922.
- Vabnick, I., Trimmer, J.S., Schwarz, T.L., Levinson, S.R., Risal, D., and Shrager, P. (1999). Dynamic potassium channel distributions during axonal development prevent aberrant firing patterns. *The Journal of Neuroscience* *19*, 747–758.
- Vacher, H., Mohapatra, D.P., and Trimmer, J.S. (2008). Localization and Targeting of Voltage-Dependent Ion Channels in Mammalian Central Neurons. *Physiological Reviews* *88*, 1407–1447.
- Voas, M.G., Lyons, D.A., Naylor, S.G., Arana, N., Rasband, M.N., and Talbot, W.S. (2007). α II-Spectrin Is Essential for Assembly of the Nodes of Ranvier in Myelinated Axons. *Current Biology* *17*, 562–568.
- Voas, M.G., Glenn, T.D., Raphael, A.R., and Talbot, W.S. (2009). Schwann Cells Inhibit Ectopic Clustering of Axonal Sodium Channels. *Journal of Neuroscience* *29*, 14408–14414.
- Volkmer, H., Leuschner, R., Zacharias, U., and Rathjen, F.G. (1996). Neurofascin induces neurites by heterophilic interactions with axonal NrCAM while NrCAM requires F11 on the axonal surface to extend neurites. *The Journal of Cell Biology* *135*, 1059–1069.
- Volkmer, H., Zacharias, U., Nörenberg, U., and Rathjen, F.G. (1998). Dissection of complex molecular interactions of neurofascin with axonin-1, F11, and tenascin-R, which promote attachment and neurite formation of tectal cells. *The Journal of Cell Biology* *142*, 1083–1093.
- Wake, H., Lee, P., and Fields, D. (2011). Control of Local Protein Synthesis and Initial Events in Myelination by Action Potentials. *Science* *333*, 1647–1651.
- Wang, X., and Schwarz, T.L. (2009). The Mechanism of Ca^{2+} -Dependent Regulation of Kinesin-Mediated Mitochondrial Motility. *Cell* *136*, 163–174.
- Wang, H., Kunkel, D.D., Martin, T.M., Schwartzkroin, P.A., and Tempel, B.L. (1993). Heteromultimeric K^+ channels in terminal and juxtaparanodal regions of neurons. *Nature* *365*, 75–79.
- Wang, H., Kunkel, D.D., Schwartzkroin, P.A., and Tempel, B.L. (1994). Localization of $\text{K}_v1.1$ and $\text{K}_v1.2$, two K channel proteins, to synaptic terminals, somata, and dendrites in the mouse brain. *The Journal of Neuroscience* *14*, 4588–4599.
- Wang, H.-S., Pan, Z., Shi, W., Brown, B.S., Wymore, R.S., Cohen, I.S., Dixon, J.E., and McKinnon, D. (1998). KCNQ2 and KCNQ3 potassium channel subunits-

- molecular correlates of the M-channel. *Science* 282, 1890–1893.
- Van Wart, A., Trimmer, J.S., and Matthews, G. (2007). Polarized distribution of ion channels within microdomains of the axon initial segment. *The Journal of Comparative Neurology* 500, 339–352.
- Watkins, T.A., Emery, B., Mulinyawe, S., and Barres, B.A. (2008). Distinct Stages of Myelination Regulated by γ -Secretase and Astrocytes in a Rapidly Myelinating CNS Coculture System. *Neuron* 60, 555–569.
- Waxman, S. (1980). Determinants of Conduction Velocity in Myelinated Nerve Fibers. *Muscle & Nerve* 3, 141–150.
- Waxman, S.G. (1974). Ultrastructural differentiation of the axon membrane at synaptic and non-synaptic central nodes of Ranvier. *Brain Research* 65, 338–342.
- Waxman, S.G. (2006). Axonal conduction and injury in multiple sclerosis: the role of sodium channels. *Nature Reviews Neuroscience* 7, 932–941.
- Waxman, S.G., and Bennett, M.V.L. (1972). Relative Conduction Velocities of Small Myelinated and Non-myelinated Fibres in the Central Nervous System. *Nature New Biology* 238, 217–219.
- Waxman, S.G., and Quick, D.C. (1977). Cytochemical differentiation of the axon membrane in A- and C-fibres. *Journal of Neurology, Neurosurgery & Psychiatry* 40, 379–385.
- Waxman, S.G., Pappas, G.D., and Bennett, M.V.L. (1972). Morphological correlates of functional differentiation of nodes of Ranvier along single fibers in the neurogenic electric organ of the knife fish *Sternarchus*. *The Journal of Cell Biology* 53, 210–224.
- Waxman, S.G., Black, J.A., Kocsis, J.D., and Ritchie, J.M. (1989). Low density of sodium channels supports action potential conduction in axons of neonatal rat optic nerve. *Proceedings of the National Academy of Sciences* 86, 1406–1410.
- Weber, P., Bartsch, U., Rasband, M.N., Czaniera, R., Lang, Y., Bluethmann, H., Margolis, R.U., Levinson, S.R., Shrager, P., Montag, D., et al. (1999). Mice deficient for tenascin-R display alterations of the extracellular matrix and decreased axonal conduction velocities in the CNS. *The Journal of Neuroscience* 19, 4245–4262.
- Weiser, M., Bueno, E., Sekirnjak, C., Martone, M.E., Baker, H., Hillman, D., Chen, S., Thornhill, W., Ellisman, M., and Rudy, B. (1995). The potassium channel

- subunit K_v3.1b is localized to somatic and axonal membranes of specific populations of CNS neurons. *The Journal of Neuroscience* *15*, 4298–4314.
- Westenbroek, R.E., Noebels, J.L., and Catterall, W.A. (1992). Elevated expression of type II Na⁺ channels in hypomyelinated axons of Shiverer mouse brain. *The Journal of Neuroscience* *12*, 2259–2267.
- Whitaker, W.R., Clare, J.J., Powell, A.J., Chen, Y.H., Faull, R.L., and Emson, P.C. (2000). Distribution of voltage-gated sodium channel α -subunit and β -subunit mRNAs in human hippocampal formation, cortex, and cerebellum. *The Journal of Comparative Neurology* *422*, 123–139.
- Wiley-Livingston, C.A., and Ellisman, M.H. (1980). Development of axonal membrane specializations defines nodes of Ranvier and precedes Schwann cell myelin elaboration. *Developmental Biology* *79*, 334–355.
- Wimmer, V.C., Harty, R.C., Richards, K.L., Phillips, A.M., Miyazaki, H., Nukina, N., and Petrou, S. (2015). Sodium channel β 1 subunit localizes to axon initial segments of excitatory and inhibitory neurons and shows regional heterogeneity in mouse brain: Regional and cellular Na_v β 1 subunit expression. *The Journal of Comparative Neurology* *523*, 814–830.
- Xiao, Z.-C., Ragsdale, D.S., Malhotra, J.D., Mattei, L.N., Braun, P.E., Schachner, M., and Isom, L.L. (1999). Tenascin-R Is a Functional Modulator of Sodium Channel Subunits. *The Journal of Biological Chemistry* *274*, 26511–26517.
- Xu, X., and Shrager, P. (2005). Dependence of axon initial segment formation on Na⁺ channel expression. *The Journal of Neuroscience Research* *79*, 428–441.
- Xu, K., Zhong, G., and Zhuang, X. (2013). Actin, Spectrin, and Associated Proteins Form a Periodic Cytoskeletal Structure in Axons. *Science* *339*, 452–456.
- Xu, M., Cao, R., Xiao, R., Zhu, M.X., and Gu, C. (2007). The Axon Dendrite Targeting of K_v3 (Shaw) Channels Is Determined by a Targeting Motif That Associates with the T1 Domain and Ankyrin G. *The Journal of Neuroscience* *27*, 14158–14170.
- Xu, M., Gu, Y., Barry, J., and Gu, C. (2010). Kinesin I Transports Tetramerized K_v3 Channels through the Axon Initial Segment via Direct Binding. *The Journal of Neuroscience* *30*, 15987–16001.
- Yang, Y., Lacas-Gervais, S., Morest, D.K., Solimena, M., and Rasband, M.N. (2004). β IV Spectrins Are Essential for Membrane Stability and the Molecular Organization of Nodes of Ranvier. *The Journal of Neuroscience* *24*, 7230–7240.

- Yang, Y., Ogawa, Y., Hedstrom, K.L., and Rasband, M.N. (2007). β IV spectrin is recruited to axon initial segments and nodes of Ranvier by ankyrinG. *The Journal of Cell Biology* *176*, 509–519.
- Yap, C.C., Vakulenko, M., Kruczek, K., Motamedi, B., Digilio, L., Liu, J.S., and Winckler, B. (2012). Doublecortin (DCX) Mediates Endocytosis of Neurofascin Independently of Microtubule Binding. *The Journal of Neuroscience* *32*, 7439–7453.
- Young, R.G., Castelfranco, A.M., and Hartline, D.K. (2013). The “Lillie Transition”: models of the onset of saltatory conduction in myelinating axons. *The Journal of Computational Neuroscience* *34*, 533–546.
- Yu, F.H., Westenbroek, R.E., Silos-Santiago, I., McCormick, K.A., Lawson, D., Ge, P., Ferriera, H., Lilly, J., DiStefano, P.S., Catterall, W.A., et al. (2003). Sodium Channel β 4, a New Disulfide-linked Auxillary Subunit with Similarity to β 2. *The Journal of Neuroscience* *23*, 7577–7585.
- Zagoren, J.C. (1984). Cation binding at the node of Ranvier. *In* “The Node of Ranvier”. J.C. Zagoren and S Fedoroff, eds. New York, Academic Press, pp.69–91.
- Zala, D., Hinckelmann, M.-V., Yu, H., Lyra da Cunha, M.M., Liot, G., Cordelières, F.P., Marco, S., and Saudou, F. (2013). Vesicular Glycolysis Provides On-Board Energy for Fast Axonal Transport. *Cell* *152*, 479–491.
- Zalc, B., Monge, M., Dupouey, P., Hauw, J.J., and Baumann, N.A. (1981). Immunohistochemical localization of the galactosyl and sulfogalactosyl ceramide in the brain of the 30-day-old mouse. *Brain Research* *211*, 341–354.
- Zalc, B., Goujet, D., and Colman, D. (2008). The origin of the myelination program in vertebrates. *Current Biology* *18*, 511–512.
- Zecevic, D. Multiple spike-initiation zones in single neurons revealed by voltage-sensitive dyes (1996). *Nature* *381*: 322–325.
- Zeng, S., and Tang, Y. (2009). Effect of clustered ion channels along an unmyelinated axon. *Phys. Rev. E* *80*, 021917.
- Zhang, X., and Bennett, V. (1998). Restriction of 480/270-kD ankyrin G to axon proximal segments requires multiple ankyrinG-specific domains. *The Journal of Cell Biology* *142*, 1571–1581.
- Zhang, A., Desmazieres, A., Zonta, B., Melrose, S., Campbell, G., Mahad, D., Li, Q., Sherman, D.L., Reynolds, R., and Brophy, P.J. (2015). Neurofascin 140 Is an Embryonic Neuronal Neurofascin Isoform That Promotes the Assembly of the

- Node of Ranvier. *The Journal of Neuroscience* 35, 2246–2254.
- Zhang, C., Susuki, K., Zollinger, D.R., Dupree, J.L., and Rasband, M.N. (2013). Membrane domain organization of myelinated axons requires β II spectrin. *The Journal of Cell Biology* 203, 437–443.
- Zhang, C.L., Ho, P.L., Kintner, D.B., Sun, D., and Chiu, S.Y. (2010). Activity-Dependent Regulation of Mitochondrial Motility by Calcium and Na/K-ATPase at Nodes of Ranvier of Myelinated Nerves. *The Journal of Neuroscience* 30, 3555–3566.
- Zhang, Y., Bekku, Y., Dzhashiashvili, Y., Armenti, S., Meng, X., Sasaki, Y., Milbrandt, J., and Salzer, J.L. (2012). Assembly and Maintenance of Nodes of Ranvier Rely on Distinct Sources of Proteins and Targeting Mechanisms. *Neuron* 73, 92–107.
- Zhong, G., He, J., Zhou, R., Lorenzo, D.N., Babcock, H.P., Bennett, V., and Zhuang, X. (2014). Developmental mechanism of the periodic membrane skeleton in axons. *eLife* 3, 1–21.
- Zonta, B., Tait, S., Melrose, S., Anderson, H., Harroch, S., Higginson, J., Sherman, D.L., and Brophy, P.J. (2008). Glial and neuronal isoforms of Neurofascin have distinct roles in the assembly of nodes of Ranvier in the central nervous system. *The Journal of Cell Biology* 181, 1169–1177.
- Zonta, B., Desmazières, A., Rinaldi, A., Tait, S., Sherman, D.L., Nolan, M.F., and Brophy, P.J. (2011). A Critical Role for Neurofascin in Regulating Action Potential Initiation through Maintenance of the Axon Initial Segment. *Neuron* 69, 945–956.

Summary

The clustering of sodium channels (Na_v) at the nodes of Ranvier is an important step in permitting rapid saltatory conduction along myelinated axons. Nodal assembly is neuron-glia dependent, mediated by myelinating oligodendrocytes of the central nervous system (CNS) and Schwann cells in the peripheral nervous system (PNS). While the mechanisms of nodal assembly are currently best characterized in the PNS, cellular and molecular mechanisms underlying their assembly in the CNS are only partially understood.

In the core of my PhD dissertation, I focused on the early developmental steps of nodal protein clustering in the CNS and show that clusters of nodal proteins, called prenodes, are detected before myelination along GABAergic axons in hippocampal neuron-glia cultures and also in the developing rodent hippocampus. Prenodal clustering requires extrinsic oligodendroglial secreted proteinaceous factors, and also the intrinsic axonal cytoskeletal scaffolding protein ankyrinG. Furthermore, the transition of sodium channels isoforms is tightly regulated along GABAergic axons during development, but this transition is lost in the absence of the physical presence of glial cells. Lastly, prenodes increase axonal conduction by a factor of 1.5x, independently of myelination and axonal caliber.

Taken together, these results further our understanding of CNS nodes of Ranvier assembly mechanisms and the developmental function of nodal clustering prior to myelin ensheathment. While conduction velocity along axons has long been thought to mostly rely on the insulating properties of myelin, these results may shed light on a new concept of axonal conduction in the absence of myelination.

Keywords: *Nodes of Ranvier, sodium channels, myelination, conduction velocity, neuron-glia interactions, GABAergic neurons*

Résumé

L'agrégation des canaux sodium (Na_v) aux nœuds de Ranvier est une étape importante pour la propagation électrique saltatoire rapide le long des axones myélinisés. L'assemblage des nœuds dépend d'interactions neurones-cellules gliales myélinisantes, les oligodendrocytes dans le système nerveux central (SNC) et les cellules de Schwann dans le système nerveux périphérique (SNP). Bien décrits dans le SNP, les mécanismes cellulaires et moléculaires restent à caractériser dans le SNC.

Lors de ma thèse, je me suis focalisé sur les étapes précoces d'assemblage des nœuds dans le SNC. Ce travail montre que des agrégats de protéines nodales (ou pré-nœuds) sont formés le long des axones de neurones GABAergiques avant la myélinisation dans des cultures neurones-glies d'hippocampe et également au cours du développement chez les rongeurs. La formation de pré-nœuds dépend de protéines sécrétées par les oligodendrocytes et de la protéine axonale d'échafaudage, ankyrineG. En outre, la transition des isoformes de Na_v le long des axones est régulée par la présence des cellules gliales. Enfin, les pré-nœuds permettent d'accélérer la vitesse de conduction de l'influx nerveux par un facteur 1,5, indépendamment de la myélinisation et du calibre axonal.

Globalement, ces résultats renforcent notre connaissance des mécanismes d'assemblage des nœuds de Ranvier dans le SNC et suggèrent une fonction développementale de l'agrégation nodale avant le début de la myélinisation. Si la vitesse de conduction a été décrite comme liée aux propriétés isolantes de la gaine de myéline, les résultats de cette thèse apportent un concept novateur de régulation de la conduction axonale en l'absence de myéline.

Mots Clés: Nœuds de Ranvier, canaux sodium, myélinisation, vitesse de conduction, les interactions neurones-gliales, neurones GABAergiques